HAWKE'S BAY REGIONAL COUNCIL
TE KAUNIHERA Ā-ROHE O TE MATAU-A-MĀUI

Meeting of the Environment and Integrated Catchments Committee

Date: 11 September 2024

Time: 9.00am

Venue: Council Chamber
Hawke's Bay Regional Council
159 Dalton Street
NAPIER

Attachments excluded from Agenda

Item	Title		Page
5.	**Biosecurity Annual Report 2023-2024 and Operational Plan 2024-2025**		
	Attachment 1:	2024-2025 Combined Pest Plant and Pest Animal Operational Plan ***online only***	2
	Attachment 2:	HBRC Biosecurity Annual Report 1 July 2023 - 30 June 2024 ***online only***	25
7.	**Our Landscapes – LiDAR partnership project with Manaaki Whenua Landcare Research**		
	Attachment 1:	Improving understanding and management of erosion with LiDAR 2024 ***online only***	51
	Attachment 2:	Mapping slope using Hawke's Bay's LiDAR digital elevation model 2024 ***online only***	103
	Attachment 3:	LiDAR-derived vegetation layers in Hawke's Bay 2024 ***online only***	125
8.	**Air Quality Monitoring update**		
	Attachment 1:	St John's Particulate Matter Monitoring Methods August 2024 ***online only***	172

2024-2025 Biosecurity Operational Plan

Regional Pest Management Plan 2018-38

August 2024
Hawkes Bay Regional Council Publication No.

HAWKES BAY
REGIONAL COUNCIL
TE KAUNIHERA Ā-ROHE O TE MATAU-A-MĀUI

ISSN 2703-2051 (Online)
ISSN 2703-2043 (Print)

Catchment Services

2024-2025 Biosecurity Operational Plan

Regional Pest Management Plan 2018-38

August 2024
Hawkes Bay Regional Council Publication No.

Prepared By:
Matt Short – Catchment Management Lead – Biosecurity

Reviewed By:
Mark Mitchell – Principal Advisor Biosecurity/Biodiversity

Approved By:
Iain Maxwell – Group Manager – Integrated Catchment Management

Contents

Introduction 5

Background 5

Integration with Annual Plan 5

Integration with Biodiversity Activities 5

Pest Categories 6

Pests contained within the RPMP 6

Principal Measures 9

Pest Plants 10

1.1. Exclusion Pest Plants 10

1.2. Eradication Pest Plants 10

1.3. Progressive Containment Pest Plants 11

1.4. Sustained Control Pest Plants 12

1.5. Biodiversity Pest Plants 15

1.6. Biological Control of Pest Plants 15

1.7. National Pest Plant Accord 15

1.8. General Advice and Information 15

Pest Animals 16

1.9. Exclusion Pest Animals 16

1.10. Eradication Pest Animals 16

1.11. Sustained Control Pest Animals 17

1.12. Site-Led Pest Animals 21

Phytosanitary Pests 21

Financial Summary 23

Measuring Performance 23

Implementation Report 24

4 September 2024 8.14 pm

Introduction

Regional councils have a mandate under Part 2 of the Biosecurity Act 1993 (the Act) to provide regional leadership in activities that prevent, reduce, or eliminate adverse effects from harmful organisms that are present in their region.

This operational plan sets out how Hawke's Bay Regional Council (HBRC) will implement the objectives set out in the Hawke's Bay Regional Pest Management Plan 2018-38 (the RPMP). This operational plan is effective from July 2024 to 30 June 2025.

Background

Hawke's Bay Regional Council is the management agency responsible for developing and implementing the Hawke's Bay Regional Pest Management Plan 2018-2038 in accordance with the Biosecurity Act 1993.

The RPMP sets out policies and rules that in combination seek to achieve the eradication or effective management of specified pests or groups of pests. It describes the biosecurity activities that will be undertaken throughout Hawke's Bay and outlines the management or eradication of specific organisms. Doing so will:

- minimise the actual or potential adverse or unintended effects associated with these organisms, and,
- maximise the effectiveness of individual actions in managing pests through a regionally coordinated approach.

As the management agency, Council is required to prepare an annual operational plan that sets out how the plan is to be implemented. Following the end of each financial year, staff will report to Council on the implementation of the operational plan.

This plan is the operational (management) response to supporting or directly achieving the objectives contained within the RPMP and is delivered by the Biosecurity team of the Catchment Services section within the Integrated Catchment Management (ICM) group.

Integration with Annual Plan

As far as practicable, the Operational Plan has been integrated with council's Annual Plan. The Annual Plan sets the overall priorities and work programmes for the organisation and provides an overview of related pest management activities for the 2024/2025 year. Implementation costs are included in the Annual Plan.

Integration with Biodiversity Activities

HBRC has responsibilities to manage biodiversity under the Resource Management Act 1991. The management of high value biodiversity areas across the region is coordinated by the Biodiversity team of the Catchment Operations team within the ICM group. Pest plant and pest animal control is a key method for managing native biodiversity, requiring ongoing investment of council resources, with resources allocated to the Priority Ecosystem programme. This programme focuses on managing the areas of highest biodiversity value in Hawke's Bay, which includes ongoing coordinated pest control. Implementation of this programme requires close coordination with the Pest Plant, Pest Animal and Predator Free Hawke's Bay teams. This work is complemented by other efforts such as deer fencing to exclude feral deer and advocating for legal protection under QEII and other covenanting agencies.

Pest Categories

Exclusion Pests

The purpose of this category is to prevent the establishment of a pest which is present in New Zealand but not yet established in the region. Eradication of an incursion exclusion pest will be attempted by the Council in conjunction with other agencies such as MPI, DOC and neighbouring Regional Councils.

Eradication Pests

The purpose of this category is to reduce the incidence or density of a pest to zero levels in an area in the short to medium term. For pests such as rooks, this could take over 30 years to achieve.

Progressive Containment Pests

The intermediate outcome for this category is to contain and reduce the geographic distribution of the pest to an area over time. Progressive containment pests are those where a pest is at high densities in parts of Hawke's Bay, but of low extent or limited range. Eradication is not feasible region-wide, but it is feasible to prevent the pest from spreading to other parts of Hawke's Bay or to eradicate the pest from parts of Hawke's Bay.

- Existing populations will be monitored and, where appropriate, systems set in place to prevent further spread.
- New technologies and methods will be investigated and introduced where possible.

Sustained Control Pests

The purpose of this category is to ensure pests are being controlled, to reduce impacts on values and spread to other properties. This may include boundary control of pest plants or suppression of a pest animal over a large geographic area where eradication is not possible.

Site Led Pests

A site-led programme is the coordinated and integrated control of pests in a defined area that aims to protect and restore specific ecological or biodiversity values which are threatened or compromised by pests. Site led programmes focus on the ecological or biodiversity values of the site rather than simply the control of pests.

Pests contained within the RPMP

Table 0-1: Number of Pest Species in the Plan.

Number of species (or groups of species) in the Regional Pest Management Plan					
Type of pest	Exclusion	Eradication	Progressive containment	Site led	Sustained control
Plants	5	8	11		9
Animals	1	2		8	5

Phytosanitary	5
Marine	2

**Note some species have more than one programme.*

Table 0-2: Pest Plant species included in RPMP

Common Name	Scientific Name	Programme
African feather grass*	*Cenchrus macrourus*	Eradication
Alligator weed*	*Alternanthera philoxeroides*	Exclusion
Apple of Sodom	*Solanum linnaeanum*	Progressive Containment
Australian sedge	*Carex longebrachiata*	Progressive Containment
Bathurst bur	*Xanthium spinosum*	Sustained Control
Blackberry	*Rubus fruticosus* agg.	Sustained Control
Cathedral bells*	*Cobaea scandens*	Eradication
Chilean needle grass*	*Nassella neesiana*	Sustained Control
Cotton thistle	*Onopordum acanthium*	Progressive Containment
Darwin's barberry*	*Berberis darwinii*	Progressive Containment
Goats rue	*Galega officinalis*	Eradication
Gorse	*Ulex europaeus*	Sustained Control
Japanese honeysuckle	*Lonicera japonica*	Progressive Containment
Marshwort*	*Nymphoides geminata*	Exclusion
Noogoora bur	*Xanthium strumarium*	Exclusion
Nassella tussock*	*Nassella trichotoma*	Progressive Containment
Nodding thistle	*Cardus nutans*	Sustained Control
Old man's beard*	*Clematis vitalba*	Progressive Containment
Phragmites*	*Phragmites australis*	Eradication
Purple loosestrife*	*Lythrum salicaria*	Eradication
Privet (Chinese and tree)	*Ligustrum sinense, L. lucidum*	Sustained Control
Ragwort	*Jacobaea vulgaris*	Sustained Control
Saffron thistle	*Carthamus lanatus*	Progressive Containment
Senegal tea*	*Gymnocoronis spilanthoides*	Exclusion
Spartina	*Spartina alterniflora, S. anglica, S. gracilis, S. maritime, S. x townsendii*	Exclusion
Spiny emex	*Emex australis*	Eradication

Common Name	Scientific Name	Programme
Variegated thistle	*Silybum marianum*	Sustained Control
Velvetleaf*	*Abutilon theophrasti*	Progressive Containment
White-edged nightshade*	*Solanum marginatum*	Eradication
Wilding Conifers	*Ref glossary pg 102*	Progressive Containment
Woolly nightshade*	*Solanum mauritianum*	Progressive Containment
Yellow bristle grass	*Setaria pumila*	Sustained Control
Yellow water lily*	*Nuphar lutea*	Eradication

** Unwanted organisms (as declared by a Chief Technical Officer)*

Table 0-3: Pest Animal species included in RPMP

Common Name	Scientific Name	Programme
Feral cat	*Felis catus*	Sustained Control, Site-led
Feral deer (incl. hybrids)	*Cervus elaphus, C. nippon, C. dama*	Site-led
Feral goat	*Capra hircus*	Sustained Control, Site-led
Feral pig	*Sus scrofa*	Site-led
Hedgehog	*Erinaceus europaeus*	Site-led
Mustelids (ferret, stoat, weasel)	*Mustelo furo, M. ermine, M. nivalis*	Sustained Control, Site-led
Possum	*Trichosurus vulpecula*	Eradication, Sustained Control, Site-led
Rabbit	*Oryctolagus cuniculis*	Sustained Control
Rat (Norway and ship)	*Rattus norvegicus, R. rattus*	Site-led
Rook*	*Corvus frugilegus*	Eradication
Wallaby (Bennett's, dama, parma, brush-tailed rock and swamp)*	*Macropus rufogriseus rufogriseus, M. eugenii, M. parma, Petrogale pencillata, Wallabia bicolour*	Exclusion

** Unwanted organisms (as declared by a Chief Technical Officer)*

Table 0-4: Marine Pests species included in RPMP

Common Name	Scientific Name	Programme
Mediterranean fanworm**	*Sabella spallanzanii*	Exclusion
Clubbed tunicate	*Styela clava*	Exclusion

*** Notifiable organism (s45 Biosecurity Act)*

Table 0-5: Phytosanitary Pests species included in RPMP

Common Name	Scientific Name	Programme
Apple black spot	*Venturia inaequalis.*	Sustained Control
Codling moth	*Cydia pomonella*	Sustained Control

Common Name	Scientific Name	Programme
European canker	*Neonectria ditissima*	Sustained Control
Fireblight	*Erwinia amylovora*	Sustained Control
Lightbrown apple moth (Leafroller)	*Epiphyas postvittana*	Sustained Control

This operational plan details the Plan objective for the control of the pests defined within the RPMP and provides a brief description of what activities HBRC will undertake to achieve the stated objective.

Principal Measures

This plan and the RPMP are based on the following core areas of HBRC's responsibility:

Regulation (standards and enforcement)

Standards, rules, and restrictions are set, and compliance enforced with penalties, when and where necessary.

Inspection

Regular property inspections ensure that rules and regulations are being met and changes in pest densities are determined over time.

Monitoring

Undertaking monitoring for pests in the region to determine their presence, distribution, and effects, and to measure the extent to which the objectives of the RPMP are being achieved.

Direct control

Funding and undertaking pest control in some circumstances as a service for regional benefit.

Advice and education

Free advice is given to raise awareness of pest problems and to provide land occupiers with the information to control their own pests.

Community initiatives

Guidance and support are provided for community driven initiatives to control pests.

Cost recovery

A full cost recovery operational service is available for pest control.

Biological control

As approved biological control agents become available, HBRC may elect to utilise them. Biocontrol is currently a key tool in the management of rabbits and various pest plant and other harmful species.

Pest Plants

1.1. Exclusion Pest Plants

Objective

Prevent the establishment of exclusion pest plants in the Hawke's Bay region.

Targets

Conduct searches in areas vulnerable to infestation, follow up on reported sightings and raise public awareness of exclusion pests. Develop partnerships with other organisations and community groups that have expertise or an interest in protecting the environment.

Eradication of exclusion species will be attempted by HBRC in conjunction with relevant Crown agencies and stakeholders where practicable.

Council will provide training to relevant council staff and stakeholders about the identification of the exclusion pests to assist in early detection. Council will provide advice, attend events, and undertake publicity campaigns to increase public awareness of exclusion pests.

Exclusion	Management Regime
Alligator weed	Develop partnerships and distribute information to interested and relevant parties to extend the area monitored for the presence of these pest plants. Investigate possible pathways for these pest plants to move into Hawke's Bay. Respond to reports of these pests, using powers under the Biosecurity Act if required. Alligator weed has been found in Hawke's Bay and a delimiting/eradication program has begun. A Management Plan has been formulated with detailed costings for this. Senegal tea has also been found in Hawke's Bay and a delimiting/eradication program has begun. A Management Plan is being drafted with detailed costings.
Marshwort	
Noogoora bur	
Senegal tea	
Spartina	

1.2. Eradication Pest Plants

Objective

Destroy all known infestations of these species within the Hawke's Bay region, prior to seed set.

Targets

Undertake direct control through service delivery at all known sites. Assessment of existing infestation points to decide whether any surveys are required. Inspection and delimit regime to be carried out at all known sites.

Control work will be undertaken annually by council staff, contractors, partners and/or stakeholders and data will be recorded in Clover.

Eradication	Management Regime
African feather grass	

Cathedral bells	HBRC will destroy all infestations prior to seed set.
Goats rue	
Purple loosestrife	
Spiny emex	
White edged nightshade	
Yellow water lily	
Phragmites	In accordance with the contract between HBRC and Ministry of Primary Industries, HBRC will destroy all infestations prior to seed set.

1.3. Progressive Containment Pest Plants

Objective

Progressively contain and reduce the geographic distribution of the pest plant either across the region or specified areas within the region.

Targets

Through a combination of direct control (service delivery) and occupier responsibility (monitoring and compliance) all known infestations will be controlled prior to seed set where practical.

Council staff will control populations within the containment area through a variety of control methods, including but not limited to spraying. The long-term goal for many of these pests is eradication but is not feasible within the short to medium term.

Council staff will also support communities to reduce the impact of progressive containment pests through regulatory and non-regulatory biosecurity programmes.

Progressive containment	Management Regime
Apple of Sodom	Occupiers are responsible for the control of Apple of Sodom, Australian sedge, Cotton thistle, Darwin's barberry, Japanese honeysuckle, Saffron thistle, Velvetleaf and Woolly nightshade on their land and may qualify for a subsidy under the incentive scheme. HBRC will at its discretion control some known infestations prior to seed set where it is practical to do so.
Australian sedge	
Cotton thistle	
Darwin's barberry	
Japanese honeysuckle	
Saffron thistle	
Velvetleaf	
Woolly nightshade	

Progressive containment	Management Regime
Nassella tussock	Occupiers are responsible for controlling Nassella tussock on their land and may qualify for a subsidy under the incentive scheme. HBRC will at its discretion control known infestations before the seeds set.
Old man's beard	As stated in the RPMP, Old Man's Beard (OMB) is not as widespread North of SH5 as it is South of this area, therefore it is beneficial to require occupiers to continue to control old man's beard north of SH5. Occupiers North of SH5 are responsible for controlling old man's beard on their land and may qualify for a subsidy under the incentive scheme. HBRC will at its discretion control some known infestations prior to seed set where it is practical to do so. There is also a progressive containment programme along the Ruahine and Kaweka ranges, to prevent the establishment of old man's beard in the ranges. HBRC, upon forming an agreed work programme with the Department of Conservation, will control all old man's beard within a 500-metre buffer zone along the edge of the Ruahine and Kaweka ranges (as per map in RPMP 2018-38). South of SH5 and outside of the 500-metre buffer zone along the edge of the Ruahine and Kaweka ranges, Council will still encourage the control of OMB but will not enforce compliance. Land users below SH5 will still be eligible for the incentive scheme for the control of OMB. HBRC will at its discretion control some known infestations before seeds reach maturity where it is practical to do so.
Wilding Conifers	Occupiers are responsible for controlling Pinus contorta on their land and may qualify for a subsidy under the incentive scheme. HBRC will at its discretion control some known infestations where it is practical to do so. Occupiers are responsible for controlling Scots pine, mountain pine and dwarf mountain pine on their land in the designated containment area and may qualify for a subsidy under the incentive scheme. HBRC will at its discretion control some known infestations where it is practical to do so. HBRC will collaborate with other stakeholders to ensure the milestones it is responsible for within the Kaimanawa and Rangitaiki Management Units are completed, and MPI are supplied with all the necessary data required.

1.4. Sustained Control Pest Plants

Objective

To provide for ongoing control of the subject, or an organism being spread by the subject, to reduce its impacts on values and spread to other properties.

Targets

Several pests are well established in Hawke's Bay, many of which have been subject to various control aspirations over time. The primary objective is to prevent or minimise the spread of these pests between neighbouring properties.

Sustained Control	Management Regime

Bathurst bur	HBRC, upon receiving a written complaint, will ensure the occupier destroys all Bathurst bur within 5 metres of the property boundary that is adjacent to the adjoining occupier complainant's boundary where the adjoining occupier is also destroying, or the land is clear of, all Bathurst bur.
Blackberry	HBRC, upon receiving a written complaint, will ensure the occupier destroys all Blackberry within 10 metres of the property boundary that is adjacent to the adjoining occupier complainant's boundary where the adjoining occupier is also destroying, or the land is clear of, all Blackberry.
Chilean needle grass	Occupiers are responsible for controlling Chilean Needle grass on their land and may qualify for a subsidy under the incentive scheme. Chilean needle grass was identified in dry summer areas of Hawke's Bay - west of Napier, and at Bay View, Puketapu, Havelock North, Maraekakaho, Poukawa, Tukituki flood plain, Otane, Patangata, Waipawa, Waipukarau, Wakarara, Omakere, Onga Onga and Porangahau (approx. 800 ha in total). There are infestations on river berm land and roadsides. Biosecurity staff will arrange to control Chilean needle grass on public land. On private land, occupiers are required to meet the rules outlined in the RPMP and control Chilean needle grass in accordance with their agreed management programmes. HBRC will at its discretion control some known infestations before the seed set where it is practical to do so. HBRC will work with Marlborough District Council and Environment Canterbury in raising awareness of CNG within New Zealand.
Gorse	HBRC, upon receiving a written complaint, will ensure the occupier destroys all Gorse within 10 metres of the property boundary that is adjacent to the adjoining occupier complainant's boundary where the adjoining occupier is also destroying, or the land is clear of, all Gorse.
Nodding thistle	HBRC, upon receiving a written complaint, will ensure the occupier destroys all Nodding thistle within 20 metres of the property boundary that is adjacent to the adjoining occupier complainant's boundary where the adjoining occupier is also destroying, or the land is clear of, all Nodding thistle.
Privet (Chinese and Tree)	Upon receipt by Council of a doctor's certificate/positive blood test clearly showing a person to be suffering a Privet allergy, Council will, within the urban area (50km speed zone or less), destroy any isolated Chinese and Tree privet plants within 50m of the residence or place of work of that person. If, upon inspection by Council, large numbers of plants exist, including as hedges, a direction will be served on the occupier to prune to prevent flowering or destroy the plants thoroughly.
Ragwort	HBRC, upon receiving a written complaint, will ensure the occupier destroys all Ragwort within 20 metres of the property boundary that is adjacent to the adjoining occupier complainant's boundary where the adjoining occupier is also destroying, or the land is clear of, all Ragwort. The presence of biological controls will be considered when a complaint is made.
Variegated thistle	HBRC, upon receiving a written complaint, will ensure the occupier destroys all Variegated thistle within 5 metres of the property boundary that is adjacent to the adjoining occupier complainant's boundary where the adjoining occupier is also destroying, or the land is clear of, all Variegated thistle.
Yellow bristle grass	HBRC will collaborate with roading authorities to manage likely vector pathways of Yellow bristle grass.

1.5. Biodiversity Pest Plants

These are plants that have a negative ecological effect which are managed outside of the RPMP. Plants that presently fall into this category are Boneseed, Climbing Spindleberry, Blue passionflower, Asiatic knotweed, Giant knotweed, Moth plant, Pampas and Purple ragwort.

1.6. Biological Control of Pest Plants

HBRC continues to support research into biological control of pest plants. HBRC's priorities for further research into bio-control agents during the life of the RPMP are Chilean needle grass, Moth plant, Nassella tussock, Old man's beard and Japanese honeysuckle. The region's biological control agents for Ragwort, Nodding thistle, and Gorse are widespread and active. A biological control agent for Californian thistle is steadily becoming established.

Over the duration of this operational plan staff will continue to work effectively to engage Māori landowners and hapu at a local and regional level in the consultation around new biocontrol releases.

1.7. National Pest Plant Accord

The Ministry of Primary Industries manages the National Pest Plant Accord, which has declared 135 plants as unwanted organisms under the Biosecurity Act. HBRC has agreed to be responsible for ensuring that people selling plants are conforming to the requirements of the Act, and not selling or propagating these plants. All pest plants and unwanted organisms are banned from sale and propagation under the Biosecurity Act. All retail outlets that are known to sell plants will be visited at least once every three years, to ensure that they are not selling any pest plant listed in the RPMP or the Pest Plant Accord.

1.8. General Advice and Information

Biosecurity staff will provide advice, attend events and undertake publicity campaigns to increase public awareness of pests. The information is intended to assist occupiers meet their obligations under the RPMP. Biosecurity staff will also assist with the general identification of plants and provide information and education material about poisonous plants.

Staff will inspect plant outlets and markets within the Hawke's Bay region for the sale and/or propagation of RPMP species. Training will be provided to relevant staff and stakeholders in identifying pests to assist in early detection.

HBRC implemented a new website called Pest Hub. It lists many pests, including those listed within the RPMP. It contains information on their impact, best practice control techniques and can report a pest to HBRC staff. It can be found here: https://www.hbrc.govt.nz/environment/pest-control/pest-hub/

Pest Animals

1.9. Exclusion Pest Animals

Objective

Prevent the establishment of exclusion pest animals in the Hawke's Bay region.

Targets

Undertake surveillance of high-risk areas/pathways. Follow up on reported sightings or reports of illegal releases and raise public awareness of exclusion pests. Develop partnerships with other organisations and community groups that have expertise or an interest in protecting the environment.

Eradication of exclusion species will be attempted by HBRC in conjunction with relevant Crown agencies and stakeholders where practicable.

Council will provide training to relevant council staff and stakeholders about identifying the exclusion pests to assist in early detection. Council will provide advice, attend events, and undertake publicity campaigns to increase public awareness of exclusion pests.

Exclusion	Management Regime
Wallaby	Undertake active surveillance of high-risk areas/pathways for these pests. Develop partnerships with interested and relevant parties to extend the area monitored for the presence of these pests. Investigate possible pathways for these pests to move into Hawke's Bay. Respond to reports of this pest, using powers under the Biosecurity Act if required.
Mediterranean fanworm	
Clubbed tunicate	

1.10. Eradication Pest Animals

Objective

Eradicate rooks from the region. Have no active rookeries within 20 years of the commencement of the RPMP. Eradicate all possums contained within Possum Eradication Areas.

Targets

Destroy all active rook nests within the Hawke's Bay region and eradicate possums within those areas identified as Possum Eradication Areas. Inspect pet shops, online sales and wildlife shelters if reports are received of the sale and/or breeding of possums and rooks. Support appropriate research initiatives, including biological control should it become available. Undertake direct control through service delivery.

Eradication	Management Regime
Possum	A Possum Eradication Area is created once written agreements have been entered into with 75% or more of the total proposed land area. The Council will undertake possum eradication work within the entire Possum Eradication Area. Once possum eradication commences, land occupiers within the area shall maintain possum eradication status in accordance with the Hawke's Bay Regional Possum Control Technical Protocol (PN 4969).

Rook	Over the duration of the Plan, all active rook nests will be destroyed within the Hawke's Bay region. Information will be provided to land occupiers on rook identification, the potential adverse effects they cause, whom to contact for rook control, and the risks of inappropriate control.

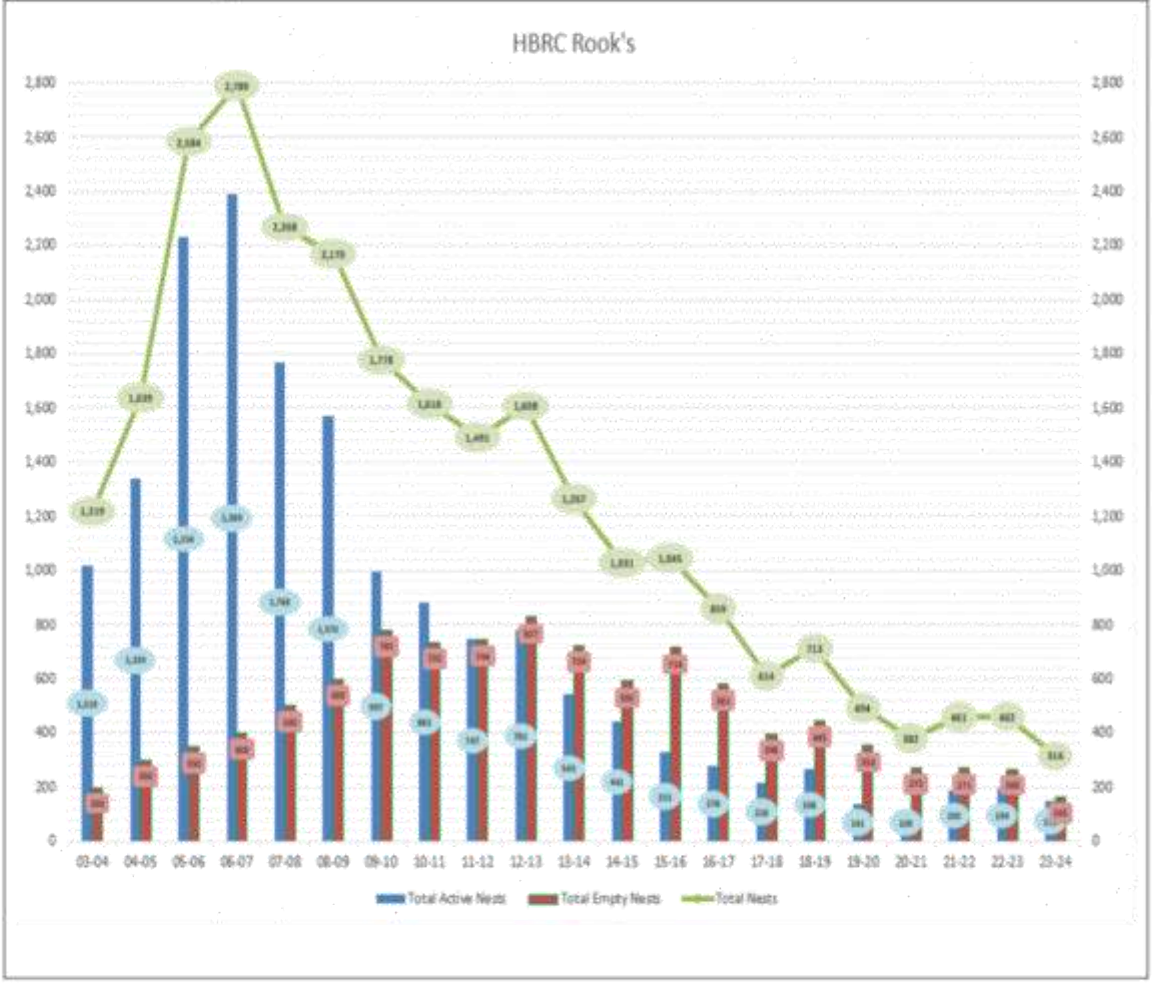

1.11. Sustained Control Pest Animals

Objective

Over the duration of the Plan, sustainably control sustained control pest animals in order to minimise adverse effects on environmental values and economic well-being within the Hawke's Bay region.

Sustained Control	Management Regime
Feral Goat	Sustainably control feral goats on land contained within Feral Goat Coordinated Management Areas to zero density or to levels specified within a Written Management Agreement approved by Hawke's Bay Regional Council.

	A Feral Goat Coordinated Management Area is created once written agreements have been entered into with 75% or more of the total land area. The Council will coordinate initial feral goat control work within the entire Feral Goat Coordinated Management Area. Once feral goats have been reduced to low levels, occupiers within the area are required to maintain feral goats in accordance with this Protocol. 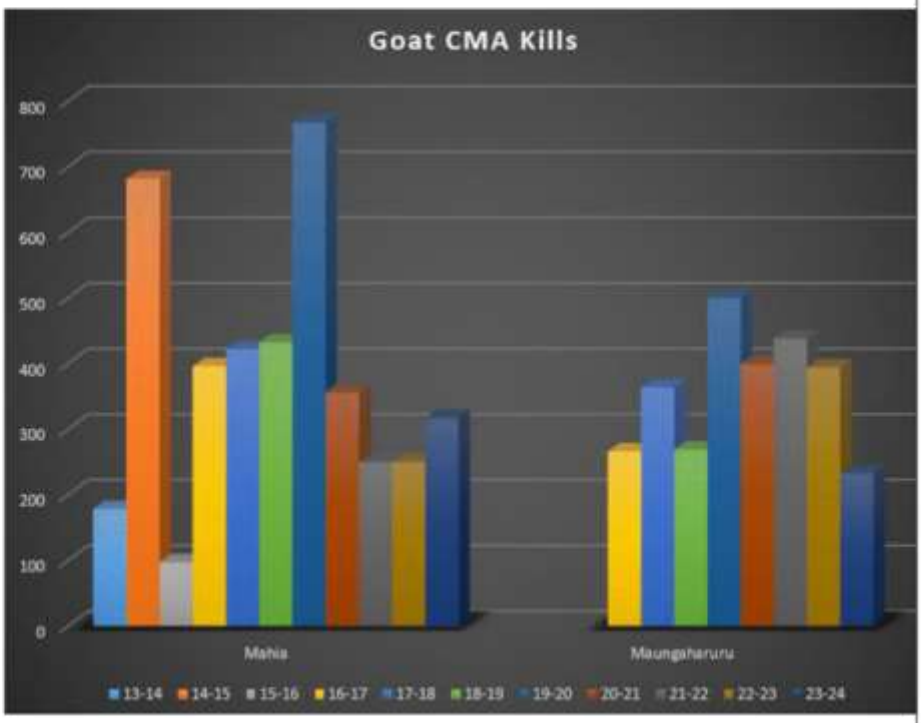
Possum	Sustainably control possums contained within Possum Control Areas to ensure population density on that land is at or below 4% residual trap catch. An occupier within a Possum Control Area shall maintain possum densities on their land at or below 4% residual trap catch, in accordance with the Hawke's Bay Regional Possum Control Technical Protocol (PN 4969). Possum monitoring will be undertaken by council on a sample of properties within the PCA area to assess if properties are meeting the plan rule. Compliance action will be undertaken for properties that fail to meet the plan rule. This includes land where the Good Neighbour Rule applies. HBRC will support land occupiers in managing possum densities through providing best practice advice, a subsidy will be provided on a range of possum control products and financial assistance for managing possums in difficult terrain. Landowners who have a QEII block less than 20 hectares on their property are eligible to receive free possum bait sufficient to control possums within the QEII area. For landowners with QEIIs greater than 20 hectares, or where several small QEIIs are collectively greater than 20 hectares, HBRC arranges and pays for possum control.

Rabbits	Sustainably control rabbits to ensure population levels are maintained below Level 4 on the Modified McLean Scale (2012). The following will be undertaken: • Conduct biannual regional rabbit night counts. (April 2021, April 2023, April 2025) • Conduct targeted biannual surveillance of rabbit prone areas. • Provide advice and education to land occupiers, including occupiers of small blocks, to help them control rabbits by the most efficient and effective means. • Monitor for compliance and where appropriate enforce the rabbit control rule. At its discretion, and as set out in an approved management programme, Council may meet up to 50% of the cost of rabbit control on rateable land where rabbit numbers exceed 4 on the McLean Scale. Council will continue to support research initiatives, including biological control, and release biological control agents for the control of feral rabbits when appropriate.
Rabbit night count locations	


Rabbit Nightcount Locations
HAWKE'S BAY REGIONAL COUNCIL
1:860,000
Nightcounts
Nightcounts
Line 1 Smedley Stn
Line 2 Glendale Stn
Line 3 Opuahi Stn
Line 4 Waipawa River
Line 5 Otrig Stn
Line 6 Woodstock Stn
Line 7 Pakaututa Farms
Line 8 McGregors
Line 9 Kaweka Farms
Line 10 Te Aue Stn
Line 11 Summerlee Stn
Line 12 Thorn Flat
Line 13 Cleeleen Stn
Line 15 Makahu Stn
Line 16 Northlands Stn
Line 17 Gwavas Stn
Line 18 Mountain Valley
Line 19 Tarawera Stn
Line 20 Big Hill Stn
Line 21 Ngamatea
Line 22 Woodlands Stn
Line 23 Rangiora Stn
NAPIER
HASTINGS

1.12. Site-led Pest Animals

Objective

Support sustainable control of site-led pests at sites of ecological importance to levels appropriate for the protection of ecological values, recreational values, and economic well-being within the Hawke's Bay region.

Targets

Coordinated and integrated control of pests in defined areas that protect and restore specific ecological or biodiversity values which are threatened or compromised by pests. Sites include:

- Priority Ecosystems (Hawke's Bay Regional Council)
- Recommended Areas for Protection (Department of Conservation)
- Sites of Special Wildlife Interest (Department of Conservation)

Site-led	Management Regime
Feral cats **Feral deer** **Feral goats** **Feral pigs** **Hedgehogs** **Mustelids** **Possums** **Rats**	Support land occupiers and community groups in managing site-led pests at areas of high biodiversity value though technical information, best practice control techniques and provision of traps or ungulate control. An agreement will be signed with the land occupier agreeing to utilise the traps and undertake best practice. HBRC staff will work with other groups to maximise outcomes of council programmes e.g., Erosion Control Scheme, Predator Free Hawke's Bay, Environmental Enhancement projects, Ecological Management and Enhancement Plans.

Phytosanitary Pests

Objective

Sustainably control apple black spot, codling moth, European canker, fireblight and lightbrown apple moth on unmanaged pipfruit production sites to protect economic well-being of the pipfruit industry within the Hawke's Bay region.

Targets

Occupiers of unmanaged pipfruit production sites shall, on receipt of a written direction from an Authorised Person, control:

- Apple black spot (Venturia inaequalis) on their land from the presence of green tips until fruit maturity/harvest; and
- Codling moth (Cydia pomonella) on their land if five (5) or more codling moths are caught in any one codling moth pheromone trap during any calendar week on their land;
- European canker (Neonectria ditissima) by inspecting all pipfruit trees on their land at least four times during the year, applying post-harvest sprays if canker is found and removing and burning all infected pipfruit tree parts showing any presence of European canker; and

- Fireblight (Erwinia amylovora) on their land during the pipfruit bloom period (from pink to petal fall); and
- Lightbrown apple moth (Leafroller) (Epiphyas postvittana) on their land once thirty (30) lightbrown apple moths are caught in any one lightbrown apple moth pheromone trap on their land from 15 December until fruit harvest.

Sustained Control	Management Regime
Phytosanitary pests	Resolving apple black spot, codling moth, European canker, fireblight or lightbrown apple moth control disputes between neighbouring parties will be undertaken by HBFGA in the first instance. If pest monitoring on the affected managed pipfruit production site over a reasonable time confirms that: • there is a clear difference in the management inputs required to control phytosanitary pests compared to the previous three years; and • monitoring results indicated that the phytosanitary pest outbreak is more severe along the boundary with the adjacent unmanaged pipfruit production site. Then HBFGA will advise the occupier of the unmanaged pipfruit production site(s), that they are deemed to be an exacerbator of phytosanitary pests. HBFGA will be entitled to give the occupier of the unmanaged pipfruit production site(s) 14 days to reach an agreement. If agreement cannot be reached and/or control is not undertaken within that time, HBFGA will advise Hawke's Bay Regional Council of the situation and seek a direction to control phytosanitary pests on the unmanaged pipfruit production site. On receiving advice regarding the situation, Hawke's Bay Regional Council will initiate appropriate enforcement procedures under the Biosecurity Act for the control of the phytosanitary pests.

Financial Summary

Council's Long-Term Plan 2021 – 2031 sets out the planned expenditure and required funding, via rates and user charges, for the operational and planning activities associated with pest management

The expenditure budgets as per the 2024-2025 Annual Plan are summarised in the table below:

Biosecurity 24/25 Annual Expenditure	24/25 LTP expenditure budget
Pest Management Strategies	$ 15,855
Pest Plant Incentive Scheme	$ 223,778
Primary production Pest Plants	$ 542,753
Environmental/human health pest plants	$ 928,987
Biological Control	$ 79,929
Rabbit control	$ 63,823
Possum control	$ 1,363,744
Site specific pest animal control	$ 52,424
Rook control	$ 167,769
Possum Bait and Rabbit Subsidy	$ 132,612
Pest Annual General Advice	$ 33,960
Pest Animal Research	$ 55,336
Marine Pests	$ 88,220
Total including Organisational Overheads	$3,749,190

Measuring Performance

The following criteria will be used to measure the success or otherwise in implementing the Operational Plan:

- Completion rate of programmes contained within this Operational Plan;
- Results from trend monitoring undertaken, and an assessment of these results;
- The education initiatives undertaken during the year;
- The number of Notice of Directions issued, the level of compliance with those notices, and any follow-up activity undertaken;
- The outcomes of all service delivery operations undertaken;

- The results of biological control research and monitoring, and the number of bio-control releases undertaken;
- All research initiatives to which contributions have been made during the year; and
- Any cross-boundary issues that arose and how they were resolved.

Implementation Report

A report on the Operational Plan and the success or otherwise of its implementation will be prepared no later than five months after the conclusion of the financial year. A copy of this report will be provided to Council.

Biosecurity Annual Report
1 July 2023 - 30 June 2024

Report on the 2023-24 Operational Plan

August 2024
Hawke's Bay Regional Council Publication No.

HAWKES BAY
REGIONAL COUNCIL
TE KAUNIHERA Ā-ROHE O TE MATAU-A-MĀUI

ISSN 2703-2051 (Online)
ISSN 2703-2043 (Print)

Catchment Operations

Biosecurity Annual Report

August 2024

Hawke's Bay Regional Council Publication No.

Prepared By:
Matt Short - Catchment Management Lead – Biosecurity
Allan Beer - Contracts Manager Pest Animals
Alice McNatty - Senior Biosecurity Advisor
Nathan Alexander - Biodiversity Advisor

Reviewed By:
Mark Mitchell – Principal Advisor Biosecurity/Biodiversity

Approved By:
Iain Maxwell, Group Manager – Integrated Catchment Management

Contents

Executive Summary **4**

1 Introduction **5**

2 Pest Plants **5**

2.1 Exclusion Pest Plants 5
2.2 Eradication Pest Plants 6
2.3 Progressive Containment Pest Plants 7
2.4 Sustained Control Pest Plants 8
2.5 Sustained Control Pest Plants – Boundary Control 9
2.6 Biodiversity Pest Plants 9
2.7 Surveillance Programme 10
2.8 Surveillance of Railway Land 10
2.9 State Highway and District Road Monitoring 10
2.10 Nurseries and Pet Shops 10
2.11 Regulatory 11
2.12 Education and Publicity 11
2.13 Biological Control 11
2.14 Plant Pest Subsidy Scheme 12
2.15 Conclusion 12

3 Pest Animals **12**

3.1 Exclusion Pest Animals 12
3.2 Eradication Pest Animals 13
3.3 Sustained Control Pest Animals 15
3.4 Site-Led Pest Animals 19
3.5 Education and Advice 20
3.6 Research Initiatives 20

4 Partial Plan Review **20**

5 Communications **20**

SEPTEMBER 2024

Executive Summary

Hawke's Bay Regional Council is the management agency responsible for developing and implementing the Hawke's Bay Regional Pest Management Plan 2018-2038 in accordance with the Biosecurity Act 1993.

The RPMP is a combination of eradicating or effectively managing specified pests or groups of pests. It describes the biosecurity activities undertaken throughout Hawke's Bay and outlines the management or eradication of specific organisms. Doing so will:

- minimise the actual or potential adverse or unintended effects associated with these organisms, and,
- maximise the effectiveness of individual actions in managing pests through a regionally coordinated approach.

As the management agency, Council is required to prepare an annual operational plan that outlines how the plan will be implemented. Following the end of each financial year, staff will report to Council on the implementation of the operational plan.

This is the Annual Report for the 2023/2024 year relating to the Operational Plan for the Hawke's Bay Regional Pest Management Plan (RPMP).

1 Introduction

Regional councils have a mandate under Part 2 of the Biosecurity Act 1993 (the Act) to provide regional leadership in activities that prevent, reduce, or eliminate adverse effects from harmful organisms in their region.

The purpose of the Hawke's Bay Regional Pest Management Plan (RPMP) is to provide for the efficient and effective management or eradication of specified harmful organisms in the Hawke's Bay Region. It builds on the 2013 Strategy and previous pest management programmes. The purpose of the Plan is to:

- Minimise the actual or potential adverse or unintended effects associated with those organisms; and
- Maximise the effectiveness of individual actions in managing pests through a regionally coordinated approach.

This Annual Report records progress in implementing the Regional Pest Management Plan via the Operational Plan 2023-2024, covering the council's biosecurity activities from 1 July 2023 to 30 June 2024. The Annual Report of regulatory activities is a statutory requirement under section 100B(2) of the Biosecurity Act 1993 (the Act).

2 Pest Plants

The RPMP lists 33 plant species as pests, divided into five management categories.

The Annual Report provides a brief description of the Council's activities in each of these pest plant categories for the 2023/2024 year.

2.1 Exclusion Pest Plants

These are pest plants that are unknown in the Hawke's Bay region and would likely have significant adverse environmental and/or economic impacts if they were to establish. The objective of this programme is to prevent their establishment.

Exclusion	Staff Days	Management Regime
Alligator weed	107	As a surveillance tool, eDNA samples were taken at a range of waterways across Hawke's Bay. A notification process has also been established, and HBRC will be alerted of any notifiable organisms detected in eDNA samples taken in Hawke's Bay. Through the above eDNA surveillance programme, alligator weed was detected at Lake Whatumā and the Mangatarata stream in Hawke's Bay in 2023. Significant ground control works have been undertaken, as well as targeted surveillance by helicopter over likely sites in the Whatumā area. An aerial spraying operation over the lake itself occurred in March after permission was granted by the Environmental Protection Agency. A management plan for Alligator weed was presented to Council, outlining operations and associated costs.
Marshwort	0	
Noogoora bur	0	
Senegal tea	27.5	
Spartina	0	

		The area infested on and around Lake Whatumā is around 15 ha in total, with isolated patches of Alligator weed being found down the Mangatarata stream (the outlet of the lake). Approximately 10 properties have alligator weed on them on the lake's eastern edge. Although control efforts to date have significantly impacted the alligator weed infestation, continued pressure will need to be applied as it can grow and spread rapidly. Ongoing monitoring and control is undertaken on the lakeside properties and Mangatarata stream. Senegal tea was discovered in Te Awa o Mokotūāraro (Clive River) in May 2024 through a positive EDNA test found in the Wilderlab public database from late 2022. Upon this discovery, the find was escalated, and staff discovered multiple infestations encompassing much of the Clive and a portion of the Karamu stream. It would be estimated that the total infestation occupies an area of less than a hectare but spans a 13km stretch of the respective waterways. As Senegal tea is a perennial plant that dies back in the winter, staff had 3 weeks to delimit the infestation and control what they found on land. A management plan is being drafted for Senegal tea to provide information on costings and staff time.

2.2 Eradication Pest Plants

These are pest plants in the Hawke's Bay region where eradication is possible. The objective is to destroy all known infestations of these species within the Hawke's Bay region before seed set. HBRC undertakes direct control through service delivery at all known sites.

Eradication	Staff days	Management Regime
African feather grass	1	Control work focussed around the Maraekakaho Stream. Localised berm maintenance meant the Ngaruroro sites could not be fully surveyed.
Cathedral bells	1.5	All known rural sites were controlled by contractors or staff. A few sites are now clear. One site at Patoka suffered significant damage and overall vegetation clearance in Cyclone Gabrielle, so it will be examined again in the next financial year.
Goats rue	1	Staff monitored all high-risk roadside areas and known infestation sites in Eskdale. Plants were only found at one roadside area in Central Hawke's Bay and in the Eskdale area.
Purple loosestrife	0.2	There are two sites in Hawke's Bay. All plants were destroyed.
Spiny emex	6	Overall, numbers remain static on the two infested properties, but at the Whakaki site, higher moisture levels across the year led to significant germination and all plants were controlled. Spiny emex has a very long seed life.
White edged nightshade	1.1	Two plants were found and destroyed.

Yellow water lily	0	After 25 years of repeated monitoring after initial control, the yellow water lily was declared eradicated from all formerly infested sites in the 2023/2024 financial year.
Phragmites	18.75	In accordance with the contract between HBRC and Ministry of Primary Industries, HBRC will destroy all infestations before seed set. The majority of this time was spent dealing with multiple small sites around Napier but with some time spent at the known sites in Havelock North and Puketitiri.

2.3 Progressive Containment Pest Plants

These are pest plants in the Hawke's Bay region, where they are too widespread to eradicate. However, there is an opportunity to progressively contain and reduce their geographic distribution either across the region or specified areas within the region. This programme is achieved through a combination of occupier responsibility and direct control by HBRC through service delivery at all known sites.

Progressive containment	Staff days	Management Regime
Apple of Sodom	25	Several farms in the Seafield Road area are the main problem areas. Improvements continue to be made each year. The time spent undertaking surveillance and control has been reduced to approximately three weeks per year. Staff removed and destroyed isolated plants.
Australian sedge	8	It is only found in the Wairoa district. Most work is subsidised through the incentive scheme and undertaken by contractors.
Cotton thistle	1.7	Due to wet conditions, numbers were static, if not lower than the previous year. Staff assisted private landowners in controlling cotton thistle to ensure control was undertaken adequately.
Darwin's barberry	18	There are two infestations, one at Gwavas and one at Puketitiri. Both were surveyed, and control work is ongoing. An extensive surveillance and control programme continued at Puketitiri, using contractors and a more significant proportion of staff time than in previous years.
Japanese honeysuckle	2	This programme applies to the Tutira area, as outlined in the RPMP. Much of this work involved administering contractors and supervising them.
Nassella tussock	3	Although plant numbers are reducing, there is a large seed bank. A site detected thirteen years ago in the Tukituki area continues to be of concern due to the high numbers of plants being found each year.
Old man's beard	54	The main control areas are north of the Napier-Taupo Highway and in areas of high biodiversity value. Areas found adjacent to the Ruahine Ranges were surveyed again and controlled. Extra resources were put into this programme due to the disruption caused by Cyclone Gabrielle last season. A significant programme of aerial works in the Wairoa area was completed this financial year, which is a real positive due to the previous two challenging years.
Saffron thistle	26	Numbers were very low this year owing to a wet autumn and spring. All known sites were controlled.

Progressive containment	Staff days	Management Regime
Velvetleaf	0.5	Known sites were assessed. Machinery hygiene was enforced. No plants were found.
Wilding Conifers	19	Pinus contorta is mainly a problem in areas that are close to conservation land. 13,042 hectares were aerially surveyed and controlled in the Napier/Taihape Rd area, including Owhaoko C7 and the Boyd Bush/Tahuhunui range on Timahanga Station. In the Rangitaiki area 3,749 hectares were surveyed and controlled which included the Te Matai 2 block and various Runanga blocks in the upper Waipunga catchment. Any Pinus contorta/Douglas fir detected were controlled. MPI have continued to help finance control programmes in the Napier/Taihape Rd area and have financed control programmes in the Rangitaiki area. However, this funding is projected to shrink somewhat.
Woolly nightshade	171	New urban sites were found this season, some quite heavily infested. This programme suffered owing to lessened access in the previous year, and as access has been reinstated, this has led to further works. Logged forestry blocks continue to provide significant numbers of seedling and sapling regrowth. One major new site was found at Mahurangi Station in the Wairoa area, and this will need repeated visits over multiple years.

2.4 Sustained Control Pest Plants

These are pest plants that are well established in Hawke's Bay, where preventing or minimising the spread of these pests between neighbouring properties is the primary objective. This includes boundary control pest plants, where a neighbouring occupier may be required to control these pests on their boundary to prevent the spread onto adjacent properties.

Chilean needle grass

Chilean needle grass is a tough weed to control. With the current control tools available, HBRC can only contain it within known areas. However, over the last seven years, an average of 21 new properties per year have been found due to a robust advocacy programme and an increased surveillance programme. This increase in properties has created extra pressure (in Spring/Summer) on staff resources and budgets at an extremely busy time for the Pest Plant team.

HBRC continues running a joint advocacy programme with Environment Canterbury and the Marlborough District Council regarding Chilean needle grass. Subdivision of properties with known Chilean needle grass infestations also increases the number of landowners contacted each year.

Chilean needle grass and river gravel extraction

Chilean needle grass is known to occupy parts of the Tukituki and Waipawa River courses in Central Hawkes Bay. Initially, a gravel extraction ban was enacted in 2020 to minimise the risk of spreading Chilean needle grass through that gravel. In response to Cyclone Gabrielle and to assist the local community in accessing gravel for rural recovery, a Controlled Area Notice was enacted to allow extraction under specific conditions. The administration of this Notice was time-consuming and accounts for a significant portion of the time spent on Chilean needle grass in the 2023/2024 financial year.

Under the terms of the Notice, 24 applications from local landowners were received, 16 of which were approved, and the balance declined due to not meeting the conditions of the Notice. A total of 6,350 cubic metres of gravel was approved for extraction, of which approximately 3,000 cubic metres of this gravel was extracted.

Of the 16 approved applicants, one was issued a Notice of Direction for unauthorised use of the gravel. The notice was served to mitigate the risk of spreading Chilean needle grass from that usage.

Surveillance of the Controlled Area was undertaken during the seeding period post-cyclone. It was deemed that the risk of spreading Chilean needle grass within the Controlled Area was low. As a result, the gravel extraction restrictions were lifted in the area from the Mangaonuku/Waipawa confluence to a point 2 kilometres downstream of Patangata bridge. Gravel extraction restrictions remain in place from the Patangata bridge down to the Tukituki mouth owing to the number of sites in the active channel.

Privet

Contractors and individual staff removed 21 Privet plants. Management programmes for hedges are ongoing. This work slowed down due to budget pressures, requiring individual staff to remove smaller trees where necessary and safe to do so with hand tools.

Yellow bristle grass

Staff worked with NZTA and Wairoa District Council to manage the risk posed by mowing regimes during seeding and the requirement for mower washdowns. High-risk landowners were also contacted.

2.5 Sustained Control Pest Plants – Boundary Control

These are pest plants that may require neighbouring occupiers to control these pest plants on their boundary. They are Bathurst bur, Blackberry, Gorse, Nodding thistle, Ragwort and Variegated thistle. This season, the amount of time spent in this area was minimal, with only 4.5 hours recorded. Complaints were related to Blackberry and Variegated Thistle.

Enforcement is the key management tool for Boundary Control plants. Controls are only enforced if their location contravenes RPMP rules (e.g., gorse within 10 metres of a neighbour's boundary, provided that boundary is clear) and only if there is a complaint.

2.6 Biodiversity Pest Plants

These plants have a negative ecological effect and are managed outside the RPMP.

Climbing Spindleberry

This plant is found in the Central Hawke's Bay area along the banks of the Waipawa and Tukituki Rivers. This season, only the most heavily infested area was controlled by contractors owing to budget pressures. Some of the remaining infested areas are difficult to move through owing to significant gorse, blackberry, and broom infestations. Staff surveyed and controlled the remaining infested areas.

Giant/Asiatic Knotweed

This plant is present in the Tuai township area and at the Waipukurau Transfer Station. A contractor sprayed the Tuai infestation, and the Waipukurau site was not checked this year owing to not having found any plants there in more than five years. It is a very invasive plant that will smother native plants, especially lower-growing species and saplings.

DIDYMO/Aquatic Pest Plants

HBRC, Fish and Game, and DOC took samples from strategic sites on the main Hawke's Bay Rivers and sent them away for DNA analysis to ascertain whether Didymo was present. All samples this year were negative for Didymo. Due to a lack of capacity to manage the student, a decision was made not to employ a summer student to run the advocacy programme.

2.7 Surveillance Programme

An increase in staff time was invested in certain pest plants, such as Woolly nightshade, Chilean needle grass, Alligator weed, and Senegal tea.

During each property inspection, staff record relevant pest plants found on individual farm maps. During monitoring, staff use previously gathered information to assess whether infestations have spread or contracted. During visits, staff take the opportunity to discuss any relevant concerns with the occupier.

Biosecurity officer visits	Properties
Rural visits	1427
High-risk sites/QEII	120
Urban visits	453
Nurseries and pet shop visits	5

2.8 Surveillance of Railway Land

Staff have a good working relationship with Treescape, the contractors responsible for vegetation control along the rail corridor in Hawke's Bay. Staff communicate with the Area Supervisor annually, identifying areas that need control. Treescape then does the work when required. This procedure enables staff to control pest plants along the railway tracks throughout the region in a timely manner.

2.9 State Highway and District Road Monitoring

A good working relationship has been developed between staff and Waka Kotahi (NZ Transport Agency) and the Central Hawke's Bay, Wairoa, and the Hastings District Councils for clearing roadside weeds. When weeds are cleared from roadsides, staff ensure the adjacent property owner clears their side. District Councils and NZTA have cooperated in setting up no-mow zones when Chilean needle grass is seeding in November/ December.

The NZTA provides an additional budget to control pest plants on its roadsides, such as Old man's beard, Japanese honeysuckle, Chilean needle grass, and Pampas. HBRC staff manages this budget, ensuring that these pest plants are controlled at the optimum time.

2.10 Nurseries and Pet Shops

MPI has indicated that nurseries in the Hawke's Bay area should be inspected at least once every three years to ensure that no plants banned for sale under the National Plant Pest Accord are being stocked. Five nurseries were visited this year. Where possible, staff focus efforts on new nurseries or informal plant sale arrangements as a higher priority.

2.11 Regulatory

One Notice of Direction was issued this year. This Notice of Direction related to the Tukituki Controlled Area Notice was complied with and revoked once conditions were met. Subdivision activities are monitored by staff to ensure compliance, which has been reasonable this year. 117.5 hours were spent on machinery inspections this year.

2.12 Education and Publicity

These activities aimed to reach a wider community than can be achieved through farm visits. Biosecurity staff worked with the Environment Education section of the Council and the Communications team. There was only one display this year at the East Coast Farming Expo.

Staff also assisted in a "Weed Swap" event in Napier where the public could swap a weed for a native plant with some success.

The following topics have been printed in the media (local newspapers, newspapers, magazines).

- Chilean needle grass
- Alligator weed
- Senegal tea
- Yellow water lily

Our Communications team also made social media posts on the following topics. Some of these were part of a series on pest plants; the data is at the end of the report.

- Alligator weed
- Moth plant
- Yellow water lily
- Woolly nightshade
- Chilean needle grass
- Caulerpa
- Senegal tea

Pamphlets on Woolly nightshade were distributed in selected urban areas throughout Hastings, Napier, and Wairoa.

Biosecurity staff worked with the Māori partnerships team to facilitate engagement with relevant iwi/hapu on the following pest plants.

- Alligator weed
- Senegal tea

2.13 Biological Control

HBRC contracted Landcare Research to:

- Develop new Biological Control Projects.
- Provide a plant identification service.

Landcare Research is continuing to evaluate/import possible biological controls for Aquatic weeds, Japanese honeysuckle, Woolly nightshade, Chinese privet, Field horsetail, Mothplant, Nassella tussock, Tradescantia, Sydney golden wattle, Chilean flame creeper, Pampas, Darwin's barberry, Wild ginger, Old man's beard, and Banana passionfruit.

Staff monitored the Californian green thistle beetle on behalf of Landcare Research, and the beetles were present at all sites monitored.

2.14 Plant Pest Subsidy Scheme

The scheme was set up to assist landowners in undertaking control programmes.

Type	Number	Amount
Rural	82	$80,572
Urban	0	0

The main pests subsidised were Chilean needle grass, Saffron thistle, Australian sedge, Darwin's barberry, and Old man's beard. Please note that this subsidy only applies to a small number of land occupier responsibility pest plants within the RPMP.

2.15 Conclusion

Most pest plant programme objectives have been achieved. With smaller budgets than in previous years, a greater portion of staff time was spent on physical works where possible, which significantly affected overall time allocations for specific pest plants.

Generally, the number of pest plants continues to decrease except for Chilean needle grass, where new properties/sites are continually being found.

The discovery of Senegal tea is another blow to the region, but it is good that it appears to be confined to the Karamu and Te Awa o Mokotūāraro (Clive River). The team responded well to this incursion, given the limited time they had to do so.

The biosecurity team's first aerial control operation for alligator weed at Lake Whatumā was successful, and the team hopes to improve upon this in subsequent years. This process was time-consuming, but a repeat of this work should be easier to manage from now on.

Surveillance and monitoring carried out this year have continued to target certain pest plants (particularly Chilean needle grass, Saffron thistle, Woolly nightshade, and exclusion pests). Staff continue targeting the areas surrounding known sites, areas of high risk, QEII covenanted sites, dump sites, creeks/drains, and rivers and areas that are presently being controlled for low-incidence plants.

3 Pest Animals

The RPMP lists 25 animal species as pests, divided into five management categories. The Annual Report provides a brief description of the activities the Council undertook in 2023/2024 for each pest category.

3.1 Exclusion Pest Animals

These are pest animals that are not known to be present in the Hawke's Bay region. If they were to establish themselves, they would likely have significant negative environmental and/or economic impacts. The objective of this programme is to prevent their establishment.

Exclusion	Management Regime
Wallaby	No positive wallaby sightings were reported over this period.
Mediterranean fanworm & Clubbed tunicate	When a vessel berths in the Inner Harbour, an Incoming Vessel Form is completed and submitted to HBRC. A risk analysis is undertaken, and if the vessel is deemed high-risk, divers inspect it. The HBRC marine biosecurity surveillance program found no marine pests this financial year. Stakeholder and Partnerships Relationships have been formed with key stakeholders, including Napier City Council, Napier Sailing Club, Port of Napier, Legasea HB, Top of the North Marine Biosecurity Partnership, Top of the South Marine Biosecurity Partnership, NIWA and Biosecurity New Zealand.

3.2 Eradication Pest Animals

These are pest animals in the Hawke's Bay region where eradication is possible. The objective is to eradicate rooks from the region and all possums contained within Possum Eradication Areas.

Eradication	Management Regime
Possum **(within the Whakatipu Mahia area)**	HBRC is in the final stages of removing possums from the 14,600ha Māhia Peninsula as part of the Whakatipu Māhia project. Land occupiers within this area have been signed up for the Possum Eradication Area programme contained within the RPMP. They will be responsible for maintaining possum eradication status in accordance with the Hawke's Bay Regional Possum Control Technical Protocol (PN 4969). The Peninsula has been split into two areas – Phase 1, the southern 5500ha – and Phase 2, the northern 9000ha. The "knockdown" using bait stations has been undertaken across the entire peninsula, and the remaining hotspots (Mahia Scenic Reserve and Grandy Lakes Forest) are being mopped up using targeted trapping in Phase 2. Over the last six months, our contractors have trapped 289 possums within the Mahia Scenic Reserve and Grandy Lakes Forest. In support of this, Andrew Richardson has trapped and poisoned approximately 80 possums from the farmland adjacent to areas that our contractors were trapping. The proof of absence network monitoring (cameras) will be reinstalled in September/October, and possum dog detector surveys will support it.
Rook	All rookeries within the Hawke's Bay Region were aerially treated using an under-slung strop man applying DRC 1339 gel directly into nests. This season, 51 active breeding rookeries were located. A total of 316 nests were treated, and of these, only 151 nests had either chicks or eggs. Post-control inspections on some of these rookeries indicate that previous control has been successful with significantly reduced activity. This year, we received an enquiry regarding rook ground control. However, after some time and effort, it was cancelled due to the infrequent presence of rooks on the feed lines.

Map: Aerial Rook Control 2023-2024

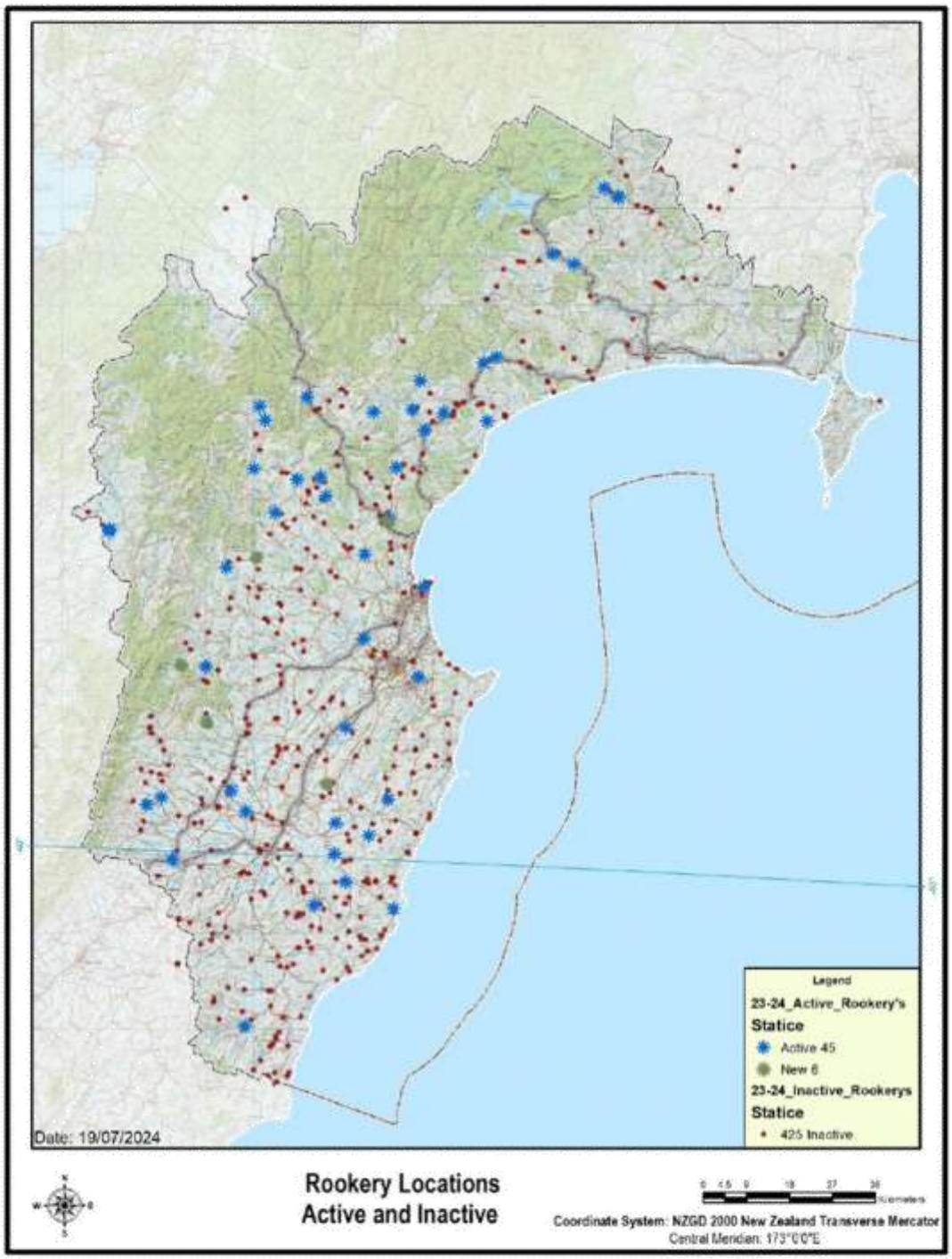

Graph 1: Rook Nests Trends

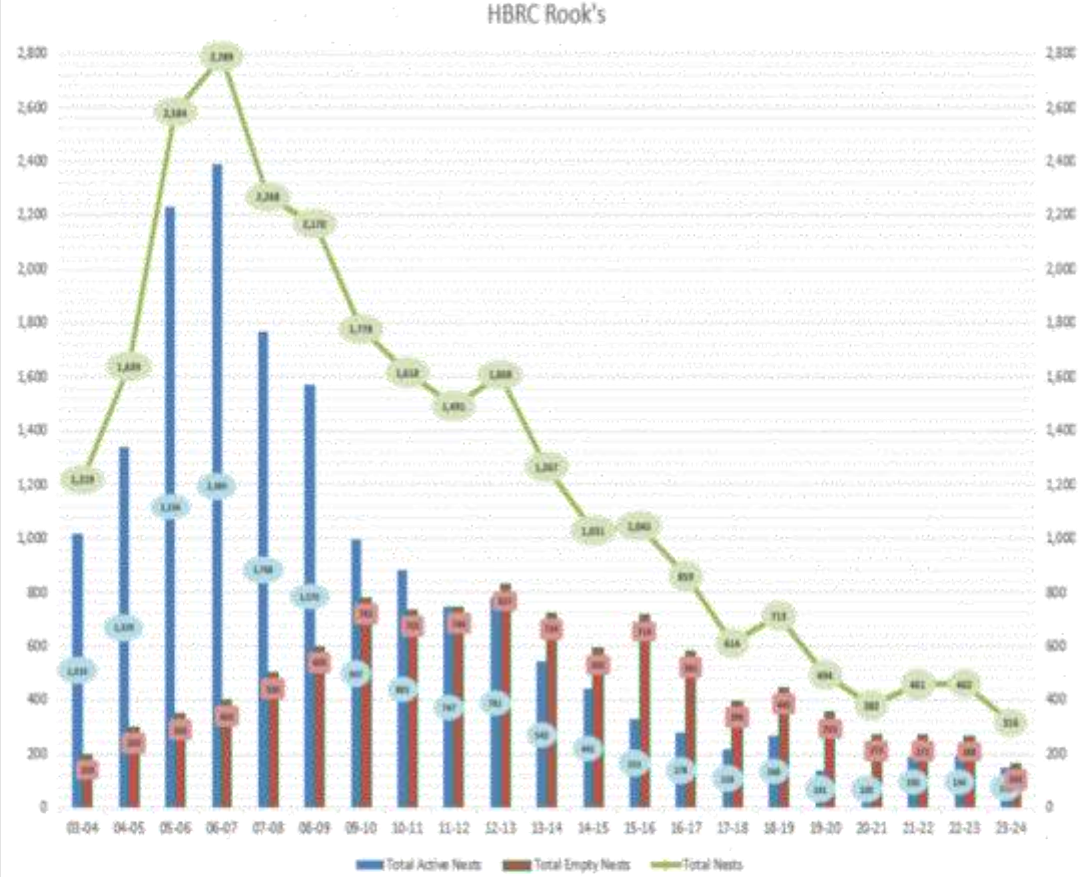

3.3 Sustained Control Pest Animals

These are pest animals that are widespread across the Hawke's Bay region. The objective is to sustainably control these pests to minimise adverse effects on the Hawke's Bay region's environmental values and economic well-being.

Sustained Control	Management Regime
Feral Goat	Feral goat control was undertaken across two feral goat coordinated management areas (CMA), Mahia (7,672 ha) and Maungaharuru (28,000 ha). A total of 550 feral goats were controlled. The Mahia goat CMA is jointly managed by HBRC, the Department of Conservation and supported by Grandy Lake Forests. It is now in the maintenance phase. The project objective is to maintain and enhance the results accomplished to date on the internal

	areas and maintain low populations within the boundary properties. Reinvasion continues to be an ongoing risk with high populations still current on most boundaries. The Maungaharuru goat CMA is jointly funded by HBRC and the Department of Conservation. It is also in the maintenance phase. Like Mahia, reinvasion continues to be an ongoing risk. **Graph 2 Goat CMA Kills** 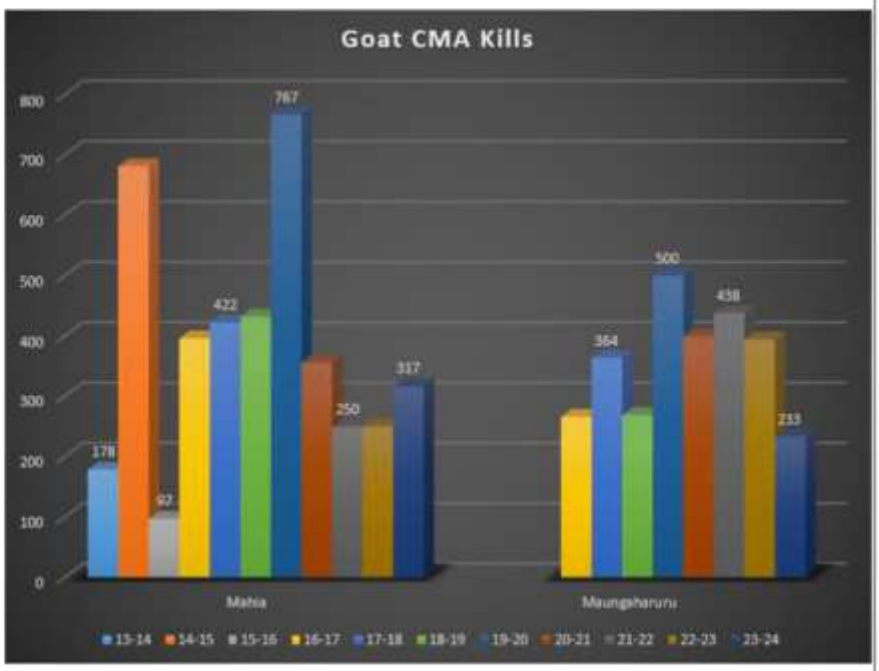
Phytosanitary pests	Occupiers are responsible for managing production pests at pipfruit production sites. Resolving apple black spot, codling moth, European canker, fireblight or light brown apple moth control disputes between neighbouring parties is undertaken by the HBFGA in the first instance. If an agreement cannot be reached, the HBFGA will advise Hawke's Bay Regional Council of the situation and seek appropriate enforcement action to be undertaken under the Biosecurity Act. HBRC has not received any requests to undertake enforcement action against phytosanitary pests.
Possum (rest of region)	Occupiers within a Possum Control Area (PCA) programme must maintain possum densities on their land at or below 4% residual trap catch (RTC). The PCA programme currently covers 774,450ha. Due to the TB outbreak in Hawke's Bay, approximately 103,213ha contained within the PCA programme are now under OSPRI management. Biosecurity staff are working closely with OSPRI, which has moved to a new geographically based operating model with staff based in the region. Possum monitoring was undertaken across 293,056ha (approximately 37% of the PCA area) of the PCA programme to monitor compliance with the RPMP rule.

PCA possum monitoring programme 2023-2024				
Occupiers	Area monitored (Ha)	Number of monitoring lines	Average Residual Trap Catch (RTC %)	Number of monitoring Lines > 4% RTC
638	293,056	2,581	2.1%	513

Although the overall trap catch rate across the area monitored was 2.1%, 513 lines were above 4%, with 15.5% or 99 of the properties monitored failing (638 properties in total monitored). Biosecurity staff are currently working with the Guardians of the Ruakituri Catchment group to resolve recent failed monitoring results in that catchment. Most other failed properties have now engaged an HBRC-approved contractor to undertake possum control, requiring no enforcement action.

HBRC supported land occupiers in managing possum densities by providing best practice advice, a 40% subsidy on a range of possum control products at Farmlands and PGG Wrightsons and financial assistance for managing possums in rugged terrain. Furthermore, 37 QEII covenants received either free possum control (covenants >20ha) or free bait sufficient to control possums within the QEII area (covenants <20ha).

HBRC used a contractor to ensure possum control on all HBRC-managed river berm land. This was done as a good neighbour, to meet HBRC's obligations under the RPMP, and to complement the control being carried out by adjacent landowners in the PCA programme.

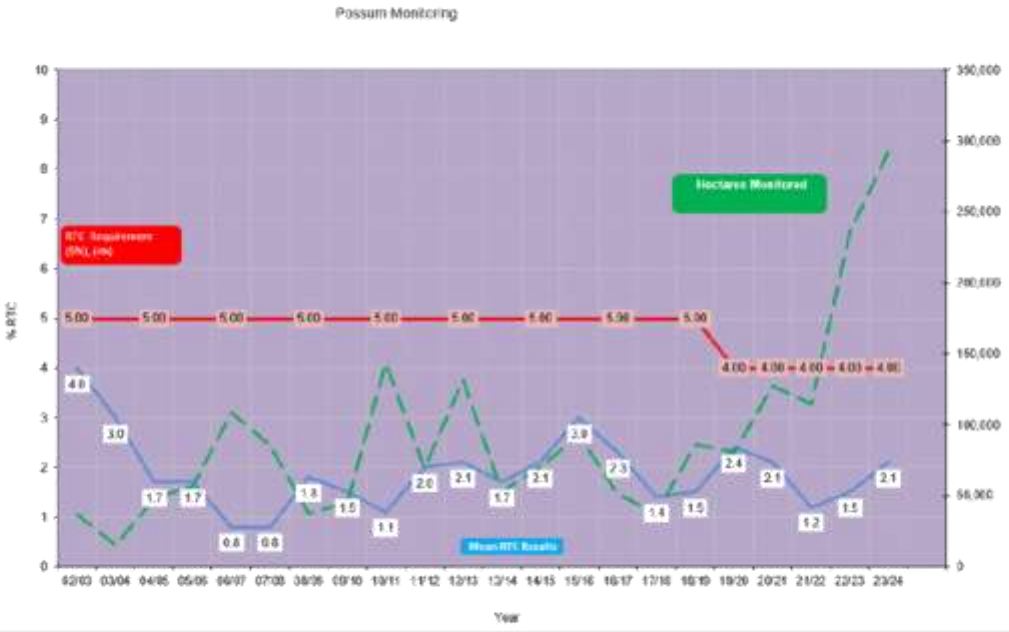

Rabbits	19 rabbit enquiries for advice and assistance were received over the last 12 months. Assistance was provided in the form of Environment Topic handouts, verbal advice, and in some cases demonstrations on the use of Pindone pellets and Magtoxin for rabbit control. **Rabbit night counts** (April 2023, April 2025) Rabbit night counts are now carried out biannually and were last undertaken in April 2023. Due to adverse weather conditions, only 10 of the 23 properties were allowed access. A summary of the data collected shows that rabbits counted per km are down in 2021, from 13.7 rabbits per km to 2.1 rabbits per km in 2023. **Graph 1: Rabbit night counts** 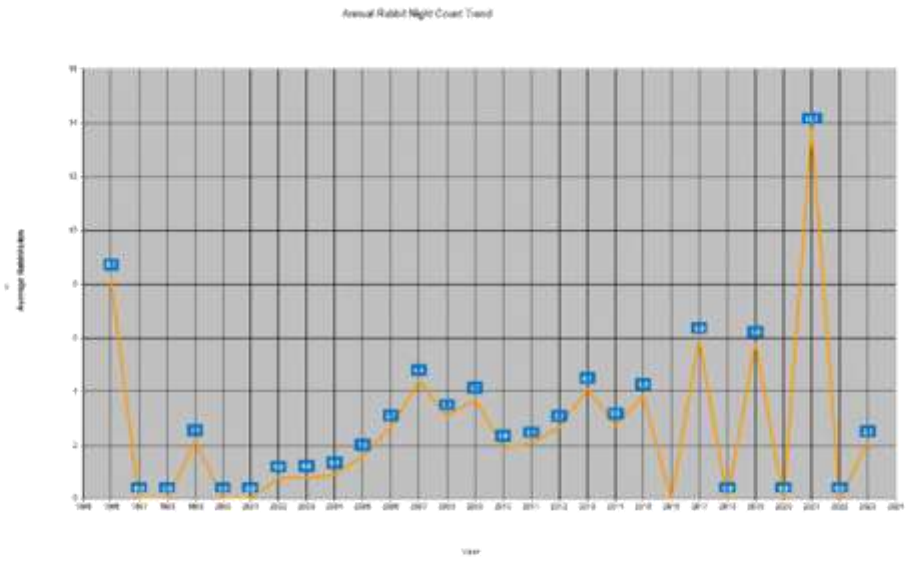

3.4 Site-Led Pest Animals

The objective is to support coordinated and integrated pest control in defined areas that protect and restore specific ecological or biodiversity values that are threatened or compromised by pests.

Site-led	Management Regime
Feral cats **Feral deer** **Feral goats** **Feral pigs** **Hedgehogs** **Mustelids** **Possums** **Rats**	The following table outlines the projects that received assistance through the site-specific programme. These projects form a wide range of initiatives, from working with individual land users to projects with significant local community involvement. The site-specific programme is only implemented at sites of ecological importance.

Project	Location	Target species
Pohue Bush	Te Pohue	Deer and goats
Henry's Bush	Whanawhana	Deer
Motumokai Bush	Porangahau	Deer
Mangatawhiti	Ruakituri	Deer and goats
Waiparere	Waiparere	Mustelids, Rats, Hedgehogs, feral cats, Possums
Puahanui Bush	Tikokino	Deer, mustelids, Rats, Hedgehogs, feral cats, Possums
Wedd Bush	Tikokino	Deer
Gillies Bush	Maraetotara	Deer
Te Aratipi	Maraetotara	Deer
Little Bush	Puketitiri	Mustelids, Rats, Hedgehogs, feral cats, Possums
Pakaututu Bush	Puketitiri	Mustelids, Rats, Hedgehogs, feral cats, Possums
Hutchinsons Reserve	Puketitiri	Mustelids, Rats, Hedgehogs, feral cats, Possums
Birch Hill	Porangahau	Mustelids, Rats, Hedgehogs, feral cats, Possums
Campbell Snelling block	Wairoa	Mustelids, Rats, Hedgehogs, feral cats, Possums

Site-led	Management Regime		
	Aramoana Reserve	Aramoana	Mustelids, Rats, Hedgehogs, feral cats, Possums
	Hinekatorangi Wetlands	Eskdale	Mustelids, Rats, Hedgehogs, feral cats, Possums

3.5 Education and Advice

The Biosecurity team continue to post regular articles in "Our Place", concentrating on rabbits, rooks, PCA updates and the use of maintenance contractors. Alongside pest plants, Pest Animal staff have worked closely with the HBRC Communications Team to implement a new HBRC Pest Hub website, including incorporating factsheets covering all aspects of pest animal control.

3.6 Research Initiatives

No research initiatives were implemented during the 2023-2024 year owing to a lack of funding.

4 Partial Plan Review

A partial plan review of the Regional Pest Management Plan was undertaken in 2022 to amend the PCA programme. The driver behind this partial plan review was community concerns regarding rising possum numbers. The PCA programme was amended to allow for HBRC to take the lead in managing possums within the PCA area through large scale contracts using professional contractors. Additional resources are required to fund the transition from land occupier responsibility to HBRC managed possum control and was going to be requested through the 2024-34 Long Term Plan. Due to the impacts of cyclone Gabrielle, this transition remains on hold until the 2027-37 Long Term Plan.

5 Communications

The 2023 biodiversity and biosecurity communication and engagement plan was designed to raise awareness about the Regional Council's biodiversity work in Hawke's Bay. Our Communications team reviewed this plan monthly and adjusted it as and when required. This included seasonal activities for public awareness and information.

The March edition of Our Environment focused particularly on biodiversity, which was promoted through CHB Mail, Hawke's Bay Today, Wairoa Star, community papers, an e-newsletter, the HBRC website, and social media.

There were a range of other activities promoted, including but not limited to:

- Biodiversity month
- Winter planting
- Chilean needle grass
- Alligator weed
- Senegal tea

Comms were delivered through media releases, radio interviews, social media, web content, and internal comms.

HBRC website: Pest Hub

The HBRC website pest hub is user-friendly for all pest plants and animals under the Regional Pest Management Plan, including marine pests and diseases. It also includes many other pests in New Zealand, including those not currently known to be found in Hawke's Bay.

The site provides the ability to report a pest, including a geo-location. The hub details our regional pests, including descriptions, photos, what harm or damage they may cause, and how they can be controlled. Management programmes and rules relating to each pest are also included, which lets people know if they need to take any steps if found on their property - https://www.hbrc.govt.nz/environment/pest-control/pest-hub/

The tables below show that the usage of all web pages increased from the 2022-2023 Financial Year to the 2023-2024 Financial Year. This is pleasing as it could be inferred that landowners and occupiers are becoming more willing to research pests and solutions to those pests themselves. Specific webpages and their subpages have also been reorganised, and Table 2 depicts some of this reorganisation.

Table 1: Web page Statistics 2022/2023

Web Page	Visits: 01 July 2022 to 30 June 2023
Pest Hub	2582
Pest Control	315
Plant Pests	297
Biosecurity	95
Chilean needle grass	16
Animal Pests	137
Marine Pests	82

Table 2: Webpage Statistics 2023/2024

Web Page	Visits: 01 July 2023 to 30 June 2024
Pest Hub	4475
Pest Control	709
Pest Plants	637
Regional Pest Management Plan	512
Animal Pests	393
Biosecurity	302
Pests On My Farm	272
Tukituki River Controlled Area Notice (now expired)	509
Predator Free Hawkes Bay	250
Marine Pests	249
Pest Hub Enquiry/Reporting Forms	194
Check Clean Dry	107
Chilean needle grass	31

Facebook: Pest Plant series, 5 Feb – 11 March 2024.

Facebook posts: 5 **Reach:** 51,826 **Impressions:** 54,554 **Interactions:** 359 **Link clicks:** 128
(All totals with definitions are in this spreadsheet Campaign Results Summary - wip.xlsx)

Comments:

- Four of five posts in this mini-series reached numbers 'higher than typical' for our Facebook posts.
- We received much positive engagement in our comments section, which is often sparse. This not only drives more interactions from new users to our page but also encourages other positive comments.
- Subsequently, the increased engagement and reach meant the content was spread further, and reach numbers continued to grow as Facebook continued to distribute the well-performing content further.
- The imagery and content served for these posts were fresh and attractive organic content.
- Language in captions was casually and easily digestible, which is attractive to readers for lighter content.

Top post: 23 February 2024 - Puahanui Bush

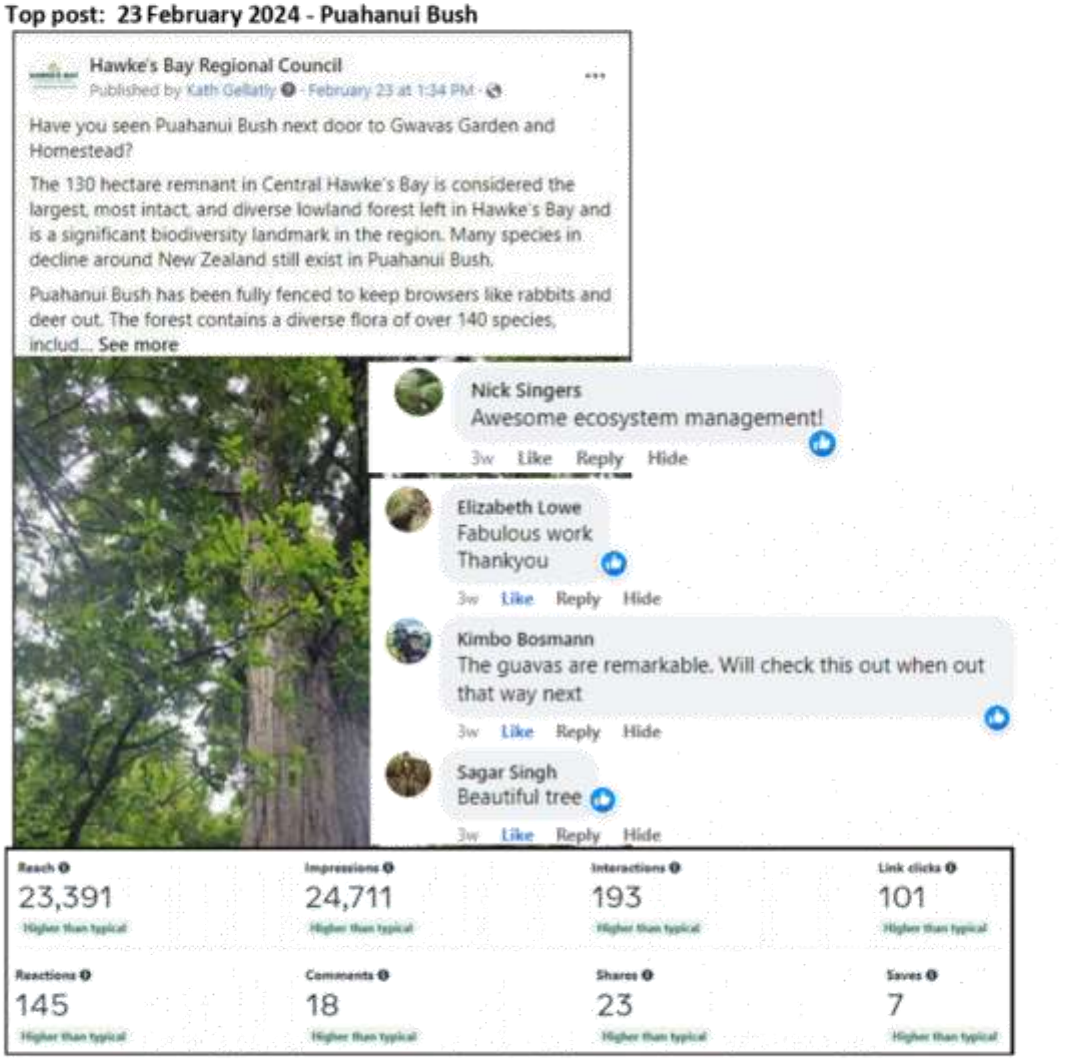

11 March 24 - Alligator Weed

Reach	Impressions	Interactions	Link clicks
12,076	12,645	123	12
Higher than typical	Higher than typical	Higher than typical	Typical

Plays	Average minutes viewed	Minutes viewed
--	0:10	1,852
	Typical	Typical

Interactions

Reactions	Comments	Shares	Saves
73	31	16	3
Higher than typical	Higher than typical	Higher than typical	Higher than typical

29 January 24 – Yellow Water Lily

Reach	Impressions	Interactions	Link clicks
8,637	8,697	114	13
Higher than typical	Higher than typical	Higher than typical	Typical

Reactions	Comments	Shares	Saves
104	7	3	0
Higher than typical	Typical	Typical	Typical

6 February 24 - Woolly Nightshade

Reach	Impressions	Interactions	Link clicks
4,694	5,192	28	2
Higher than typical	Typical	Typical	Lower than typical

Reactions	Comments	Shares	Saves
18	4	5	1
Typical	Typical	Typical	Typical

16 February 24 – Caulerpa

Reach	Impressions	Interactions	Link clicks
3,028 Typical	3,309 Typical	15 Typical	--

Reactions	Comments	Shares	Saves
9 Typical	2 Typical	4 Typical	0 Typical

Improving understanding and management of erosion with LiDAR

Prepared for: Hawke's Bay Regional Council June 2024

Hawkes Bay Regional Council Publication No. 5659

HAWKES BAY REGIONAL COUNCIL

TE KAUNIHERA Ā-ROHE O TE MATAU-A-MĀUI

ISSN 2703-2051 (Online)
ISSN 2703-2043 (Print)

HAWKES BAY REGIONAL COUNCIL
TE KAUNIHERA Ā-ROHE O TE MATAU-A-MĀUI

(06) 835 9200
0800 108 838
Private Bag 6006 Napier 4142
159 Dalton Street . Napier 4110

Environmental Science

Improving understanding and management of erosion with LiDAR

Prepared for: Hawke's Bay Regional Council June 2024

Hawkes Bay Regional Council Publication No. Report number S659

Reviewed By:
Dr Ashton Eaves – Senior Land Scientist

Approved By:
Sam French – Science Manager

ISSN 2703-2051 (Online)
ISSN 2703-2043 (Print)

Manaaki Whenua
Landcare Research

Improving understanding and management of erosion with LiDAR

Prepared for: Hawke's Bay Regional Council

May 2024

Improving understanding and management of erosion with LiDAR

Contract Report: LC4466

Hugh Smith, Andrew Neverman, Harley Betts, Alex Herzig

Manaaki Whenua – Landcare Research

Reviewed by:	*Approved for release by:*
Simon Vale	Sam Carrick
Researcher - Geomorphology	Portfolio Leader – Characterising Land Resources
Manaaki Whenua – Landcare Research	Manaaki Whenua – Landcare Research

Contents

Summary v
1 Introduction 1
1.1 Objectives 1
2 Background 1
2.1 Regional shallow landslide susceptibility model 1
2.2 Regional SedNetNZ model 3
3 Methods 5
3.1 LiDAR pre-processing for erosion modelling 5
3.2 Digital stream network 7
3.3 Data collection for model parameterisation 9
3.4 Upgraded regional shallow landslide susceptibility model 13
3.5 Upgraded regional SedNetNZ model 15
4 Results 24
4.1 Regional shallow landslide susceptibility 24
4.2 Regional SedNetNZ erosion and sediment load model 28
5 Conclusions 38
6 Acknowledgements 39
7 References 39

Appendix 1 45
Appendix 2 46

Summary

Project and client

- Hawke's Bay Regional Council (HBRC) in collaboration with Manaaki Whenua – Landcare Research (MWLR) identified the opportunity to use the 2020–2021 regional LiDAR coverage to improve understanding and management of erosion in the Hawke's Bay region.
- The scope of work involved upgrading the existing shallow landslide susceptibility and SedNetNZ models for the region to use higher resolution LiDAR-derived topographic data alongside the targeted acquisition of new data for improved model parameterisation.

Objectives

- The project had the following objectives.
  - Upgrade the model of rainfall-induced shallow landslide susceptibility previously applied in Hawke's Bay.
  - Improve the spatial representation of the digital stream network as part of the SedNetNZ model development.
  - Upgrade the regional SedNetNZ erosion and sediment load model.

Methods

- The LiDAR-based upgrade to the existing regional shallow landslide susceptibility model involved: a) assembling an inventory of landslides located in areas with LiDAR coverage; b) re-applying the binary logistic regression (BLR) model and evaluating model performance; c) predicting landslide susceptibility at 5 m resolution across the region.
- Predictive performance of the BLR model was assessed using cross-validation. Model classification (i.e. landslide versus non-landslide points) was evaluated using receiver operating characteristic curves (ROC) and calculating the area under curve (AUC) based on 100 model iterations.
- The digital stream network was generated from a sink-filled 5 m digital elevation model (DEM) derived from the regional LiDAR coverage using a flow direction and accumulation algorithm and a 10-ha channel initiation threshold. The digital network underwent both automated and manual refinement.
- Development of the SedNetNZ model to use LiDAR-derived DEMs focused on the shallow landslide, surface, and riverbank erosion sub-models, as well as the representation of sediment entering floodplain storage.
- The new LiDAR-based version of SedNetNZ now integrates high-resolution landslide susceptibility with the shallow landslide erosion sub-model. The surface erosion sub-model is now based on a full implementation of the Revised Universal Soil Loss Equation (RUSLE) using LiDAR-derived topographic inputs.
- The previous riverbank erosion sub-model has been replaced with a data-driven approach that draws on expanded data sets of channel planform change (this

increased from 77 to over 800 km of mapped channels) and bank height for model parameterisation.

- The extent of floodplain alongside channels where flows may go overbank and deposit sediment is now determined from the LiDAR-based 5 m DEM. This replaces the previous representation of floodplains based on New Zealand Land Resource Inventory (NZLRI) mapping at 1:63,360 scale.

Results

- The upgrade to the shallow landslide susceptibility model has improved predictive performance based on LiDAR-derived topographic inputs and an expanded landslide inventory. The LiDAR DEM–based model achieved a median AUC of 0.91 in cross-validation compared to an AUC of 0.75 for the pre-LiDAR model that used the national 15 m DEM and a smaller inventory (56,000 vs 116,000 mapped landslides).
- Region-wide predictions of shallow landslide susceptibility were produced as raster layers with probability- and class-based scales for contemporary land cover and for land cover where all mapped forestry land was converted to grass cover. This forestry-to-grass conversion provided a common reference condition for comparing the inherent susceptibility of forestry and pastoral land.
- The new LiDAR-based SedNetNZ model estimated a total region-wide suspended sediment load delivered to the coast of 8.0 Mt yr^{-1}, which compared to 7.2 Mt yr^{-1} using the previous model.
- The shallow landslide, surface, and riverbank erosion loads increased when estimated using the LiDAR-version of the model compared to the previous model. However, the percentage contributions from the erosion processes are similar between model versions with shallow landslide erosion (64%) contributing the largest proportion on average in the upgraded model, followed by surface erosion (19%) and then by riverbank erosion (12%).
- Mean annual suspended sediment loads predicted using the LiDAR-based version of SedNetNZ showed improved agreement compared to the previous model with estimates of mean annual loads from stream gauging sites in the region.

Conclusions

- The benefits of using higher resolution LiDAR-derived DEMs in erosion and sediment load modelling include: a) improved model parameterisation and predictive performance due to the more accurate representation of topography (e.g. slope angle, curvature); b) better representation of the stream network (e.g. channel sinuosity, channel slope, bank height); c) the ability to provide higher resolution raster layers for selected erosion processes.
- The regional shallow landslide susceptibility layers provide land managers with higher resolution, data-driven spatial information that may be used to better target tree planting to those areas of pastoral land most susceptible to slope instability.
- The upgraded SedNetNZ model provides both improved predictions of contributions from erosion processes to suspended sediment loads as well as high resolution raster layers for shallow landslide and surface erosion not previously available; these may be used to better support land and water planning in the region.

1 Introduction

Hawke's Bay Regional Council (HBRC) in collaboration with Manaaki Whenua – Landcare Research (MWLR) identified the opportunity to use existing regional LiDAR coverage to improve understanding and management of erosion in the Hawke's Bay region. This project builds on work previously completed for HBRC by MWLR to quantify spatial patterns in: a) susceptibility to rainfall-induced shallow landslides using statistical modelling; b) erosion and suspended sediment loads using the SedNetNZ model for the region.

The present report outlines the work undertaken to improve these models using the 2020–2021 regional LiDAR coverage. The scope of work agreed with HBRC involved using the regional LiDAR to upgrade the models to use the higher resolution LiDAR-derived topographic data alongside the targeted acquisition of new data for improved model parameterisation.

1.1 Objectives

The project had the following objectives.

- Upgrade the model of shallow landslide susceptibility previously applied in Hawke's Bay.
- Improve the spatial representation of the digital stream network as part of the SedNetNZ model development.
- Upgrade the regional SedNetNZ erosion and sediment load model.

2 Background

2.1 Regional shallow landslide susceptibility model

The HBRC previously commissioned work to produce a regional rainfall-induced shallow landslide susceptibility layer (Smith 2020). This statistical landslide susceptibility modelling used data from over 27,000 landslide scars (source areas) mapped in southern Hawke's Bay following the April 2011 storm event; these data were augmented by landslide mapping data collected elsewhere for the Smarter Targeting Erosion Control (STEC) MBIE research programme (2018–2023).

Smith (2020) used logistic regression and random forest (RF) models to classify landslide and non-landslide points based on a database comprising over 56,000 scars. The models draw on national spatial data sets for elevation (i.e. a 15 m digital elevation model [DEM]), land cover (NZ Land Cover Database [LCDB]), rock type (NZ Land Resources Inventory [NZLRI]) and morphometric variables (e.g. slope, aspect etc) derived from the DEM. Cross-validation was used to evaluate model predictive performance and assessed using the receiver operating characteristic (ROC) curves and calculation of the area under curve

(AUC). The logistic regression model was found to outperform the RF model when trained and tested with data from independent study areas (Smith 2020; Smith et al. 2021).

A combination of topographic and land cover inputs was selected for the previous region-wide modelling of shallow landslide susceptibility at 15 m resolution (Figure 1). This balanced model performance (mean AUC = 0.75) with the extent of regional coverage (92% complete). Rock type was not included due to the lack of landslide data for the full range of rock types present in the region. Inclusion of rock type achieved only minor improvement in predictive performance (AUC = 0.76) but led to a large reduction in regional coverage (63% complete). Shallow landslide susceptibility layers were produced for the region using spatial probability and class-based scales (Figure 2).

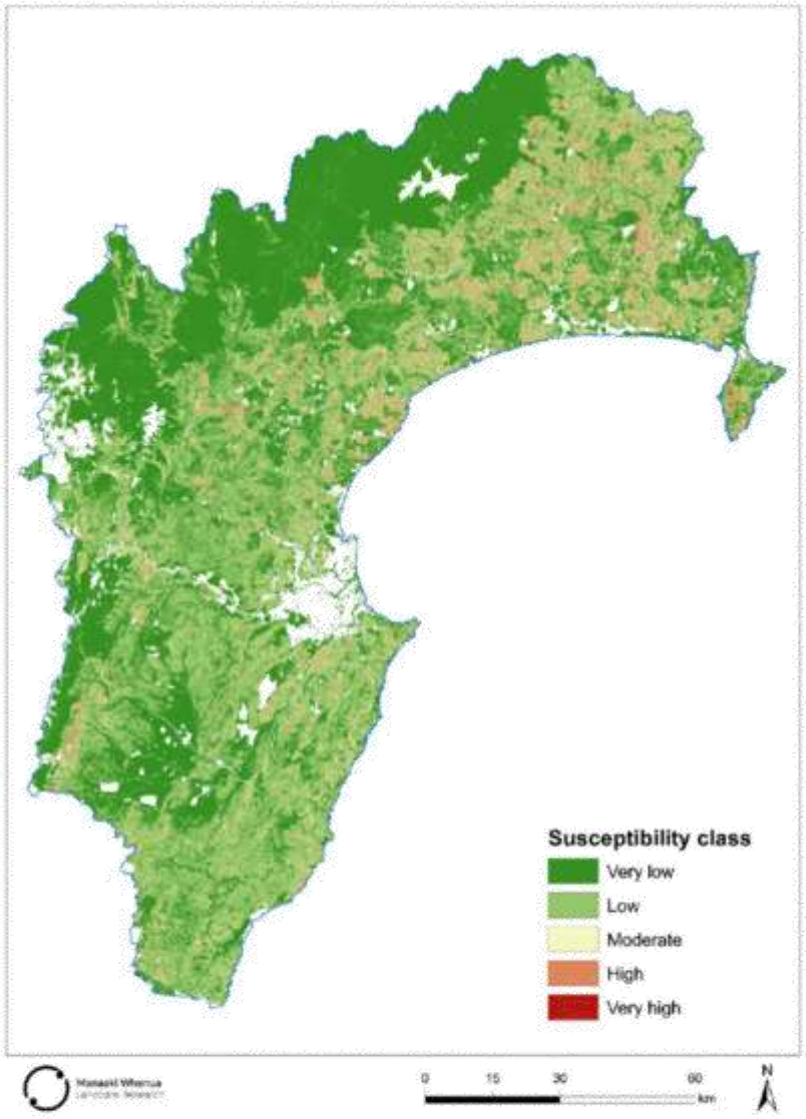

Figure 1. Previous rainfall-induced shallow landslide susceptibility layer for the Hawke's Bay region based on the 15 m national digital elevation model (DEM) (Source: Reproduced from Smith 2020, Fig. 3.)

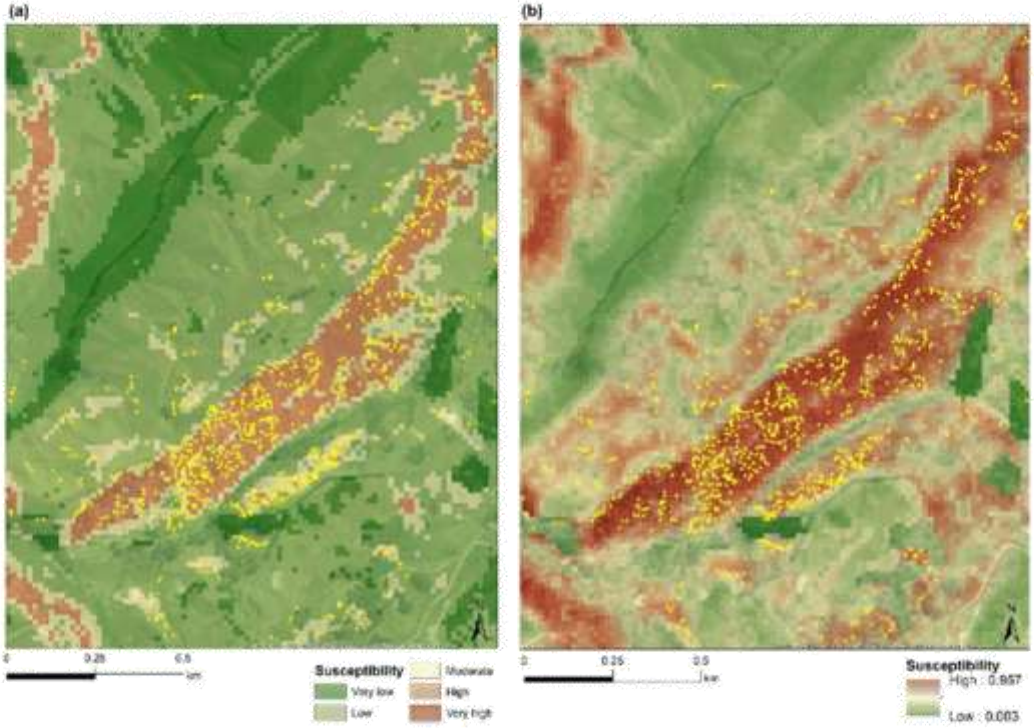

Figure 2. Comparison of an area in southern Hawke's Bay affected by the April 2011 storm event: (a) class-based susceptibility scale; (b) probability-based susceptibility scale. The yellow points represent the location of mapped landslide scars. (Source: Reproduced from Smith 2020, Fig. 5)

The upgrade to the existing shallow landslide susceptibility layer involves an increase in resolution (from 15 m to 5 m pixels) based on the regional LiDAR-derived DEM. We also draw on an expanded landslide database compiled from mapping completed within the STEC programme combined with mapping commissioned by HBRC from the March 2022 storm events that affected northern Hawke's Bay (Betts et al. 2023).

2.2 Regional SedNetNZ model

SedNetNZ is a sediment budget model that represents the range of erosion processes that occur in New Zealand and their contribution to suspended sediment loads. SedNetNZ includes surface (sheet/rill), shallow landslide, earthflow, gully, and riverbank erosion processes (Dymond et al. 2016; Betts et al. 2017; Smith et al. 2019a). In the non-LiDAR based version of SedNetNZ, hillslope erosion processes are computed on a 15 m grid while bank erosion is estimated for each segment of the digital stream network developed for the River Environment Classification v2 (REC2). The sediment loads from these processes are combined and routed through the digital stream network while accounting for losses due to floodplain deposition and trapping in lakes to estimate the mean annual suspended sediment load for each REC2 subwatershed across a region.

Previous SedNetNZ modelling was commissioned by HBRC in three parts. These focused on 1) the Tukituki catchment (Palmer et al. 2017); 2) Tūtaekurī, Ahuriri, Ngaruroro, and Karamu catchments (together referred to as TANK), together with the South Coast and Pōrangahau catchments (Palmer et al. 2016); and 3) the catchments in northern Hawke's Bay (Spiekermann et al. 2017). Subsequently, HBRC commissioned MWLR to update the bank erosion component of SedNetNZ (Smith et al. 2020). This work also compiled the separate catchment level SedNetNZ model outputs into a single regional shapefile that was supplied to HBRC (Figure 3). The version of the SedNetNZ model previously applied in Hawke's Bay did not account for lake sediment trapping.

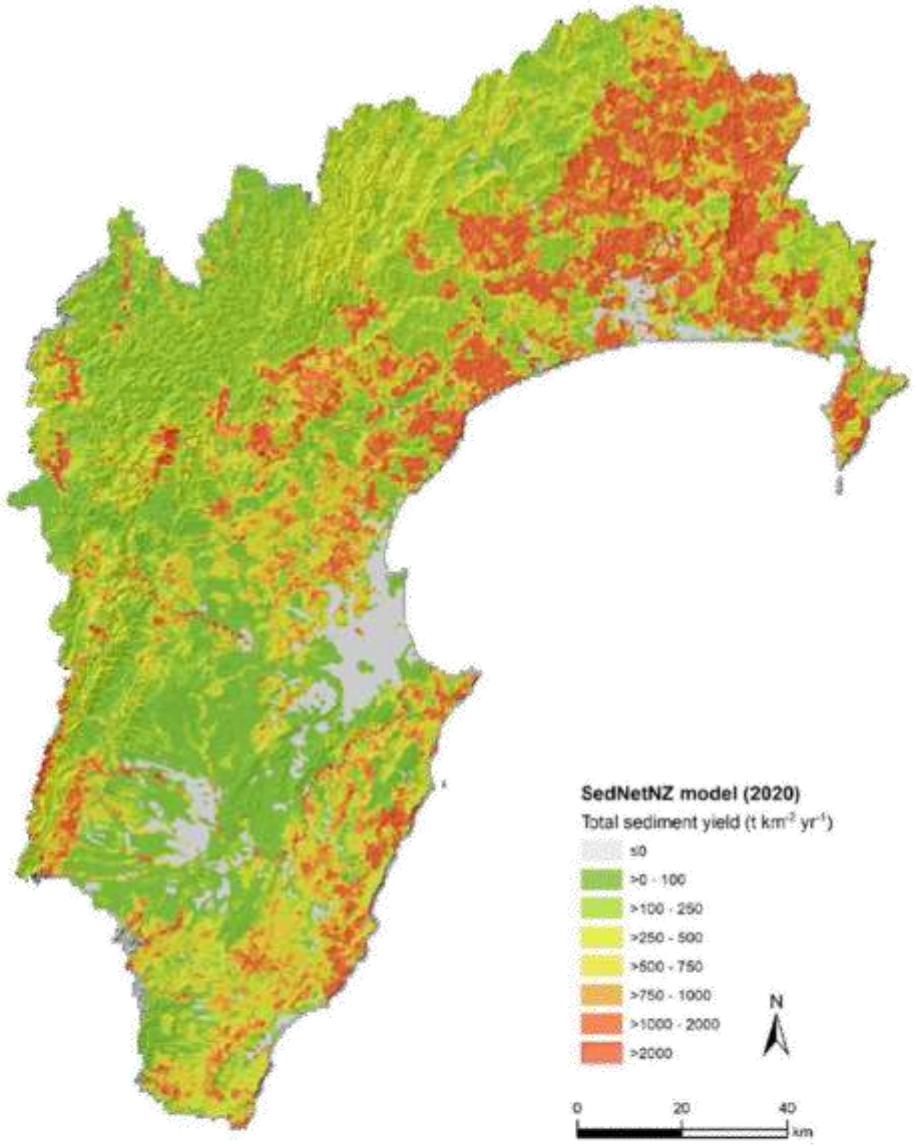

Figure 3. Previous SedNetNZ modelled total suspended sediment yield per REC2 subwatershed for the Hawke's Bay region based on the national 15 m DEM. (Source: Based on data from Smith et al. 2020)

The upgrade to the SedNetNZ model involves: a) generating new digital stream network and subwatershed layers using the LiDAR-derived 5 m DEM; b) obtaining new data to improve model parameterisation; c) implementing changes to model algorithms that represent surface, bank and shallow landslide erosion as well as sediment entering floodplain storage to use the higher resolution topographic data. We agreed with HBRC that the gully and earthflow components of the model would not be upgraded at this stage as there is presently insufficient data. Therefore, these components remain unchanged.

3 Methods

3.1 LiDAR pre-processing for erosion modelling

The HBRC supplied the 2020-2021 regional LiDAR data set to MWLR in August 2022. MWLR processed the classified point cloud and produced digital elevation models (DEM), digital surface models (DSM), and canopy height models (CHM) for use within the MWLR–HBRC LiDAR partnership project. The Hawke's Bay LiDAR survey did not extend into the Gisborne District which covers the headwaters of the Wairoa catchment (Figure 4). Representation of the complete hydrological catchment is required for erosion and sediment modelling. Therefore, data from the Gisborne LiDAR survey was obtained and used to extend the LiDAR coverage to include the whole Wairoa catchment.

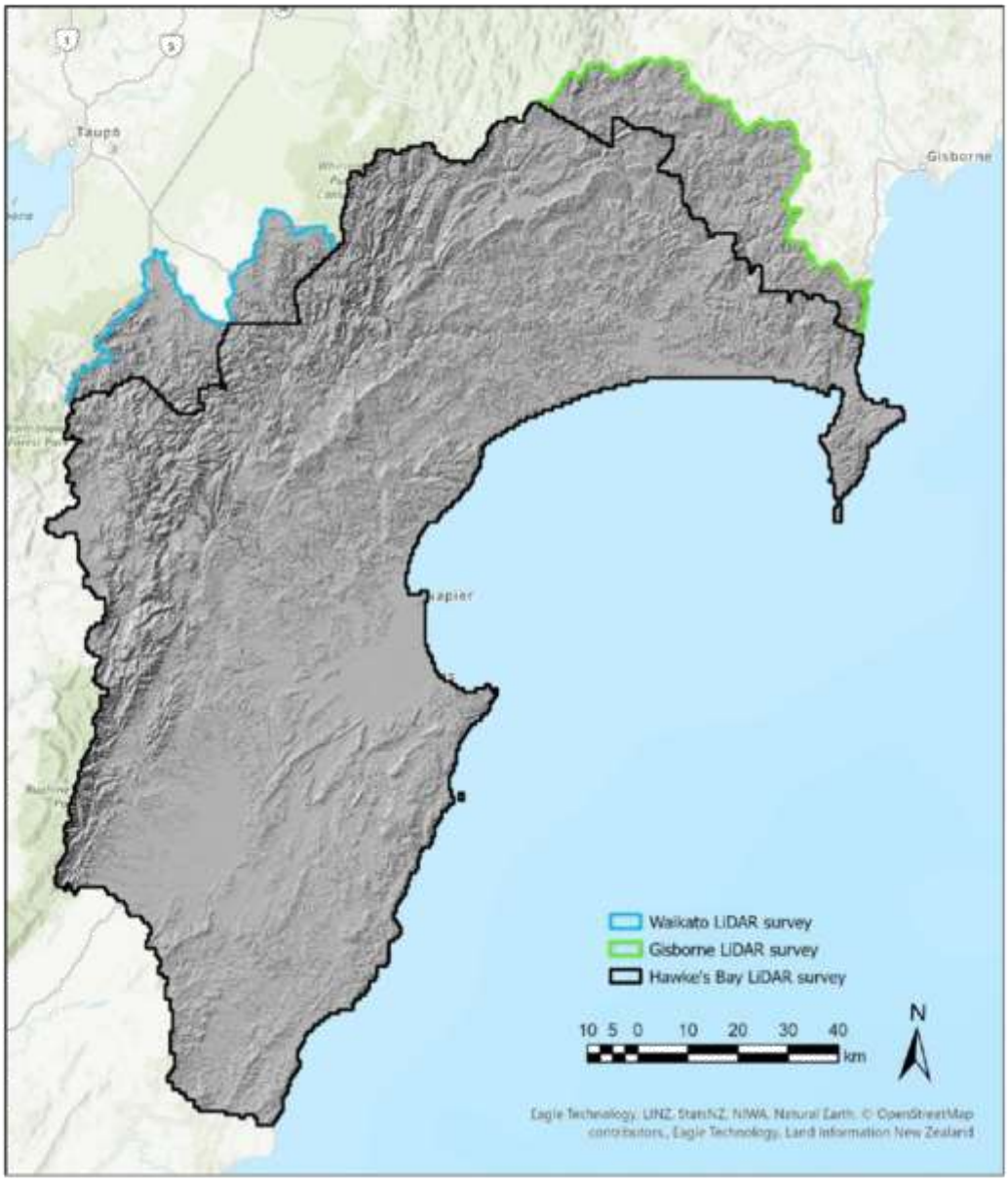

Figure 4. Shaded relief map based on the combined LiDAR-derived 5 m DEMs from the Hawke's Bay (black polygon), Gisborne (green), and Waikato (blue) LiDAR surveys.

Between May and November 2023 HBRC supplied LiDAR data captured by the Waikato survey (blocks G and E) that covered the headwaters of the Mohaka and Ngaruroro Rivers (Figure 4) as well as the final refined version of the Hawke's Bay LiDAR point cloud. These data sets were processed to produce the final DEM, DSM and CHM spanning the full regional extent, including those parts of the Gisborne District that drain into the Hawke's Bay region.

3.2 Digital stream network

The digital stream network and subwatershed layers were produced specifically for use in regional-scale erosion and sediment load modelling. The digital network was derived from the 5 m DEM and included the headwaters of the Wairoa catchment that extend into the Gisborne District. The network was generated from the sink-filled DEM using a D8 flow direction and accumulation algorithm and a 10-ha channel initiation threshold. The D8 algorithm models flow direction from a cell to its steepest downslope neighbour.

Each segment within the digital network has a corresponding subwatershed draining to the segment. Individual stream segments are related to their subwatershed by their HydroID. The NextDownID gives the HydroID of the next downstream segment or subwatershed within the network. Where a segment has a NextDownID = -1, this indicates that there are no further downstream segments.

The total length of the LiDAR DEM-derived network depends on the choice of channel initiation threshold (i.e. the upstream contributing area required to initiate a first-order stream segment) (Table 1). A potential LiDAR-based approach to detecting channel head locations was not applied due to the small size of incipient channels that are likely to sit below the minimum vertical accuracy (e.g. non-vegetated areas ≤ 0.2 m at a 95% confidence interval) for the LiDAR point cloud (Land Information New Zealand 2020), while vertical accuracy will be further reduced for areas under woody vegetation cover. The difference in network length compared to the REC2 digital network is not only a function of initiation threshold, but also of channel sinuosity. The LiDAR DEM-derived networks better represent the sinuous planform of channels compared to the REC2 network (Figure 5a).

Table 1. Comparison of total unrefined length of the stream network based on REC2 and LiDAR-derived 5 m DEM with different channel initiation thresholds (10, 20, 30 ha)

Digital network	Network length (km)
REC2	24,595
LiDAR 5 m DEM 30 ha	24,935
LiDAR 5 m DEM 20 ha	29,749
LiDAR 5 m DEM 10 ha	40,327

The choice of a region-wide channel initiation threshold involves a trade-off between a higher headwater stream density (Figure 5b) versus an increase in the number and length of low-order stream segments in lowlands. A lower initiation threshold produces a larger number of spurious segments in lowland areas, such as those situated within wide river channels (Figure 5c). For erosion and sediment load modelling, we selected the channel network based on a 10-ha initiation threshold. This network provides reasonable representation of headwater channels while limiting the formation of spurious channels in lowlands.

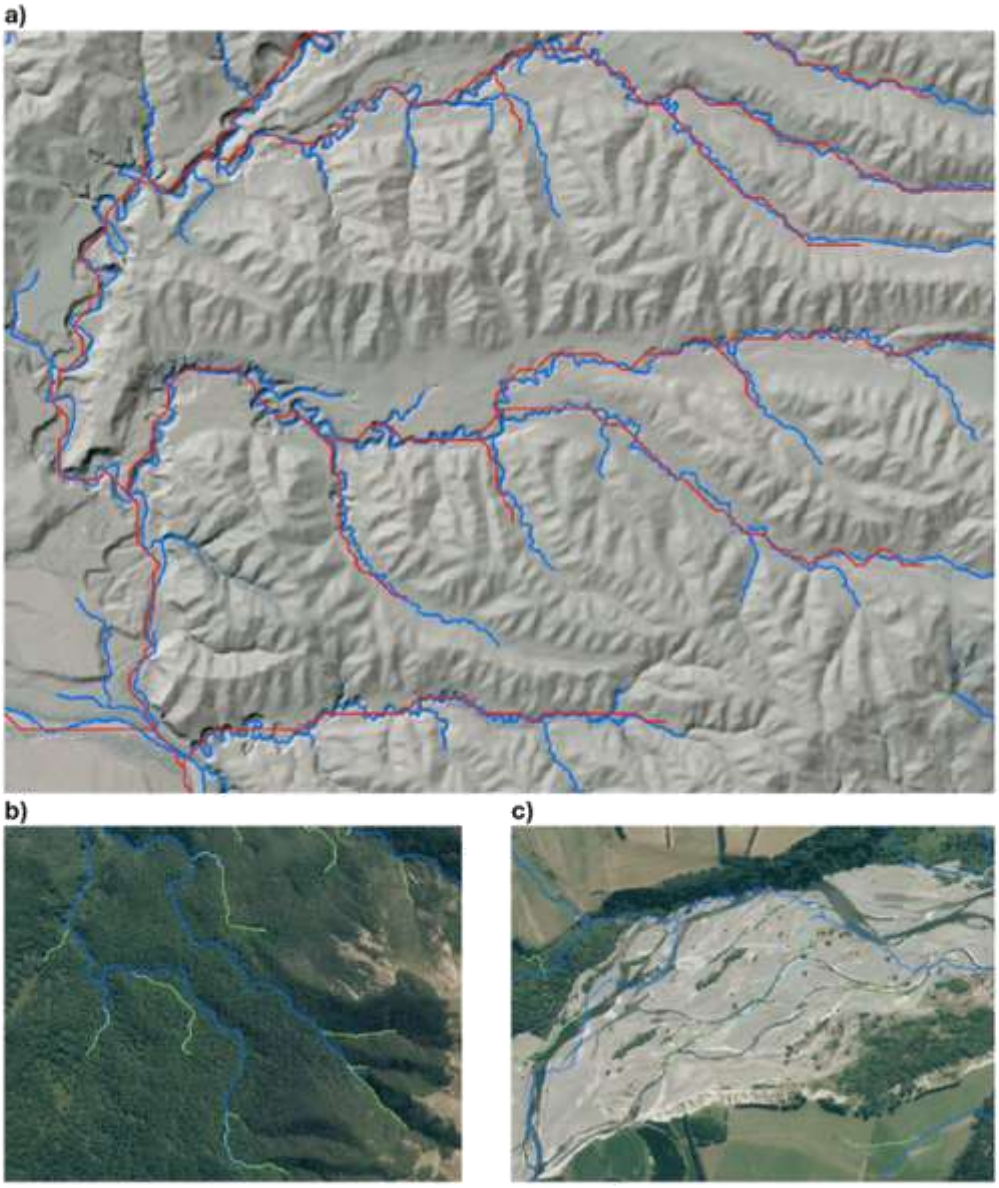

Figure 5. Examples of networks. a) REC2 digital network (red) versus LiDAR DEM-derived digital network (blue) showing improved planform accuracy; b) headwater streams networks versus c) lowland streams networks using different initiation thresholds (30 ha – dark blue, 20 ha – light blue, 10 ha – light green).

The 10-ha digital network and subwatershed layers underwent automated and manual refinement procedures to improve network representativeness. These procedures included those listed in the following bullets.

- Removal of stream segments draining away from Hawke's Bay (i.e. any segments that do not ultimately drain to coastal Hawke's Bay were excluded).

- Removal of first-order segments where much of the segment lies within a lake or larger river channel. This tends to occur along the lower reaches of rivers such as the Ngaruroro and Tukituki where spurious first-order segments are produced fully or largely within the wide channels of these rivers.
- Editing of the network in low-lying areas near the coast or very low-relief areas surrounding inland lakes that form natural sinks. The presence of infrastructure (road bridges, culverts, urban drainage etc.) within these areas also affects derivation of the stream network based on the LiDAR-derived DEM (i.e. where the modified drainage does not follow the steepest slope or where infrastructure creates obstacles that impede the digital network from following the natural drainage line).
- Filling areas that form natural sinks in the DEM to generate the stream network. However, the resulting flat surfaces prevented the algorithm from producing a representative network. Therefore, the stream network in these areas was removed and a simplified network was manually digitised from aerial imagery (source: HBRC), while the associated subwatersheds were merged. As it was not possible to separate these filled areas into discrete stream segments and subwatersheds, we instead represented them by merged multi-part segments with a single HydroID and a corresponding merged subwatershed.

As a result of these procedures, not all subwatersheds have an associated stream segment. Within the updated SedNetNZ model, the presence of a stream segment is the basis for applying the riverbank erosion sub-model and thus only those subwatersheds with a stream segment are considered potential sources of bank erosion. Subwatersheds without stream segments are retained as these may contain sediment load contributions from other erosion processes (e.g., surface erosion). The subwatershed layer is used to summarise and route suspended sediment loads to the coast.

The final refined 10-ha stream network has a total length of 39,487 km.

3.3 Data collection for model parameterisation

Targeted data collection is required to support model development and parameterisation for the Hawke's Bay region. This section describes mapping to obtain data on a) shallow landslide locations for use in modelling landslide susceptibility, as well as b) bank migration rate and c) bank height data for modelling bank erosion. The modelling described in the present report also draws on pre-existing data used in previous parameterisation and implementation of both the regional landslide susceptibility and SedNetNZ models for Hawke's Bay.

3.3.1 Shallow landslide mapping

Shallow landslide data are required for landslide susceptibility modelling. To upgrade the Hawke's Bay regional landslide susceptibility layer, we require landslide mapping data that overlap with available LiDAR coverages. This includes the existing landslide data for southern Hawke's Bay. However, no landslide data was available for northern Hawke's Bay at the time of the previous modelling (Smith 2020).

Following the March 2022 storm events over northern Hawke's Bay, HBRC contracted MWLR to complete semi-automated mapping using object-based image analysis (OBIA) across the storm impacted area (3,200 km^2). This work focused on mapping post-storm landslides and debris deposits using 0.5 m 4-band Airbus Pleiades satellite imagery followed approximately 12 months later by an aerial survey that captured 0.3 m 4-band orthophotography. The resulting OBIA-mapped polygons underwent a process of manual refinement to remove false positives.

These landslide data from northern Hawke's Bay were used to augment existing MWLR landslide inventories that intersect with available LiDAR coverages.

3.3.2 Channel planform mapping

Riverbank migration rate data is required for calibrating the riverbank erosion sub-model within SedNetNZ. Mapping of channel planform change from repeated aerial imagery (i.e., 2010-11 and 2019-20 surveys) was used to estimate reach-average bank migration rates.

The selection of river channel reaches for mapping was based on our analysis of the annual maximum flows recorded at HBRC river gauging stations. We compared the mean annual flood (MAF) recorded during the 9-year mapping interval versus the full gauge record where ≥ 30 years of annual data were available for analysis. This comparison allowed us to target river reaches for mapping where the difference in MAF between the mapping interval and full record was minimised. In turn, this limited the potential for bias in the data resulting from mapping reaches where the MAF over the shorter imagery interval deviated significantly from the longer-term record.

We identified 21 gauging stations out of a total of 36 where the MAF was not significantly different (Mann-Whitney *U* test; $P > 0.05$) between the mapping interval versus the full record. The catchments corresponding to the gauged rivers are shown in Figure 6. Our channel mapping focused on reaches located up and downstream of gauging stations with the same stream order as the gauged reach.

Examples of the channel planform mapping are shown in Figure 7. Shaded areas show zones of erosion. We computed the reach-average lateral bank migration rate (m yr^{-1}) for each segment of the digital stream network that intersected the mapped reaches. Approximately 420 km of channel were mapped in the Hawke's Bay region. These data were supplemented by the inclusion of selected reaches from a) low-order streams in lowlands and b) bedrock confined reaches as data was lacking for these channel types where lateral change was negligible. In addition, bank migration data from repeated channel planform mapping for the Greater Wellington region was used to augment the data from Hawke's Bay for model calibration and testing. The Greater Wellington mapping followed the same procedure and produced data for 386 km of channel.

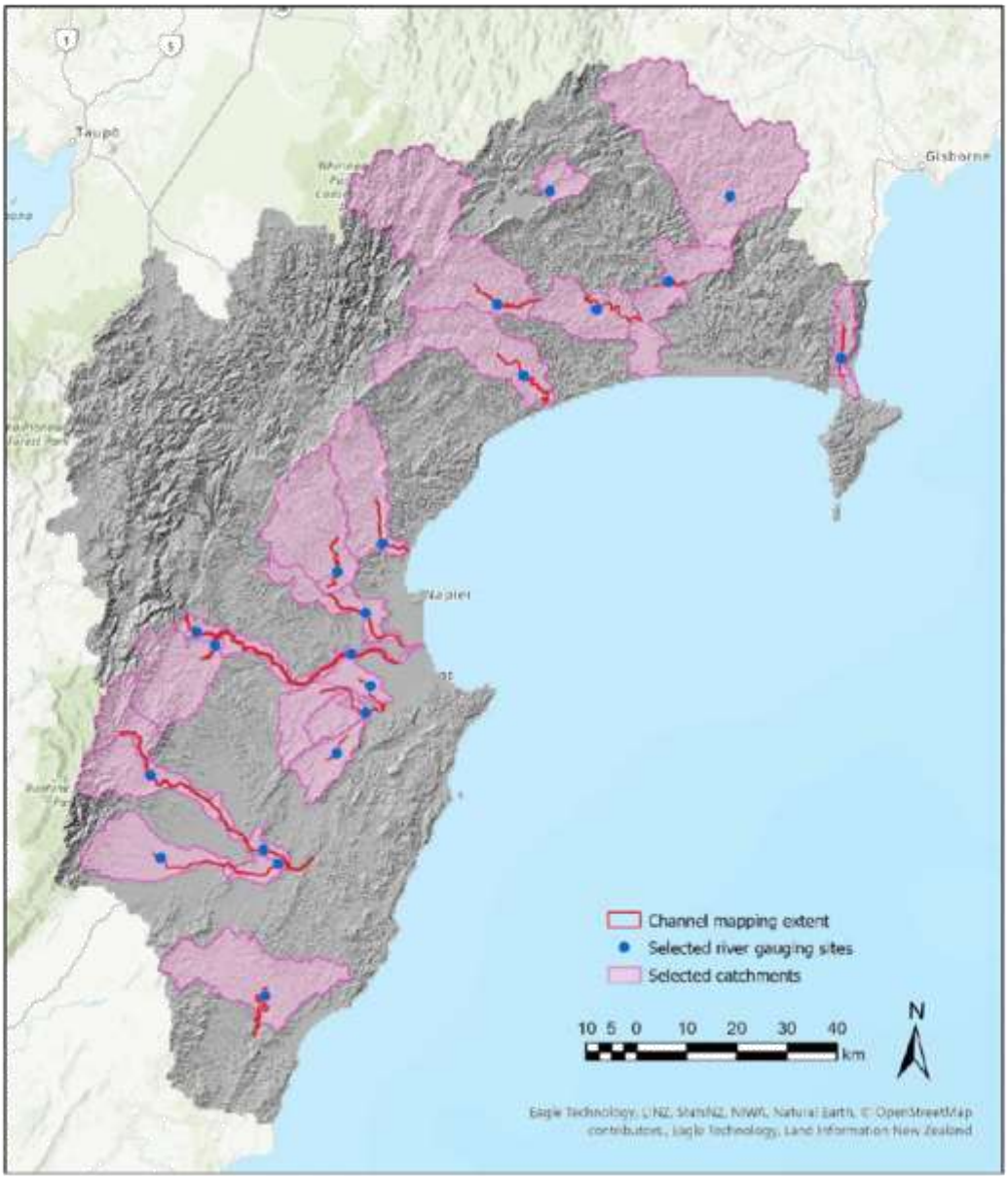

Figure 6. Selected reaches (red lines) for channel planform mapping using the regional orthophotography for 2010–11 and 2019–20. Blue points show river gauging stations (*n* = 21) used to estimate mean annual flood (MAF); pink shading shows catchment areas.

Figure 7. Examples of channel planform mapping showing areas of erosion (yellow shading) with mapped channel banks from 2010–11 (yellow line) and 2019–20 (red line) aerial imagery.

3.3.3 Bank height mapping

Reach-average bank heights are required as a model input for predicting suspended sediment loads from bank erosion. Previous modelling of bank erosion in the region lacked region-specific data on bank heights and instead relied on a general relationship relating bank height to mean annual discharge (Dymond et al. 2016; Smith et al. 2020). We address this limitation here by using the LiDAR-derived 1 m DEM to estimate bank heights for selected reaches across the region.

Bank heights were mapped along transects perpendicular to the flow direction spaced at 50 m intervals (Figure 8). Bank heights were measured by placing a point at the bank top and toe and calculating the elevation difference between the two points for both left and right banks. Reach selection focused on channels spanning a range in stream orders with visible banks using both the regional orthophotography and hillshade computed for the 1 m DEM to locate the bank top and toe.

A total of 10,431 discrete banks were mapped using this approach. The reach-average bank height was then determined per stream segment. These manual measurements were used to assess predictions of reach-average bank height (described in section 3.5.3).

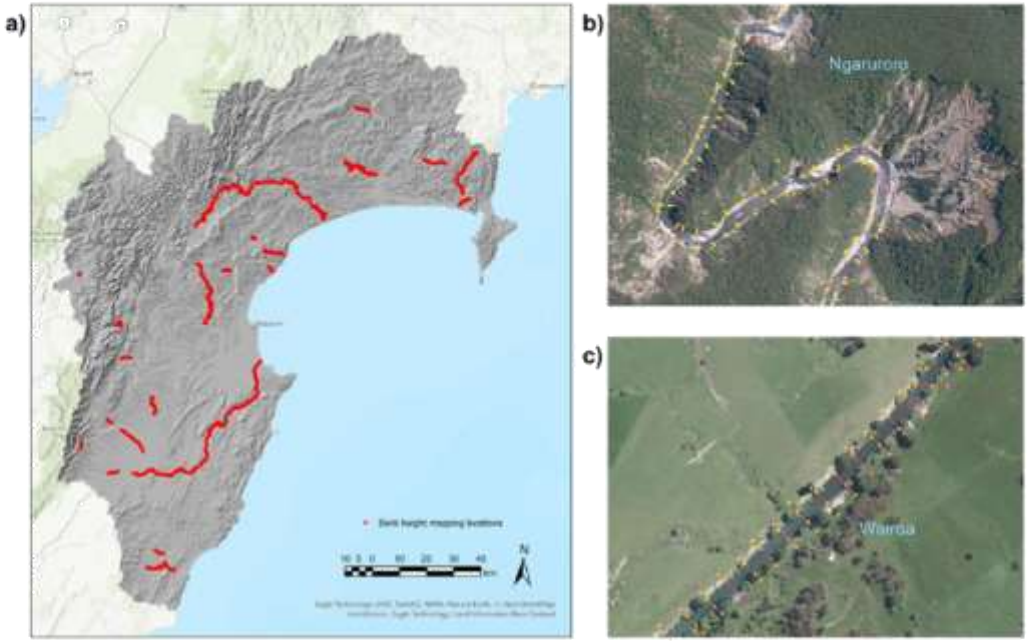

Figure 8. Bank heights; a) mapping locations; b) and c) examples of reaches with bank top and toe points marked along transects. Pink lines denote channel transects while yellow dots show the mapped locations of the top and toe of banks.

3.4 Upgraded regional shallow landslide susceptibility model

The LiDAR-based upgrade to the existing regional rainfall-induced shallow landslide model involved: a) assembling a data set comprising landslides located in areas with LiDAR coverage; b) re-applying the logistic regression model and evaluating model performance; c) predicting landslide susceptibility at 5 m resolution across the region.

The data set comprises shallow landslides (over n = 116,000) mapped in southern and northern Hawke's Bay as well as from the Greater Wellington region in areas overlapping with LiDAR coverage (Table 2). The data set has more than doubled in size compared to the 56,000 landslides available for use in the previous landslide susceptibility modelling (Smith 2020). Non-landslide locations were randomly selected from within the landslide mapping areas to produce a balanced sample comprising equal numbers of landslide and non-landslide points for modelling (Smith et al. 2021).

Binary logistic regression (BLR) was used to classify landslide and non-landslide locations. BLR requires spatial data corresponding to landslide/non-landslide locations for variables that may influence susceptibility. The analysis draws on spatial data sets for elevation (5 m LiDAR-derived DEM), land cover (NZ LCDB) and rock type (NZLRI; Newsome et al. 2008). Slope angle (continuous variable), aspect (categorical variable with 8 classes), profile (categorical: convex, concave, planar) and planform curvature (categorical: convergent, divergent, planar) were also derived from the DEM. These input variables were selected for use in statistical modelling because: a) there is a potential physical basis for how each

variable may influence landslide susceptibility (Smith et al. 2021); b) model inputs can be derived for all areas.

Table 2. Summary information for the study areas with LiDAR coverage contributing data to the shallow landslide data set used for the upgraded landslide susceptibility modelling

Study area no.	Location	Study area (km^2)	Period	Number of landslides	Imagery sources (resolution)	Data source
1	Southern Hawke's Bay	175	Event (2011)	27,170	Orthorectified aerial photography and Worldview-2 (0.4 m)	Smith et al. (2021)
2	Northern Hawke's Bay	3,162	Multi-event (2022)	45,879	Orthorectified aerial photography (0.3 m) and Pleiades (0.5 m)	Betts et al. (2023)
3	Wairarapa, Greater Wellington	843	Multi-event (2005-10)	43,069	Orthorectified aerial photography (0.4 m)	Spiekermann et al. (2021)

Binary logistic regression has been widely applied internationally for landslide susceptibility analysis (Reichenback et al. 2018) and was used by Smith (2020) for predicting landslide susceptibility in Hawke's Bay. BLR is a type of generalised linear model (GLM) that uses a logistic function with a binary dependent variable (landslide presence/absence). It relates the probability (P) of landslide presence ($Y = 1$) to the spatial explanatory variables ($x_1, x_2 \ldots x_n$) where $\beta_0, \beta_1, \beta_2 \ldots \beta_n$ are fitted constants (equation 1):

$$P(Y = 1) = \frac{1}{1 + e^{-(\beta_0 + \beta_1 x_1 + \beta_2 x_2 \cdots \beta_n x_n)}} \quad (1)$$

Model predictive performance was assessed using k-fold cross-validation. The data set comprising landslide and non-landslide locations was randomly shuffled and then split into $k = 5$ folds, where $k - 1$ folds were used for model training and each remaining fold (20% of the data) was used once for testing. Sensitivity to the location of non-landslide points was also tested by repeating the randomised placement of absence points five times. The procedure was repeated to produce a total of 100 data partitions for model fitting and testing.

Model classification performance (i.e. landslide versus non-landslide) was evaluated using receiver operating characteristic (ROC) curves and calculation of the AUC based on the 100 iterations. ROC curves and AUC values are widely used in the landside susceptibility literature to assess model performance (Reichenbach et al. 2018). ROC curves plot the true positive rate ($TPR = \frac{TP}{TP + FN}$) versus the false positive rate ($FPR = \frac{FP}{TN + FP}$) to give an indication of sensitivity (probability of detection) versus 1 – specificity (specificity refers to the true negative rate) (Conoscenti et al. 2016). An AUC value of 0.5 corresponds to performance no better than a random guess, while a value of 1 indicates perfect classification. Model performance is generally considered 'fair' above 0.7, 'good' between 0.8-0.9, and 'excellent' above 0.9 (Carter et al. 2016).

The fitted BLR model was used to produce spatial predictions of shallow landslide susceptibility at 5 m resolution. The model was applied in the region with the set of explanatory variables as raster inputs and used to predict shallow landslide susceptibility, which is expressed as a spatial probability (range 0-1).

3.5 Upgraded regional SedNetNZ model

The upgrade to SedNetNZ for the region focused on shallow landslide, surface erosion, and riverbank erosion sub-models, as previously agreed with HBRC. We also revised the floodplain deposition component of SedNetNZ. During the scoping phase for this project, we identified that we presently lack sufficient data on gully and earthflow erosion processes to upgrade these sub-models. Therefore, the gully and earthflow erosion sub-models are included unchanged from previous applications of the model in the Hawke's Bay region.

SedNetNZ computes a sediment budget for the subwatershed draining to each segment in the LiDAR DEM-derived digital stream network. Each sediment budget comprises erosion process (i.e. surface, shallow landslide, gully, earthflow, and riverbank) sediment loads delivered to the stream segment less any sediment entering floodplain storage. The resulting net suspended sediment load is then routed to the next downstream segment and through the network to the coast, while accounting for deposition in lakes.

Predictions of mean annual surface and shallow landslide erosion using the LiDAR DEM–based sub-models were produced on a 5 m grid, while bank erosion was estimated for each stream segment in the digital network.

3.5.1 Shallow landslide sub-model

Shallow landslides are considered the most common form of erosion in New Zealand hill country (Eyles 1983). Shallow landslides are typically < 2 m deep and individual source areas (scars) are generally small (median size 50–100 m^2) (Betts et al. 2017; Smith et al. 2021). Landslide-triggering storm events occur episodically and thus the contribution of shallow landslides to suspended sediment loads will exhibit significant inter-annual variation. For this reason, SedNetNZ averages across a multi-decadal period to estimate the longer-term contribution of shallow landslides to mean annual suspended sediment loads rather than attempting to estimate the contribution for any given year.

In previous applications of SedNetNZ, including to the Hawke's Bay region, the mass of soil eroded by shallow landslides and delivered to the stream network per square kilometre per year (EL) was estimated by:

$$EL = \rho \, SDR \, d_l f(s) \quad (2)$$

where ρ is the bulk density of soil (t m^{-3}), SDR is the sediment delivery ratio, d_l is the mean depth of landslide failure (m), and $f(s)$ is the expected area of landslide scars per square kilometre per year at slope angle s (m^2 km^{-2} yr^{-1}) for terrain under grass cover.

Shallow landslide erosion was estimated for those erosion terrains[1] (Dymond et al. 2010) identified as being susceptible to landslide erosion; ρ is set to 1.5 t m^{-3} (Dymond et al. 2016); SDR values are typically 0.5 in hill country and 0.1 in hard rock mountain areas (Dymond et al. 2016); d_l is set to 1 m (Page et al. 1994; Reid & Page 2002; Betts et al. 2017; Phillips et al. 2021); and $f(s)$ is determined from previous calibration of SedNetNZ using multi-temporal landslide mapping data from historical aerial imagery spanning approximately 70 years for study areas in the Manawatū catchment (Dymond et al. 2016; Betts et al. 2017). The difference in SDR between hill country and hard rock mountain areas reflects the tendency for landslides in mountains to contain a larger proportion of rock (Dymond et al. 2016).

Permanent woody cover is estimated to reduce shallow landslide erosion by 90% compared with pasture (Basher 2013; Dymond et al. 2016; Phillips et al. 2020; Smith et al. 2023), while an 80% reduction may be applied under exotic plantation forest (Vale et al. 2021). The lower reduction estimated for plantation versus permanent forest recognises the effectiveness of forest cover for reducing shallow landslides (Marden 2012; Smith et al. 2023) for much of the rotation while acknowledging the period spanning several years between harvest and canopy closure of the replanted crop during which there is an increase in susceptibility to shallow landslide erosion (Phillips et al. 2018, 2020).

Upgraded shallow landslide sub-model

In the present report, we combine the LiDAR-based modelling of shallow landslide susceptibility with the shallow landslide erosion sub-model in SedNetNZ. This new approach replaces the use of the erosion terrains layer with higher resolution (5 m resolution) spatial predictions of shallow landslide susceptibility based on the LiDAR-derived DEM (see section 3.4).

We related landslide-eroded area to slope using photogrammetrically derived 2-m DEMs from the Manawatū study areas that span soft and hard rock areas. These DEMs were resampled to 5 m for consistency with the Hawke's Bay 5 m DEM. These revised landslide-eroded area versus slope relationships (Figure 9b) replace the single landslide-slope relationship originally based on the national 15 m DEM (Dymond et al. 2016; Figure 9a). We derived the soft rock landslide-slope relationship using data from landslide mapping of hill country areas under mostly grass cover (Betts et al. 2017). The hard rock relationship was based on landslide mapping data for greywacke ranges under woody vegetation (Fuller et al. 2016). Therefore, the lower landslide eroded area per 1-degree slope bin for hard rock terrain in Figure 9b reflects the influence of both woody cover and rock type on landslide erosion.

The sediment load from shallow landslide erosion was distributed across the landscape based on the spatial probabilities from the modelled landslide susceptibility. The 2018

[1] An erosion terrain is a land type with a distinct combination of erosion processes and rates leading to characteristic sediment generation and yields. Erosion terrains were derived from New Zealand Land Resource Inventory data and are based on combinations of rock type/parent material, topography, rainfall, and erosion process type and severity.

land cover from LCDB v5.0 was reclassified into woody cover on hard rock areas and grass cover on non-hard rock terrain. This reclassified cover layer was used to predict landslide susceptibility and the resulting susceptibility layer formed the basis for applying the landslide-slope relationships across the region. This was achieved using a 'percentile matching' approach whereby percentiles derived from the pixel-based spatial probabilities from the susceptibility layer were separately matched to the equivalent slope percentiles in 1-degree increments (bins) for the woody cover on hard rock and grass on non-hard rock domains. This enabled the landslide eroded area per 1-degree slope bin (i.e. $f(s)$) to be distributed spatially at 5 m resolution across the region for each domain.

Given the difference in the reference vegetation cover (grass versus woody) for the rock type-based landslide calibration data (Figure 9), the reduction in landslide erosion by 80% (exotic plantation) or 90% (permanent woody cover) was only applied on non-hard rock terrain where woody vegetation was present. In contrast, landslide erosion was increased by an inverse proportion (i.e. 10-fold) in those hard rock areas under non-woody vegetation to represent the higher rates of landslide erosion that generally occur in the absence of woody cover.

To prevent small amounts of landslide erosion from occurring on very slow slope land, a slope threshold of 6 degrees was applied below which landslide erosion was deemed negligible. This threshold corresponds to an approximate susceptibility value of 0.01, representing the land least susceptible to instability. Landslide susceptibility was not modelled for LCDB-mapped urban areas due to insufficient data, thus landslide erosion was not estimated for these areas.

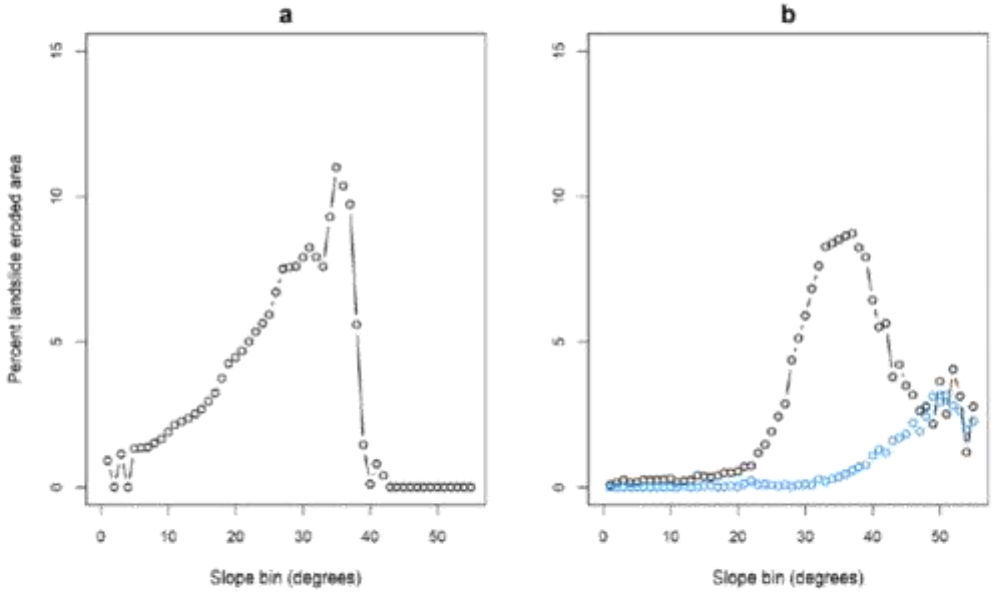

Figure 9. Plots of landslide eroded area (expressed as a percentage of each slope bin) per 1-degree slope bin for: a) national 15 m DEM (previous SedNetNZ model; Dymond et al. 2016); b) 5 m DEM for soft rock under grass (black circles) and hard rock under woody vegetation (blue circles) terrain based on multitemporal polygon mapping (70-year interval) of shallow landslide erosion in the Manawatū catchment.

3.5.2 Surface erosion sub-model

Surface erosion (i.e. sheet and rill erosion from raindrop impacts and overland flow) was previously estimated in SedNetNZ using the NZ Universal Soil Loss Equation (NZUSLE) (Dymond et al. 2010, 2016). The version of the NZUSLE originally applied in the Hawke's Bay region (Palmer et al. 2016, 2017; Spiekermann et al. 2017) is given by:

$$ES = a\,P^2\,K\,(\frac{L}{22})^{0.5}SC \quad (3)$$

where ES is surface erosion (t km^{-2} yr^{-1}), a is a constant (t km^{-2}yr^{-1}mm^{-2}), P is mean annual rainfall (mm), K is a soil erodibility factor (0.25 for loam soil [Dymond et al. 2010]), L is slope length (m), S is a slope steepness factor given by $0.065 + 4.56\,s + 65.41\,s^2$ where s is slope gradient, and C is a vegetation cover factor (1 for bare ground, 0.01 for pasture, 0.005 for forest).

Revised NZUSLE

The NZUSLE surface erosion sub-model has undergone several refinements since the original applications of SedNetNZ in Hawke's Bay. These include changes to:

- **Soil erodibility:** the constant value for K has been replaced with a spatially variable soil erodibility term based on soil mapping data (Neverman et al. 2021) represented by:

$$K = \frac{2.1(12-OM)M^{1.14}10^{-4}+3.25(SS-2)+2.5(PP-3)}{7.59\times100} \quad (4)$$

  where OM is the soil organic matter content, M is the particle size parameter, SS is the soil structure code, and PP is the soil profile permeability code (Wang et al. 2001; Yang et al. 2018). We use 6 PP classes, adapted from Rosewell and Loch (2002). M is calculated as a function of the proportion silt and clay:

$$M = Silt(100 - Clay) \quad (5)$$

  where $Silt$ and $Clay$ are the percentages of silt and clay in the soil, respectively.

- **Slope length:** The term related to slope length (i.e., $(\frac{L}{22})^{0.5}$) has been replaced with a term that better represents the effect of topography on the size of convergent upslope areas contributing overland flow and surface erosion (Smith et al. 2019b), as described by Desmet and Govers (1996):

$$L = \frac{(A+D^2)^{m+1}-A^{m+1}}{D^{m+2}\times x^m \times 22.13^m} \quad (6)$$

  where L is slope length factor for a given raster cell (pixel), A is the upstream catchment area (m^2) at the cell inlet, D is the raster cell width (m), m is the slope length exponent, x = sin a+cos a, with α being the slope aspect.

The slope length exponent m is calculated depending on the rill to inter-rill ratio β and the slope gradient θ (Foster et al. 1977 and McCool et al. 1989 cited in Renard 1997):

$$\beta = \frac{\sin\theta / 0.896}{3\times(\sin\theta)^{0.8}+0.56} \quad (7)$$

$$m = \frac{\beta}{1+\beta} \quad (8)$$

- **Slope steepness:** The slope steepness factor S has been replaced by a term from the Revised Universal Soil Loss Equation (RUSLE) (Renard 1997), which is calculated according to a threshold in slope gradient sp (%):

$$S = \begin{cases} 10.8 \times \sin\theta + 0.03 & with\ sp < 9\% \\ 16.8 \times \sin\theta - 0.5 & with\ sp \geq 9\% \end{cases} \quad (9)$$

Implementation of RUSLE using the LIDAR-derived DEM

In the present work, we replace the NZUSLE with RUSLE (Renard et al. 1997) within SedNetNZ and use RUSLE to estimate suspended sediment loads delivered to streams from surface erosion across the Hawke's Bay. RUSLE and the earlier Universal Soil Loss Equation (USLE) (Wischmeier & Smith 1978) are empirical models developed using an extensive erosion data set obtained from plot measurements on predominantly agricultural land (Renard et al. 1997). The USLE/RUSLE was originally developed in the United States and has since been widely applied globally, including in New Zealand using the national 15 m DEM (Donovan 2022).

Most terms in the revised version of the NZUSLE described above are the same as those used in RUSLE, except the term representing the influence of rainfall on surface erosion rates. To fully implement RUSLE within SedNetNZ using the 5 m LiDAR-derived DEM, we replaced aP^2 in equation (3) with a spatial input for rainfall erosivity. We also excluded channel areas based on the new digital stream network from surface erosion estimates.

Rainfall erosivity (R) refers to the power of rainfall available to drive erosion at the soil surface (Nearing et al. 2017). The spatial distribution in annual rainfall erosivity was previously estimated across New Zealand by Klik et al. (2015) using high-resolution (10-min interval) rainfall data from 35 stations to calculate the product of total kinetic energy and maximum 30-min rainfall intensity for all rainstorms over the years of record (Klik et al. 2015). Regression analysis was used to derive climatic region-specific relationships between the estimates of rainfall erosivity and annual precipitation (Klik et al. 2015). We have used the regional relationships described in Klik et al. (2015) to estimate rainfall erosivity across Hawke's Bay.

We have replaced the previous aP^2 term which was computed using the Land Environments New Zealand (LENZ)-based estimate of mean annual rainfall (1950–1980) (Leathwick et al. 2003) with the rainfall erosivity estimate derived using the more recent estimate of mean annual rainfall for the period 1981-2010 that was produced for the Ministry for the Environment.

The NZUSLE was originally calibrated with measurements of surface erosion rates from across New Zealand (Dymond et al. 2013, 2016). We do not have LiDAR coverages that overlap with the calibration data and thus cannot apply an updated calibration to the LiDAR-based RUSLE estimate of surface erosion. Instead, the RUSLE is used with a sediment delivery ratio that approximates the previously calibrated NZUSLE to estimate the total net load delivered to the stream network from surface erosion.

3.5.3 Riverbank erosion sub-model

The total mass of material eroded from riverbanks each year is a function of bank height, reach length, and bank migration rate (Dymond et al. 2016):

$$B_j = \rho M_j H_j L_j \quad (10)$$

where B_j is the total eroded mass for the j-th stream segment (t yr^{-1}), ρ is the bulk density of the bank material (t m^{-3}), M_j is the bank migration rate (m yr^{-1}), H_j is the mean bank height (m) and L_j is the length (m) of the j-th stream segment.

The predicted mass of material eroded from riverbanks represents the gross contribution of sediment supplied to the river channel per year. This does not account for redeposition and storage of eroded bank material on banks, within the channel bed or the lateral accretion of material on bars with channel migration. Hence, net bank erosion in SedNetNZ was previously estimated as one-fifth of gross bank erosion, based on reach-scale sediment budgets comparing bank erosion and accretion (De Rose & Basher 2011).

Bank migration rate was originally estimated using a simple empirical relationship between mean annual flood and bank migration rate (Dymond et al. 2016). This earlier version was replaced by an improved sub-model to better represent the spatial variability in factors influencing bank migration (Smith et al. 2019a). The application of this improved sub-model in Hawke's Bay was described by Smith et al. (2020).

The previously updated sub-model represented the mean annual bank migration rate as a function of six factors, as follows (Smith et al. 2019a):

$$M_j = SP_j Sn_j T_j V_j (1 - PR_j)(1 - PW_j) \quad (11)$$

where M_j is the bank migration rate (m yr^{-1}) of the j-th stream link, SP_j is the stream power of the mean annual flood (MAF) for the j-th stream link (where SP_j is the product of MAF and channel slope), Sn_j is the channel sinuosity rate factor of the j-th link, T_j is the soil texture-based erodibility factor of the j-th link, V_j is the valley confinement factor of the j-th link, PR_j is the proportion of riparian woody vegetation of the j-th link, and PW_j is the fraction of bank protection works for the j-th link. See Smith et al. (2019a) for a full explanation of the derivation of equation 11.

The MAF was estimated across the digital stream network using a fitted power function ($MAF = 39q^{0.8}$; R^2 = 0.84; n = 26) between modelled mean annual discharge (q) and MAF measured at river gauging stations across the Hawke's Bay region (Smith et al. 2020). Mean annual discharge was previously estimated for each link in the REC2 digital network based on an empirical water balance model (Woods et al. 2006; Elliott et al. 2016). These

estimates of discharge ($m^3 s^{-1}$) were converted to runoff (mm yr^{-1}) and used to re-compute mean annual discharge for the LiDAR DEM-derived digital network based on the upstream contributing area of each stream segment.

There are several important constraints on previous estimates of bank erosion. These relate to the limited data available on: a) bank migration rates for model calibration; b) bank heights that are required to convert bank migration rate to gross bank erosion; c) storage of eroded bank material within channels to estimate the net contribution of bank erosion to sediment loads. These constraints have been addressed in the present work through a focus on targeted data collection to support model development.

Bank migration rates

We compared the predictive performance of four sub-model versions that adopt an increasingly data-driven approach to estimate bank migration rates. The sub-models are outlined below.

1 **Process – Original (Process – O):** process-based model described by Smith et al. (2019a) applied with the original bank migration data available for model calibration. This is the same sub-model version applied in Hawke's Bay without LiDAR derived model inputs (Smith et al. 2020). This approach comprises a priori variable selection to represent process relationships while model calibration involves fitting variables related to channel sinuosity and bank erodibility (Smith et al. 2019a).

2 **Process – Updated (Process – U):** same sub-model as above with a priori variable selection but model calibration uses the expanded bank migration data set described in section 3.3.2 in combination with LiDAR derived inputs for modelling.

3 **General Additive Model (GAM):** the GAM approach allows both linear and non-linear relationships between variables and bank migration rate. We applied GAM with automated variable selection using a penalised likelihood approach (termed LASSO – least absolute shrinkage selection operator) implemented within the gamsel package in R (Chouldechova & Hastie 2022). Applying GAM with LASSO fits sparse models to reduce overfitting.

4 **Random Forest (RF):** random forest is a machine learning algorithm where there are no constraints on variable relationships. RF comprises multiple individual decision trees fitted by taking a random sample from the data with the remaining data used to measure error, while predictions are averaged across all trees. The R package 'randomForest 4.6-14' (Liaw & Wiener 2002) was used to implement Breiman and Cutler's random forest regression algorithm (Breiman 2001).

The predictive performance of the different sub-model versions was assessed using cross-validation. This involved randomly shuffling the bank migration data and splitting into folds, where $k-1$ folds were used for model fitting and each remaining fold used once for testing. Performance of the 'Process – O' sub-model is based on results reported in Smith et al. (2019a) and does not use LiDAR-derived DEM inputs. The 'Process – O' performance was previously evaluated using 2-fold cross-validation due to the smaller amount of data available (Smith et al. 2019a). In contrast, the performance of the other sub-models that use LiDAR inputs are compared directly using 5-fold cross-validation repeated 200 times

to give 1,000 iterations in total. The sub-model with the best predictive performance is used to estimate bank migration rates in the upgraded SedNetNZ model (refer section 4.2.3).

Bank height

Previously, mean bank height (H_j) for each stream segment was estimated from a simple regional relationship with mean annual discharge (Dymond et al. 2016). This produced a bank height that increased downstream with discharge, and did not account for reach-to-reach variations in bank height that reflected local river channel form. We sought to improve on this approach using the LiDAR DEM to estimate reach-average bank heights across the region.

Our approach estimated bank heights from transects located perpendicular to the digital stream network at 50 m intervals. The width of transects varied per stream segment as a function of mean discharge and the inverse of mean lateral slope (as a proxy for valley confinement) to approximate variations in bankfull width. The elevation along each transect was computed using the 1 m DEM for a range of percentiles and the bank height approximated using difference between the 75^{th} – 5^{th} percentile elevations with a minimum bank height set to 0.2 m. We compared the resulting bank height estimates with the independent point-based height measurements described in section 3.3.3.

Net bank erosion

Estimating the net contribution of bank erosion to suspended sediment loads requires information on the redeposition and storage of eroded bank material on banks, within the channel bed or the lateral accretion of material on bars with channel migration. Such information is not widely available. Net bank erosion was previously estimated at one-fifth of gross bank erosion – based on results from a detailed empirical study using repeated aerial photography and LiDAR surveys in the Waipaoa River catchment (De Rose & Basher 2011).

We sought to estimate net bank erosion based on the channel planform mapping for comparison with the previous Waipaoa based estimate. Planform mapping using the repeated aerial imagery (2010-11 to 2019-20) identified areas of both erosion and accretion within channels for each digital stream segment (n = 1,308 mapped segments) over the mapping interval. These areas were converted to mean annual rates of reach-average lateral erosion or accretion (m yr^{-1}). Average erosion and accretion volumes per segment per year were then approximated using the average of the maximum and minimum mapped bank heights per transect, respectively. The mean net bank erosion (P_{net}) as a proportion of the mean gross bank erosion (E_v) was computed as

$$P_{net} = (E_v - A_v)/E_v \quad (12)$$

where A_v is the mean accretion volume per segment per year.

This analysis assumes that, for laterally migrating channels, the outer eroding bank is typically higher than the opposite accreting bank. In practice, bank heights may vary

between erosion and accretion zones, while some reaches may experience erosion or accretion along both banks. Nonetheless, this assumption provides a first-order approximation for estimating net bank erosion based on a significantly larger data set (805 km of channel length) for comparison with the previous estimate based on 44 km of mapped channel length in the Waipaoa catchment.

3.5.4 Sediment routing and floodplain storage

SedNetNZ estimates the mean annual suspended sediment load delivered by each erosion process to the digital stream network. This sediment is then routed through the network to the coast. The version of SedNetNZ originally applied to the Hawke's Bay did not include representation of sediment storage in lakes, which has since been added to the model (Neverman et al. 2021). The representation of floodplain deposition has also been refined (Vale et al. 2021). Previously, sediment deposited on floodplains was assumed to spread evenly across the floodplain for each major river catchment. The revised floodplain deposition algorithm estimates the amount of sediment entering floodplain storage along the stream network based on upstream loads rather than averaging the load deposited on floodplains across major catchments (Vale et al. 2021).

The mass of sediment (t yr^{-1}) entering floodplain storage in the ith subwatershed (F_i) is calculated as:

$$F_i = pS_t \frac{L_i accS_i^2}{\sum L_i accS_i^2} \quad (13)$$

where p is the proportion of the sediment load generated by hillslope erosion per lake or sea-draining catchment that is deposited on floodplains in the catchment, set to 5% based on previous SedNetNZ parameterisation carried out in the Manawatū (Dymond et al. 2016), S_t is the total sediment load (t yr^{-1}) generated by hillslope erosion per lake or sea-draining catchment, L_i is the segment length (m) on floodplain in the ith subwatershed, and $accS_i$ is the total accumulated (upstream) sediment load from hillslope erosion (t yr^{-1}) in the ith subwatershed.

Previous applications of SedNetNZ, including those in the Hawke's Bay, used the (NZLRI mapping to define the spatial extent of floodplains. The NZLRI was mapped at a scale of 1:63,360 and may not capture smaller areas of floodplain. In the present work, we use the LiDAR-derived 5 m DEM for Hawke's Bay to identify the extent of floodplains along the digital stream network. For the upgraded SedNetNZ model, we did not seek to model the area of floodplain inundated by the largest flood on record. Instead, we represented the length of channel where flows may go overbank and deposit sediment on floodplains on average over a multi-decadal period (i.e. L_i in equation 13). Therefore, we defined floodplains as areas of low slope land adjacent to the active channel which may be inundated by the average annual maximum flow.

The estimated depth of the average annual maximum flow varied by stream order (1–8) and was defined with reference to annual maximum flows measured at 77 water level gauges across the Hawke's Bay with a mean 27 years of data. The estimated maximum height of floodplains above the channel ranged from 1–5 m, and these were used to identify subwatersheds where sediment may enter floodplain storage. The stream bed and

banks were excluded from the floodplain extent using a 7.5 m buffer either side of the streamlines (i.e. total width of 3 pixels), or mapped extents (i.e., approximating bankfull) for wider channels (Smith & Betts 2021), and a slope threshold of 5 degrees.

To account for sediment trapping through lakes, we applied a lake-specific sediment passing factor (SPF) to the net sediment load at the end of a subwatershed draining to a lake. We calculated SPF using an adaptation of Gill's (1979) approximation of Brune's (1953) trap efficiency (the inverse of passing factor) curve for medium sediment:

$$SPF = 1 - \frac{V/I}{1.02(V/I)+0.012} \quad (14)$$

where V is the lake volume, and I is the annual inflow to the lake.

4 Results

4.1 Regional shallow landslide susceptibility

Rainfall-induced shallow landslide susceptibility was predicted for the Hawke's Bay region, including the area within the Wairoa catchment that extends into the Gisborne region using the BLR model and the LiDAR-derived 5 m DEM (Figure 10). In the present analysis, the BLR model achieved a median AUC of 0.91 in cross-validation. This improves on the predictive performance of the previous BLR model (AUC = 0.75) used to produce the pre-LiDAR landslide susceptibility layer (15 m resolution) for the region based on the national DEM (Smith 2020).

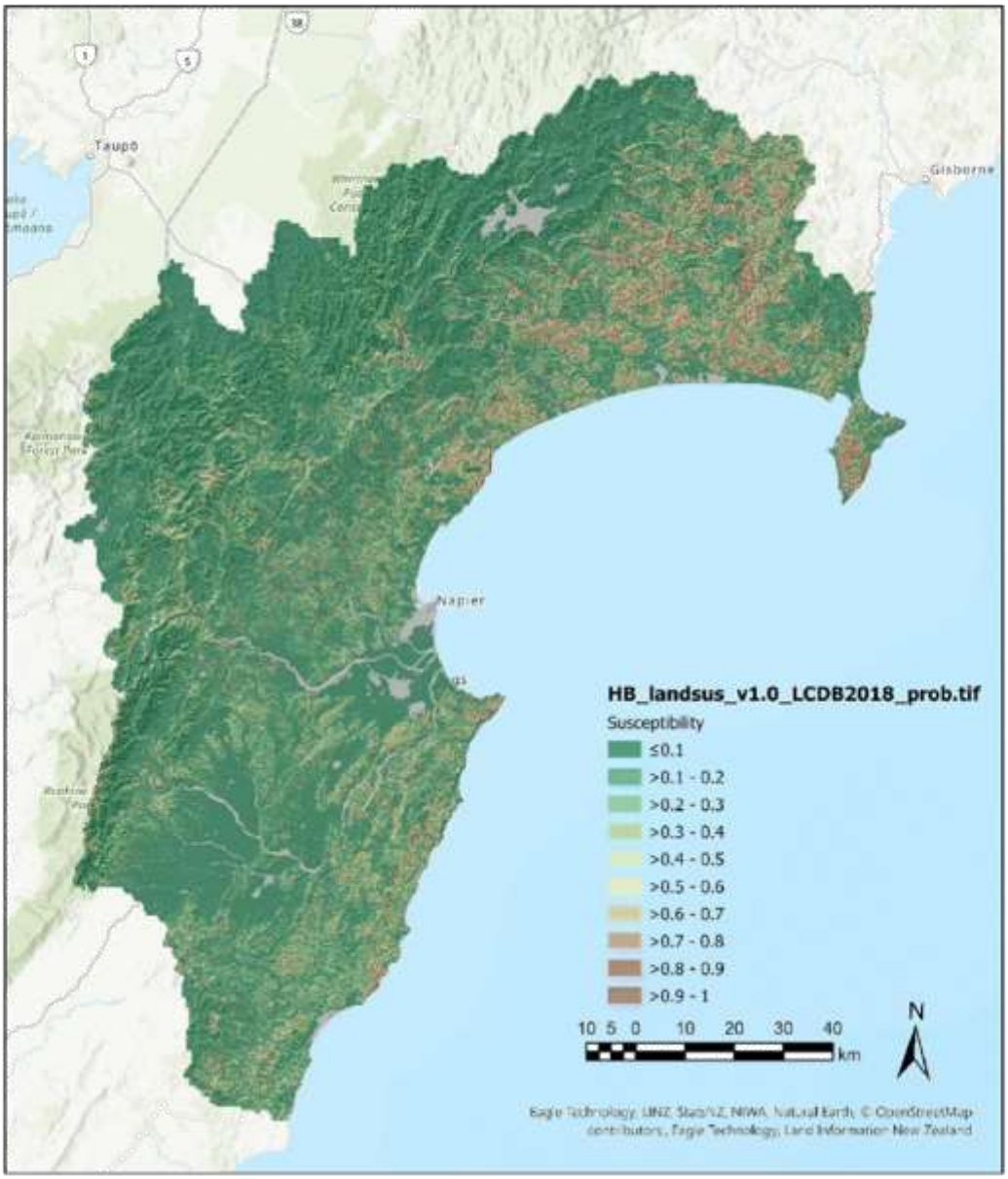

Figure 10. Shallow landslide susceptibility (probability scale) for the Hawke's Bay region based on the LiDAR-derived 5 m DEM and 2018 land cover from LCDB v5.0. Gaps in susceptibility predictions (grey) occur where this information is currently unavailable or for areas that do not produce landslides (e.g., lake water surface).

The improvement in BLR model predictive performance translates to better discrimination of areas with high and low susceptibilities. This is evident from a close-up view comparing spatial probabilities of an area near Frasertown in the Wairoa catchment based on the previous susceptibility layer (15 m resolution) versus the LiDAR-based (5 m) layer (Figure 11). The probability values (range 0–1) represent the spatial likelihood of a future landslide occurring for a given location and not the temporal probability of occurrence. This comparison highlights how the previous layer contains more probability values close to

0.5 (Figure 11a), which shows the lesser ability of this earlier model to discriminate locations as stable or unstable. In contrast, the updated model combined with the LiDAR-derived 5 m DEM produced a susceptibility map which is better able to separate stable (near 0) and unstable (near 1) areas (Figure 11b).

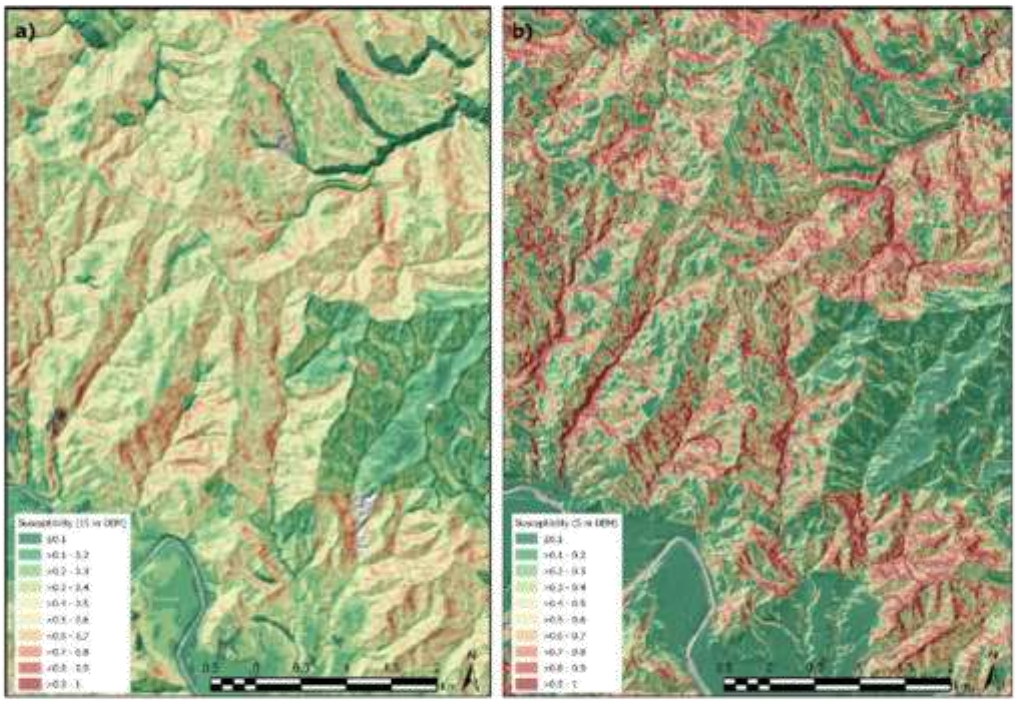

Figure 11. Comparison of shallow landslide susceptibility (probability scale) for an area in the Wairoa catchment (lower Waiau River, northwest of Frasertown) using different approaches: a) susceptibility based on the national 15 m DEM (Smith 2020); b) susceptibility based on the LiDAR-derived 5 m DEM (present report) for 2018 land cover from LCDB v5.0.

The LiDAR-based shallow landslide susceptibility layers were supplied as raster maps (5 m resolution) using probability and class-based scales. These probability values may be converted to a class-based scale. Class thresholds were determined by ranking the landslides used to fit the model by their probability values in decreasing order. 'High' susceptibility corresponds to 80% of the mapped landslides which have probability values ≥ 0.609. 'Moderate' corresponds to a further 15% of the mapped landslides with probability values between 0.282 and < 0.609. 'Low' relates to the remaining 5% of landslides with values < 0.282.

Both the previously supplied 15 m resolution landslide susceptibility layers and the LiDAR-based layers used the same 2018 land cover data from LCDB v5.0. In the present report, we also produced layers where forestry land has been converted to grass cover. Specifically, this involved converting 'Exotic Forest' and 'Forest – Harvested' cover classes in LCDB v5.0 to grass. This provides a common reference condition (i.e. removes woody cover) for comparing the inherent susceptibility of forestry and pastoral land. A summary of the LiDAR-based landslide susceptibility layers supplied with this report is given in Appendix 1.

The data-driven approach for defining classes adopted in the present study differs from the literature-based approach used in Smith (2020) where five susceptibility classes were defined (ranging from 'very low' to 'very high') based on probability threshold values from Rossi et al. (2010). The data-driven approach may be considered an improvement as it relates class thresholds to the underlying landslide data used to train the BLR model and provides a quantitative basis for defining class thresholds. However, this approach still requires a choice of probability thresholds based on a predetermined proportion of the landslide data. In the present case, we used 80% of the landslide inventory to define the 'high' class threshold, as has been applied previously (Spiekermann et al. 2022), and this should ensure a large proportion of future landslides occur within this area.

While acknowledging the difference in derivation of susceptibility classes between Smith (2020) and the present report, it is still possible to compare areas of land within each class to understand the extent of change between the layers. To do this, the 'very low' and 'low' classes from Smith (2020) were combined into 'low' while the 'high' and 'very high' classes were combined into 'high' to compare with the low/moderate/high classes used in the LiDAR-based susceptibility layers (Table 3).

Table 3. Comparison of areas for landslide susceptibility classes based on the national 15 m DEM (Smith 2020) versus the LiDAR-derived 5 m DEM (present report)

National 15 m DEM (Smith 2020)			LiDAR-derived 5 m DEM (present report)		
Susceptibility class	Area (km^2)	Area (%)	Susceptibility class	Area (km^2)	Area (%)
Low[a]	12,312	87	Low	12,363	81
Moderate	1,015	7	Moderate	1,702	11
High[b]	770	5	High	1,125	7

[a] Low combines 'very low' and 'low' susceptibility classes from Smith (2020).

[b] High combines the 'high' and 'very high' susceptibility classes from Smith (2020).

A comparison of layers showed a decrease in the percentage area under the 'low' class and an increase in the area under 'moderate' and 'high' classes with the LiDAR-based landslide susceptibility layer (Table 3). The percentage of land classed as 'moderate' or 'high' increased from 12% to 18% using the LiDAR-based layer. This equates to an increase in area of 'moderate' or 'high' susceptibility land from 1,785 to 2,827 km^2 under 2018 land cover. It was also possible to predict susceptibility for a larger area in our LiDAR-based layers (15,190 km^2) compared to the previous layer (14,097 km^2). Areas without a susceptibility prediction occur where there is either insufficient information to fit the model or the areas do not produce landslides (e.g. lake and river water surfaces).

4.2 Regional SedNetNZ erosion and sediment load model

The regional layers associated with the LiDAR-based version of SedNetNZ that accompany the present report are summarised in Appendix 2.

4.2.1 Shallow landslide erosion

Shallow landslide erosion may be expressed as the mean annual suspended sediment yield from shallow landslides delivered to the stream network. This representation of shallow landslide erosion does not imply landslide erosion occurs every year but instead averages on an annual basis the sediment load generated by discrete landslide-triggering events that occur over multi-decadal intervals. This approach allows for the construction of sediment budgets where the contributions from each erosion process may be expressed in the same units: either as suspended sediment loads (t yr^{-1}) or yields (t km^{-2} yr^{-1}).

The spatial pattern in net sediment yields from shallow landslides across the Hawke's Bay region is shown in Figure 12. This figure presents the estimated mean annual net sediment yield per pixel. These pixel-based yields form the basis for computing the landslide sediment load for each subwatershed in the digital stream network. The highest net sediment yields (> 2,000 t km^{-2} yr^{-1}) from shallow landslide erosion occur most extensively in the Wairoa catchment in northern Hawke's Bay, and on comparable soft rock pastoral hill country terrain in central and southern areas of the region. In contrast, the forested hard rock terrain has significantly lower net sediment yields (< 500 t km^{-2} yr^{-1}) from landslide erosion, which reflects the lower susceptibility of this terrain to the occurrence of landslides (Figure 10).

The total net suspended sediment load delivered to the stream network from shallow landslide erosion amounted to 5.4 Mt yr^{-1} for the region using the upgraded shallow landslide sub-model with the LiDAR-derived DEM.

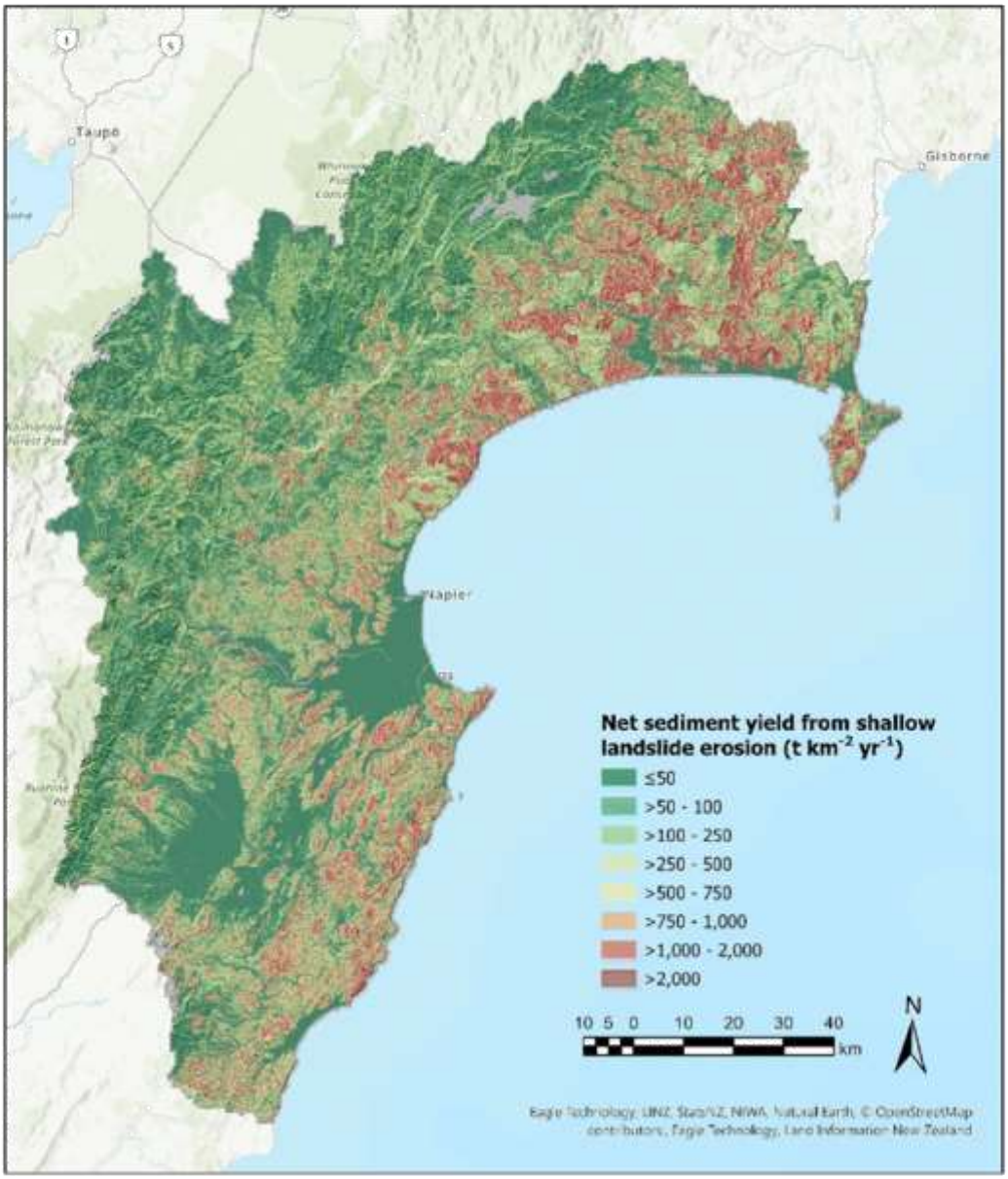

Figure 12. Mean annual suspended sediment yield (t km^{-2} yr^{-1}) from rainfall-induced shallow landslide erosion delivered to the stream network based on 2018 land cover from LCDB v5.0 and displayed over the underlying hillshade layer.

4.2.2 Surface erosion

Net suspended sediment yields from surface erosion (sheet and rill erosion) delivered to the stream network are shown in Figure 13. The spatial pattern in surface erosion reflects spatial variations in the RUSLE factors. Higher rainfall erosivity tends to occur over elevated terrain due to orographic effects that produce higher rainfall. Soil erodibility increases where surface soils have lower organic matter and higher silt content. Steep and convergent terrain concentrates surface runoff that may increase erosion, while vegetation

cover has a critical role in protecting the soil surface from raindrop impact and increasing surface roughness that reduces overland flow velocities.

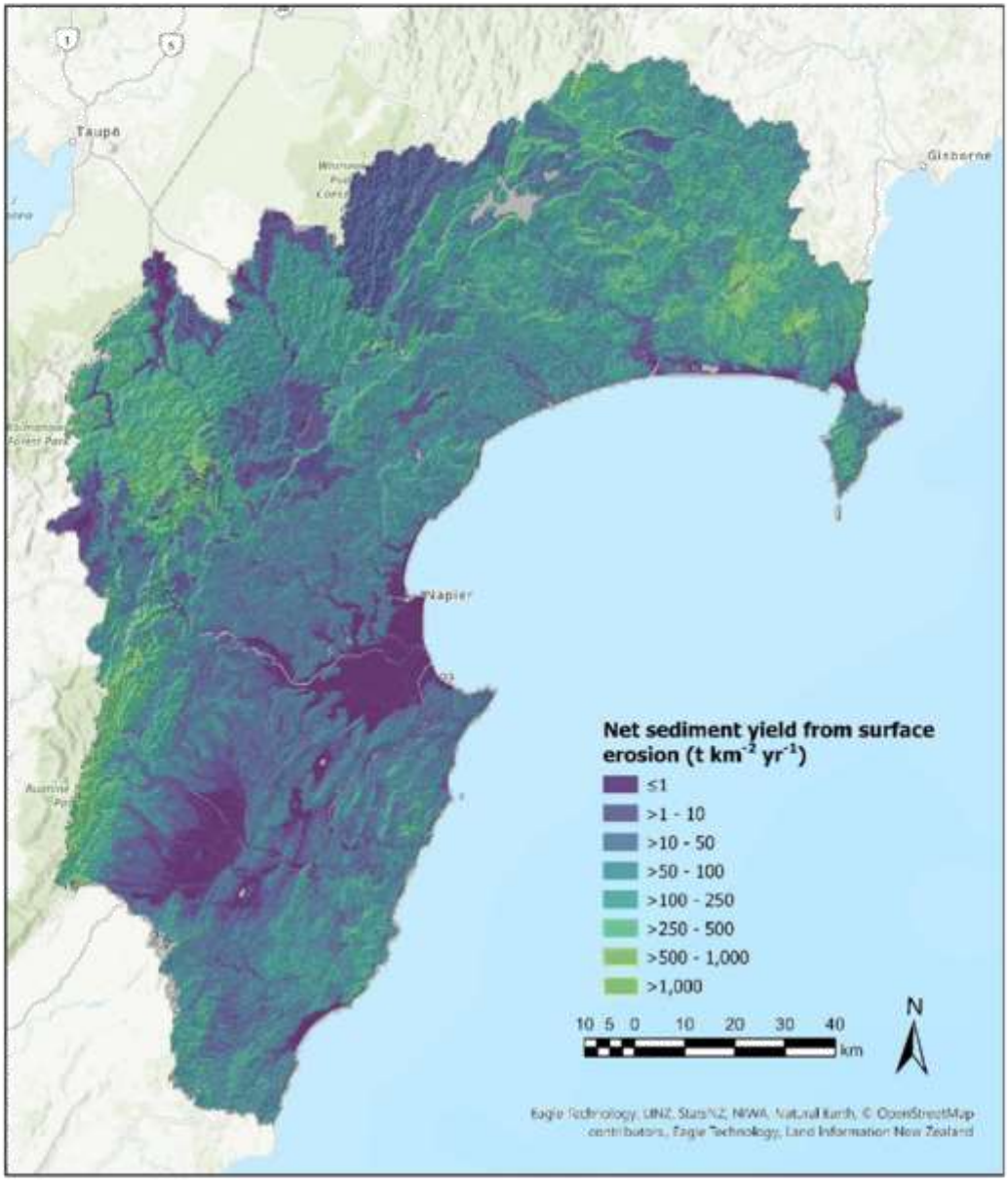

Figure 13. Mean annual suspended sediment yield (t km^{-2} yr^{-1}) from surface erosion delivered to the stream network based on 2018 land cover from LCDB v5.0 displayed over the underlying hillshade layer.

Within the Hawke's Bay region, the highest surface erosion rates (>1000 t km^{-2} yr^{-1}) tend to occur in hilly and mountainous areas with higher rainfall and steep, convergent terrain (Figure 13). Within these areas, those locations lacking vegetation cover or where soils tend to have higher silt content exhibit higher surface erosion rates. The net suspended

sediment load delivered to the stream network from surface erosion amounted to 1.7 Mt yr^{-1} for the region using the RUSLE sub-model with the LiDAR-derived DEM.

4.2.3 Riverbank erosion

Bank migration sub-models were compared based on differences between measured and modelled reach-averaged migration rates. Sub-model fitting in each case used all the data, whereas predictive performance was evaluated independently through cross-validation. The original 'Process – O' results were assessed with nearly 40 km of channel mapping data from the Manawatū catchment and do not include LiDAR-derived DEM inputs (Smith et al. 2019a), whereas this model was fitted using 77 km of channel data (Manawatū augmented with data from the Kaipara harbour catchment) when applied in the Hawke's Bay region (Smith et al. 2020). In contrast, sub-model calibration for the remaining three sub-models based on LiDAR DEM inputs was performed with over 800 km of channel change data.

There is a general reduction in RMSE and MAE (expressed in units of m yr^{-1}) between the 'Process – O', 'Process – U', GAM, and RF sub-models (Table 4). The 'Process – O' results reflect the previous sub-model performance using the limited data originally available for calibration. The 'Process – U', GAM, and RF cross-validation results based on the expanded data set show RF produced the least error both in fitting and prediction (Table 4). Therefore, the RF sub-model was selected for use in predicting reach-average bank migration rates.

Table 4. Comparison of error statistics from sub-model fitting using all data and predictive performance in cross-validation (RMSE = root mean square error; MAE = mean absolute error)

Procedure	Error statistic	Sub-models			
		Process - O	Process - U	GAM	RF
Fitting	RMSE	0.78	0.38	0.36	0.15
	MAE	0.65	0.14	0.17	0.06
Prediction	RMSE	1.1	0.37	0.39	0.31
	MAE	0.76	0.14	0.18	0.14

The new approach for estimating mean bank height for stream segments significantly improved on the previous approach based on mean annual discharge. Figure 14 shows the improved correlation between the estimated mean bank height compared to direct point-based measurements using the DEM. The coefficient of determination (R^2) relative to the 1:1 line increased from 0.40 to 0.66 for estimates of mean bank height based on mean annual discharge versus the LiDAR based approach, respectively. Despite this improvement, the scatter in bank height values suggests that there may be some scope for further refinement in the future.

Net bank erosion as a proportion of gross bank erosion was estimated at 0.28 based on the channel planform and bank height mapping data from Hawke's Bay. This is

comparable to the 0.20 estimate used in previous SedNetNZ modelling. While both estimates are subject to considerable uncertainty, their consistency suggests that these values may provide a reasonable approximation for determining net bank erosion. Further work to quantify erosion and accretion at reach scale could use repeated LiDAR surveys and compare the difference in DEMs to quantify volumetric changes.

The updated estimate of net suspended sediment loads from riverbank erosion combined bank migration rates from the RF sub-model with the LiDAR-based estimates of mean bank height per stream segment, and the revised estimate of the proportion of net to gross bank erosion based on the newly acquired mapping data. The RF sub-model was fitted 100 times (mean R^2 = 0.87) using all available bank migration data and the mean predicted bank migration rate per stream segment was used for estimating suspended sediment loads from bank erosion.

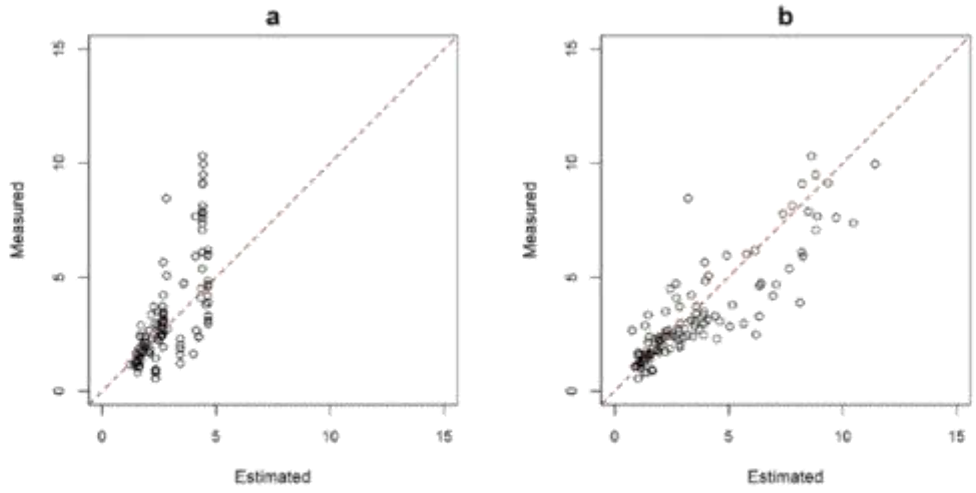

Figure 14. Reach-average bank height (m) correlations based on: a) previous bank height relationship with mean annual discharge versus measured bank heights; and b) LiDAR-based spatial estimate versus measured bank heights. The measured bank heights are based on mean values for stream segments (*n* = 110) with ≥30 discrete height measurements (total *n* = 5,643 measurements).

The mean net suspended sediment load from bank erosion equated to 1.0 Mt yr^{-1} for the region. The variance associated with repeated fitting of the RF sub-model was low (standard deviation = 0.02 Mt yr^{-1}). This total net load compares with 0.70 Mt yr^{-1} based on the previous estimate for the region (Smith et al. 2020). Most of this increase in sediment load from bank erosion was attributable to the increase in the length of the digital stream network. The length of the REC2 digital network is 24,595 km compared to 39,487 km for the LiDAR DEM–derived digital network with a 10-ha channel initiation threshold. This increase in network length partly reflects the improved representation of channel sinuosity based on the LiDAR-derived DEM. The mean net suspended sediment load per metre length of channel decreased slightly from 0.028 to 0.026 t m^{-1} yr^{-1} between the previous and the LiDAR-based estimates. Figure 15 shows the spatial pattern in net suspended sediment yields from bank erosion per metre of stream segment.

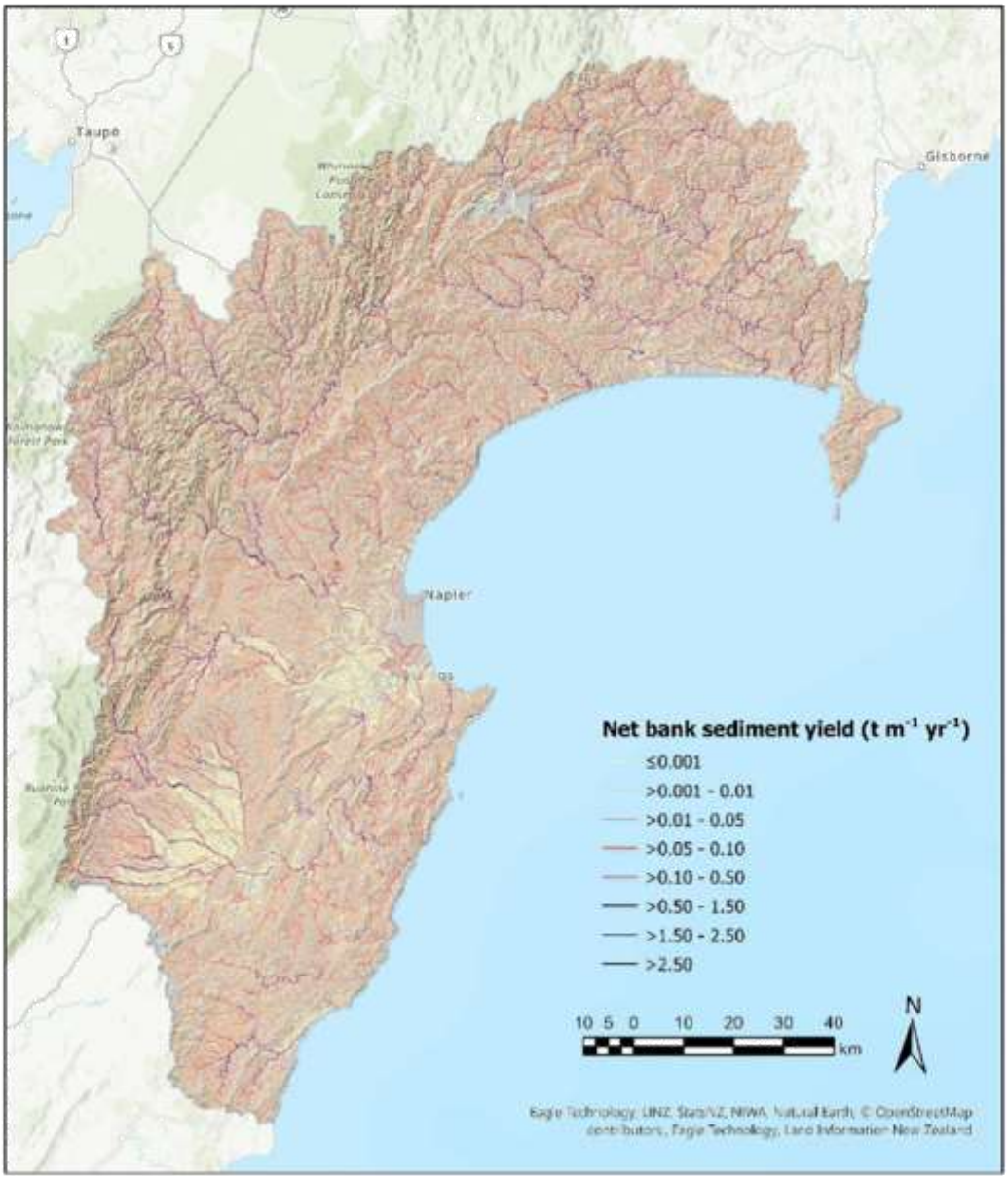

Figure 15. Predicted reach-averaged net bank suspended sediment yield (t m^{-1} yr^{-1}) per stream segment length for each segment in the LiDAR DEM-derived digital network.

4.2.4 Region-wide suspended sediment budget

The erosion process contributions to suspended sediment loads in the LiDAR-based SedNetNZ sediment budget for the region are summarised in Table 5. We compared these loads with estimates for the previous version of SedNetNZ applied in the region. The shallow landslide, surface, and riverbank erosion loads increased when estimated using the LiDAR-version of the model compared to the previous model version. However, the percentage contributions from the erosion processes are similar between model versions with shallow landslide erosion contributing the largest proportion on average followed by

surface erosion and riverbank erosion (Table 5). While no modifications were made to the gully and earthflow process representation in the LiDAR-based version of the model, minor differences in load arise due to differences in land cover between the present report (LCDB v5.0 from 2018) and the earlier modelling in the region that used LCDB v4.1 (from 2012).

Table 5. Comparison of region-wide suspended sediment loads estimated using the LiDAR based SedNetNZ versus the previous version of the model applied in Hawke's Bay

Estimated sediment loads delivered to the stream network	Previous SedNetNZ		LiDAR SedNetNZ	
	Suspended sediment load (Mt yr^{-1})	Percentage contribution to total load	Suspended sediment load (Mt yr^{-1})	Percentage contribution to total load
Shallow landslide erosion	4.9	66	5.4	64
Surface erosion	1.5	19	1.7	19
Riverbank erosion	0.70	9	1.0	12
Gully erosion	0.13	2	0.15[a]	2
Earthflow erosion	0.27	4	0.27[a]	3
Total load delivered to the stream network	7.5		8.5	
Total net load delivered to the coast[b]	7.2		8.0	

[a] Differences in gully and earthflow suspended sediment loads reflect differences in land cover between the present report (LCDB v5.0, 2018) versus earlier SedNetNZ modelling in Hawke's Bay that was based on LCDB v4.1 (2012). These erosion process sub-models did not undergo modification.

[b] Total net load delivered to the coast = total load delivered to the stream network less the sediment load entering long-term storage in lakes and on floodplains.

The total suspended sediment load delivered to the stream network increased from 7.5 to 8.5 Mt yr^{-1} between the previous and LiDAR model versions, respectively, while the net load delivered to the coast increased from 7.2 to 8.0 Mt yr^{-1} (Table 5). The total suspended sediment load per subwatershed is shown in Figure 16. These are net suspended sediment loads that accumulate downstream while accounting for losses of sediment into long-term storage in lakes and on floodplains. By ranking coast-draining subwatersheds (i.e. NextDownID = -1), we can identify those rivers with the largest mean annual suspended sediment loads reaching the coast. The top five ranked rivers (and their loads) comprise the Wairoa (2.4 Mt yr^{-1}), Ngaruroro including Tūtaekurī (1.3 Mt yr^{-1}), Tukituki (1.1 Mt yr^{-1}), Mohaka (0.87 Mt yr^{-1}), and Pōrangahau (0.54 Mt yr^{-1}).

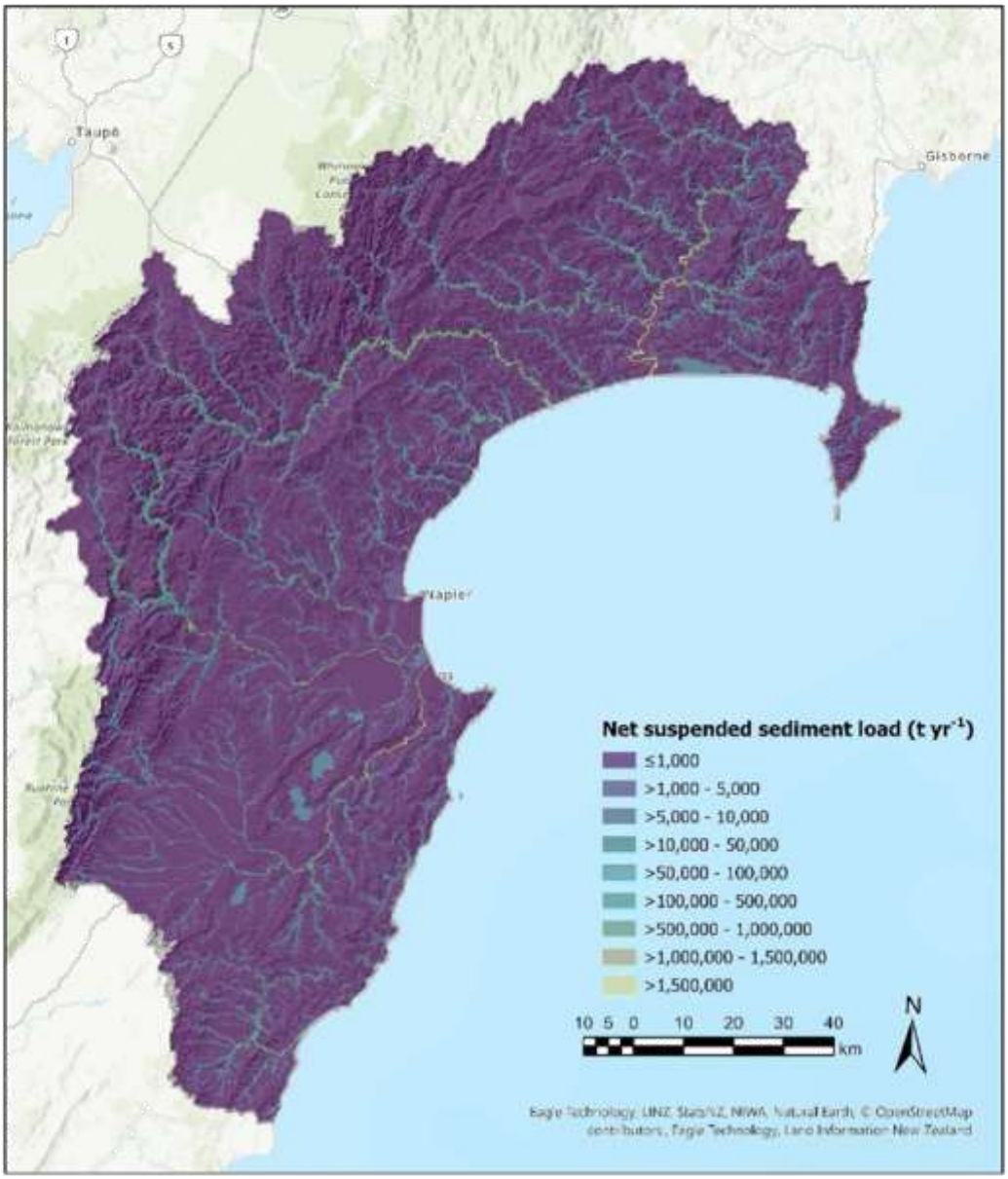

Figure 16. Net suspended sediment load (t yr^{-1}) accumulated downstream based on 2018 land cover from LCDB v5.0 displayed for subwatersheds over the underlying hillshade layer.

Figure 17 shows the spatial pattern in suspended sediment yields (t km^{-2} yr^{-1}) per subwatershed across the region. The sediment yield was calculated as the sum of net suspended sediment loads from each erosion process present within each subwatershed divided by the subwatershed area. This does not account for downstream storage of sediment in lakes and on floodplains. The largest sediment yields typically occur in areas of pastoral hill country on erodible, soft rock terrain as well as along sections of eroding river channel. Lower sediment yields occur in areas with woody vegetation cover or low slope. In a few cases, high yields (t km^{-2} yr^{-1}) occur in subwatersheds despite having relatively low erosion (t yr^{-1}) due to the very small areas of these subwatersheds (< 0.005 km^2).

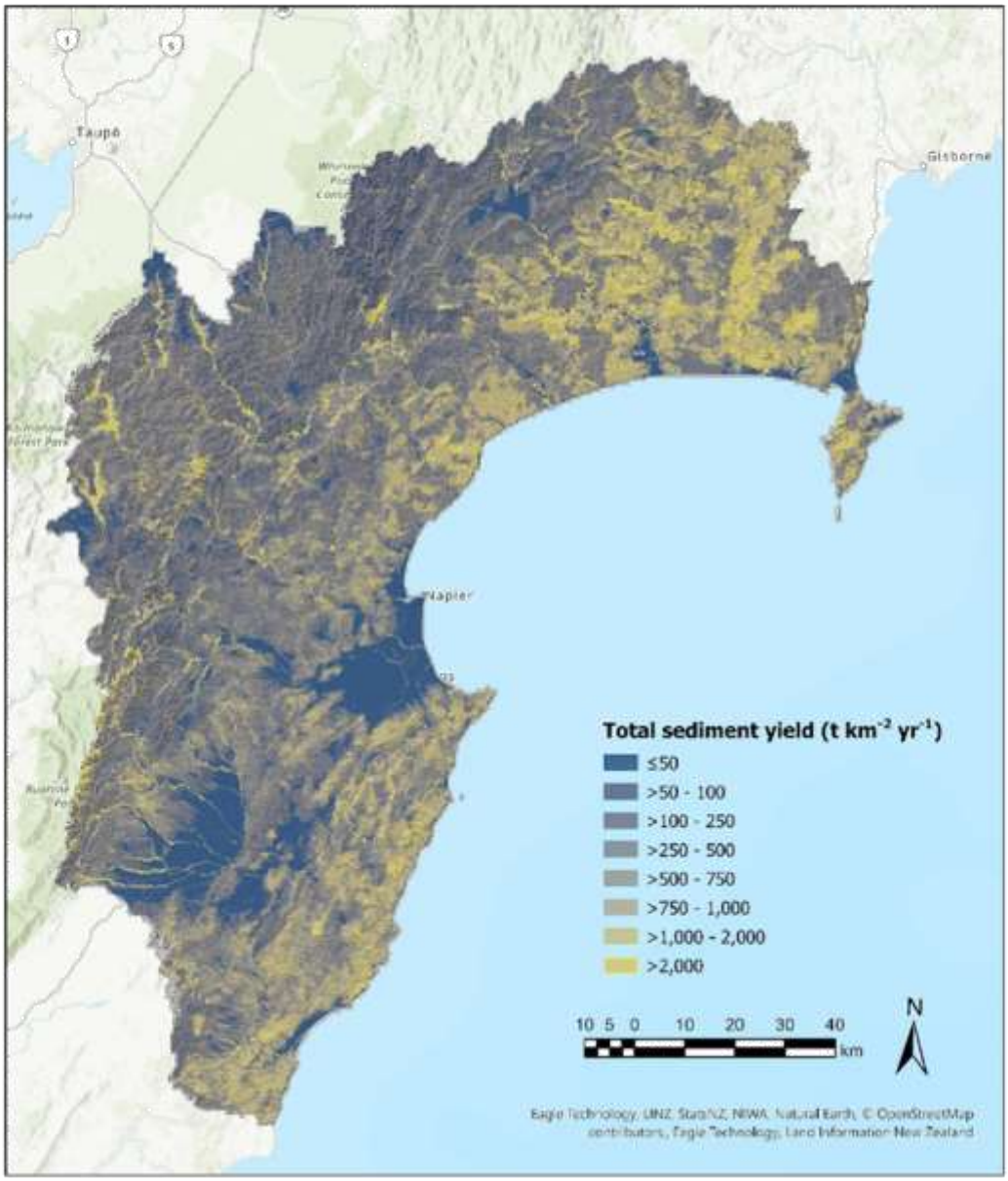

Figure 17. Total suspended sediment yield (t km^{-2} y^{-1}) per subwatershed for the LiDAR-based digital network based on 2018 land cover from LCDB v5.0 displayed over the underlying hillshade layer.

4.2.5 SedNetNZ model evaluation

SedNetNZ is designed to predict spatial patterns in erosion and suspended sediment load on a mean annual basis for periods spanning decades. It is difficult to quantify a model's performance over such time scales other than through comparison with measurements of suspended sediment load, which has been the main form of SedNetNZ model evaluation (Basher et al. 2018). Often, longer term suspended sediment load data are unavailable. However, various rivers have been monitored in the Hawke's Bay region and the resulting

suspended sediment concentration (SSC) and discharge (Q) data have been used to estimate mean annual suspended sediment loads via SSC-Q rating curve methods (Hicks et al. 2019).

Comparing the LiDAR-based SedNetNZ estimates of mean annual suspended sediment loads with the SSC-Q rating curve estimates gives an R^2 = 0.67 (n = 16) relative to the 1:1 line. While this improves on the previous non-LiDAR SedNetNZ estimates of sediment loads (R^2 = 0.55), there is considerable scatter in both relationships (Figure 18). One limitation of these rating curve-based estimates of mean annual suspended sediment load relates to the monitoring period. The suspended sediment and flow data end before 1997 for the sites in Hawke's Bay (Hicks et al. 2019), thus reflecting periods that experienced differences in hydro-climatic conditions, land cover, and the extent of erosion control (i.e. tree planting etc.) compared to the contemporary state. Nonetheless, these rating curve-based estimates span multi-decadal periods – and that has an important averaging effect, that is essential when comparing with SedNetNZ load predictions. Shorter records are more likely to be influenced by the specific rainfall, river flow, and sediment transport conditions observed during those intervals. For instance, short monitoring intervals may not capture the impact of landslide-triggering events that occur episodically and contribute significant quantities of sediment to the stream network.

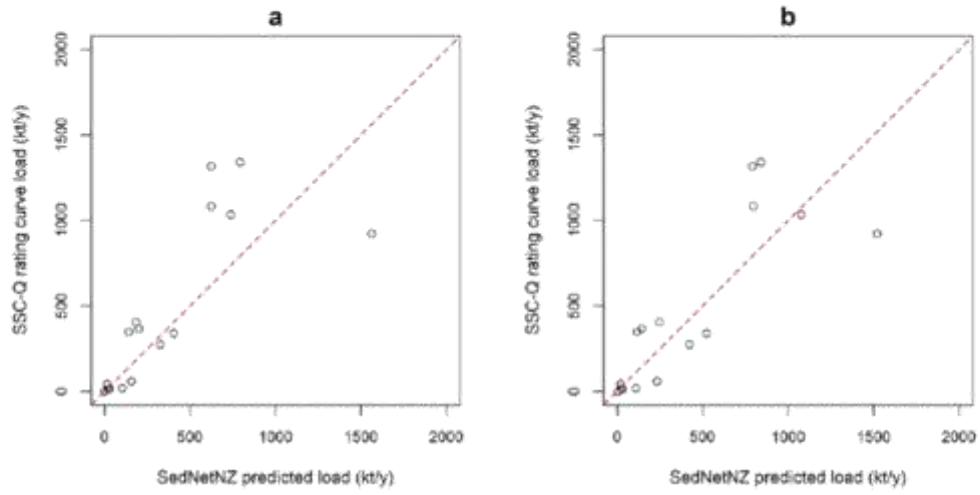

Figure 18. Comparison of SSC-Q rating curve estimates of mean annual suspended sediment load versus model predictions for: a) previous SedNetNZ; and b) LiDAR-based SedNetNZ loads.

5 Conclusions

The present report describes work undertaken to improve erosion models in the Hawke's Bay region using the 2020–2021 regional LiDAR coverage. The scope of work involved upgrading the existing regional landslide susceptibility and SedNetNZ sediment budget models to use the higher resolution LiDAR-derived topographic data alongside the targeted acquisition of new data for improved model parameterisation.

The benefits of using higher resolution LiDAR-derived DEMs in erosion and sediment load modelling include: a) improved model parameterisation and predictive performance due to the more accurate representation of topography (e.g. slope angles, curvature); b) better representation of the stream network (e.g. channel sinuosity, channel slope, bank height); c) the ability to provide higher resolution raster layers for selected erosion processes, namely shallow landslide, and surface erosion.

The upgrade to the shallow landslide susceptibility model improved predictive performance based on LiDAR-derived topographic inputs and an expanded landslide inventory (56,000 to 116,000 mapped landslides). The susceptibility model based on LiDAR-derived 5 m DEMs achieved a median AUC of 0.91 in cross-validation compared to an AUC of 0.75 for the pre-LiDAR landslide susceptibility model that was based on the national 15 m DEM.

Region-wide predictions of landslide susceptibility were produced as raster layers with probability and class-based scales for contemporary land cover (LCDB v5.0 2018) and for land cover where LCDB-mapped forestry land was converted to grass cover. This forestry-to-grass conversion provided a common reference condition for comparing the inherent susceptibility of forestry and pastoral land. The landslide susceptibility layers give land managers higher resolution, data-driven spatial information that may be used to better target tree planting to those pastoral areas most susceptible to slope instability.

Upgrading the SedNetNZ model to use LiDAR-derived DEMs focused on the shallow landslide, surface, and riverbank erosion sub-models. The new LiDAR-based version of SedNetNZ now incorporates high-resolution landslide susceptibility in the shallow landslide erosion sub-model. The surface erosion sub-model is based on a full implementation of the RUSLE model using LiDAR-derived topographic inputs. The previous riverbank erosion sub-model has been replaced with a data-driven approach that draws on expanded data sets of channel planform change (increased from 77 to over 800 km of mapped channels) and bank height.

As part of the upgraded SedNetNZ model, we produced and refined the digital stream network and subwatershed layers using the LiDAR-derived 5 m DEM. The subwatershed layer forms the basis for constructing suspended sediment budgets. The new LiDAR-based SedNetNZ model estimated a total region-wide suspended sediment load delivered to the coast of 8.0 Mt yr^{-1}, which compares to 7.2 Mt yr^{-1} using the previous model. The LiDAR-based model also showed improved agreement with longer term estimates of mean annual suspended sediment loads from stream gauging sites in the region.

The upgraded SedNetNZ model provides both improved predictions of contributions from erosion processes to suspended sediment loads as well as high resolution raster layers for shallow landslide and surface erosion not previously available that may be used to better support land and water planning in the region.

6 Acknowledgements

We acknowledge Hawke's Bay Regional Council (HBRC) and Manaaki Whenua – Landcare Research (MWLR) for jointly funding this work as part of the HBRC-MWLR LiDAR Partnership Project. MWLR's contribution to the project was supported by the Strategic Science Investment Fund (SSIF) allocated to MWLR. We specifically acknowledge and thank Ashton Eaves, Tim Farrier, Anna Madarasz-Smith, Therese Kaul, Kathleen Kozyniak, and Andrew Burton from the HBRC for their advice and input to the project and the work described in this report.

7 References

Basher LR 2013. Erosion processes and their control in New Zealand: ecosystem services in New Zealand – conditions and trends 2013. Lincoln, Manaaki Whenua Press. Pp. 363–374.

Basher L, Spiekermann R, Dymond J, Herzig A, Ausseil A-G 2018. SedNetNZ, SLUI and contaminant generation. Part1: Sediment and water clarity. Manaaki Whenua – Landcare Research contract report LC3135, prepared for Horizons Regional Council.

Betts H, Basher L, Dymond J, Herzig A, Marden M, Phillips C 2017. Development of a landslide component for a sediment budget model. Environmental Modelling & Software 92: 28–39.

Betts H, Smith HG, Neverman A, Tsyplenkov A, 2023. Wairoa shallow landslide and debris deposit mapping following storm events in March 2022. Landcare Research Contract Report LC4331 for Hawke's Bay Regional Council.

Breiman L 2001. Random forests. Machine Learning 45: 5-32.

Brune GM 1953. Trap efficiency of reservoirs. Eos, Transactions American Geophysical Union 34(3): 407–418.

Carter JV, Pan J, Rai SN, Galandiuk S 2016. ROC-ing along: evaluation and interpretation of receiver operating characteristic curves. Surgery 159: 1638–1645.

Chouldechova A, Hastie T 2022. gamsel: Fit regularization path for generalized additive Models. R package version 1.8-2. https://CRAN.R-project.org/package=gamsel

Conoscenti C, Rotigliano E, Cama M, Caraballo-Arias N, Lombardo L, Agnesi V 2016. Exploring the effect of absence selection on landslide susceptibility models: a case study in Sicily, Italy. Geomorphology 261: 222–235.

De Rose R, Basher LR. 2011. Measurement of river bank and cliff erosion from sequential LiDAR and historical aerial photography. Geomorphology. 126:132–147.

Desmet P, Govers G 1996. A GIS procedure for automatically calculating the USLE LS factor on topographically complex landscape units. Journal of Soil and Water Conservation 51(5): 427–433.

Donovan M, 2022. Modelling soil loss from surface erosion at high-resolution to better understand sources and drivers across land uses and catchments: a national-scale assessment of Aotearoa, New Zealand. Environmental Modelling & Software 147: 105228. https://doi.org/10.1016/j.envsoft.2021.105228

Dymond JR, Betts HD, Schierlitz CS 2010. An erosion model for evaluating regional land-use scenarios. Journal of Environmental Modelling Software 25(3): 289–298.

Dymond JR, Herzig A, Basher L, Betts HD, Marden M, Phillips CJ, Ausseil A-G, Palmer DJ, Clark M, Roygard J 2016. Development of a New Zealand SedNet model for assessment of catchment-wide soil-conservation works. Geomorphology 257: 85–93.

Dymond J, Herzig A, Betts H, Marden M, Phillips C, Basher L 2013. Parameterisation of SedNetNZ for the Manawatu catchment. Landcare Research Contract Report LC1503 prepared for AgResearch and the Ministry of Business, Innovation and Employment.

Elliott AH, Semadeni-Davies AF, Shankar U, Zeldis JR, Wheeler DM, Plew DR, et al. 2016. A national-scale GIS-based system for modelling impacts of land use on water quality. Environmental Modelling & Software 86: 131–144.

Eyles GO 1983. The distribution and severity of present soil erosion in New Zealand. New Zealand Geographer 39(1): 12–28.

Foster GR, Meyer LD, Onstad CA 1977. A runoff erosivity factor and variable slope length exponents for soil loss estimates. Transactions of the ASAE 20(4): 683–687.

Fuller IC, Riedler RA, Bell R, Marden M, Glade T 2016. Landslide-driven erosion and slope-channel coupling in steep, forested terrain, Ruahine Ranges, New Zealand, 1946–2011. Catena 142: 252–268.

Gill MA 1979. Sedimentation and useful life of reservoirs. Journal of Hydrology 44(1): 89-95.

Hicks DM, Semadeni-Davies A, Haddadchi A, Shankar U, Plew D 2019. Updated sediment load estimator for New Zealand. NIWA Client Report 2018341CH prepared for Ministry for the Environment. Christchurch, NIWA.

Klik A, Haas K, Dvorackova A, Fuller IC 2015. Spatial and temporal distribution of rainfall erosivity in New Zealand. Soil Research 53: 815–825.

Leathwick J, Wilson G, Rutledge D, Wardle P, Morgan F, Johnston K, McLeod M, Kirkpatrick R 2003. Land Environments of New Zealand. Auckland, David Bateman.

Land Information New Zealand (LINZ) 2020. PGF Version: New Zealand National Aerial LiDAR base specification. Land Information New Zealand.

Liaw A, Wiener M. 2002. Classification and regression by randomForest. R News 2(3): 18–22.

Marden M 2012. Effectiveness of reforestation in erosion mitigation and implications for future sediment yields, East Coast catchments, New Zealand: a review. New Zealand Geographer 68: 24–35.

McCool DK, Foster GR, Mutchler CK, Meyer LD 1989. Revised slope length factor for the universal soil loss equation. Transactions of the ASAE 32(5): 1571–1576.

Nearing MA, Yin S, Borrelli P, Polyakov VO 2017. Rainfall erosivity: an historical review. Catena 157: 357-362.

Neverman AJ, Smith HG, Herzig A, Basher L 2021. Modelling baseline suspended sediment loads and load reductions required to achieve Draft Freshwater Objectives for Southland. Landcare Research Contract Report LC3749 prepared for Environment Southland.

Newsome PFJ, Wilde RH, Willoughby EJ 2008. Land Resource Information System spatial data layers: data dictionary. Palmerston North, Landcare Research. http://digitallibrary.landcareresearch.co.nz/cdm/ref/collection/p20022coll14/id/67.

Page MJ, Trustrum NA, Dymond JR 1994. Sediment budget to assess the geomorphic effect of a cyclonic storm, New Zealand. Geomorphology 9(3): 169–188.

Palmer D, Dymond J, Basher L, Ausseil A-G, Herzig A, Betts H, Spiekermann R 2017. SedNetNZ modelling to evaluate and quantify sediment sources from the Tukituki catchment, Hawke's Bay. Manaaki Whenua – Landcare Research Contract Report LC1991 prepared for Hawke's Bay Regional Council.

Palmer D, Dymond J, Mueller M, Herzig A, Spiekermann R, Basher L 2016. SedNetNZ modelling to estimate sediment sources from the TANK, South Coast, and Porangahau watersheds. Manaaki Whenua – Landcare Research Contract Report LC2599 prepared for Hawke's Bay Regional Council.

Phillips C, Basher L, Spiekermann R 2020. Biophysical performance of erosion and sediment control techniques in New Zealand: a review. Landcare Research Contract Report LC3761 prepared for the Smarter Targeting of Erosion Control (STEC) MBIE research programme.

Phillips C, Hales T, Smith H, Basher L 2021. Shallow landslides and vegetation at the catchment scale: a perspective. Ecological Engineering173: 106436. https://doi.org/10.1016/j.ecoleng.2021.106436.

Phillips C, Marden M, Basher LR 2018. Geomorphology and forest management in New Zealand's erodible steeplands: an overview. Geomorphology 307: 107-121.

Reichenbach P, Rossi M, Malamud BD, Mihir M, Guzzetti F 2018. A review of statistically-based landslide susceptibility models. Earth-Science Reviews 180: 60–91.

Reid LM, Page MJ 2002. Magnitude and frequency of landsliding in a large New Zealand catchment. Geomorphology 49: 71-88.

Renard KG 1997. Predicting soil erosion by water: a guide to conservation planning with the Revised Universal Soil Loss Equation (RUSLE). Washington, DC, United States Government Printing.

Rosewell CJ, Loch RJ 2002. Estimation of the RUSLE soil erodibility factor. In: McKenzie N, Coughlan K, Cresswell H eds. Soil physical measurement and interpretation for land evaluation. Melbourne, Australia, CSIRO Publishing. Pp. 361–369.

Rossi M, Guzzetti F, Reichenbach P, Mondini AC, Peruccacci S 2010. Optimal landslide susceptibility zonation based on multiple forecasts. Geomorphology 114: 129–142.

Smith HG 2020. A region-wide assessment of shallow landslide susceptibility in Hawke's Bay. Landcare Research Contract Report LC3720 for Hawke's Bay Regional Council.

Smith HG, Betts H 2021. Memorandum on implementing a national index for susceptibility to streambank erosion. Landcare Research Contract Report LC3998 prepared for the Ministry for the Environment.

Smith HG, Herzig A, Dymond J, Basher L 2019b. Application of a revised SedNetNZ model to the Oreti and Aparima catchments, Southland. Landcare Research Contract Report LC3507 prepared for the Our Land and Water National Science Challenge.

Smith HG, Neverman AJ, Betts H, Spiekermann R 2023. The influence of spatial patterns in rainfall on shallow landslides. Geomorphology 437: 108795. https://doi.org/10.1016/j.geomorph.2023.108795

Smith HG, Spiekermann R, Betts H, Neverman AJ 2021. Comparing methods of landslide data acquisition and susceptibility modelling: Examples from New Zealand. Geomorphology 381: 107660. https://doi.org/10.1016/j.geomorph.2021.107660

Smith HG, Spiekermann R, Dymond J, Basher L 2019a. Predicting spatial patterns in riverbank erosion for catchment sediment budgets. New Zealand Journal of Marine and Freshwater Research 53: 338–362.

Smith HG, Spiekermann R, Herzig A, Dymond J 2020. Application of a revised bank erosion model to update SedNetNZ results for Hawke's Bay. Landcare Research Contract Report LC3740 prepared for Hawke's Bay Regional Council.

Spiekermann R, Betts H, Dymond J, Basher L 2017. Volumetric measurement of river bank erosion from sequential historical aerial photography. Geomorphology 296: 193–208.

Spiekermann RI, McColl S, Fuller I, Dymond J, Burkitt L, Smith HG 2021. Quantifying the influence of individual trees on slope stability at landscape scale. Journal of Environmental Management 286: 112194. https://doi.org/10.1016/j.jenvman.2021.112194

Spiekermann RI, Smith HG, McColl S, Burkitt L, Fuller IC 2022. Quantifying effectiveness of trees for landslide erosion control. Geomorphology 396: 107993. https://doi.org/10.1016/j.geomorph.2021.107993

Vale SS, Smith HG, Neverman A, Herzig A 2021. Application of SedNetNZ with land management and climate change scenarios and temporal disaggregation in the Bay of Plenty Region. Manaaki Whenua – Landcare Research contract report LC4002, prepared for Bay of Plenty Regional Council.

Wang G, Gertner G, Liu X, Anderson A 2001. Uncertainty assessment of soil erodibility factor for revised universal soil loss equation. Catena 46(1): 1–14.

Wischmeier WH, Smith DD 1978. Predicting rainfall erosion losses– a guide to conservation planning, agriculture handbook. Indiana, USA, United States Department of Agriculture.

Woods R, Hendrikx J, Henderson R, Tait A 2006. Estimating mean flow of New Zealand rivers. Journal of Hydrology New Zealand 45(2): 95–109.

Yang X, Gray J, Chapman G, Zhu Q, Tulau M, McInnes-Clarke S 2018. Digital mapping of soil erodibility for water erosion in New South Wales, Australia. Soil Research 56(2): 158–170.

Appendix 1

Table A1.1. Summary of the rainfall-induced shallow landslide susceptibility layers based on the LiDAR-derived 5 m DEM supplied with the present report

Layer name	Description
HB_landsus_v1.0_LCDB2018_prob.tif	Raster layer (5 m grid) of rainfall-induced shallow landslide susceptibility based on a spatial probability scale (0-1) from the BLR model predictions using 2018 land cover from LCDB v5.0.
HB_landsus_v1.0_forestrytograss_prob.tif	Raster layer (5 m grid) of rainfall-induced shallow landslide susceptibility based on a spatial probability scale (0-1) from the BLR model predictions using 2018 land cover from LCDB v5.0 where 'Exotic Forest' and 'Forest – Harvested' classes have been converted to grass cover. This provides a common reference condition (i.e., removes woody cover) for comparing the inherent susceptibility of forestry and pastoral land.
HB_landsus_v1.0_LCDB2018_class.tif	Raster layer (5 m grid) of rainfall-induced shallow landslide susceptibility based on 2018 land cover from LCDB v5.0 where the probability scale has been converted to a class-based scale (i.e., High/Moderate/Low). Class thresholds were determined by ranking the landslides used to fit the model by their probability values in decreasing order. 'High' susceptibility corresponds to 80% of the mapped landslides which have probability values ≥ 0.609. 'Moderate' corresponds to a further 15% of the mapped landslides with probability values between 0.282 and < 0.609, while 'Low' relates to the remaining 5% of landslides with values < 0.282.
HB_landsus_v1.0_forestrytograss_class.tif	Raster layer (5 m grid) of rainfall-induced shallow landslide susceptibility based on 2018 land cover from LCDB v5.0 where the probability scale has been converted to a class-based scale (i.e., High/Moderate/Low) and 'Exotic Forest' and 'Forest – Harvested' LCDB classes have been converted to grass cover. The probability thresholds used to define the High/Moderate/Low classes are the same as for HB_landsus_v1.0_LCDB2018_class.tif.

Appendix 2

Table A2.1. Summary of layers associated with the LiDAR-based version of SedNetNZ supplied with the present report

Layer name	Description
Stream_network_v1.0.shp	Digital streamlines representing the drainage network with a 10-ha upstream area threshold for channel initiation.
Subwatersheds_v1.0.shp	Subwatersheds draining to segments within the digital stream network.
HB_LiDAR_SedNetNZ_v1.0.shp	LiDAR-based SedNetNZ suspended sediment budget for each subwatershed in the Hawke's Bay region based on 2018 land cover from LCDB v5.0. The shapefile contains the following fields: • HydroID – unique identifier of each subwatershed • NextDownID – HydroID of the next downstream subwatershed • AreaKM2 – subwatershed area in km^2 • LandslYld – mean annual suspended sediment yield (t km^{-2} yr^{-1}) from shallow landslides delivered to the stream segment within a subwatershed • SurfaceYld – mean annual suspended sediment yield (t km^{-2} yr^{-1}) from surface erosion delivered to the stream segment within a subwatershed • EarthflYld – mean annual suspended sediment yield (t km^{-2} yr^{-1}) from earthflow erosion delivered to the stream segment within a subwatershed • GullyYld – mean annual suspended sediment yield (t km^{-2} yr^{-1}) from gully erosion delivered to the stream segment within a subwatershed • RivBankYld – mean annual suspended sediment yield (t km^{-2} yr^{-1}) from net riverbank erosion delivered to the stream segment within a subwatershed • TotalSedYld – total mean annual suspended sediment yield (t km^{-2} yr^{-1}) delivered to the stream segment from all erosion processes present within a subwatershed • FldplnLoad – suspended sediment load entering floodplain storage along a stream segment (t yr^{-1}) • AccNetLoad – net suspended sediment load that accumulates downstream while accounting for losses of sediment into long-term storage in lakes and on floodplains (t yr^{-1})
HB_ShallowLandslideErosion_v1.0.tif	Raster layer (5 m grid) of mean annual suspended sediment yield (t km^{-2} yr^{-1}) from rainfall-induced shallow landslide erosion delivered to the stream network for 2018 land cover from LCDB v5.0. For sediment budgeting, the sediment yield from shallow landslide erosion is derived by averaging across all pixels within a subwatershed.
HB_SurfaceErosion_v1.0.tif	Raster layer (5 m grid) of mean annual suspended sediment yield (t km^{-2} yr^{-1}) from surface erosion delivered to the stream network for 2018 land cover from LCDB v5.0. At the pixel scale, very high sediment yields from surface erosion occur when expressed per km^2 in some cases due to the combination of high erosion rates and the small pixel size (1 pixel = 25 m^2). For sediment budgeting, the sediment yield from surficial erosion is derived by averaging across all pixels within a subwatershed.

Mapping slope using Hawke's Bay's LiDAR digital elevation model

Prepared for: Hawke's Bay Regional Council June 2024

Hawkes Bay Regional Council Publication No. 5661

HAWKES BAY REGIONAL COUNCIL

TE KAUNIHERA Ā-ROHE O TE MATAU-A-MĀUI

ISSN 2703-2051 (Online)
ISSN 2703-2043 (Print)

HAWKES BAY
REGIONAL COUNCIL
TE KAUNIHERA Ā-ROHE O TE MATAU-A-MĀUI

(06) 835 9200
0800 108 838
Private Bag 6006 Napier 4142
159 Dalton Street . Napier 4110

Environmental Science

Mapping slope using Hawke's Bay's LiDAR digital elevation model

Prepared for: Hawke's Bay Regional Council June 2024

Hawkes Bay Regional Council Publication No. Report number 5661

Reviewed By:
Dr Ashton Eaves – Senior Land Scientist

Approved By:
Sam French – Science Manager

ISSN 2703-2051 (Online)
ISSN 2703-2043 (Print)

Manaaki Whenua
Landcare Research

Mapping slope using Hawke's Bay's LiDAR digital elevation model

Prepared for: Hawke's Bay Regional Council

June 2024

Mapping slope using Hawke's Bay's LiDAR digital elevation model

Contract Report: LC4482

Nathan P Odgers

Manaaki Whenua – Landcare Research

Reviewed by:	*Approved for release by:*
Balin Robertson	Sam Carrick
Pedologist	Portfolio Leader – Characterising Land Resources
Manaaki Whenua – Landcare Research	Manaaki Whenua – Landcare Research

Contents

Summary v
1 Introduction 1
2 Objective 1
3 Methods 1
3.1 Digital elevation model 1
3.2 Slope gradient 3
3.3 Slope classification 5
4 Results 6
4.1 Slope gradient 6
4.2 S-map/LUC slope classes 8
4.3 Intensive Winter Grazing slope classes 10
5 Conclusions 12
6 Acknowledgements 13
7 References 13

Appendix 15

Summary

Project and client

- Hawke's Bay Regional Council contracted Manaaki Whenua – Landcare Research to produce raster layers of slope and slope class for the Hawke's Bay – Wairoa catchment region using the council's new LiDAR digital elevation model (DEM).

Objective

- The objective of the project was to produce layers of slope gradient, S-map / land-use capability slope class, and intensive winter grazing slope class using 1 m- and 5 m-resolution mosaics of Hawke's Bay Regional Council's LiDAR DEM, that should be appropriate for land management at the farm scale.

Methods

- We used a conventional 'moving window' approach to compute a raster slope layer from each of the 1 m and 5 m DEMs. The dimensions of the moving window depended on the grid resolution of the DEM but were set so that the spatial footprint associated with the slope estimates was 400 m^2. This was done in order to emulate the intensive winter grazing rules for slope. The dimensions of the moving windows required for a 400 m^2 footprint were 21×21 grid cells and 5×5 grid cells for the 1 m- and 5 m-resolution DEMs respectively.
- We computed raster layers of S-map / land-use capability and intensive winter grazing slope classes for each DEM by allocating the slope estimates to the relevant class based on simple sets of rules.

Results

- Three raster layers were produced for each DEM: slope measured in degrees, S-map / land-use capability slope classes, and intensive winter grazing slope classes.

Assumptions and limitations

- We assume that the slope estimates produced using the specified combination of parameters is a reasonable estimate of the slope required for implementation of the IWG rules.
- Using large moving windows to compute slope has a smoothing effect on the apparent slope compared to using a traditional 3×3-cell moving window. The larger the moving window, the greater the smoothing effect. At LiDAR grid resolution, use of the traditional moving window would reveal microtopographic- rather than landscape- or management-scale slope, which is undesirable with respect to the most likely use cases for our slope layers.
- Using our method to estimate slope, single grid cells or small clusters of cells with elevations that differ strongly from the surroundings may have a strong influence on the estimated slope.

- We advise caution when applying the slope maps to support decision-making, as further analysis, interpretation or contextual information may be required in order to make sensible, well-informed decisions.

Conclusions

- The slope estimates have a footprint of 400 m^2 and are gridded at very high resolution, so they should be useful for informing land management decisions at the farm scale.
- The slope estimates should also be useful sources of information for supporting region-wide activities, such as the mapping of land-use capability and/or the implementation of intensive winter grazing rules.

1 Introduction

Slope is an important parameter of the terrain. Geometrically it is the first derivative of elevation and describes the rate of change of elevation in the direction of steepest descent (Evans & Cox 1999; Gallant & Wilson 2000). Slope is of great significance in hydrology and geomorphology due to its effect on the velocity of water (Gallant & Wilson 2000). It influences many processes occurring in the landscape, including the rate of infiltration of water into the soil profile, and therefore the soil water content (Morbidelli et al. 2018). It also influences erosion potential (Mitasova et al. 1996) and many other processes.

The advent of LiDAR digital elevation models (DEMs) has allowed terrain parameters such as slope to be estimated at very fine spatial resolutions. Due to their fine vertical and horizontal resolution, LiDAR DEMs have been revolutionary for understanding the topography of certain types of landscape, such as low-relief areas.

Hawke's Bay Regional Council (HBRC) have a LiDAR DEM that covers their entire region, and they are interested in exploring the use of terrain parameters such as slope to inform the application of Land Use Capability (LUC) and Intensive Winter Grazing (IWG) rules.

2 Objective

The objective of this project was to produce layers of slope gradient, S-map / land-use capability slope class, and intensive winter grazing slope class using 1 m- and 5 m-resolution mosaics of Hawke's Bay Regional Council's LiDAR DEM.

3 Methods

We prepared DEMs of the Hawke's Bay region at 1 m and 5 m resolution. We then used the DEMs to compute the slope gradient in degrees, and classified the slope according to the S-map/LUC slope classification and the IWG slope classification. All calculations were implemented in the Python programming language.

3.1 Digital elevation model

We prepared DEMs of the Hawke's Bay region at 1 m and 5 m resolution. The DEMs included the Gisborne District part of the Wairoa catchment (Figure 1).

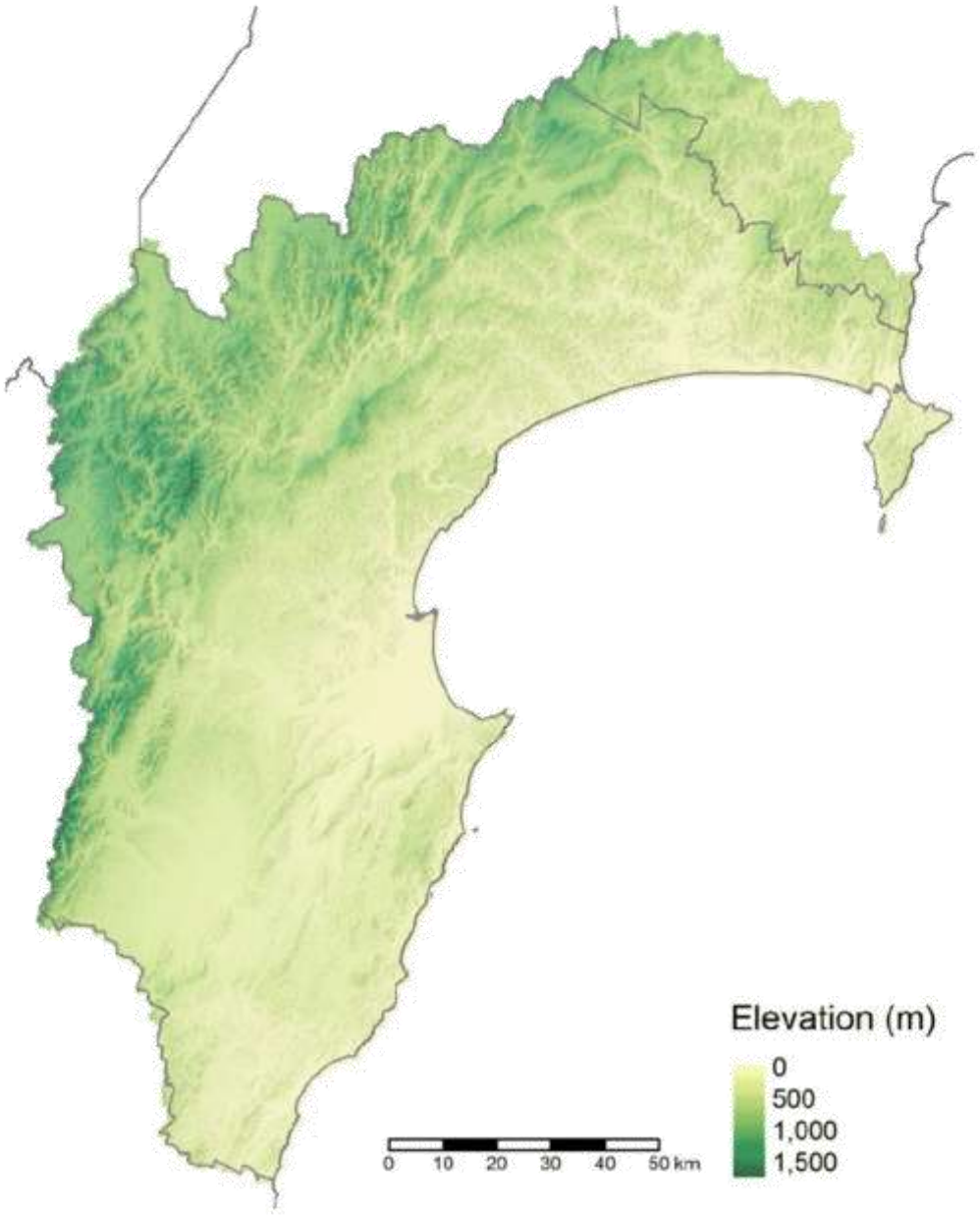

Figure 1. Digital elevation model for the Hawke's Bay – Wairoa catchment area.

3.2 Slope gradient

3.2.1 Moving window

Slope gradient in degrees was derived from each DEM using Evans's (1979) method, which uses a moving window to estimate the slope at each grid cell based on the cell's elevation and the elevations of its eight immediate neighbours. As such, the moving window is a square with dimensions (width and height) of $d = 3$ grid cells. It also has a real-world footprint of g metres on each side, or an areal footprint of $G = g \times g$ square metres, where g is computed as follows:

$$g = (d - 1) \times r \quad (1)$$

where r is the grid resolution of the DEM in metres.

The size or spatial footprint of this moving window may be too small to suit certain applications when applied to high-resolution LiDAR DEMs. For example, on a DEM that has resolution $r = 1$ m, slope estimates derived using a moving window of width and height $d = 3$ would have a footprint of $g = 2$ m, or $G = 4$ m^2, which would reveal the slope of the microtopography rather than the landscape-scale slope. The landscape-scale slope is more useful for land management.

The IWG Module (Ministry for Primary Industries & Ministry for the Environment 2022) requires estimates of slope measured over 'any 20 m distance of the land'. We interpret this specification as $g = 20$ m, or $G = 400$ m^2. Working backwards, we compute the required d as follows:

$$d = \frac{g+r}{r} \quad (2)$$

This equates to $d = 21$ cells for the 1 m-resolution DEM and $d = 5$ cells for the 5 m-resolution DEM. Using moving windows of this size has a smoothing effect on the apparent slope compared to slope derived using the traditional moving window of size $d = 3$. It is this effect that removes the appearance of microtopography and allows us to estimate a slope that may be useful for land management at paddock to farm scales. Generally, the larger the d, the greater the smoothing effect.

3.2.2 Slope calculation

Slope is computed using the first derivatives of elevation z along the x and y Cartesian axes, δx and δy. For the conventional moving window with $d = 3$, δx and δy are computed as follows.

$$\delta x = (z_3 + z_6 + z_9 - z_1 - z_4 - z_7)/6r \quad (3)$$

$$\delta y = (z_1 + z_2 + z_3 - z_7 - z_8 - z_9)/6r \quad (4)$$

The $z_i, i = 1,2,3,\ldots 9$ refers to elevations at specific cells of the moving window, as indicated in Figure 2. The central cell with elevation z_5 is the cell for which the slope is being estimated.

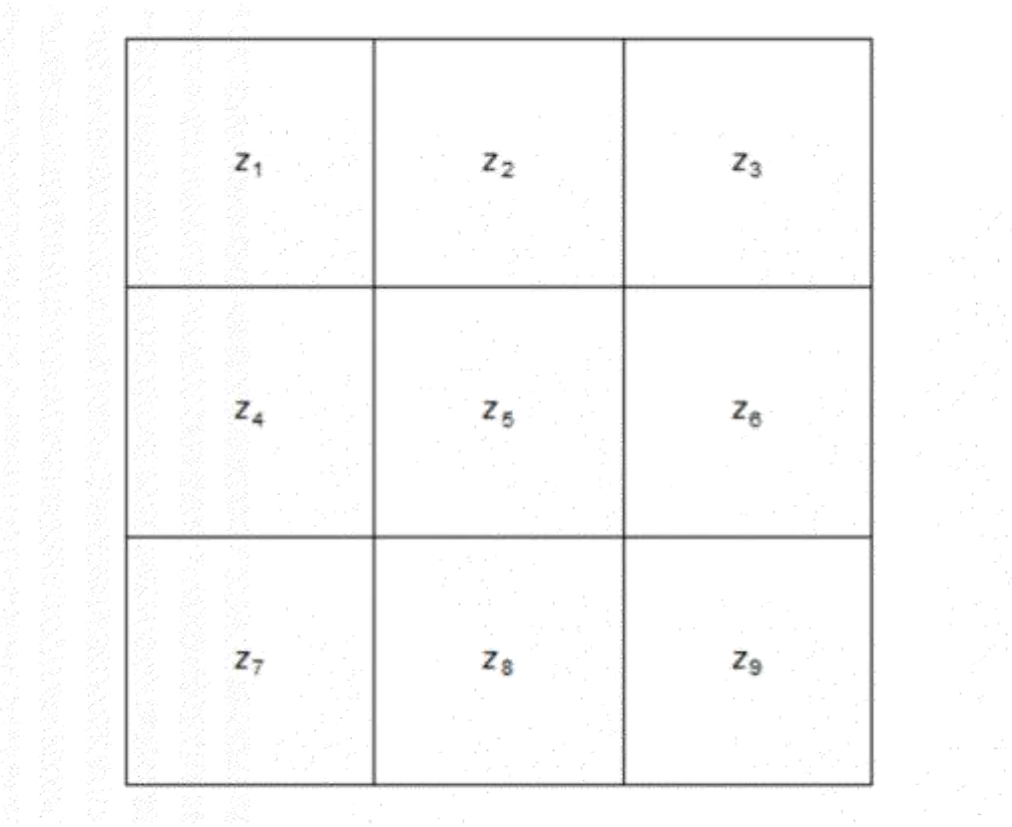

Figure 2. A moving window neighbourhood of length and width $d = 3$ grid cells.

The slope in radians, s_{rad} is then computed as follows.

$$s_{\text{rad}} = \arctan\left(\sqrt{\delta x^2 + \delta y^2}\right) \quad (5)$$

Finally, the slope in degrees, s_{deg} is computed as follows.

$$s_{\text{deg}} = s_{\text{rad}} \times \frac{180}{\pi} \quad (6)$$

We need to generalise equations 3 and 4 to compute slope using moving windows of size $d > 3$. To do this we shift the neighbour cells to the corners and edge midpoints of the neighbourhood, as demonstrated in Figure 3.

Figure 3. A moving window neighbourhood of length and width d = 5 grid cells.

We then use equations 7 and 8 to compute δx and δy:

$$\delta x = (z_{d,1} + z_{d,(d+1)/2} + z_{d,d} - z_{1,1} - z_{1,(d+1)/2} - z_{1,d})/(3rd - 3r) \quad (7)$$

$$\delta y = (z_{1,1} + z_{(d+1)/2,1} + z_{d,1} - z_{1,d} - z_{(d+1)/2,d} - z_{1,d})/(3rd - 3r) \quad (8)$$

This method is in the spirit of the method one might use to estimate slope in the field. One limitation of the method is that single grid cells or small clusters of grid cells with elevations that differ strongly from the surroundings will exert a strong influence on the estimated slope, despite the smoothing effect engendered by the size of the moving window. Care should be taken when interpreting the slope with respect to whether spurious slope values represent important landscape phenomena or can be disregarded.

3.3 Slope classification

We allocated the raster slope values to slope classes in two commonly used slope classifications: the S-map / land-use capability (LUC) slope classification (Lilburne et al. 2012; Lynn et al. 2021), and the intensive winter grazing slope classification (Ministry for Primary Industries & Ministry for the Environment 2022). Separate raster files were produced for each classification system using the slope gradient raster derived from each DEM.

3.3.1 S-map / land-use capability slope classes

S-map and the LUC classification share the same system of slope classes, described in Table 29 of Lilburne et al. 2012 and Table 6 of Lynn et al. 2021. The raster classification rules are given in Table 1, alongside the raster value used to represent each class.

Table 1. Rules used to allocate slope gradient to an S-map/LUC slope class

Slope class	Classification rule	Raster value
A	$0 \leq s_{deg} < 4$	1
B	$4 \leq s_{deg} < 8$	2
C	$8 \leq s_{deg} < 16$	3
D	$16 \leq s_{deg} < 21$	4
E	$21 \leq s_{deg} < 26$	5
F	$26 \leq s_{deg} < 35$	6
G	$s_{deg} \geq 35$	7

3.3.2 Intensive winter grazing slope classes

The IWG slope rules are described in Ministry for Primary Industries & Ministry for the Environment 2022. The raster classification rules are given in Table 2. Rules used to allocate slope gradient to an IWG slope class.

Table 2. Rules used to allocate slope gradient to an IWG slope class.

Slope class	Classification rule	Raster value
Grazeable	$0 \leq s_{deg} \leq 10$	1
Not grazeable	$s_{deg} > 10$	2

4 Results

Results are presented for the 5 m-resolution output.

4.1 Slope gradient

The slope layer for the Hawke's Bay – Wairoa catchment area, based on the 5 m-resolution DEM, is presented in Figure 4. The 5 m-resolution slope for the vicinity of Te Mata Peak, which encompasses a broad range of physiography, is presented in more detail in Figure 5. The smoothing effect referred to in Section 3.2.1 is evident in the figure legends, where the maximum slope estimate in the detail area is in the order of 60°. One may expect slopes steeper than this on the very rugged topography of Te Mata Peak. They may exist over horizontal distances shorter than g, but a smaller d would be required to reveal them.

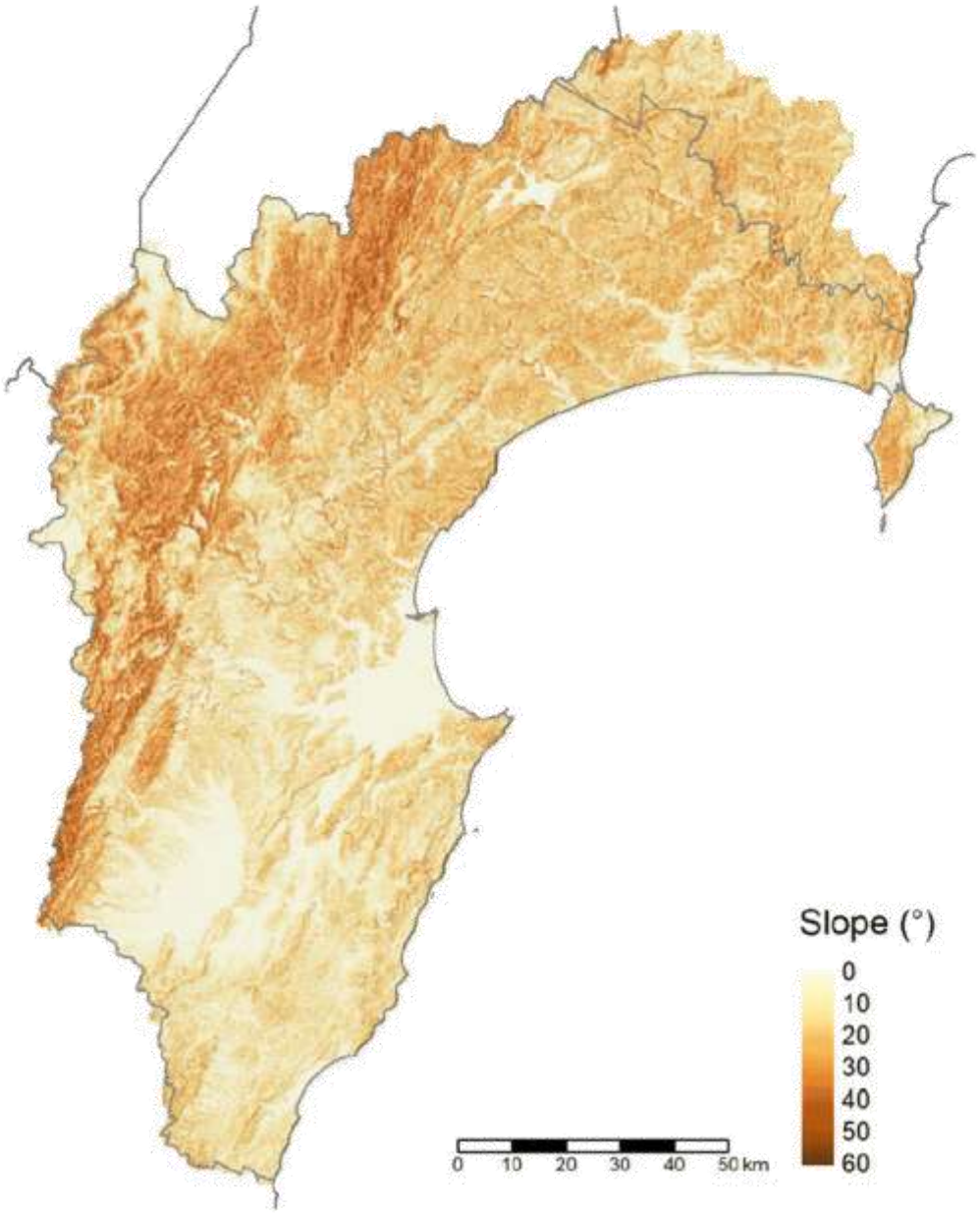

Figure 4. Slope layer for the Hawke's Bay – Wairoa catchment area.

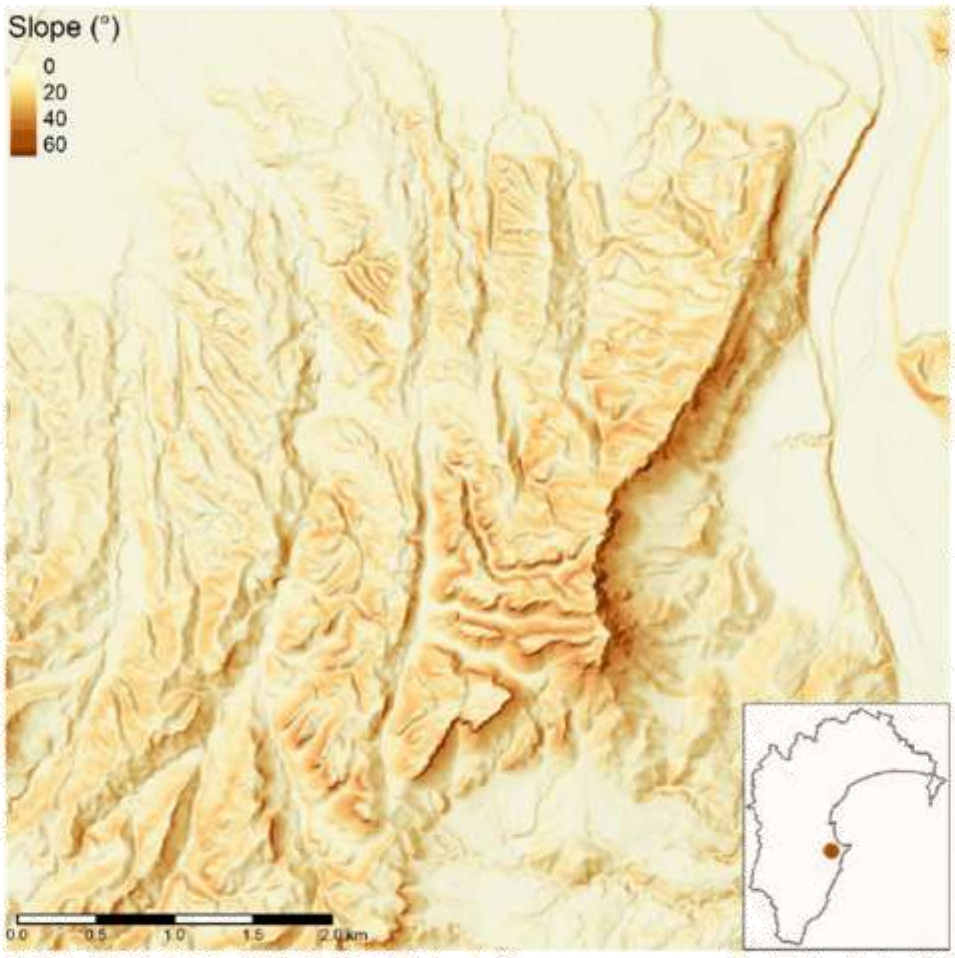

Figure 5. Detail of 5 m-resolution slope layer for the area around Te Mata Peak.

4.2 S-map/LUC slope classes

The S-map/LUC slope class layer for the Hawke's Bay – Wairoa catchment area, based on the 5 m-resolution DEM, is presented in Figure 6. The 5 m-resolution slope class layer for the vicinity of Te Mata Peak is presented in more detail in Figure 7.

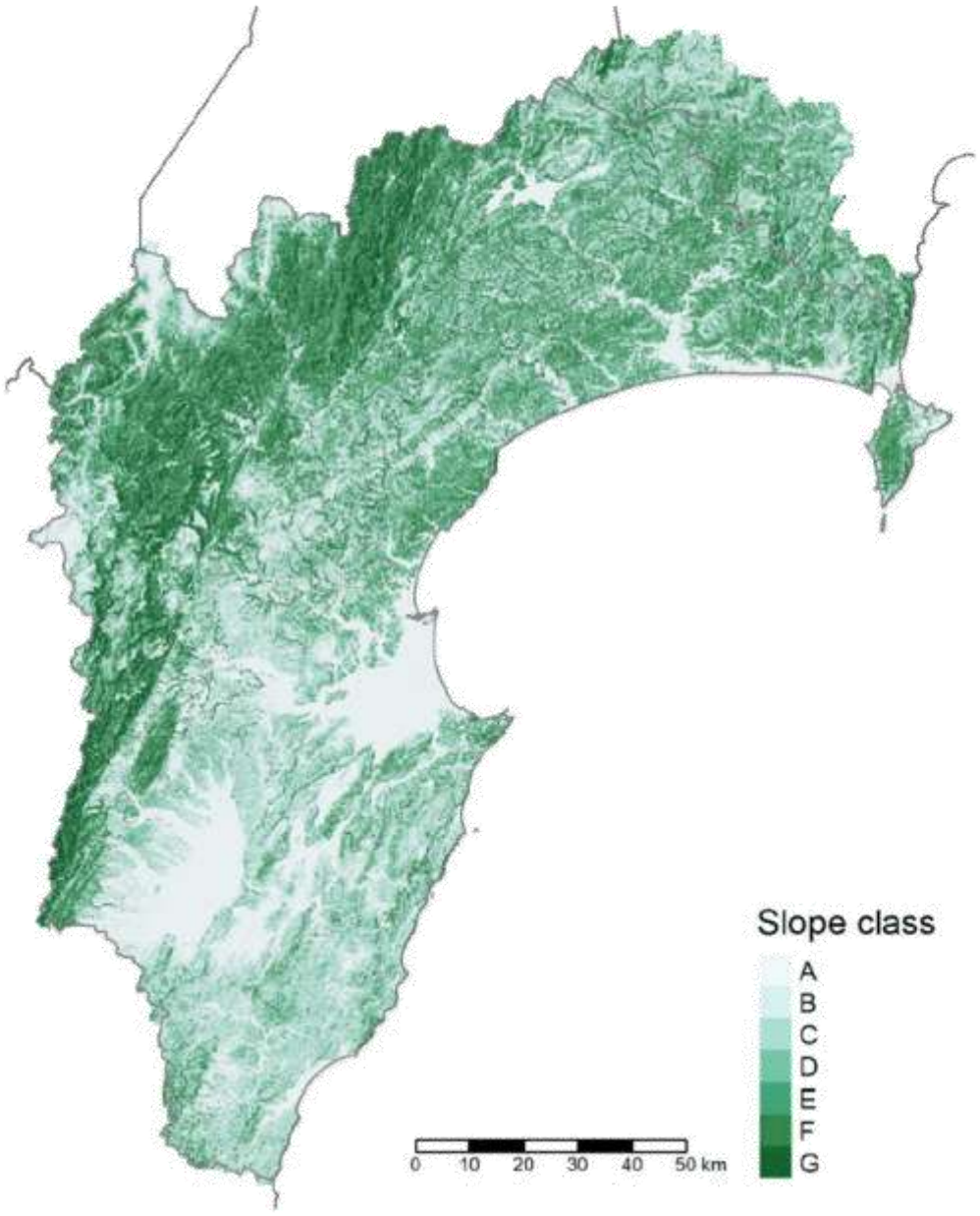

Figure 6. S-map/LUC slope class layer for the Hawke's Bay – Wairoa catchment area.

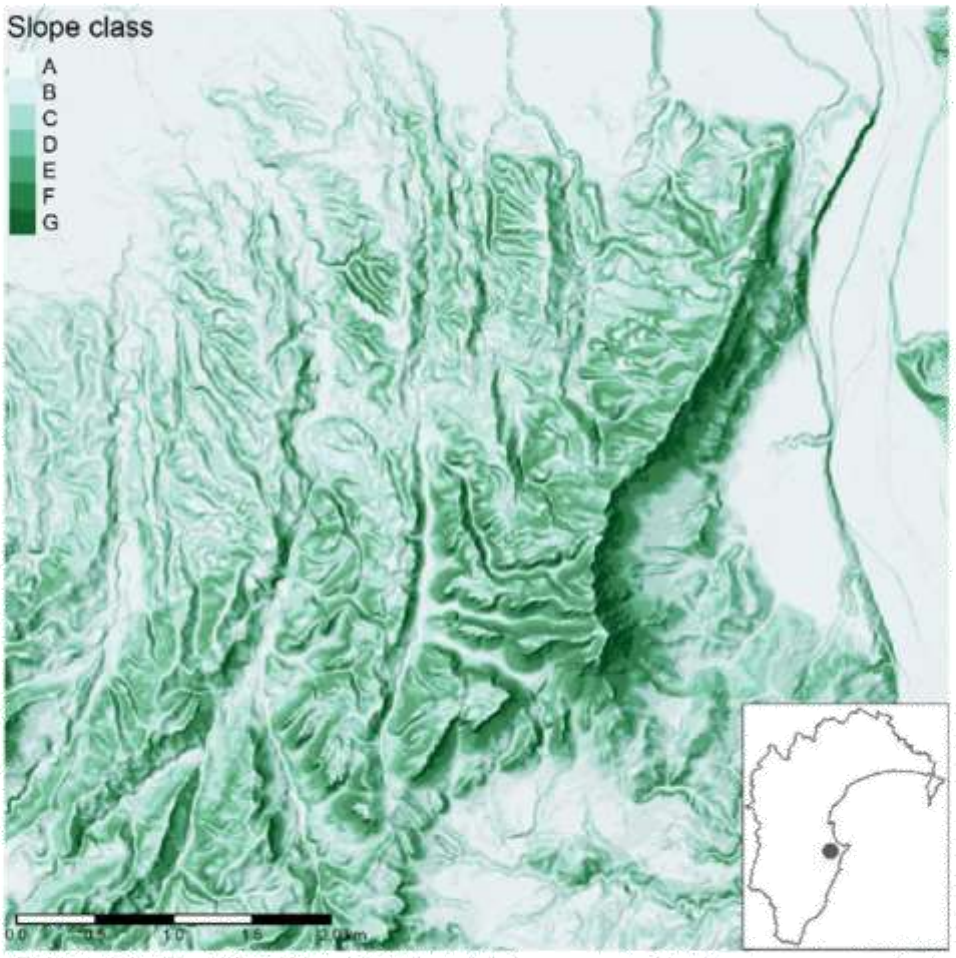

Figure 7. Detail of 5 m-resolution S-map/LUC slope class layer for the area around Te Mata Peak.

4.3 Intensive winter grazing slope classes

The IWG slope class layer for the Hawke's Bay – Wairoa catchment area, based on the 5 m-resolution DEM, is presented in Figure 8. The 5 m-resolution IWG slope class layer for the vicinity of Te Mata Peak is presented in more detail in Figure 9. We advise caution when using this map to apply the IWG rules as further analysis, interpretation or contextual information may be required to make sensible decisions. This is because not all land mapped as less-than-10° slope may be suitable for grazing in winter. For example, an area of land that is otherwise suitable may be too small or too inaccessible to graze.

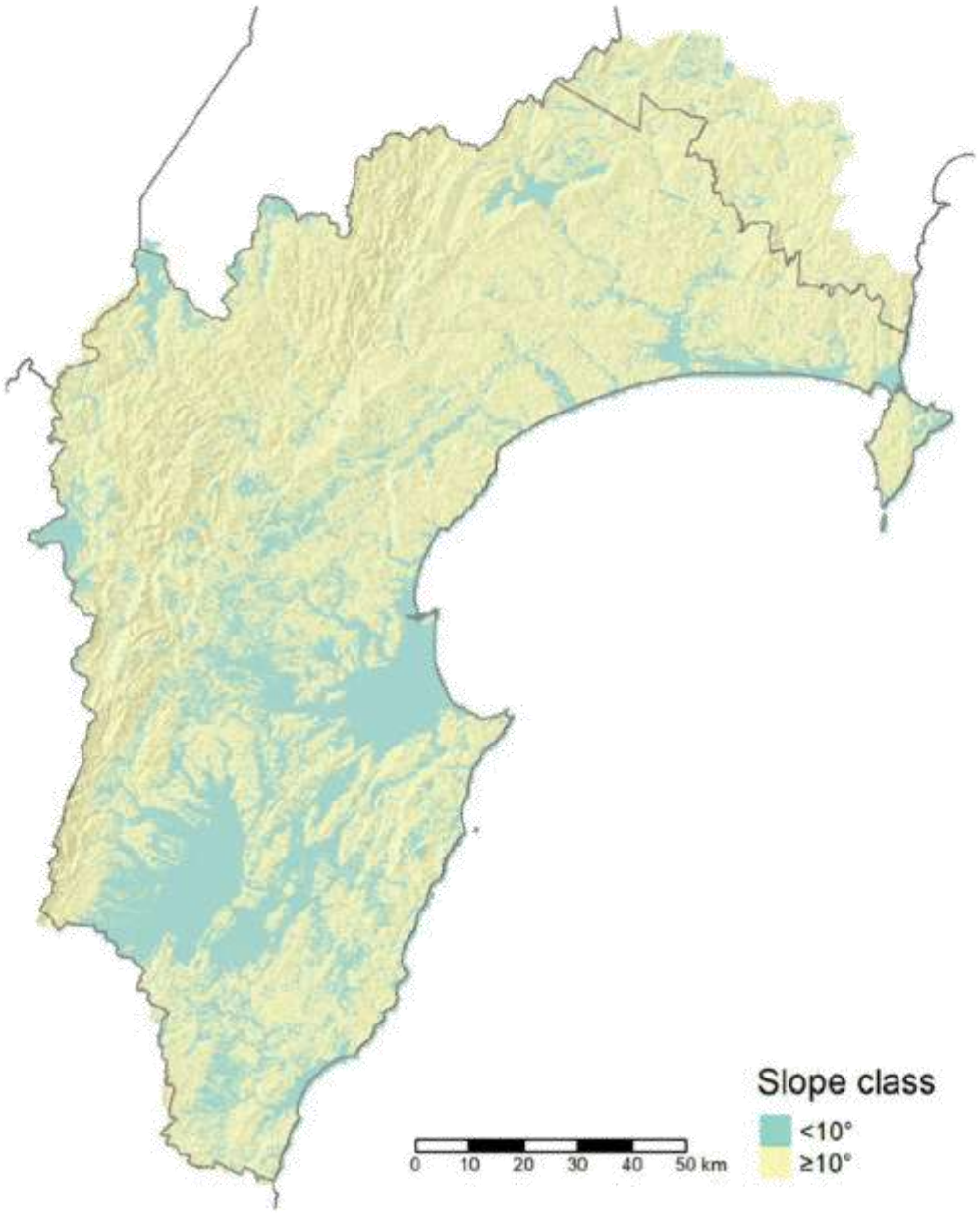

Figure 8. IWG slope class layer for the Hawke's Bay – Wairoa catchment area.

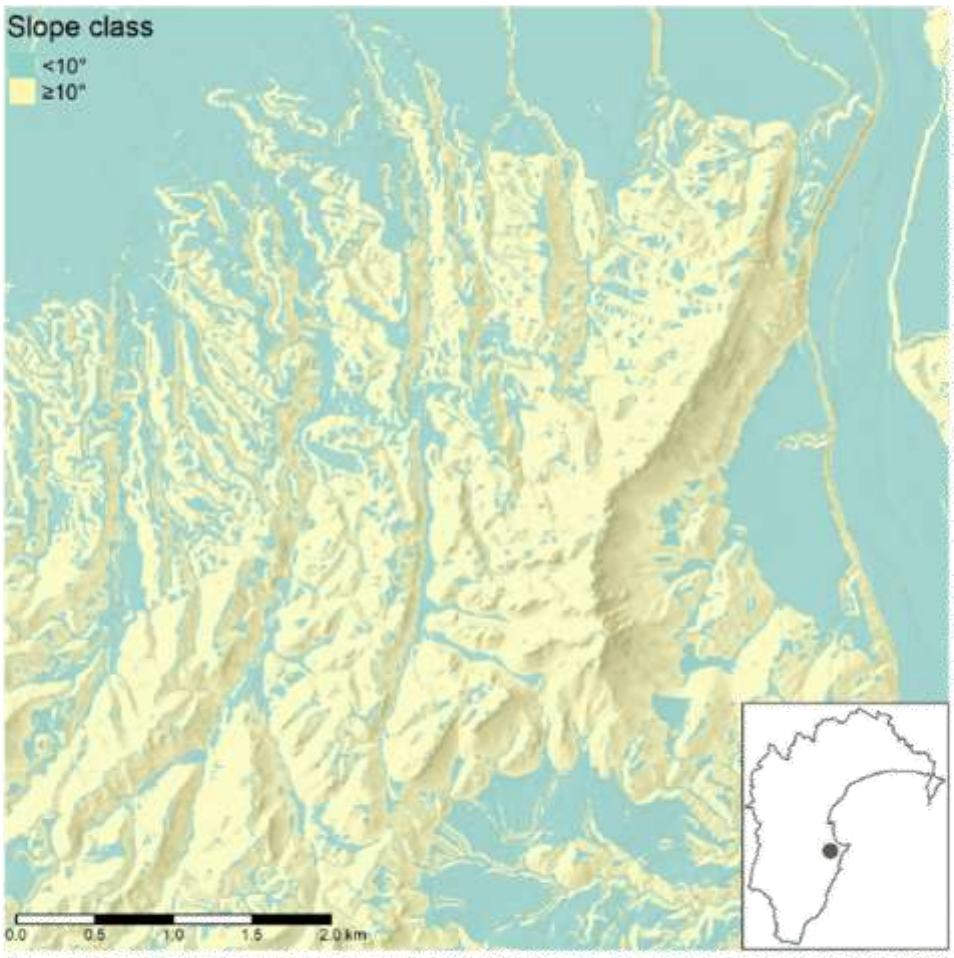

Figure 9. Detail of 5 m-resolution IWG slope class layer for the area around Te Mata Peak.

5 Conclusions

We computed the slope gradient in degrees for the 1 m and 5 m Hawke's Bay DEMs. We allocated the slope to classes in the S-map/LUC and IWG slope classifications. Because the slope estimates have a footprint of 400 m^2 and are gridded at very high resolution, we anticipate they will be useful for informing land management decisions at the farm scale. They will also be useful for supporting region-wide activities, such as the mapping of LUC and/or implementation of IWG rules. We advise caution when applying the slope maps to support decision-making, as further analysis, interpretation or contextual information may be required in order to make sensible, well-informed decisions.

6 Acknowledgements

We are grateful to Hawke's Bay Regional Council for providing the 1 m-resolution LiDAR elevation model.

7 References

Evans IS 1979. An integrated system of terrain analysis & slope mapping. Durham, England, University of Durham.

Evans IS, Cox NJ 1999. Relations between land surface properties: altitude, slope and curvature. In: Hergarten S, Neugebauer HJ eds. Process modelling and landform evolution. Lecture notes in earth sciences, vol. 78. Berlin, Heidelberg, Springer. Pp. 13–45. https://doi.org/10.1007/BFb0009718

Gallant JC, Wilson JP 2000. Primary topographic attributes. In: Wilson JP, Gallant JC eds. Terrain analysis: principles and applications. New York, Wiley. Pp. 51–85.

Lilburne LR, Webb TH, Hewitt AE, Lynn IH 2012. S-map database manual version 1.3. Landcare Research Contract Report LC478.

Lynn IH, Manderson AK, Page MJ, Harmsworth GR, Eyles GO, Douglas GB, et al. 2021. Land use capability survey handbook: a New Zealand handbook for the classification of land (3rd ed., revised and reprinted). Hamilton, AgResearch Ltd.

Ministry for Primary Industries, Ministry for the Environment 2022. Intensive Winter Grazing Module. Wellington, Ministry for Primary Industries.

Mitasova H, Hofierka J, Zlocha M, Iverson LR 1996. Modelling topographic potential for erosion and deposition using GIS. International Journal of Geographical Information Systems 10(5): 629–641. doi: 10.1080/02693799608902101

Morbidelli R, Saltalippi C, Flammini A, Govindaraju RS 2018. Role of slope on infiltration: a review. Journal of Hydrology 557. doi: 10.1016/j.jhydrol.2018.01.019

Appendix – File specifications

List of files

The files derived from the 1 m-resolution DEM are listed in Table A1. Files derived from the 1 m-resolution digital elevation model and those derived from the 5 m-resolution DEM are listed in Table A2. Files derived from the 5 m-resolution digital elevation model

Table A1. Files derived from the 1 m-resolution digital elevation model

File
hbrc_wairoa_dem_1m_slope_degrees_r10.tif
hbrc_wairoa_dem_1m_slope_degrees_r10.tif.iso19139.xml
hbrc_wairoa_dem_1m_slope_iwg_r10.tif
hbrc_wairoa_dem_1m_slope_iwg_r10.tif.aux.xml
hbrc_wairoa_dem_1m_slope_iwg_r10.tif.iso19139.xml
hbrc_wairoa_dem_1m_slope_smap7_r10.tif
hbrc_wairoa_dem_1m_slope_smap7_r10.tif.aux.xml
hbrc_wairoa_dem_1m_slope_smap7_r10.tif.iso19139.xml

Table A2. Files derived from the 5 m-resolution digital elevation model

File
hbrc_wairoa_dem_5m_slope_degrees_r2.tif
hbrc_wairoa_dem_5m_slope_degrees_r2.tif.aux.xml
hbrc_wairoa_dem_5m_slope_degrees_r2.tif.iso19139.xml
hbrc_wairoa_dem_5m_slope_iwg_r2.tif
hbrc_wairoa_dem_5m_slope_iwg_r2.tif.aux.xml
hbrc_wairoa_dem_5m_slope_iwg_r2.tif.iso19139.xml
hbrc_wairoa_dem_5m_slope_smap7_r2.tif
hbrc_wairoa_dem_5m_slope_smap7_r2.tif.aux.xml
hbrc_wairoa_dem_5m_slope_smap7_r2.tif.iso19139.xml

The files with extension .tif are cloud-optimised GeoTIFF (COG) files that contain the raster data. The files with extension .tif.iso19139.xml contain the ISO19139-compatible metadata for the raster files. The files with extension .tif.aux.xml contain raster attribute tables (in GDALRasterAttributeTable format) for the S-map/LUC and IWG slope class rasters that relate the integer raster values to class names.

Raster file specifications

The coordinate reference system of all raster files is New Zealand Transverse Mercator. Other specifications of the raster files are described in Table A3. Raster file specifications.

Table A3. Raster file specifications.

File	Rows (cells)	Columns (cells)	Resolution (m)	Data type	File size (GB)
hbrc_wairoa_dem_1m_slope_degrees_r10.tif	213120	171360	1	32-bit floating point	92.7
hbrc_wairoa_dem_1m_slope_iwg_r10.tif	213120	171360	1	8-bit unsigned integer	0.6
hbrc_wairoa_dem_1m_slope_smap7_r10.tif	213120	171360	1	8-bit unsigned integer	1.9
hbrc_wairoa_dem_5m_slope_degrees_r2.tif	42624	34272	5	32-bit floating point	3.8
hbrc_wairoa_dem_5m_slope_iwg_r2.tif	42624	34272	5	8-bit unsigned integer	0.0
hbrc_wairoa_dem_5m_slope_smap7_r2.tif	42624	34272	5	8-bit unsigned integer	0.2

LiDAR-derived vegetation layers in Hawke's Bay

Prepared for: Hawke's Bay Regional Council June 2024

Hawkes Bay Regional Council Publication No. 5658

HAWKES BAY REGIONAL COUNCIL

TE KAUNIHERA Ā-ROHE O TE MATAU-A-MĀUI

ISSN 2703-2051 (Online)
ISSN 2703-2043 (Print)

HAWKES BAY REGIONAL COUNCIL
TE KAUNIHERA Ā-ROHE O TE MATAU-A-MĀUI

(06) 835 9200
0800 108 838
Private Bag 6006 Napier 4142
159 Dalton Street . Napier 4110

Environmental Science

LiDAR-derived vegetation layers in Hawke's Bay

Prepared for: Hawke's Bay Regional Council June 2024

Hawkes Bay Regional Council Publication No. Report number 5658

Reviewed By:
Dr Ashton Eaves – Senior Land Scientist

Approved By:
Sam French – Science Manager

ISSN 2703-2051 (Online)
ISSN 2703-2043 (Print)

Manaaki Whenua
Landcare Research

LiDAR-derived vegetation layers in Hawke's Bay

Prepared for: Hawke's Bay Regional Council

June 2024

LiDAR-derived vegetation layers in Hawke's Bay

Contract Report: LC4470

Jan Schindler

Manaaki Whenua – Landcare Research

Reviewed by:

James Shepherd
Research Area Leader, Remote Sensing and Data Science

Brent Martin
Senior Researcher - Data Science
Manaaki Whenua – Landcare Research

Approved for release by:

Sam Carrick
Portfolio Leader – Characterising Land Resources
Manaaki Whenua – Landcare Research

Contents

Summary v
1 Introduction 1
2 Background 1
3 Objectives 2
4 Methods 3
4.1 Aerial LiDAR survey 3
4.2 LiDAR tile processing 5
4.3 Deep learning for semantic segmentation 14
4.4 Tree canopy and short vegetation layers 15
4.5 Forest layer 15
4.6 Individual tree layer 16
4.7 Shelter belt layer 16
4.8 Pine / exotic forest layer 20
5 Results 25
5.1 Regional LiDAR raster products 25
5.2 Regional LiDAR vegetation layers 27
6 Conclusions and recommendations 36
7 Acknowledgements 39
8 References 39

Summary

Project and client

The 'LiDAR tools partnership' programme was a collaborative initiative between the Environmental Science section of the Hawke's Bay Regional Council (HBRC) and Manaaki Whenua – Landcare Research (MWLR).

The purpose of the programme was to maximise the benefit from the new acquisition of LiDAR data for the Hawke's Bay region through taking a partnership approach and explore how the aerial LiDAR data, captured over the region in 2021/2022, can address five key environmental science questions about how LiDAR data can: (i) help improve understanding and management of erosion; (ii) improve land characterisation; (iii) map vegetation classes; (iv) quantify ecosystem services; (v) making LiDAR information available. This report presents findings from sub-project (iii) on mapping vegetation types.

Objectives

The project aimed to produce high-resolution vegetation layers that could be used for identifying and mapping different types of vegetation. The list of desired classes was subject to technical feasibility and the priorities of the HBRC team. All data sets were to be generated for the entire region. The final list of deliverables included:

- delivering LiDAR rasterised at very high resolution, i.e. 30 cm pixel size, into digital models of canopy height, surface, ground and modelled daylight/shadow
- focusing on these specific spatial vegetation layers (agreed in discussions with HBRC): individual trees, forests, tree canopy, short vegetation, shelter belts, pine/exotic forest
- investigating experimental LiDAR case studies, as needed by HBRC.

The purpose of this work was not only to generate one-off data products, but to create baseline methods and data that can be updated and refined in the future. All methods were designed to be transparent and repeatable.

Methods

We used MWLR-internally developed software code and workflows to process large-scale aerial point clouds and multi-band imagery. For both the LiDAR processing and vegetation detection models, we used a collection of open-source Python-based software packages. We also applied state-of-the-art computer vision and deep learning models for detection of vegetation features in aerial LiDAR data.

Results

About one Terabyte of aerial LiDAR was processed and translated into regional maps of vegetation information. The layers provide unprecedented detail of land surface and vegetation structure for the Hawke's Bay Region and include low vegetation, tree canopy and individual trees, forests, shelter belts, and pine stands. The data cover all land-cover

types, including agricultural areas, rural hill-country, forests and urban; and will act as a baseline vegetation layer at regional scale in New Zealand enabling detailed change mapping in the future.

Recommendations

Based on the project's outcomes and experiences, we make the following recommendations to HBRC.

- Working on clear class definitions, e.g. minimum height, side lengths, spacing between features, to filter the data sets of shelter belts, pine, and fields to further reduce uncertainties in the data set and make the layers more useful for specific use cases.
- Once the rules have been defined, these should also be applied to the training data set; the models should then be retrained on the more specific requirements to optimise accuracy and loss metrics. This will greatly improve the results and reduce error screening needs.
- We recommend councils (i.e. HBRC) investigate the potential combination of existing environmental layers to derive secondary datasets and establish rule sets that can be applied at broader (regional) scale.
- We recommend exploring different AI and more traditional algorithm options for future vegetation change analysis, to ensure the consistency of the map results.
- That councils (i.e. HBRC) conduct simultaneous acquisitions of LiDAR and aerial photography to increase the usefulness of the technologies and improve classification of vegetation types and tree species.
- That councils (i.e. HBRC) use state-of-the-art computer vision methods such as convolutional encode-decoder networks, which showed promise in this work and can be potentially used for tree species classification in NZ regional RGB imagery.
- We recommend councils (i.e. HBRC) investigate acquiring purpose-driven, high-density aerial and under-canopy LiDAR measurements to enable analysis of mid-tier and understorey of forests.

1 Introduction

The 'LiDAR tools partnership' programme is a collaborative initiative between the Environmental Science section of the Hawke's Bay Regional Council (HBRC) and Manaaki Whenua – Landcare Research (MWLR).

The purpose of the programme is to maximise the benefit from the new acquisition of LiDAR data for the Hawke's Bay region through taking a partnership approach and explore how the aerial LiDAR data, captured over the region in 2021/2022, can address five key environmental science questions: how LiDAR data can: (i) help improve understanding and management of erosion; (ii) improve land characterisation; (iii), map vegetation classes; (iv), quantify ecosystem services; (v), making LiDAR information available. This report presents findings from sub-project (iii) on mapping vegetation types.

The project was structured into four phases. First, the teams from HBRC and MWLR identified priority vegetation classes and, depending on availability and resolution of HBRC input data sets, worked with HBRC to define the feasible mapping scope. Key input data were then collated from HBRC and the 3D aerial LiDAR point clouds for the region were processed and converted to useful raster representations for further downstream analysis.

Second, ground truth data labels were manually created for vegetation classes that required model training. Third, algorithms and processing workflows for the vegetation classes were developed and initial proof of concept layers were created.

Finally, the methods were refined, and manual training data extended to capture remaining uncertainties. The final region-wide vegetation layers were produced, and a technical report written.

2 Background

The HBRC has partnered with Land Information New Zealand (LINZ) to invest in LiDAR coverage of the Hawke's Bay region, as part of the wider LINZ National Elevation Programme outlined at https://www.linz.govt.nz/data/linz-data/elevation-data. The regional LiDAR coverage was made available for use by August 2022. Following acquisition of LiDAR coverage, HBRC also decided to invest through the HBRC 2021–31 Long Term Plan in using the LiDAR data across a range of applications to support its activities to implement objectives under Te Tiriti, Freshwater, Biodiversity, and Sustainable Land Management themes.

MWLR has also recognised the step-change opportunity that regional LiDAR coverage creates for its scientific research, and in particular application of its science to support its regional council partners. For this reason, MWLR has decided to co-operate on and co-fund a programme of work with HBRC. MWLR envisions that the application of its LiDAR-enabled science in the Hawkes Bay region, will benefit future applications in other regions that MWLR partners with.

Between May and August 2021 simultaneous scoping exercises were carried out in both organisations to ascertain current uses of LiDAR and ideas for possible uses. At the same time, representatives from both organisations (as the LiDAR programme scoping group) came together to articulate the success factors for the project and to determine prioritisation criteria to select preferred projects to fund. The prioritisation criteria used have been summarised into the following list of outcomes for a successful programme.

- Support improved relationships and engagement with iwi and with Hawke's Bay communities and provide information that is accessible.
- Empower iwi to exercise kaitiakitanga through use of this data.
- Produce information, tools and approaches that are useful for informing policy, decision-making, regulation and implementation in HBRC.
- Provide real-world benefit to HBRC and their stakeholders within 5 years.
- Support collaboration and capability building across the partner organisations.

Over 120 ideas were submitted in the scoping process. This list was filtered based on the following criteria: combining similar ideas; was the idea possible with level of data resolution available; did the idea align with both the organisations' strategies; was the idea 'business as usual' for the council. This reduced the original list to approximately 40. These 40 ideas were re-examined to see if any of them could be combined to make one, bigger project. Based on this scoping and subsequent workshops, a refined set of projects were invited to develop up the more detailed project plans which are the basis of the final programme.

The programme consists of five synergistic projects.

1 Improving understanding and management of erosion with LiDAR.

2 Improving land characterisation with LiDAR.

3 Vegetation layer from LiDAR and aerial imagery.

4 Quantifying ecosystem services (seed funding).

5 Making LiDAR information available (extension and testing).

There is an interdependency between most but not all of the proposals, with the LiDAR data being the common thread.

3 Objectives

The project aimed to produce high-resolution vegetation layers that could be used for identifying and mapping different types of vegetation. The list of desired classes was subject to technical feasibility and the priorities of the HBRC team. All data sets were to be generated for the entire region. The final list of deliverables included:

- Delivering LiDAR rasterised at very high resolution, i.e. 30 cm pixel size, into digital models of canopy height, surface, ground and modelled daylight/shadow

- focusing on these specific spatial vegetation layers (agreed in discussions with HBRC): individual trees, forests, tree canopy, short vegetation, shelter belts, pine/exotic forest
- investigating experimental LiDAR case studies, as needed by HBRC.

The purpose of this work was not only to generate one-off data products, but to create baseline methods and data that can be updated and refined in the future. All methods were designed to be transparent and repeatable.

4 Methods

4.1 Aerial LiDAR survey

The Hawke's Bay Region LiDAR 2020 project was undertaken by iXblue as part of the Land information New Zealand (LINZ) National Elevation Programme. The project encompasses the areas of HBRC that overlap with the Wairoa District Council (WDC), Hastings District Council (HDC), Napier City Council (NCC) and Central Hawke's Bay District Council (CHBDC) administration boundaries (Farrier, 2021).

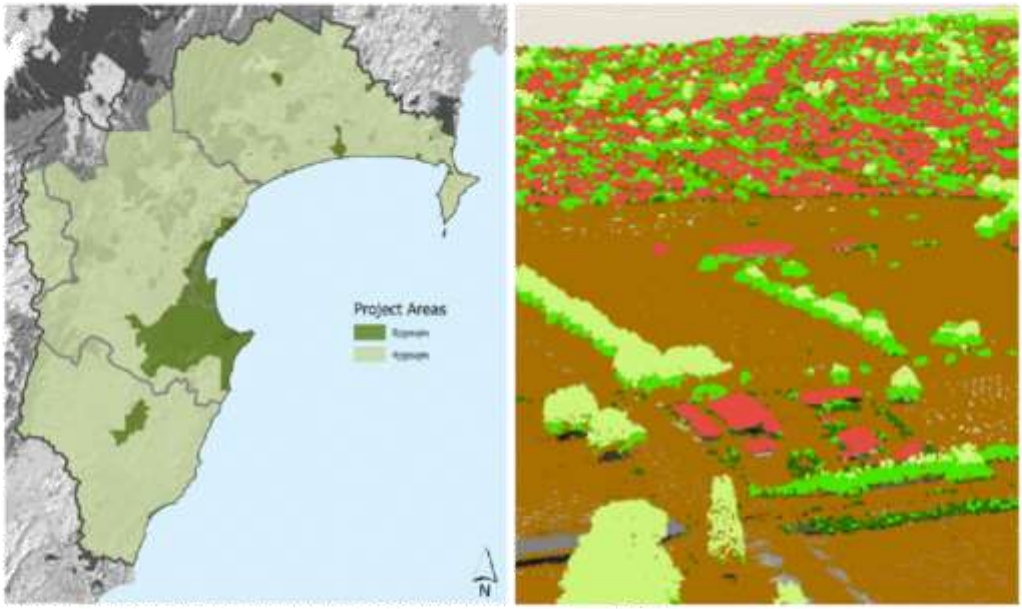

Figure 1. Project specifications and parameters. (Left) Project area extent and base pulse density specification; (Right) Classified point cloud. (Source: Both taken from Farrier 2021).

The aerial LiDAR survey was conducted between 2020 and 2021 with a pulse density of 4 points per m^2 (ppsm) over rural areas and 8 ppsm in urban areas (Figure 1). The initial survey area was later complemented by a similar LiDAR survey from the Waikato region adding the missing area in the north-west (Figure 2). For data acquisition, iXblue used a Leica TerrainMapper-LN LiDAR sensor system mounted on a fix-winged aircraft. This aircraft was flown at an altitude of about 2 km above ground level with a circular scanning pattern (Table 1).

Table 1. LiDAR sensor and collection parameters for the 8 points per square metre (ppsm) urban setting. (Source: Taken from Farrier 2021.)

Parameter	Variable
Average Pulse Density	8.9 pulses per square metre
Maximum Pulse Spacing: Across Track	0.45 m
Maximum Pulse Spacing Along Track	0.50 m
Average Pulse Spacing	0.34 m
LiDAR Pulse Repetition Rate	1,500,000 Hz
Scanner Pattern	Circular
Nominal Altitude Above Ground Level	1,950 m
Aircraft Ground Speed	Target 145 knots, but not exceeding 163 knots
Field of view	+/-20 degrees
Laser wavelength	1,064 nm
Laser divergence	0.25 mrad
Return Pulses	Programmable up to 15
Intensity digitisation	14 bits

Projects undertaken as part of the Provincial Growth Fund-LiDAR programme are required to use the PGF Version: New Zealand National Aerial LiDAR Base Specification (Land Information New Zealand 2020). The raw point cloud was pre-processed and classified by the vendor (iXblue) to PGF Version: New Zealand National Aerial LiDAR Base Specification standard CL2.

The data product was tiled into NZTopo50 1:1,000 map tiles. Each tile is about 482 × 720 metre in size. The total survey area covers about 14,737 km^2. They are in New Zealand Transverse Mercator 2000 map project (code EPSG:2913) and with NZVD2016 normal-orthometric heights (EPSG:7839). In total, there are 42,467 tiles, i.e. point cloud data files in the LAZ file format, with about 963 Gigabyte (GB) in size.

Figure 2. Aerial LiDAR data in Hawke's Bay. (Left) Full coverage; (Middle) Individual LiDAR tiles shown in yellow; (Right) Zoomed-in view as example over Wairoa.

4.2 LiDAR tile processing

The LiDAR tiles are processed individually and in parallel using the Slurm[1] workload manager on the High-Performance Computer (HPC). The entire workflow takes about 5-10 minutes per tile depending on the number of points and all 42,467 tiles can be processed in about 3-4 hours during a typical New Zealand eScience Infrastructure (NeSI) HPC workload while competing with other running jobs. All individual image tiles are then stitched together to create image mosaics. Mosaic creation is more time consuming because it is a single-thread process and can take up to 24 hours for very large raster data. The method is set up to work on both the city- and region-wide LiDAR surveys.

All our processes run on the HPC infrastructure of NeSI. We use freely available open-source software. Most of the LiDAR workflow was developed as an MWLR internal package for previous projects in pure Python and optimised in places using Numba (Lam et al. 2015) and C++ code.

The tile-based processing workflow produces regional mosaics of key raster outputs at a 30 cm pixel resolution. The workflow performs the following steps: (1) buffering around LiDAR tiles; (2) noise removal; (3) generating a digital elevation model (DEM) and shaded terrain map (hillshade); (4) normalising the point cloud to ground height; (5) generating a digital Surface Model (DSM) and surface hillshade; (6) generating a daylight / shadow model; (7) generating a canopy height model (CHM); (8) tree crown segmentation; (9) generating region-wide mosaics of these products.

[1] https://slurm.schedmd.com/

4.2.1 Buffered LiDAR tiles

The original LiDAR tiles do not overlap, so to ensure seamless processing, we create new tiles with an additional buffer. This approach prevents border artefacts and makes parallel processing easier. We use the spatial tile index vector file as a look-up table to find neighbouring LiDAR tiles; and then new tiles are created with buffer around the central tile (Figure 3). We do this using GeoPandas[2] and PDAL[3] (Point Data Abstraction Library) merge and crop filters. For each LiDAR tile, the 8 neighbouring tiles are identified, merged and then clipped back to the central tile extent with a 60 m buffer region.

Figure 3. Creation of buffered LiDAR tile data. (Left) Original. (Middle) For each LiDAR tile, the eight neighbouring tiles are merged; (Right) The merged tiles are then clipped to the central tile extent with a 60 metre buffer area.

[2] https://geopandas.org/

[3] https://pdal.io/

4.2.2 Noise removal

The raw LiDAR data contains typical LiDAR noise, which needs to be removed. The vendor has already pre-classified noisy measurements, but we have chosen to apply additional filtering to ensure clean point clouds (Figure 4). We do this using 'statistical outlier removal' from the PDAL library.

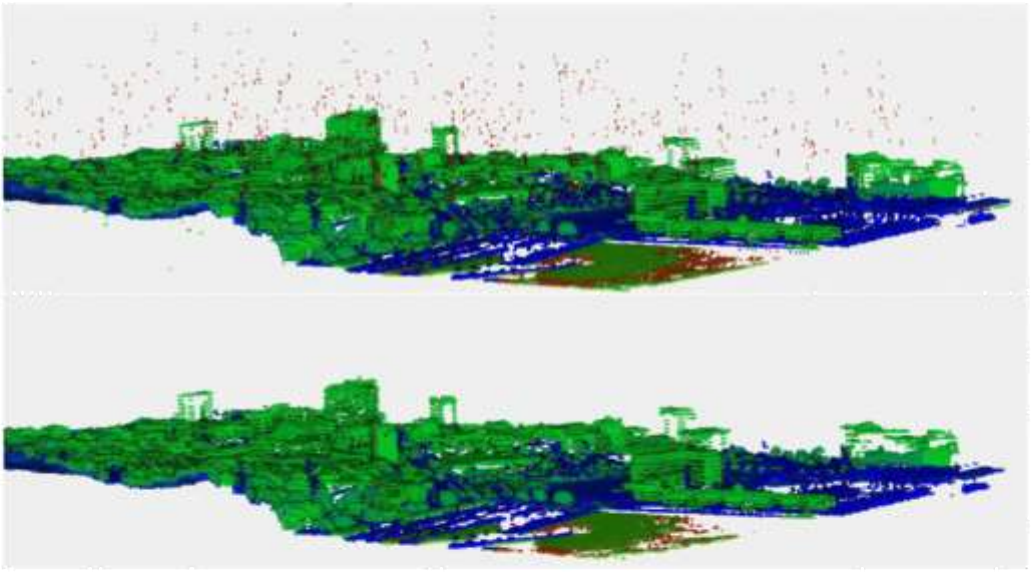

Figure 4. Noise removal of an aerial point cloud. (Top) Before; (Bottom) After. (Example is from another data set in Wellington.)

4.2.3 Generate the digital elevation model (DEM)

We use a point-to-grid methodology to assign the minimum ground point to a pixel (at 30 cm pixel resolution). We use the LiDAR classification code (ground: 2) from the vendor. To account for the width of the LiDAR beam at ground we generate 8 additional points in circular fashion around the central point with radius 20 cm, effectively mimicking the local binning method Point2Grid from Kim et al (2006). We then interpolate missing values using Natural Neighbour Interpolation (NNI). We developed a Python package for NNI with bindings to the C++ CGAL[4] functions and used OpenMP[5] to parallelise the point look-up table. This led to performance increases of several orders of magnitude compared to the PYNGL[6] NNI implementation. Hillshade rasters, which are a pseudo 3D representation of the terrain are rendered in greyscale, are created using GDAL's *gdaldem* method. Figure 5 shows examples of the DEM adjustments and hillshade.

[4] https://www.cgal.org/

[5] https://www.openmp.org/

[6] https://www.pyngl.ucar.edu/Functions/Ngl.natgrid.shtml

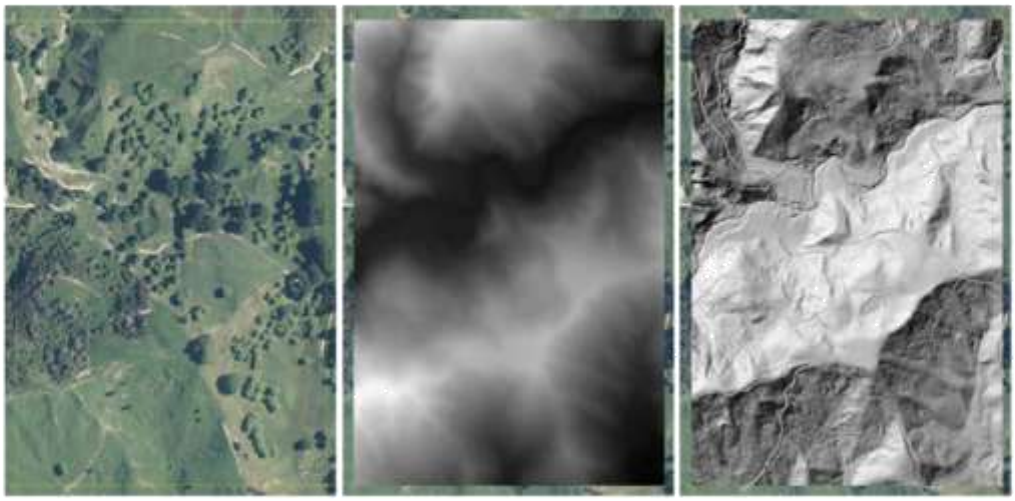

Figure 5. Examples of DEM adjustments. (Left) Original view; (Middle) With DEM; (Right) With DEM hillshade.

4.2.4 Normalise point cloud to ground height

We calculate height above ground using the ground elevation model and replaced the height (*Z*) value in the point cloud (Figure 6). This is done with PDAL's *hag_dem* filter which uses the DEM raster value below a 3D point to calculate its absolute height above ground. Absolute height of individual points is needed to inform tree and canopy height in the next steps.

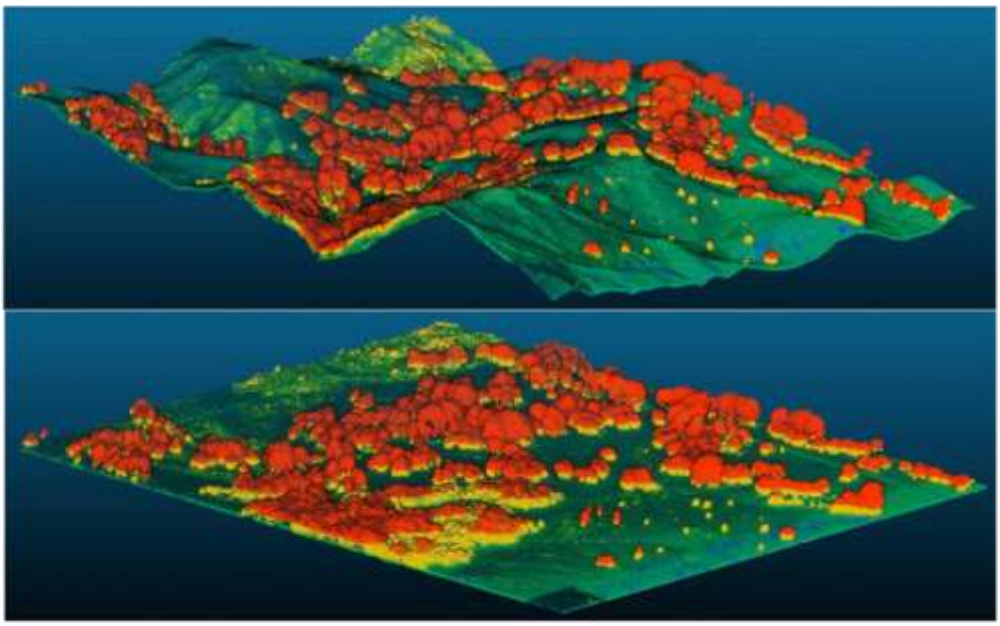

Figure 6. Height normalisation of a 3D LiDAR point cloud (Top) Before; (Bottom) After. Tall vegetation in red, short vegetation in yellow and green colours depict ground.

4.2.5 Digital surface model (DSM)

We use a similar process to DEM generation to create the DSM – but instead of binning using the minimum value, the maximum value is chosen to generate the DSM at a 30 cm pixel resolution. We then apply a 3 × 3 pixel convolutional median filter to smooth the surface model. We also compute a hillshade from the DSM (Figure 7).

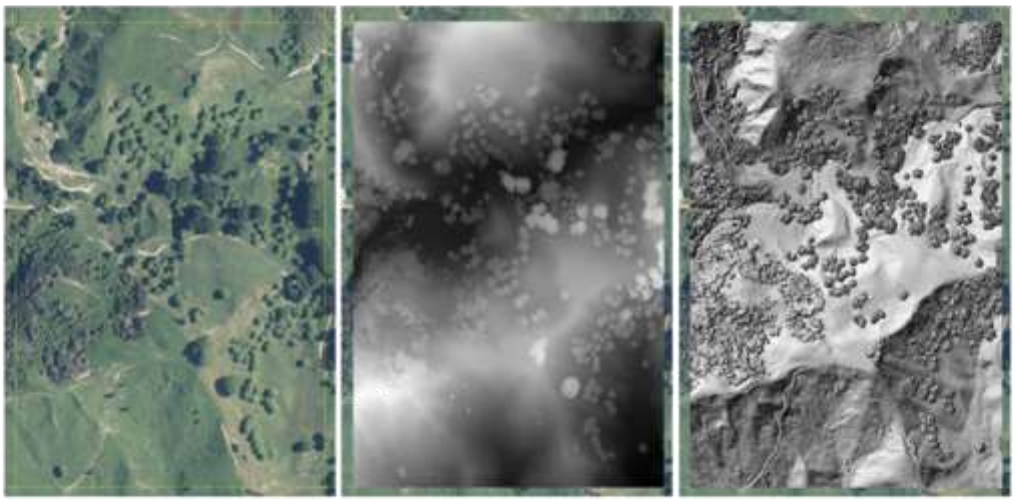

Figure 7. Example for DSM and DSM hillshade generation. (Left) Original view; (Middle) With DSM; (Right) With DSM hillshade.

4.2.6 Daylight / Shadow model

We model the proportion of time a location is within daylight, i.e. outside of an area of shadow cast by a local object, using the module 'TimeInDaylight' from the WhiteboxTools Open Core[7] software suite (Lindsay 2016). The result is a smooth and realistic shadow estimate of tree canopies, man-made structures, and other structures (Figure 8). The high-resolution (30 cm) surface model leads to extremely detailed and realistic daylight / shadow representations.

Figure 8. Daylight modelling. (Left) Original: (Right) With daylight computation.

[7] https://www.whiteboxgeo.com/manual/wbt_book/available_tools/geomorphometric_analysis.html?highlight=daylight#timeindaylight

4.2.7 Canopy height model (CHM)

We use the original LiDAR classification by the vendor to filter for vegetation points – this means buildings and other objects are discarded in this process. It is important to note that the classification is not 100% perfect, and any errors (e.g. misclassification of buildings as vegetation) will carry over to the CHM-derived layers. We use the point-to-grid method for binning canopy height (highest point in a 30 cm window) to 30 cm pixel resolution; and the raster is then smoothed using a 3 × 3 median filter, and with filling data values in pixels with no data (Figure 9).

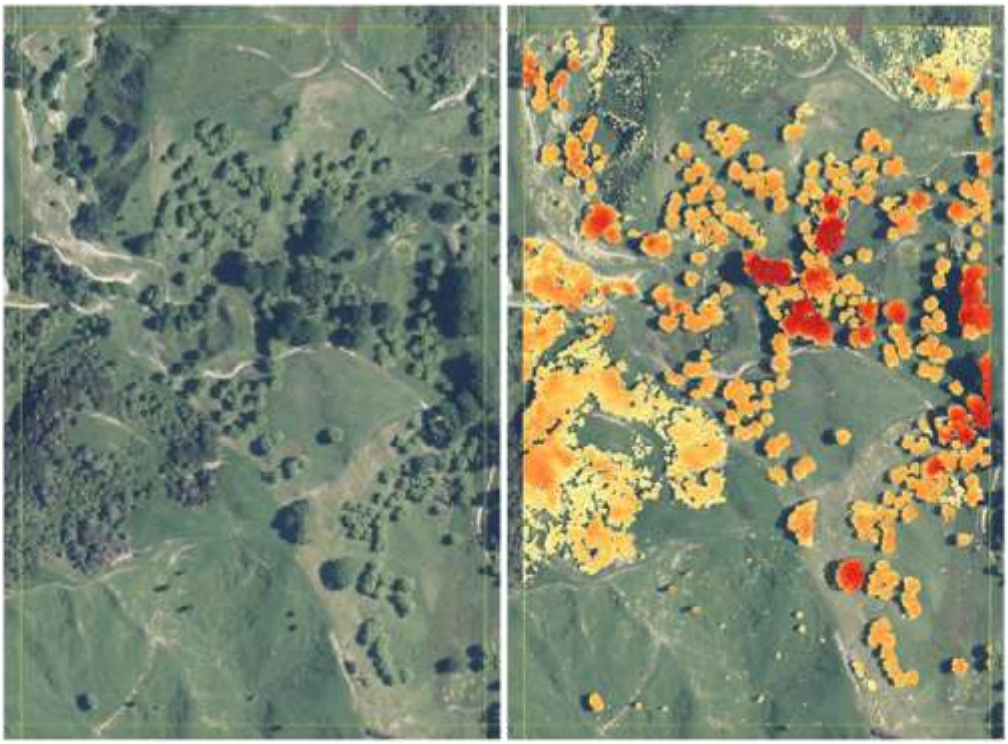

Figure 9. Canopy height model (CHM). (Left) Original; (Right) Example with yellow colours representing short vegetation and darker red colours representing taller vegetation.

4.2.8 Tree crown segmentation

We apply the MWLR-internally developed PyCrown algorithm (Zörner et al. 2018a, 2018b) to segment individual tree crowns and label trees with a unique identifier. PyCrown is a parameterised circular region-growing algorithm with local maxima as initial seeds (Dalponte et al. 2016) and works in three steps: i) smoothing the CHM; ii) identifying tree top locations; and iii) delineating crown boundaries (Figure 10). The algorithm requires a set of parameters describing rules for tree segmentation from the CHM. We used a minimum tree height of 3 metres, a maximum height of 60 metres, applied a spatial median filter with size of 3 metres, and a local maximum filter to detect tree top location with a filter size of 2 metres. We used the standard settings from (Zörner et al. 2018) describing the rule-based threshold system for running the region-growing algorithm.

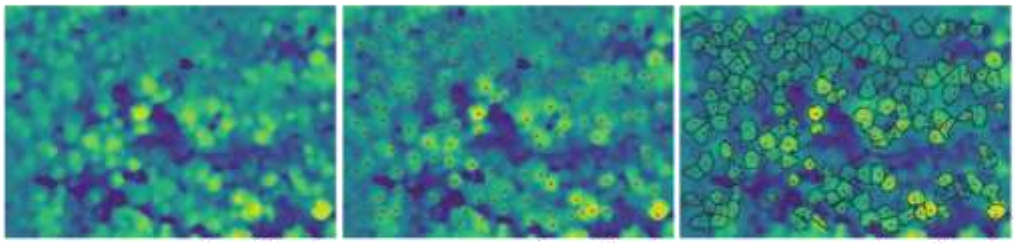

Figure 10. PyCrown tree identification process. (Left) Original. (Middle) Treetop locations are approximated using a local maximum filter. (Right) A seeded region-growing algorithm is then applied to generate crown outlines.

We then export the treetop locations and crown polygons (Figure 11) as GeoPackage files, which is an open format for geospatial information. Treetop height information and calculated crown diameter are added as attributes in the feature table, available for each tree object. The mean diameter is approximated by, first, calculating the minimum bounding rectangle of each crown and, then, calculating the mean of the minor and major axis side lengths. Information on tree height and diameter can be readily extract and visualised (Figure 12).

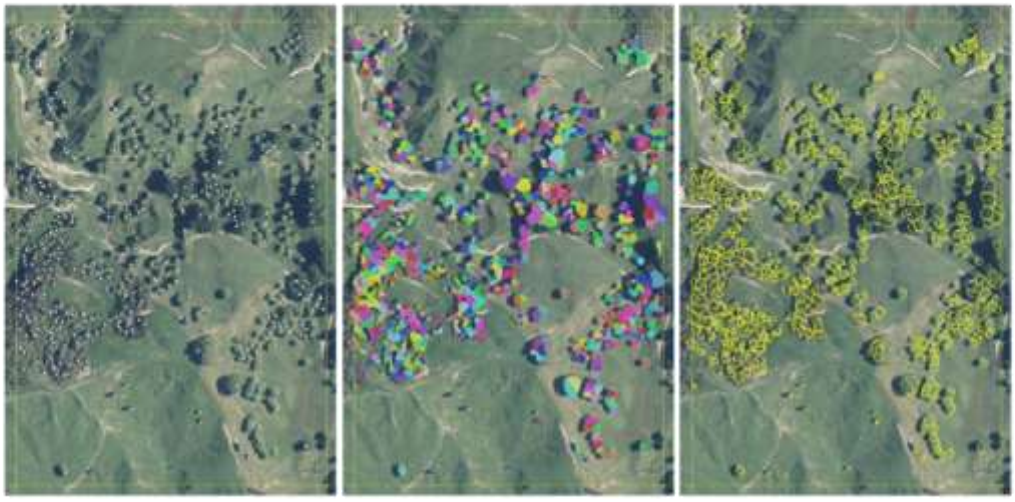

Figure 11. Treetop location refinements. (Left) Example for treetop location; (Middle) Rasterised raw PyCrown objects labels with random colouring. (Right) Individual tree crown polygon data.

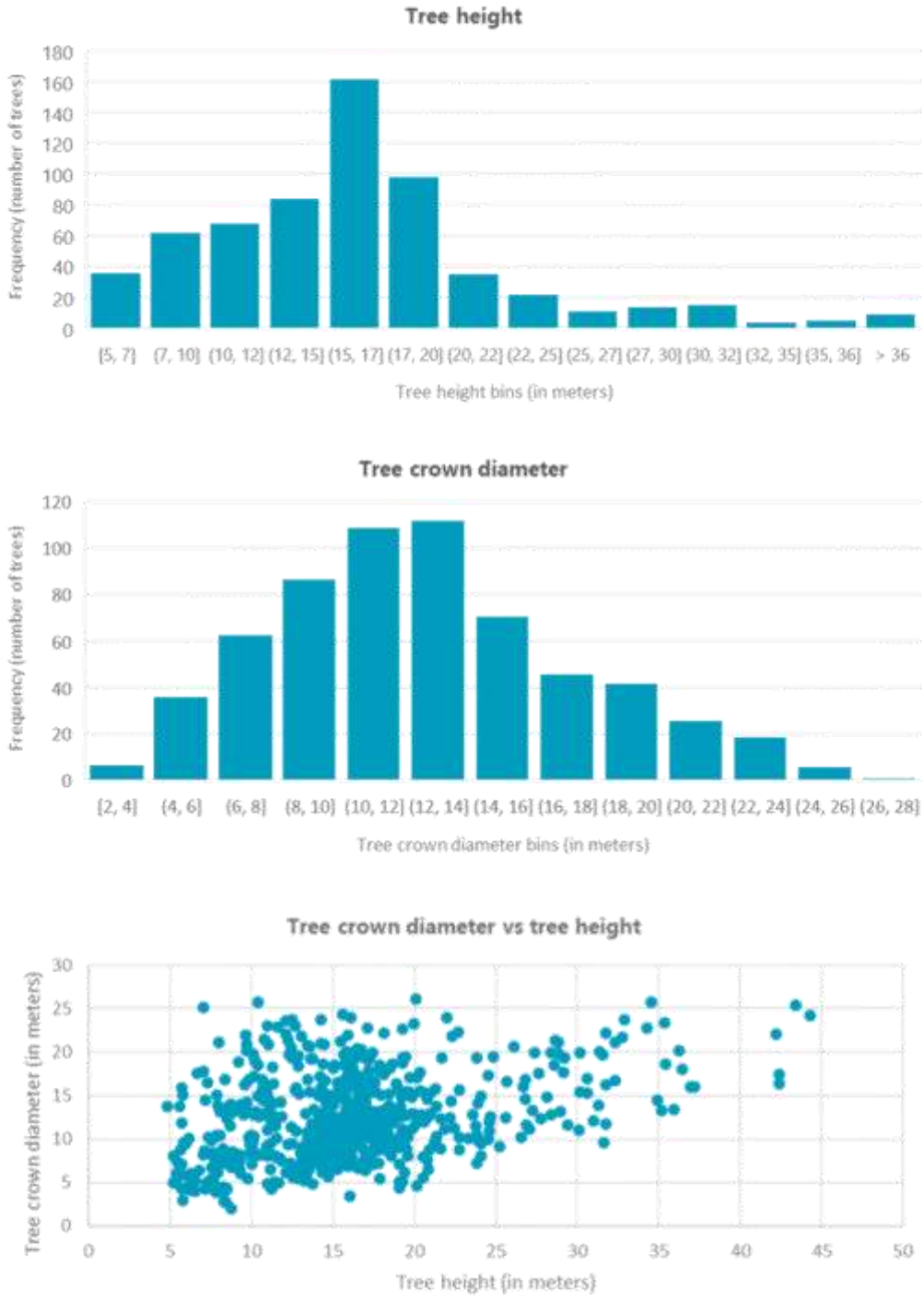

Figure 12. Example of individual tree statistics (for same tile as in Figure 13) that are automatically populated in the tree point data set. (Top) Histogram of tree height, corresponding to the highest CHM values within the crown polygon; (Middle) Histogram of crown diameter, estimated by approximating by the crown polygon shape; (Bottom) Scatterplot of crown radius vs tree height.

4.2.9 Region-wide LiDAR raster mosaics

We cut off the added buffer around each LiDAR tile product, i.e. the CHM, DEM, DSM, daylight and all hillshade rasters, and group all tiles into virtual raster files using the gdal *gdalbuildvrt* tool. We then convert the virtual rasters into large regional mosaics in the efficient KEA format using the gdal command *gdal_translate*.

For compatibility reasons we also create mosaics in a more commonly used raster format which is the cloud optimized GeoTIFF with a LERC_DEFLATE compression with PREDICTOR=2 and a MAX_Z_ERROR=0.01 (in metres). The latter provides lossy compression to the second decimal place, which is adequate for the vertical resolution of the LiDAR products.

4.3 Deep learning for semantic segmentation

Deep learning approaches and especially encoder–decoder convolutional neural networks (CNNs) have quickly become the state-of-the-art in computer vision tasks such as semantic segmentation (e.g. for land cover mapping in aerial imagery) because of their superior classification accuracy and low level of pixel noise. Deep learning encoder–decoder networks translate one image to another, with the second image being generally less complex than the first. The network is trained by repeatedly applying it to pairs of input and output images, and incrementally adjusting the model's parameters to gradually improve overall performance on the task. This approach can be readily applied to mapping automation by training the encoder–decoder network on a rasterised version of the current map and the imagery originally used to generate it. The model is trained on a subset of the area of interest, where examples of the target type have been extensively mapped. The model is then applied to the rest of the area.

Deep learning networks typically produce a semantic raster, in which each pixel represents the class of the corresponding image pixel. However, the model can also generate a *probability* raster, where intensity represents the model's confidence in each pixel being of the target class. As well as learning to perform the mapping task, encoder–decoder networks can potentially improve on the original map if there are errors; this is because these errors contradict the general patterns learned, and so are ignored during training and corrected when the model is run over the same imagery. This approach has the potential to discover additional, i.e. not previously labelled, target objects within the training area.

We explored using deep learning encoder–decoder networks to transform canopy height models at high resolution (30 cm) and medium resolution (1 metre) into probability rasters that suggest candidate areas for pine forests and shelter belts, respectively.

4.4 Tree canopy and short vegetation layers

The high-resolution regional CHM can be visualised and colour-coded based on different threshold levels. However, it is useful to have stand-alone layers of discrete classes such as tree canopy and short vegetation. We create such rasters by dividing the canopy height model into two classes: above 3 metre (tree canopy) and below 3 metres (low vegetation) (Figure 13).

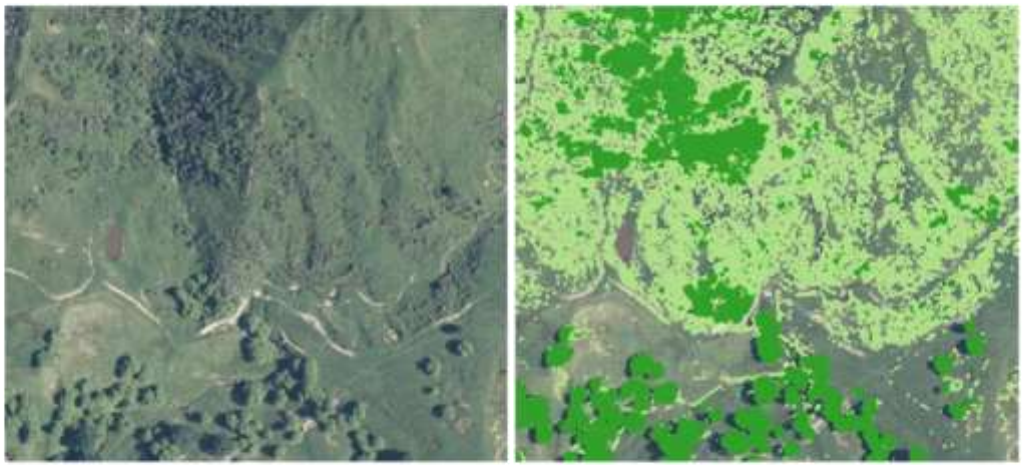

Figure 13. Layer visualisation. (Left) Original; (Right) Example for low (< 3m) vegetation (light green) and tree canopy (dark green) layers.

4.5 Forest layer

Any definition of forest extent depends on the mapping purpose and specific requirements will probably change. Therefore, our definition of forest extent just provides a baseline and should provide a more high-level interpretation of contiguous tree canopy with a minimum mapping unit. We apply a transparent method, which can be replicated and adapted to future needs.

The forest layer is derived from the regional canopy height raster with a minimum mapping unit of 1 ha (100 × 100 m). The 30 cm resolution CHM is reduced to a 1 metre pixel grid using cubic interpolation, because the fine detail is not necessary. Again, a minimum threshold of 3 metres for tree canopy is applied. The resulting data still contains many small fragments, is noisy around edges of canopy, and can also contain many small holes. We decided to run a series of binary morphological operations to smooth out the raster. We, first, applied a binary operation followed by a binary closing operation using a circular filter (3 m diameter). This smooths out edges of canopy objects. We then removed objects smaller than 1 ha in size and also removed small holes of larger objects, also applying a 1 ha threshold. The forest raster layer (Figure 14) was then polygonised using the *gdal_polygonize* tool and, again, simplified to 1 metre resolution using the "ogr2ogr -simplify 1" tool. This results in a smooth and consistent forest layer for the entire region.

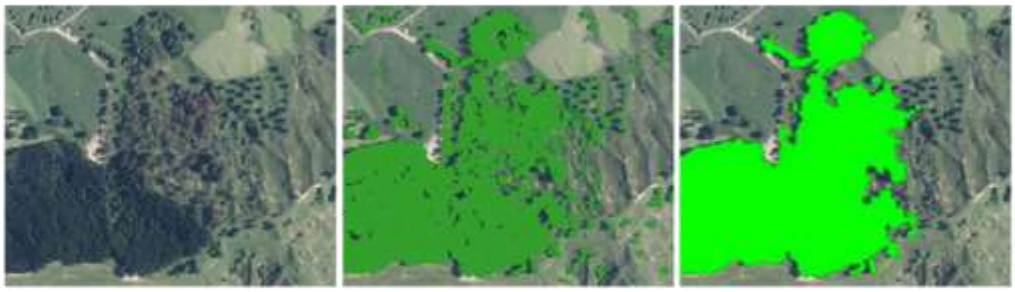

Figure 14. Forest layer comparisons. (Left) Original; (Middle) Tree canopy layer; (Right) Forest layer. The forest layer provides a more high-level interpretation of contiguous tree canopy with a minimum mapping unit of 1 ha.

4.6 Individual tree layer

The tree location information from each individual LiDAR is merged into one large vector file and includes the tree height and crown radius attributes.

In addition to the LiDAR-derived tree estimates we also tested the experimental deep learning-based tree detection methods developed in other MWLR-led research projects and applied a pre-trained YOLO (Redmon et al. 2016) model from Greater Wellington to the 30 cm aerial RGB photography from 2021–2022 over the whole of the Hawke's Bay region. The aerial image-based solution can supposedly give an independent estimate of tree counts over the region useful for comparison.

4.7 Shelter belt layer

We follow a semi-supervised object delineation approach in which we: (1) manually label an extensive training data set of shelter belts; then (2) train a deep learning model to recognise this vegetation class purely from the rasterised canopy height data.

The training data was designed to capture a variety of different shelter belt representations, landscape types and areas in which no shelter belts appear (Figure 15). No concrete definition of how shelter belts must look like were available at the time, so this is a best effort of delineating likely shelter belt areas.

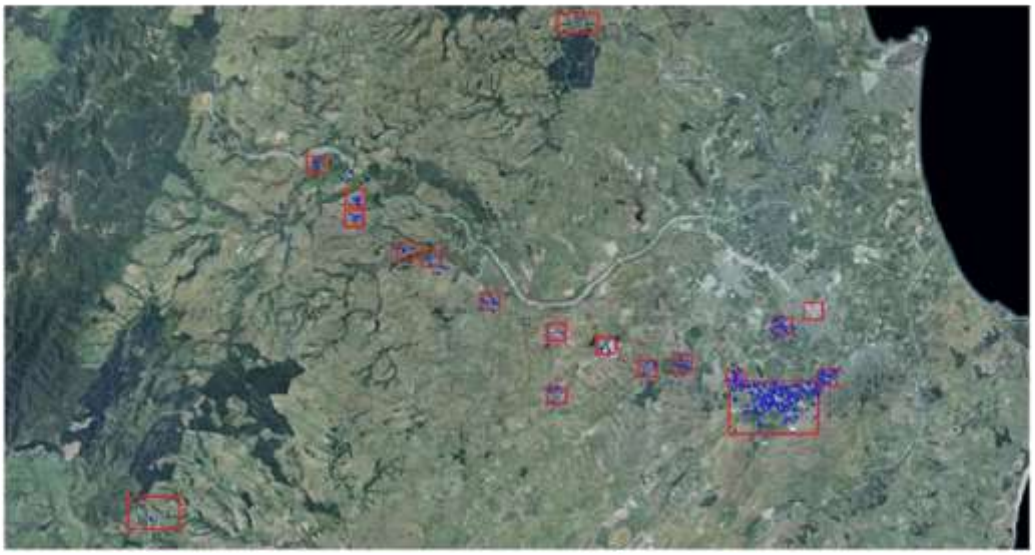

Figure 15. Training areas (red polygons) capturing different landscapes and shelter belt types. Blue polygons depict manually drawn shelter belts.

The manual digitisation was conducted in a GIS and all visible shelter belts within the training areas delineated. In total, 540 shelter belts of different sizes were mapped in 18 training areas covering an area of 51.59 km^2. The CHM was overlaid over the aerial RGB photography as visual aid to guide the manual mapping. Manual digitisation of shelter belts is complicated by the fact that many subjective decisions have to be taken when drawing polygons (e.g. what is the minimum height, what are the minimum and maximum side lengths, how far apart can trees be located to still form a shelter belt, and more). In many cases, decisions depend on the local context and many factors play together. This means we have created a training data set which provides a general interpretation of shelter belts, which are not too short and not too wide (Figures 16 and 17). Our training data set can be adapted in the future to cater for more specific requirements.

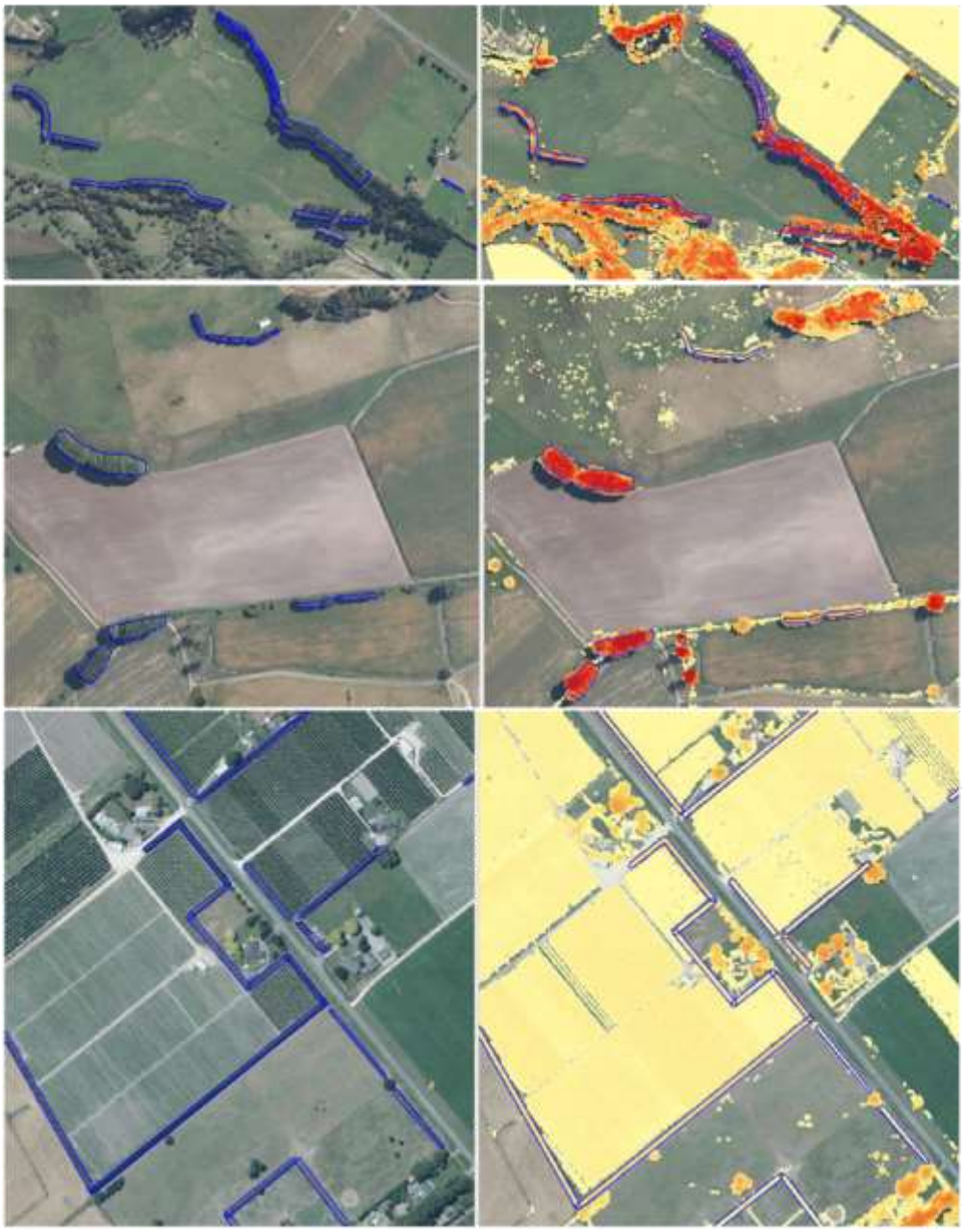

Figure 16. Shelt belt layer training data. Examples of shelter belt polygons (blue polygons) manually drawn in a GIS with aerial photograph in background; (Right top, middle and bottom) shows the corresponding canopy height with yellow depicting short vegetation and red taller vegetation.

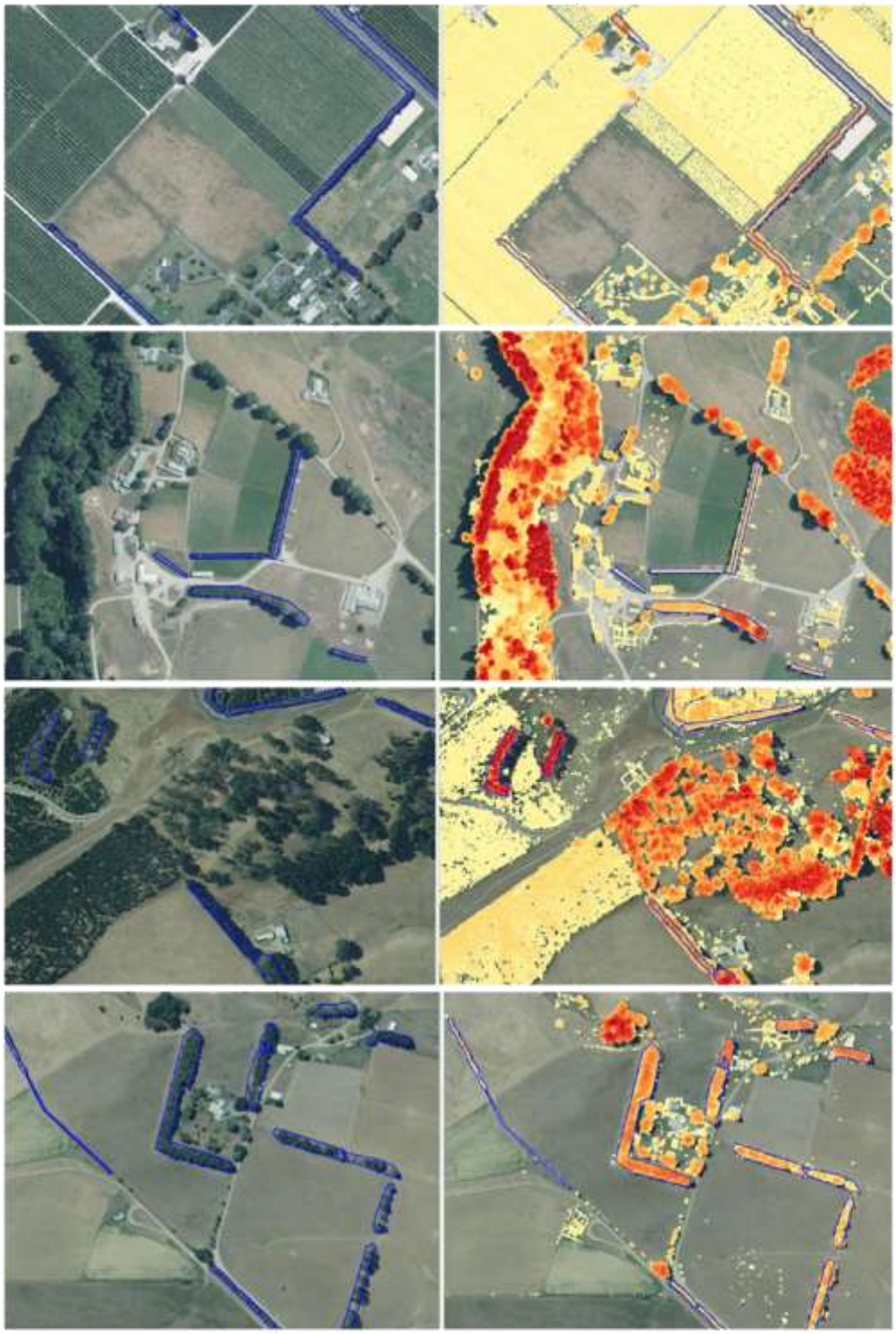

Figure 17. Shelt belt layer training data. Examples of shelter belt polygons (blue polygons) manually drawn in a GIS with aerial photograph in background; (Right top, middle and bottom) shows the corresponding canopy height with yellow depicting short vegetation and red taller vegetation.

The canopy height raster was split into small square tiles within each training area with 512 × 512 pixels. We conducted a random sampling approach, splitting up the image and label data set into 80% training and 20% validation sets. We then trained a UNet-type CNN model (Ronneberger et al. 2015) with a Resnet101 encode backbone pretrained on the imagenet data set, using the PyTorch framework with focal loss with gamma = 2, a batch size of 16, a learning rate of 0.0001 and the following augmentations: horizontal and vertical flip, transpose, and random rotation of 90 degrees. We trained the model for 1.5 hours on a NVIDIA A100 GPU until the validation loss and accuracy reached their maximum and stabilised (Figure 18).

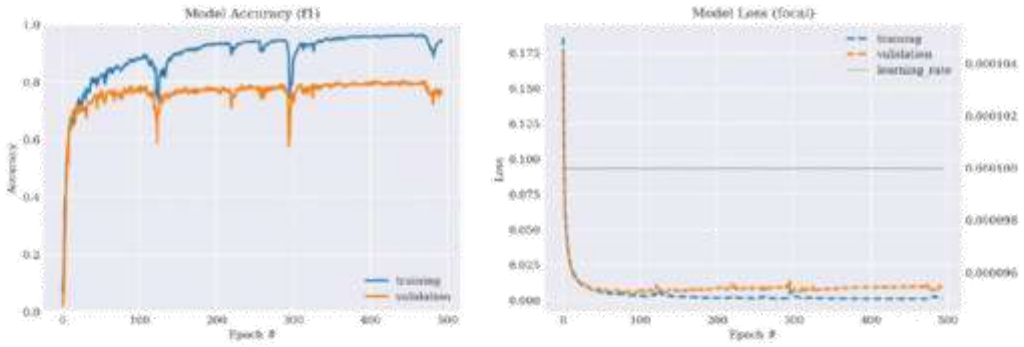

Figure 18. Deep learning model training curves of accuracy and loss for shelter belt segmentation.

4.8 Pine / exotic forest layer

The HBRC requested we separate out exotic from native forests. We decided that it is easier to focus on classifying pine from the CHM than trying to identify a complex native forest class. Pine forest is distinct in shape and structure and can be visually distinguished from mixed, native forest (Figure 19).

We follow a similar mapping approach as for the shelter belt layer by: (1) generating spatial training labels from the CHM; (2) training a deep learning model; (3) running the prediction over the entire region.

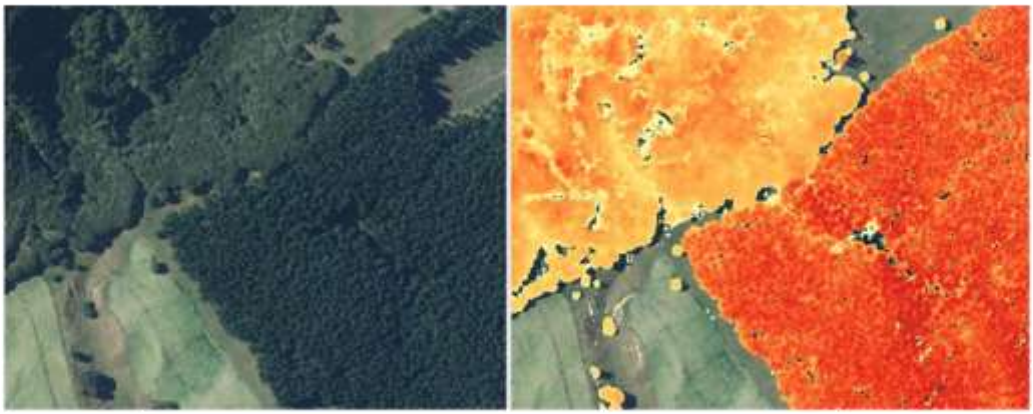

Figure 19. Different structural appearance of pine (lower right in both images) and native forest (upper left in both images). (Left) Aerial photograph; (Right) 30 cm canopy height model with shorter trees in yellow and taller trees in red. The aerial photo was taken later, and a patch of pine forest has been removed.

We used the high-resolution CHM at 30 cm pixel resolution because the distinct shape and structure of both young and mature pine trees is clearly visible at this fine scale. At lower resolution CHM, e.g. the standard 1 metre CHM products, this signal becomes blurry, and it is harder to detect the structure of individual trees (Figure 21).

We first created training data for various types of pine forests (i.e. young plantation, medium and mature stands) and trained a UNet model on this. The resulting predictions indicated a strong correlation of freshly planted pine forest with vineyards and orchards because of similar planting patterns as observed in the CHM (Figure 22). We, therefore, extended the initial training data set by explicitly including fields. One possibility is to add training areas over fields and just ignore all values, by using these as false negative areas. Alternatively, we could create a separate class which can be later used to identify fields in CHM raster directly. We decided to take the latter approach and test how useful such an experimental class can be.

We manually digitised 166 pine forest polygons as well as 538 fields polygons in 20 training areas covering a total area of 205.6 km^2 (Figure 20). Again, the training areas are designed to capture different landscape types including urban, native forest, water, and agricultural areas.

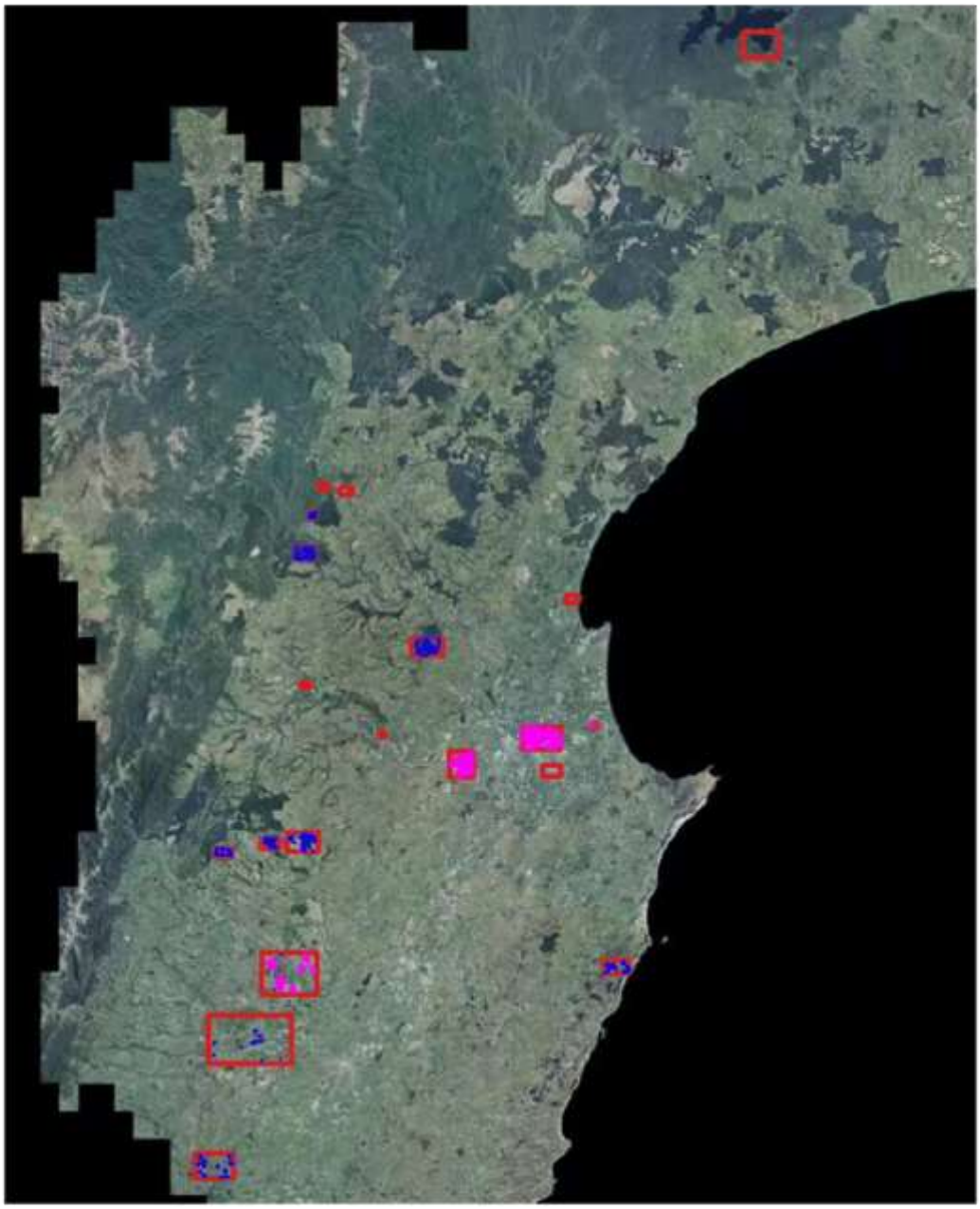

Figure 20. Training areas (red lines) for pine forest detection. Blue polygons indicate manually mapped pine forest and pink areas indicate fields (vineyards/orchards) used as separate class.

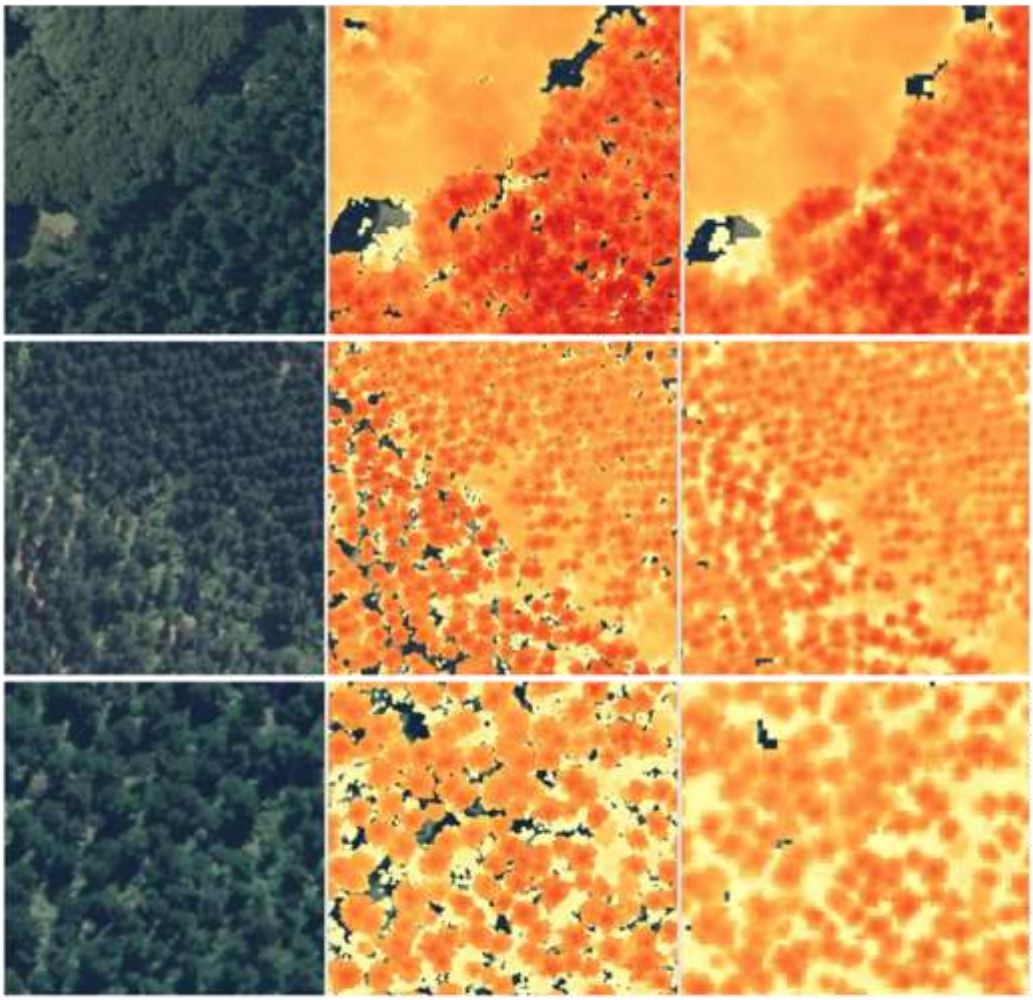

Figure 21. Impact of raster resolution on pine forest detection. (Left) Aerial photography; (Middle) The 30 cm CHM can resolve the fine structure and shape of pine trees at different age classes. (Right) The signal becomes less pronounced at lower resolutions, i.e. the standard 1 m CHM product.

Figure 22. Training polygons (pink) around fields, including orchards and vineyards; these features can appear structurally similar to freshly planted pine forest. (Left) Aerial photography; (Right) 30 cm canopy height model.

5 Results

5.1 Regional LiDAR raster products

We generated eight regional raster products, all at 30 cm pixel resolutions: a DEM, DEM hillshade, DSM, DSM hillshade, CHM, tree canopy, low vegetation, and the daylight/shadow model (Figure 23). All data is stored in the efficient cloud-optimised GeoTIFF format with internal pyramid layers (GIS overviews) computed, totalling about 954.5 GB on disk. The extremely fine resolution of the data sets provides unprecedented detail of the ground (Figure 25) and canopy surface of the entire region. The daylight/shadow layer is not only useful as GIS base layer for realistic-looking 3D visualisation but gives indication of the shadowing effect of trees and man-made structures (Figure 24).

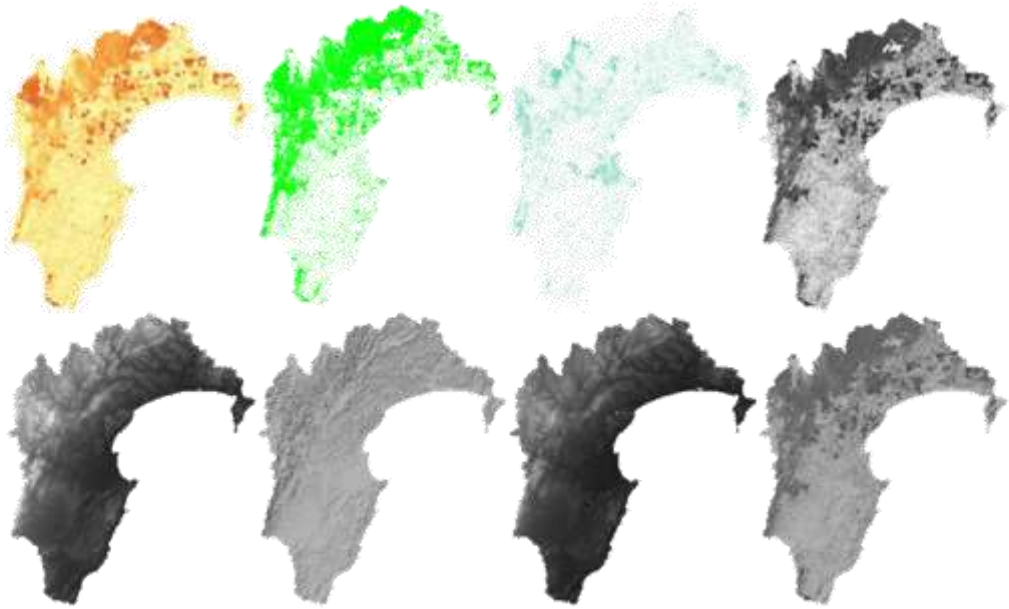

Figure 23. Regional LiDAR products at 30 cm. (Top, left to right) CHM, tree canopy, low vegetation, daylight/shadow. (Bottom, left to right) DEM, DEM hillshade, DSM, DSM hillshade.

Figure 24. Daylight and canopy height. (Left) Daylight/shadow layer; (Right) Daylight/shadow layer with the canopy height overlaid.

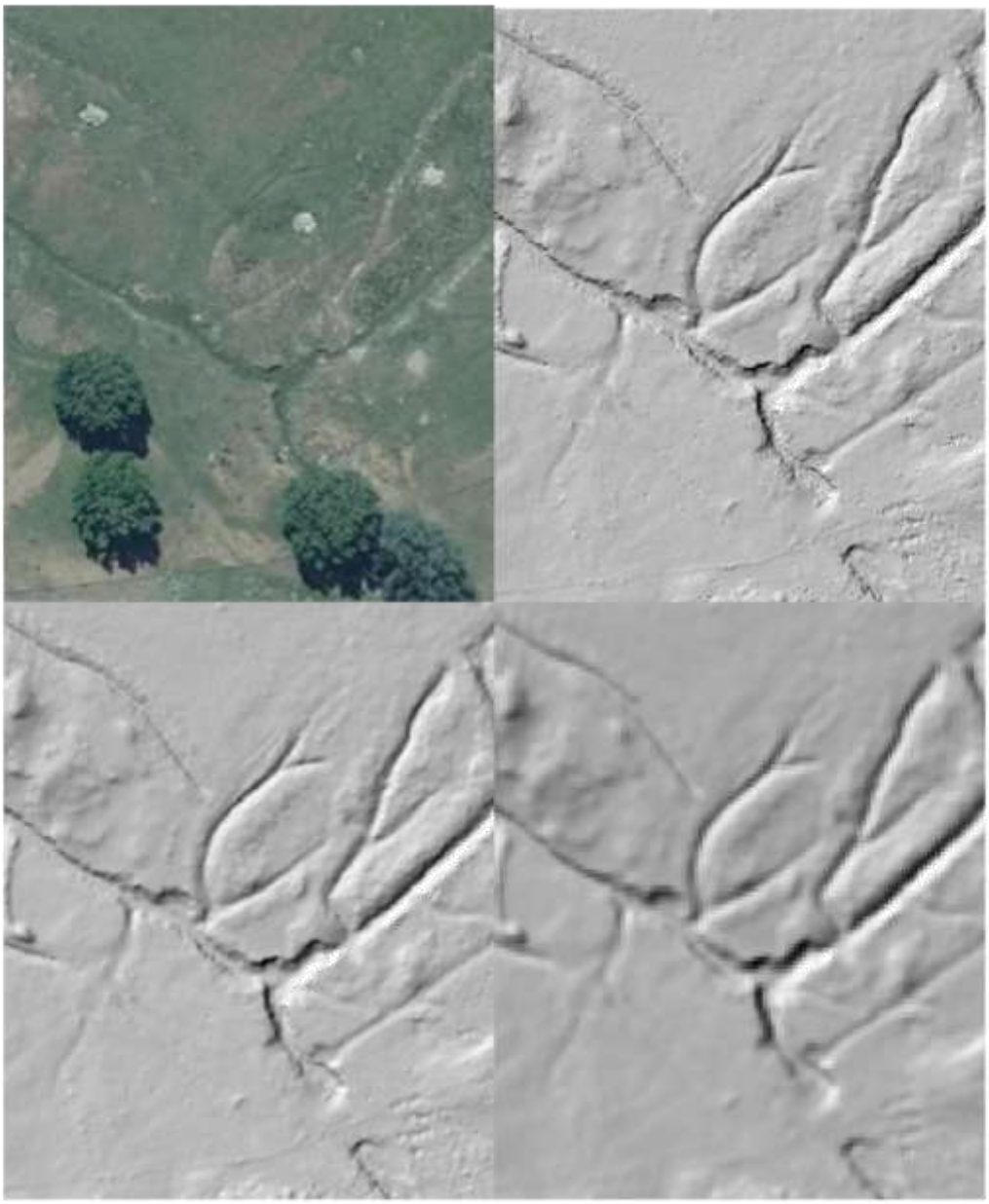

Figure 25. Comparisons of resolutions. (Top left) Original; (Top right) Spatial detail of the very fine 30 cm resolution elevation model; (Bottom left) In the 50 cm DEM model; (Bottom right) In the traditional 1 m DEM.

5.2 Regional LiDAR vegetation layers

We derived a total of seven LiDAR-derived vegetation products consisting of: single trees, tree canopy, short vegetation, shelter belts, forest cover, pine/exotic forest, and an experimental fields layer (Figure 26), totalling 7.3 GB with the single tree layer alone occupying 6.9 GB. This gives an extremely detailed picture (Figure 27) of the vegetation status at the LiDAR acquisition date and provides a baseline for future change analysis. It also vastly surpasses the spatial detail of previous large-scale land cover products such as the Land Cover Database of New Zealand (LCDB v.50) of Manaaki Whenua – Landcare Research (2020).

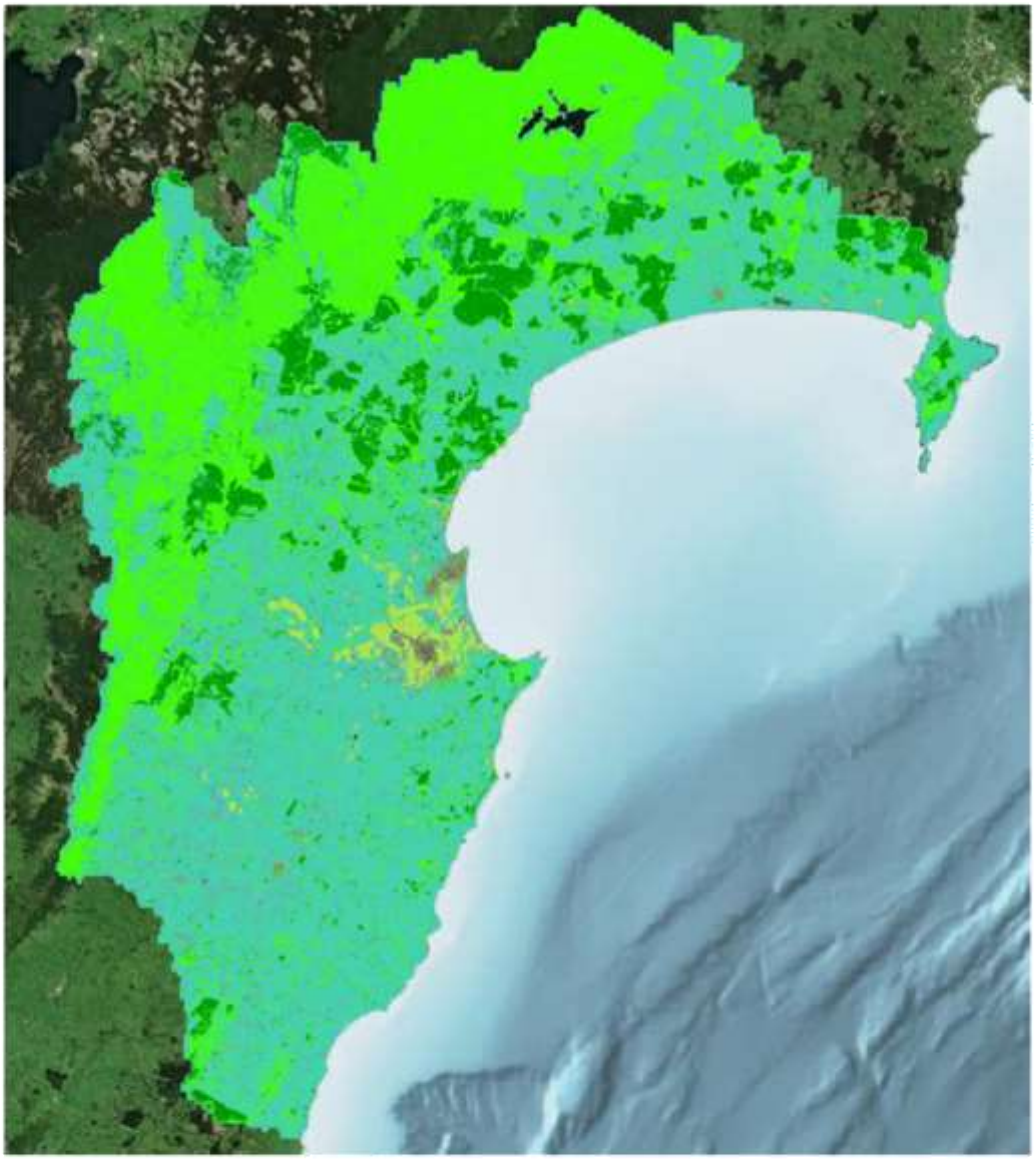

Figure 26. Overview and extent of region-wide vegetation layers for Hawke's Bay region depicting forest cover in bright green, low vegetation in pale green, individual trees, shelter belts in pink, fields in yellow and pine forest in dark green. Buildings are indicated in red.

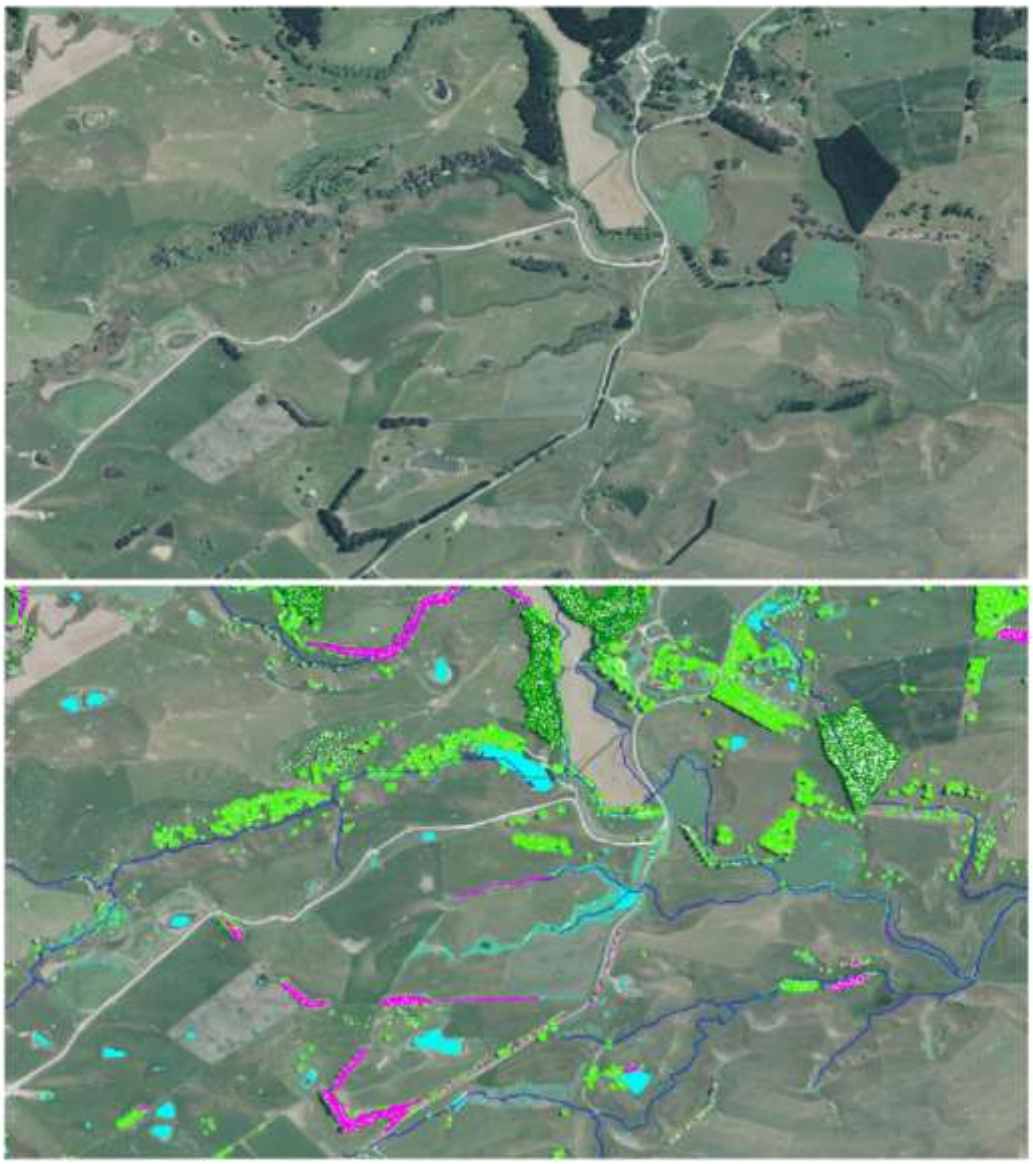

Figure 27. Example of vegetation classification. (Top) Original. (Bottom) With classification (water bodies in cyan, individual trees as white dots, tree cover in bright green, low vegetation in pale green, pine in dark green, shelter belts in pink and river network in blue). The intersection between buffered water area and vegetation types may help categorise riparian vegetation and wetlands.

5.2.1 Individual tree layer

All tree information from the individual LiDAR tiles was merged to form a point vector layer for the region (Figure 28). In total, we counted 57,293,929 trees > 3 metre over all forest, rural and urban landscapes.

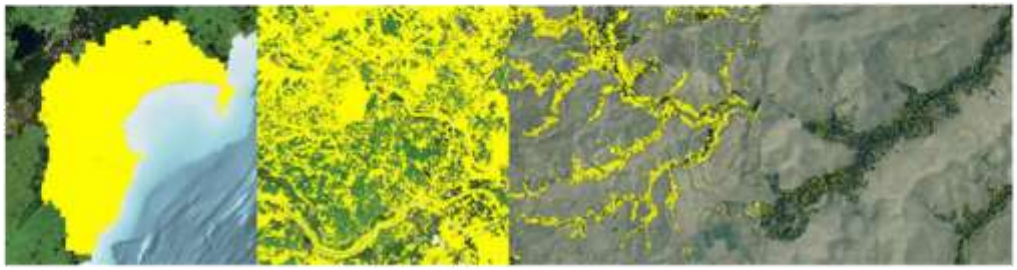

Figure 28. The individual tree layer (yellow dots) for Hawke's Bay, capturing trees in all landscapes. The panels (left to right) show zoom-ins.

We conducted an experiment to identify trees from the regional aerial photography using a deep learning approach and compared it to the LiDAR-derived individual tree layer. While PyCrown estimated about 57.3 million trees, the YOLO deep learning model estimates around 58.2 million trees, which was very close to the LiDAR-estimate. While the overall numbers are similar, there are interesting differences at local scale (Figure 29). The LiDAR-based approach is highly parameterised and many decisions have to be made to define minimum tree height or minimum spacing between trees, whereas for the deep learning based approach no height information is used and the prediction of tree locations depends more on the training data and model structure. In this experiment, we found that both solutions work well at identifying trees of various sizes and shapes. The PyCrown approach gave a consistent and interpretable result which can be adapted and fine-tuned to specific tree types if required. The deep learning approach worked without setting any rules, can identify very short trees, and uses the optical RGB information to find trees – which is often much more informative than the CHM structural information alone.

Figure 29. PyCrown LiDAR-derived tree locations (red dots) vs YOLO deep learning estimates (yellow triangles). (Top) Rural scene; (Bottom) Urban scene in Napier. The red PyCrown predictions are on top of the green YOLO predictions leading to some of the latter not being visible. PyCrown used a 3 m tree height threshold, whereas no height threshold was used in the image-based approach.

5.2.2 Shelter belt layer

The UNet model was applied to the CHM of Hawke's Bay and the pixel-wise predictions were converted into polygon vector layer of shelter belts (Figure 30). In total, we counted 39,798 shelter belts.

Figure 30. Region-wide layer of shelter belts in Hawke's Bay. Shelter belts depicted as polygons with pink outline. (Left): Entire study extent; (Right) Zoom-in.

The overall accuracy on the validation data set is high with a F1-score of 80% (with 100% being a perfect classification). The F1-score metric represents the pixel-wise classification score; however, it is not ideal for evaluating how good the classifier actually was at detecting shelter belts. This metric merely reflects how well the predicted shelter belt polygons match the manually labelled training polygons – which can be quite different on purpose. Training polygons were drawn outlining linear features of shelter belts, but not perfectly delineating the vegetation belonging to a particular shelter belt. The model might learn vegetation features more broadly and training labels and predicted labels might differ slightly (Figures 31 and 32). We therefore considered it would be useful to estimate the number of correctly detected shelter belts and compare the areas of the manual labels with the predicted areas. Specifically, we asked the following three questions – and received the answers shown.

1 How many of the shelter belt polygons (not part of the tiles used for training) were detected by the prediction?

Answer: 100% of manually digitised shelter belts were predicted (partly or fully).

2 How much of the manually labelled area (not part of the tiles used for training) is covered by the predicted shelter belt area?

Answer: 97%; almost all the labelled shelter belts pixels were successfully predicted.

3 How much of the predicted shelter belt area was outside the training labels?

Answer: 23%; the prediction produced more shelter belt pixels compared to the manual labels.

Deep learning predictions are difficult to interpret, and it is impossible to explain in natural language why some predictions in specific locations were made and some not. We inspected over 1,000 individual polygons and can confirm that the model, overall, learned the general patterns of shelter belts from the training data set well. However, there were also spurious predictions and instances in which a human operator would take a different decision. This predominantly occurred either in areas that are inconclusive (where an operator might struggle too), or along linear vegetation features such as riparian or other plantings (which are difficult to tell apart from shelter belts in a single band CHM). The data set needs filtering based on rule sets to define which predictions can be confirmed as shelter belts and the same rules should be applied in the future to the training data to re-fit the model and refine predictions.

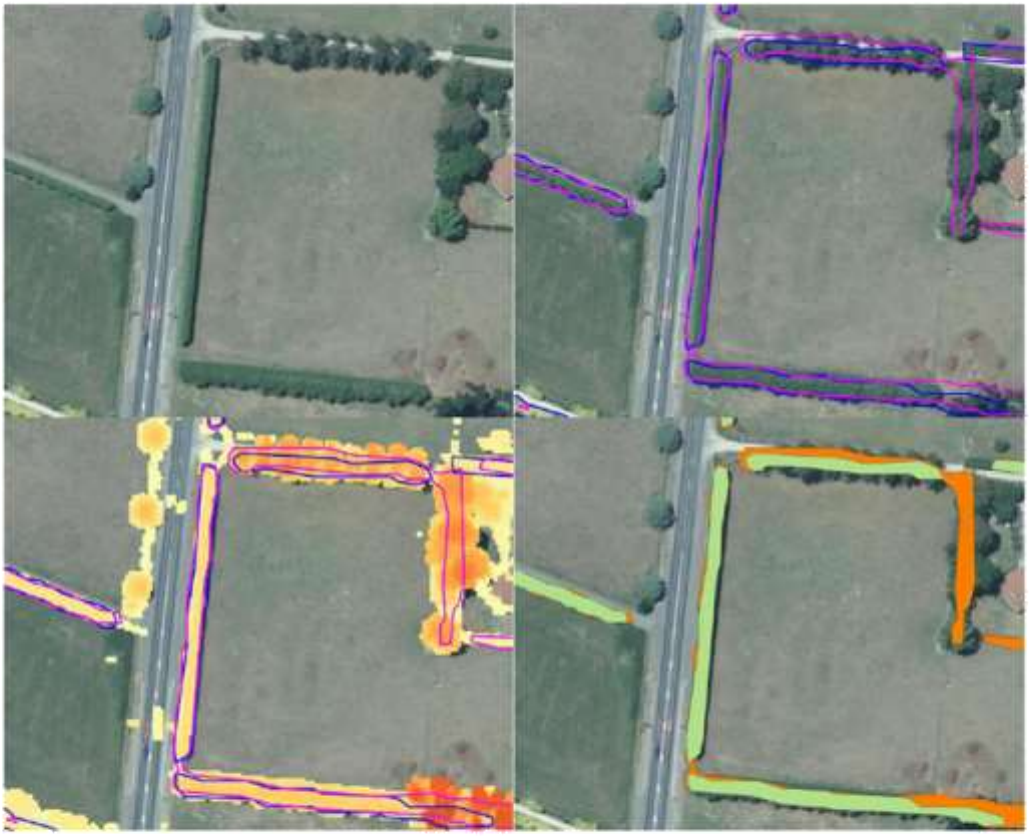

Figure 31. Example of the shelter belt model performance. (Top left) Aerial photography; (Top right and bottom left) Shelter belt predictions (pink outlines) compared to the manual labels (blue outlines). (Bottom left) Canopy height is displayed; (Bottom right) Comparison of the true positives (green shading) and false positives (orange shading). In many cases the model was better than the training data. Here, the false positives actually indicate areas that are probably shelter belts but weren't properly labelled for training.

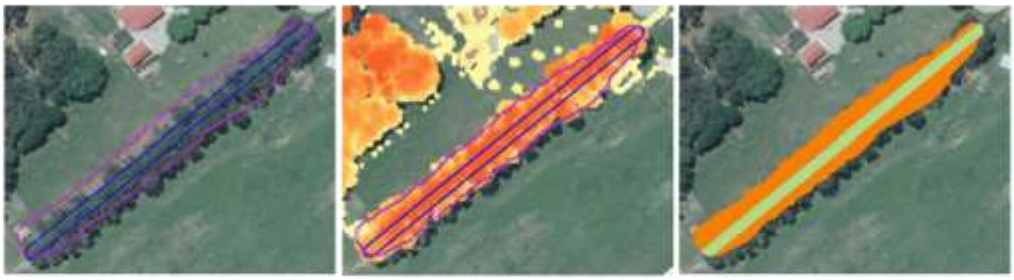

Figure 32. Examples of differences and learning. (Left) Difference between manual labels (blue outlines) and model predictions (pink outlines); (Middle) Same as left panel, but with CHM overlaid (Right) Showing the model classifying correctly but learning to expand to the vegetation canopy, rather than predicting artificial, straight lines. True positives (green shading) and false positives (orange shading).

5.2.3 Pine forest layer

The UNet model was applied to the CHM of Hawke's Bay and the pixel-wise predictions were converted into a polygon vector layer of pine forests (Figure 33). A total of 18,662 polygons were produced covering total area of 1,511.8 km^2. Similarly to the shelter belt layer results, the UNet model was able to improve the manual labelling in places and delineate smoother outlines (Figure 34). We found 94.8 % of the manually labelled pine forest polygons were detected by the model. The model F1-score for the pine class (i.e. the pixel-wise semantic segmentation accuracy) against the validation data set was very high at 96.9 %. False positives were rare but may occur over agricultural plantings with similar structural properties.

Figure 33. Region-wide layer of pine forest (green polygons) in Hawke's Bay. (Left) Result for entire study extent; (Right) Zoom-in.

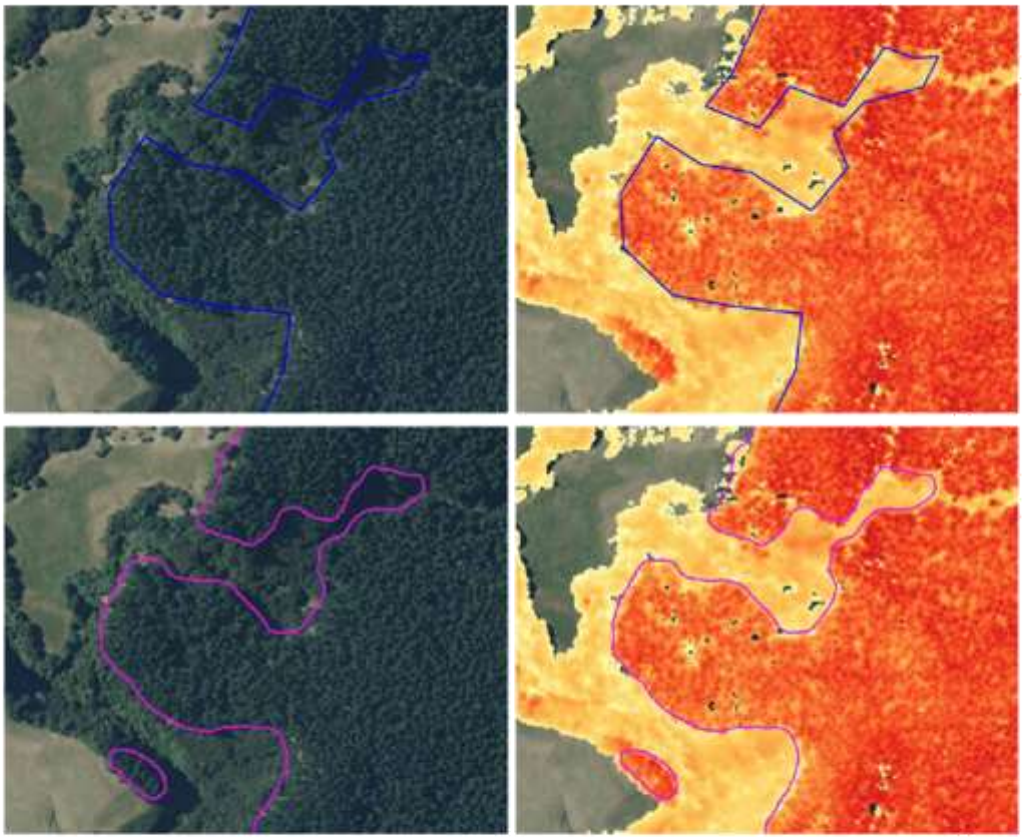

Figure 34. Examples of the model performance on the pine forest layer. (Left) Aerial photography; (Right) Canopy height model. Manual labels (blue lines) are coarse, but the predictions are smooth and more detailed. Unmapped pine is also picked up by the model.

5.2.4 Experimental fields layer

The UNet model that was trained on pine forest included a separate class called 'fields' that was meant to capture orchards and vineyards with similar structural and planting behaviours to young pine stands. The model successfully learned to pick up these regular patterns and was able to identify such fields from the CHM. The model predicted 3,948 fields with an area of about 142.8 km^2 (Figure 35). We found 99.6 % of the manually labelled fields were detected by the model and the F1-score of the fields class against the validation data set was very high at 97.3 %. It is worth noting that false positives were very rare and young pine forest was never falsely predicted as 'field' – whereas the opposite is true as discussed before.

The model output gave a comprehensive estimate of agricultural fields of various types, and was not limited to orchards and vineyards. It was not possible from the CHM to detect fields with no or very short vegetation. This limited the usefulness of the output but still captured the state of vegetation on fields at the LiDAR acquisition date.

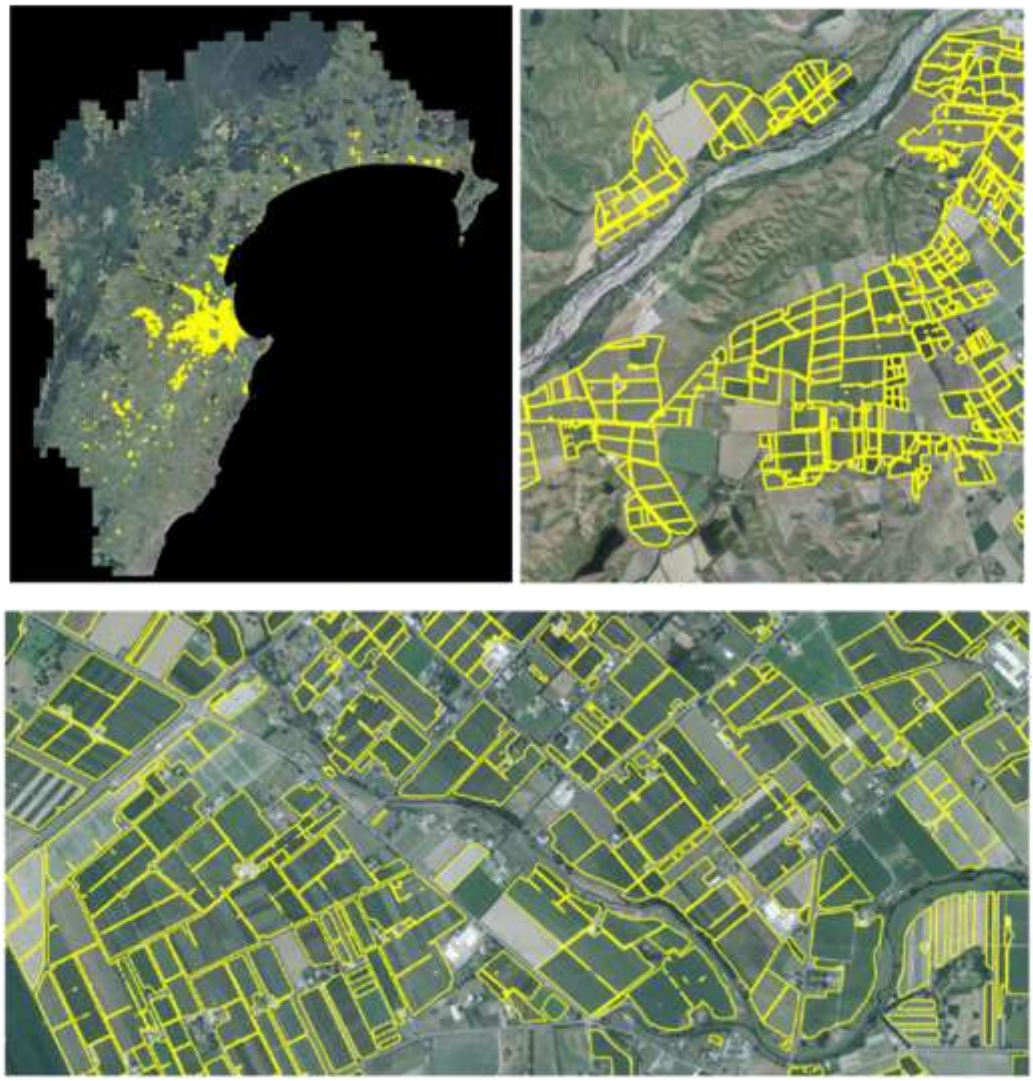

Figure 35. 'Experimental fields' (orchards/vineyards – yellow polygons) predictions from LiDAR for Hawke's Bay. (Top left) Result for entire study extent; (Top Right and Bottom) Zoom-ins.

5.2.5 Forest cover

The CHM-derived forest layer was generated with a minimum mapping unit of 1 ha, i.e. the minimum area of a forest patch (Figure 36). The total forest cover was c. 5,505.6 km^2 which is about 37.3 % of the LiDAR survey area.

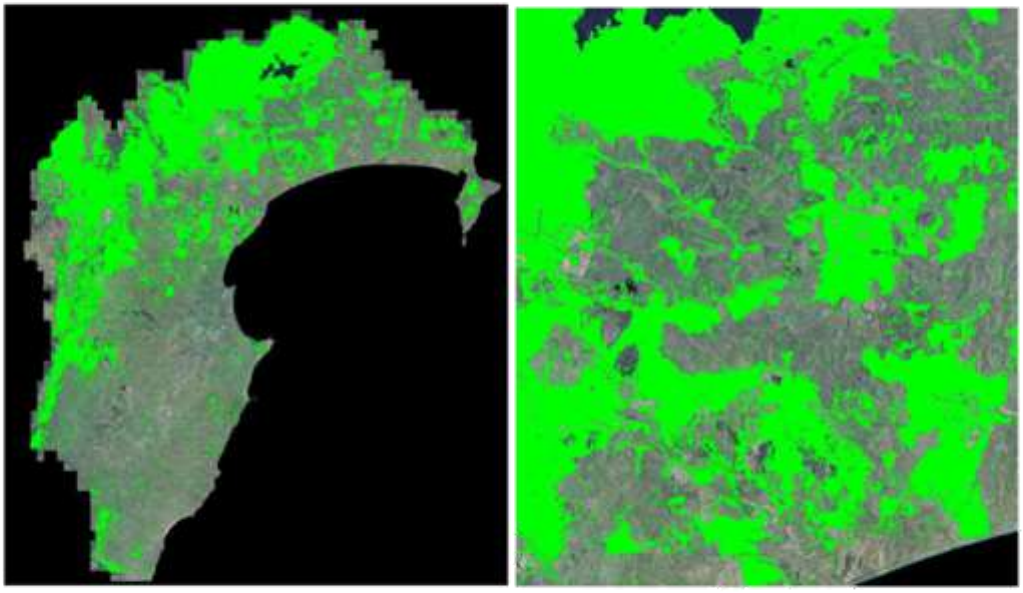

Figure 36. Forest cover (green areas) in Hawke's Bay. (Left) Result for entire study extent; (Right) zoom-in.

6 Conclusions and recommendations

The collaborative LiDAR partnership programme between HBRC and MWLR aimed to maximise the benefit from the LiDAR acquisition for the Hawke's Bay region and explored how this 3D data set can address key environmental science questions. The project was aimed at producing high-resolution spatial layers that could be used for identifying and mapping different types of vegetation. About one Terabyte of aerial LiDAR was processed and translated into regional maps of vegetation information. The raster layers provide unprecedented detail of land surface and vegetation structure for the Hawke's Bay region. This canopy height information overlaid with vector objects of forests, shelter belts, pine stands, and individual trees provides a comprehensive vegetation layer at regional scale in New Zealand. It also vastly surpasses the spatial detail of previous large-scale land cover products such as the Land Cover Database of New Zealand (LCDB v.5.0) created by Manaaki Whenua – Landcare Research (2020).

We applied efficient software workflows to process large-scale aerial point clouds and multi-band imagery as well as state-of-the-art computer vision and deep learning models for detection of vegetation features in rasterized LiDAR data. The purpose of this work was not only to generate one-off data products, but to create baseline methods and data sets

which can be updated and refined in the future and used for change detection. The methods described in this report are transparent and repeatable.

We note the following and make several related recommendations.

1 Our methods were developed to produce consistent vegetation maps for the entire region, prioritising regional coverage over detailed local mapping. The project scope did not allow for time-consuming manual refinement of the layers, and we acknowledge this as a limitation. In addition, there exist different types of uncertainties in the derived vegetation products. We used the LiDAR classification provided by the vendor to filter for vegetation points. It is important to note that the classification is not 100% perfect, and any errors, e.g. misclassification of buildings as vegetation, will carry over to the CHM-derived layers. While the deep learning-based methods achieve high mapping accuracy, even small error percentages (e.g. 3.1% for pine forest) may lead to a large number of small erroneous polygons that need to be manually inspected and screened. The rules and threshold-based tree identifying algorithm catered for all types of trees without being optimised to a specific species, which is also likely to lead to errors.

   - We recommend councils (i.e. HBRC) work on clear class definitions, e.g. minimum height, side lengths, spacing between features, to filter the data sets of shelter belts, pine, and fields to further reduce uncertainties in the data set and make the layers more useful for specific use cases.
   - Once the rules have been defined, these must be also applied to the training data set and models should be re-trained on the more specific requirements to optimise accuracy and loss metrics – which will greatly improve the results and reduce error screening later on.

2 The vegetation layers are useful on their own but become more powerful when combined with additional information, such as, knowledge of nearby water areas. The intersection between wet areas and vegetation types may help categorise wetlands and riparian vegetation. The latter could be directly derived by buffering around the stream network and intersecting with the vegetation layers.

   - We recommend councils (i.e. HBRC) investigate the potential combination of existing environmental layers to derive secondary datasets and establish rule sets that can be applied at broader (regional) scale.

3 This project applied both traditional algorithms and novel AI techniques to the LiDAR data sets. We demonstrated that encoder–decoder networks are very flexible; they can be trained to detect different vegetation types from canopy height models alone or can use multi-band aerial photography as input for detection tasks. They are also able to improve initial training data sets, e.g. through improving shelter belt labels or drawing smoother pine forest outlines, during the prediction stage. They are relatively easy to train (i.e. just by providing appropriate training data sets) and no domain-specific rules are required for initial predictions. However, deep learning predictions are difficult to interpret, and it is impossible to explain in natural language why some predictions in specific locations were made and some not. Hand-crafted algorithms, on the other hand, can be highly parameterised and many domain-specific decisions

have to be made to get intial results, which limits transferability to new problems, e.g. different vegetation classes.

- Because both types of systems have their strengths and weaknesses, we strongly recommend exploring different AI and hand-crafted options for future vegetation change analysis, to ensure consistency of the map results.

4 A major strength of the deep learning approach is that no height information is required. This can greatly reduce cost as RGB aerial photography can be used on its own for vegetation classification and analysis (except height/volumetric change). The convolutional neural network is able to extract both spectral and structural from the photography, which often contains more information than the pure CHM. It was not practical in this project to combine the RGB photography with LiDAR canopy height, because the surveys were conducted at different times, and for some areas were over a year apart; this lead to mismatches due to temporal change, and to misalignment issues due to the different measurement geometries and systems.

- We recommend simultaneous acquisitions of LiDAR and RGB imagery to increase usefulness of the technologies and improve classification of vegetation types and tree species.

5 Councils may want to use LiDAR data for applications beyond broad vegetation mapping, e.g. targeting smaller areas with specific objectives which are not practical at the regional scale. This may include more detailed tree species (different native species or other exotics) or field type classification (distinguishing between different types of orchards and vineyards). For such exercises, a substantial amount of training data must be generated, supported by expert knowledge and ground-truthed observations. We conducted a short trial to identify willow trees from the CHM but with limited success due to the small training data size and lack of colour information from photography.

- We recommend that councils (i.e. HBRC) use state-of-the-art computer vision methods such as convolutional encode-decoder networks, which showed promise in this work and can be used for tree species classification from NZ regional RGB imagery (e.g. Spiekermann et al. 2023).

6 Another potential application for the LiDAR data is forest structure analysis and damage assessment, e.g. assessment of understorey damage due to browsing animals. The typical regional aerial LiDAR surveys in New Zealand are mainly conducted to map the ground surface and to generate medium-resolution raster products of man-made and vegetation surfaces. This means surveys are flown at low pulse rates leading to limited vegetation penetration and poor vertical structure information of native forests.

- We recommend councils (i.e. HBRC) investigate acquiring purpose-driven high-density aerial and under-canopy LiDAR measurements to enable analysis of mid-tier and understorey of forests.

7 Acknowledgements

The report is based on discussions with Annabel Beattie, Ashton Eaves and Tim Farrier from Hawke's Bay Regional Council.

8 References

Dalponte M, Coomes DA 2016. Tree-centric mapping of forest carbon density from airborne laser scanning and hyperspectral data. Methods in Ecology and Evolution 7(10): 1236– 1245.

Farrier T 2021. Hawke's Bay regional LiDAR 2020. (2021) Dataset report. November 2021. Hawkes Bay Regional Council Publication No. 5566. Available online at: https://catalogue.data.govt.nz/dataset/hawkes-bay-regional-lidar-2020-dataset-report3 (accessed 06 May 2024)

Kim, H., Arrowsmith, J.R, Crosby, C.J., Jaeger-Frank, E., Nandigam, V., Memon, A., Conner, J., Badden, S.B., and Baru, C (2006) An efficient implementation of a local binning algorithm for digital elevation model generation of LiDAR-ALSM datasets, Eos (Transactions, American Geophysical Union), Fall Meeting, 2006, Abstract G53C-0921.

Lam S-K, Pitrou A, Seibert S 2015. Numba: a LLVM-based Python JIT compiler. In: Proceedings of the Second Workshop on the LLVM Compiler Infrastructure in HPC (LLVM '15). Association for Computing Machinery, New York, NY, USA. Article 7: 1–6. Available online at: https://doi.org/10.1145/2833157.2833162

Land Information New Zealand (LINZ) 2020. PGF Version: New Zealand national aerial LiDAR base specification, January 2020. Available online at: https://www.linz.govt.nz/sites/default/files/pgf_version_new_zealand_national_aerial_lidar_base_specification.pdf (accessed 06 May 2024).

Lindsay JB 2016. Whitebox GAT: A case study in geomorphometric analysis. Computers & Geosciences 95: 75–84.

Manaaki Whenua – Landcare Research 2020. LCDB v5.0 - Land Cover Database version 5.0, Mainland, New Zealand. Available online at: https://doi.org/10.26060/W5B4-WK93

Redmon J, Divvala S, Girshick R, Farhadi A 2016. You only look once: unified, real-time object detection. In: 2016 IEEE Conference on Computer Vision and Pattern Recognition (CVPR), Las Vegas, NV, USA, 2016, pp. 779-788. Available online at: https://doi.org/10.1109/CVPR.2016.91

Ronneberger, O., Fischer, P., & Brox, T. (2015). U-net: Convolutional networks for biomedical image segmentation. In Medical image computing and computer-assisted intervention–MICCAI 2015: 18th international conference, Munich, Germany, October 5-9, 2015, proceedings, part III 18 (pp. 234-241). Springer International Publishing.

Spiekermann RI, van Zadelhoff F, Schindler J, Smith H, Phillips C, Schwarz M 2023. Comparing physical and statistical landslide susceptibility models at the scale of

individual trees. Geomorphology 440: 108870. https://doi.org/10.1016/j.geomorph.2023.108870

Zörner J, Dymond J, Shepherd J, Jolly B 2018a. PyCrown – Fast raster-based individual tree segmentation for LiDAR data. Landcare Research NZ Ltd. Available online at: https://doi.org/10.7931/M0SR-DN55

Zörner J, Dymond JR, Shepherd JD, Wiser SK, Bunting P, Jolly B 2018b. LiDAR-based regional inventory of tall trees – Wellington, New Zealand. Forests 9: 702–71.

St John's Particulate Matter Monitoring Method

Co-location and demonstrated equivalence of particulate matter monitoring methods at St John's College, Hastings.

August 2024
Hawkes Bay Regional Council Publication No. 5612

HAWKES BAY
REGIONAL COUNCIL
TE KAUNIHERA Ā-ROHE O TE MATAU-A-MĀUI

ISSN 2703-2051 (Online)
ISSN 2703-2043 (Print)

Version

HAWKES BAY
REGIONAL COUNCIL
TE KAUNIHERA Ā-ROHE O TE MATAU-A-MĀUI

(06) 835 9200
0800 108 838
Private Bag 6006 Napier 4142
159 Dalton Street . Napier 4110

Environmental Science

St John's Particulate Matter Monitoring Methods

Co-location and demonstrated equivalence of particulate matter monitoring methods at St John's College, Hastings.

August 2024
Hawkes Bay Regional Council Publication No. 5612

Prepared By:
Jeremy Kidd – Scientist - Air Quality

Reviewed By:
Dr Kathleen Kozyniak – Team Leader Air & Land Science

Approved By:
Sam French – Acting Manager Science

ISSN 2703-2051 (Online)
ISSN 2703-2043 (Print)

Version

Contents

Executive summary 5

1 Introduction 6

2 Methodology 7

2.1 Monitoring Site 7

2.2 Instrumentation 8

2.3 Study Period 9

2.4 Data Analysis 9

3 Results 11

3.1 Monitoring Results 11

3.2 Methods Comparison and Demonstrated Equivalence 13

3.3 Temporal Variation 16

3.4 Meteorological Conditions 20

4 Discussion 22

4.1 PM_{10} 22

4.2 $PM_{2.5}$ 23

4.3 Implications of switching monitoring methods 23

5 Acknowledgements 24

6 Glossary of abbreviations and terms 24

7 References 25

Version

Tables

Table 2-1: Summary of instrumentation used for the colocation study. 9
Table 2-2: PM threshold concentrations used for this study. 10
Table 3-1: Summary statistics of PM monitoring results from the different study methods. 11
Table 3-2: Summary of the demonstrated equivalence analysis. 15
Table 3-3: Summary of the demonstrated equivalence analysis after data adjustment. 15

Figures

Figure 2-1: Map of the Hastings area and the location of the St John's air quality monitoring site. 7
Figure 2-2: The number of days exceeding the NESAQ PM_{10} standard of 50 µg/m3 as a 24-hour average at the HBRC St John's College monitoring site in Hastings. 8
Figure 3-1: 24-hour average PM_{10} values for all methods across the study period. 12
Figure 3-2: 24-hour average $PM_{2.5}$ values for all methods across the study period. 13
Figure 3-3: Plots comparing 24-hour average values for: A) Reference vs BAM PM_{10}, B) Reference vs Fidas PM_{10}, C) BAM vs Fidas PM_{10}, D) Reference vs BAM $PM_{2.5}$, E) Reference vs Fidas $PM_{2.5}$, and F) BAM vs Fidas $PM_{2.5}$. 14
Figure 3-4: Monthly average PM_{10} across all three measurement methods for the study period. 16
Figure 3-5: Percentage difference between the mean seasonal PM_{10} concentrations of the different measurement methods. 17
Figure 3-6: Monthly average $PM_{2.5}$ across all three measurement methods for the study period. 18
Figure 3-7: Percentage difference between the mean seasonal $PM_{2.5}$ concentrations of the different measurement methods. 18
Figure 3-8: Time Variation plot of PM_{10} measurements from the BAM and Fidas for the study period. 19
Figure 3-9: Time Variation plot of $PM_{2.5}$ measurements from the BAM and Fidas for the study period. 20
Figure 3-10: Frequency of wind direction and wind speed during the study period (left) and the entire data record (right) at the HBRC St John's Air Quality site. 21
Figure 3-11: Frequency of wind direction and speed by season for the study period. 21
Figure 3-12: Monthly average temperatures for the study period and the entire data record at St John's Air Quality site. 22

Version

Executive summary

A colocation study was undertaken at the HBRC air quality monitoring site located at St John's College in Hastings using FH-62 beta attenuation monitors (BAM), a Fidas 200E aerosol spectrometer and E-SEQ-FRM gravimetric reference samplers. The aim of the study is to compare PM_{10} and $PM_{2.5}$ measurements from the BAM and Fidas and determine whether they are equivalent to each other and the reference method. PM_{10} and $PM_{2.5}$ data were collected from 6 April 2022 to 20 April 2023. Equivalence between instruments was assessed using an orthogonal regression of 24-hour average values as set out in the standard AS/NZS 3580.9.17:2018. The threshold of 25% expanded relative uncertainty was used to determine whether instruments are equivalent.

Key findings from the study are:

- The Fidas demonstrated equivalence to the reference method for PM_{10} measurement.
- The BAM demonstrated equivalence to the reference method for $PM_{2.5}$ measurement.
- BAM PM_{10} and Fidas $PM_{2.5}$ are not equivalent to the reference method.
- The Fidas and BAM are not equivalent to each other for PM_{10} or $PM_{2.5}$ and Fidas measurements are higher than BAM measurements.
- The Fidas measures higher concentrations than the two other methods when PM is dominated by biomass burning sources (winter).
- The reference method measures higher concentrations than the other methods when marine aerosols make a greater contribution to PM (summer).

The implications of the study are that switching to the Fidas for regulatory monitoring will result in an apparent increase in PM_{10} and $PM_{2.5}$ concentrations, as well as more exceedances of the NESAQ PM_{10} standard and WHO guidelines. However, this would be a more accurate representation of PM_{10} concentrations which is important for assessing compliance with the NESAQ for PM_{10}. The orthogonal regressions from this study can be used to adjust data for trend analysis, continuity of the data record and/or equivalence to reference method.

Version

1 Introduction

The Hawke's Bay Regional Council (HBRC) has monitored particulate matter (PM) since 2005 and currently operates 3 regulatory monitoring stations in the Awatoto, Napier and Hastings airsheds. The purpose of the monitoring stations is to determine whether levels of PM_{10} meet the National Environmental Standards for Air Quality (NESAQ) set out in the Resource Management Act 1991 (RMA). HBRC currently uses beta attenuation monitors (BAMs) to assess compliance with the NESAQ.

Monitoring using BAMs meets the requirements of the NESAQ, but it involves a substantial amount of time and/or money to maintain the instruments and manage sometimes noisy data. New measurement technologies have emerged in recent years, which offer a range of benefits when compared to BAMs. These include less time/cost of maintenance, better data quality (less noise) and the ability to measure PM in multiple size fractions and at a high time resolution. Optical instruments have gained regulatory certifications in Europe and the US and are being used by some regional councils in New Zealand to replace older regulatory monitoring instruments.

The aim of this study is to compare the measurements of PM_{10} and $PM_{2.5}$ from the newer optical method with the incumbent BAM methodology. The measurements are also compared with a gravimetric reference method to assess equivalence of the continuous methods to the reference method. The expected outcomes of this study are to determine whether the different monitoring instruments are equivalent to each other. This will inform whether adjustment of monitoring data is needed to keep continuity of the data record, for trend analysis and to achieve equivalence with the reference method.

Version

2 Methodology

2.1 Monitoring Site

The HBRC air quality monitoring site used for this study is located at St John's College in Mayfair, Hastings. It is situated in a residential area about 1km east of the town centre (Figure 2-1). Hastings sits on the Heretaunga Plains in Hawke's Bay, roughly 10km from the nearest coastline.

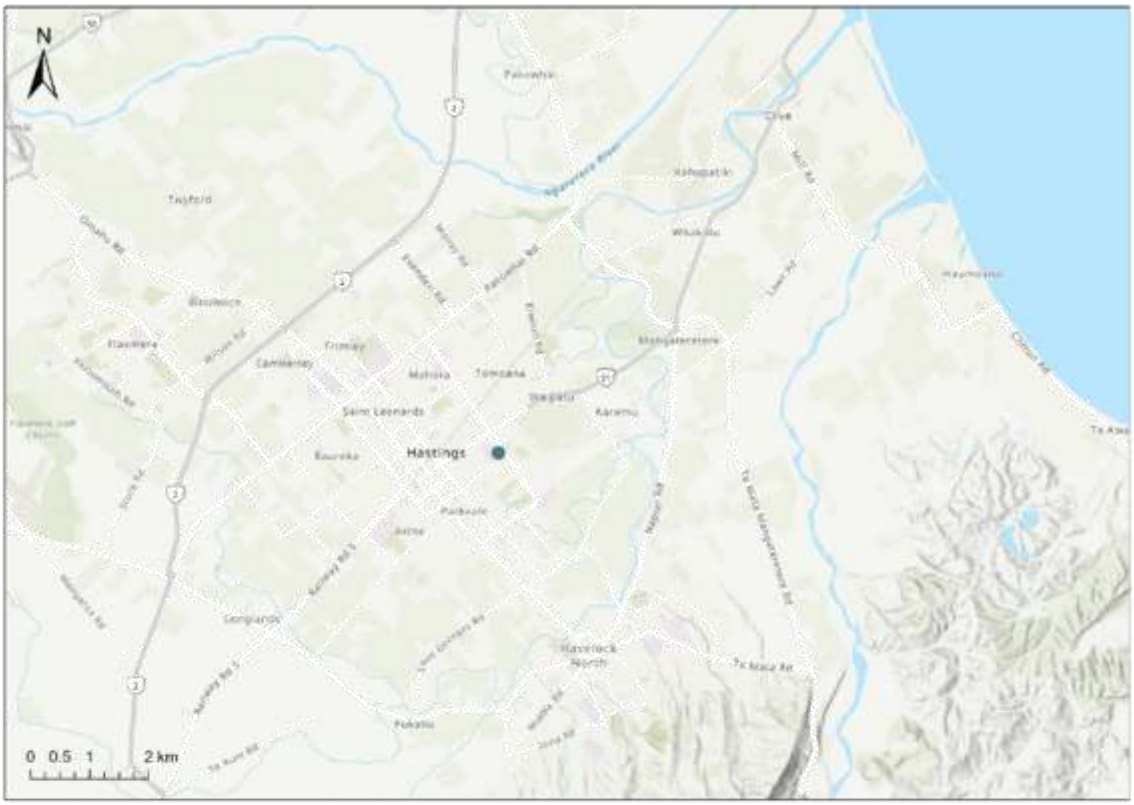

Figure 2-1: Map of the Hastings area and the location of the St John's air quality monitoring site. The site is represented by the blue dot.

The climate of Hawke's Bay is characterised by high sunshine hours and variable rainfall. Hastings generally has warm summer afternoons and cold winter nights, with median minimum temperatures of 3-5°C. Low wind speeds compared to other coastal parts of New Zealand lead to frequent frosts during the cooler months of the year (Chappell, 2013).

Biomass burning is a major source of PM in Hastings, making up 30% of average PM_{10} and 55% of average $PM_{2.5}$. Marine aerosols are also a major contributor at 36% and 22% of average PM_{10} and $PM_{2.5}$ respectively. Motor vehicles, soil (PM_{10} only) and secondary sulphates make up the remaining contributions (Davy & Trompetter, 2024). The number of days exceeding the NESAQ PM_{10} standard has reduced substantially since HBRC began monitoring but exceedances can still occur during favourable meteorological conditions (Figure 2-2).

Version

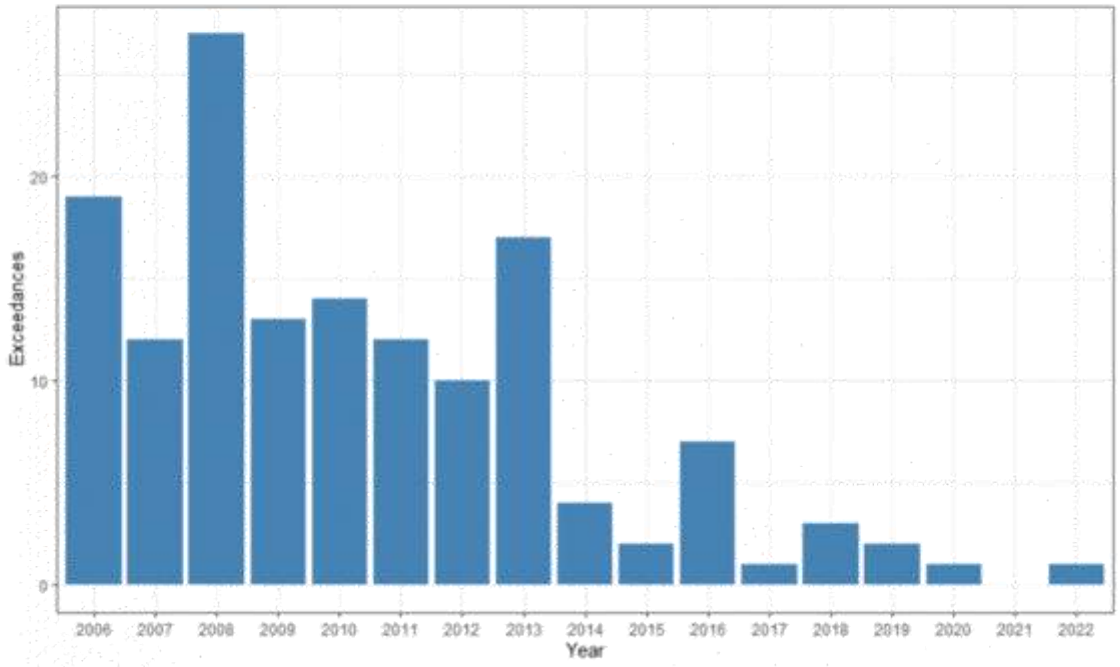

Figure 2-2: The number of days exceeding the NESAQ PM_{10} standard of 50 µg/m3 as a 24-hour average at the HBRC St John's College monitoring site in Hastings. The PM_{10} data used for assessing compliance with the NESAQ were collected using an FH-62 BAM.

2.2 Instrumentation

Three different instruments for measuring PM are used in this study:

- Thermo Scientific™ FH-62 C14 Continuous Particulate Monitor.
- Palas Fidas® 200E Dust Aerosol Spectrometer.
- Met One E-SEQ-FRM Sequential Reference Method Sampler.

The FH-62, otherwise called the BAM in this report, measures PM by way of beta attenuation and is an approved method for assessing compliance with the NESAQ for PM_{10} in New Zealand. It is also certified for PM_{10} measurement by the United States Environmental Protection Agency (US EPA), but not for $PM_{2.5}$ (Table 2-1). This is the current methodology used for regulatory monitoring by HBRC, with NESAQ compliance reported monthly. Air is drawn through a size selective inlet head (PM_{10} or $PM_{2.5}$), through a heated inlet pipe (to remove moisture) and through a glass fibre filter tape. Beta particles are fired through the filter tape and the attenuation of these particles determines the weight of deposited PM. Negative values are relatively common in BAM data as moisture and other volatile particles deposited on the filter tape evaporate off, reducing the weight of matter on the filter tape. The instrument provides 10-minute average PM data as well as a 24-hour average. For this study 10-minute average data were recorded and used to calculate 1-hour and then 24-hour averages.

The Fidas 200E measures PM through optical light scattering of individual particles, providing data across multiple size fractions. It is not on the list of approved methods for regulatory monitoring in New Zealand but has certifications in the UK and Europe (Table 2-1). The measurement range of the instrument is 0.18 – 18 µm with a time resolution of 1 second up to 24 hours. Operating temperature range is from 5 to 40°C.

To be consistent with the FH-62 data, 10-minute average data were recorded from the instrument and used to calculate 1-hour averages, from which the 24-hour averages used in this study are calculated.

The E-SEQ-FRM (referred to as FRM in this report) is a gravimetric sampler, drawing air through a sample filter and determining a PM concentration from the weight of PM deposited on the filter. It is certified as a reference method by the US EPA (Table 2-1). Filters are weighed before and after sampling and the weight of deposited PM is calculated from the difference between the two measurements. A size selective inlet determines whether PM_{10} or $PM_{2.5}$ is measured. Time resolution is set by the user and for this study was set to 24 hours. For this study Whatman PTFE membrane filters with a 47mm diameter and 0.4µm pore size were used to collect particulate matter. The supply, conditioning and weighing of filters to determine PM gravimetric mass were carried out by GNS Science as part of a source apportionment study for the Hastings airshed (Davy & Trompetter, 2024).

Table 2-1: Summary of instrumentation used for the colocation study.

Instrument	Measurement Method	Certification	PM Metric	Samples (% Valid data capture)
Thermo Scientific FH-62 C14	Continuous beta attenuation	US EPA Equivalent PM_{10} Method	PM_{10}	373 (98.4%)
Thermo Scientific FH-62 C14	Continuous beta attenuation	Not certified for $PM_{2.5}$ measurement	$PM_{2.5}$	370 (97.6%)
Palas Fidas 200E	Continuous optical	TUV(Germany), MCERTS(UK), EN 15267	PM_{10} and $PM_{2.5}$ (Also PM_{1}, PM_{4}, PM_{total})	355 (93.7%)
Met One E-SEQ-FRM	Discrete Gravimetric	US EPA Reference Method	PM_{10}	135 (87.1%)
Met One E-SEQ-FRM	Discrete Gravimetric	US EPA Reference Method	$PM_{2.5}$	134 (93.1%)

2.3 Study Period

The study period ran from 6th April 2022 to 20th April 2023. During this time the E-SEQ-FRM samplers operated on a 1 in 3-day schedule for all months except the months of May to August, when samples were taken on a 1 in 2-day basis. The sampling frequency was increased during the coldest months of the year to have a better chance of sampling high-pollution days, which most frequently occur during this time of the year. Sampling frequency was also increased to 1 in 2-day during March and April 2023, following the flooding that occurred during Cyclone Gabrielle.

2.4 Data Analysis

The analysis carried out in this study has been guided by the Australian and New Zealand Standard for Demonstration of equivalence for ambient particulate matter monitoring methods (AS/NZS 3580.9.17:2018). As set out in the standard, the relationship between the 24-hour averages of the reference method (RM) and the candidate method (CM) is determined using an orthogonal regression. The

Version

results of the orthogonal regression govern whether the CM can be considered equivalent to the RM. The condition for accepting the CM data as equivalent is:

- The expanded relative uncertainty is ≤25%

The expanded relative uncertainty is calculated at a specific threshold concentration. The threshold concentrations used for this study are set out in Table 2-2. The PM_{10} threshold is the NESAQ standard for 24-hour average PM_{10}, and the $PM_{2.5}$ threshold is taken from the World Health Organisation (WHO) Air Quality Guidelines Global Update (WHO, 2006). It is a strategic goal of the Hawke's Bay Regional Council to have regional air quality meeting the WHO guidelines by 2025, and the 2005 guidelines were current at the time the strategic plan was created. The WHO 2021 guidelines (WHO, 2021) are also included for reference as they are the most recent version of the guidelines and may be incorporated into regulatory standards in the future. The 2021 guidelines are not used as the thresholds for determining equivalence in this study.

Table 2-2: PM threshold concentrations used for this study. All PM concentrations are 24-hour averages in units of $\mu g/m^3$.

PM Measurement	Threshold for determining equivalence	WHO 2021 Guideline
PM_{10}	50	45
$PM_{2.5}$	25	15

If the expanded relative uncertainty condition is not met, then the results of the following slope and intercept tests determine how to adjust/correct the CM data:

- The slope must be insignificantly different from 1:
  $|b - 1| \leq 2 \times u(b)$
  where b is the slope and u(b) is the uncertainty of the slope
- The intercept is insignificantly different from 0:
  $|a| \leq 2 \times u(a)$
  where a is the intercept and u(a) is the uncertainty of the intercept

Data from this study were analysed using the openair package in the statistical software R (Carslaw & Ropkins, 2012). The orthogonal regression analysis required for equivalence testing was carried out using the Orthogonal regressions and equivalence test utility worksheet version 2.9 (Beijk, 2012).

3 Results

3.1 Monitoring Results

There were 127 valid data points recorded across all three methods for PM_{10} and 125 valid data points for $PM_{2.5}$. Summary statistics are shown in Table 3-1. The BAM recorded the lowest mean, lowest maximum value and least exceedances of thresholds/guidelines for both particle sizes. Mean PM_{10} was highest for the FRM but the greatest PM_{10} maximum was recorded by the Fidas. $PM_{2.5}$ mean values were closer between the Fidas and FRM but the Fidas recorded a greater $PM_{2.5}$ maximum and recorded more days above the threshold and guideline values.

Table 3-1: Summary statistics of PM monitoring results from the different study methods. All values are in units of $\mu g/m^3$.

Instrument	PM_{10} Mean	PM_{10} Max	PM_{10} > 50	PM_{10} > 45	$PM_{2.5}$ Mean	$PM_{2.5}$ Max	$PM_{2.5}$ > 25	$PM_{2.5}$ > 15
FH-62 BAM	9.7	41.1	0	0	6.9	40.5	4	16
Fidas 200E	13.3	63.5	2	3	8.2	54.5	9	17
E-SEQ-FRM	16.5	58	1	2	8.5	45.2	5	16

Time series of the measured PM_{10} values shows that higher concentrations occurred during the cooler months of the year (May – September) with the Fidas recording higher concentrations compared to the other two methods. During the warmer months of the year concentrations are generally lower and the FRM recorded the highest concentrations of all the methods. There is also a sizeable gap in the data from mid-July to mid-August which was caused by instrument malfunction (Figure 3-1).

Version

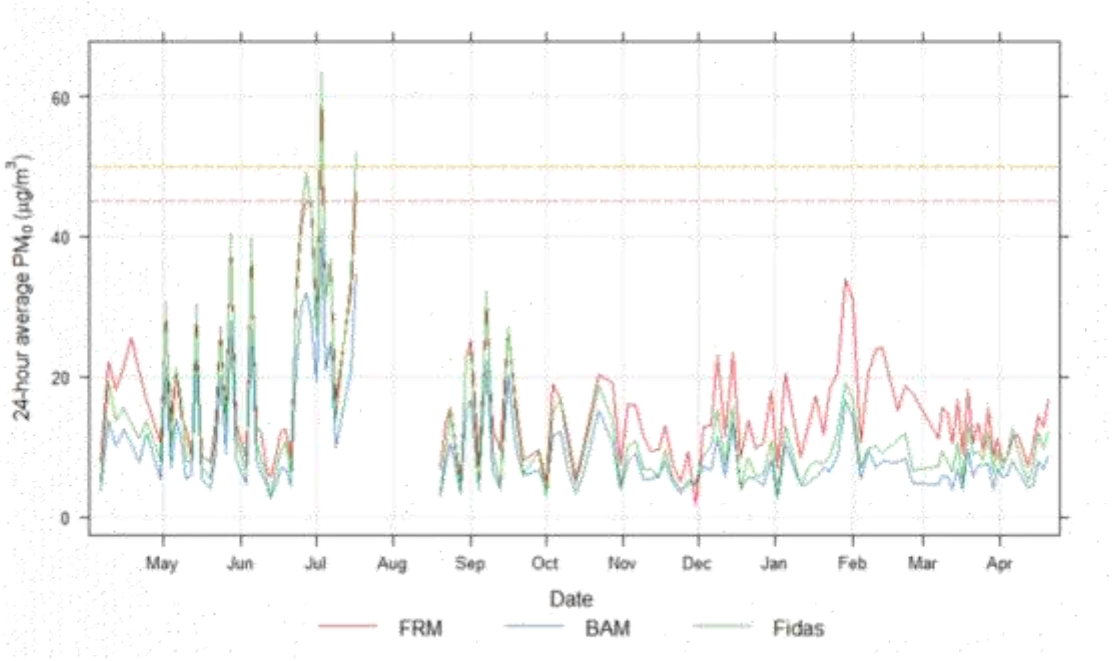

Figure 3-1: 24-hour average PM_{10} values for all methods across the study period. The orange dashed line represents the NESAQ of 50 µg/m³. The red dashed line represents WHO 2021 guideline of 45 µg/m³.

The time series for $PM_{2.5}$ is shown in Figure 3-2. As seen in the PM_{10} time series, peak concentrations occur during the months of May through September and are generally low during the rest of the study period. Fidas concentrations were the highest of the methods for the May through September period while the FRM recorded higher concentrations during summer months. There are two gaps in the $PM_{2.5}$ data, from late June to early July (caused by instrument failure) and from mid-February to the beginning of March (due to power failure after Cyclone Gabrielle).

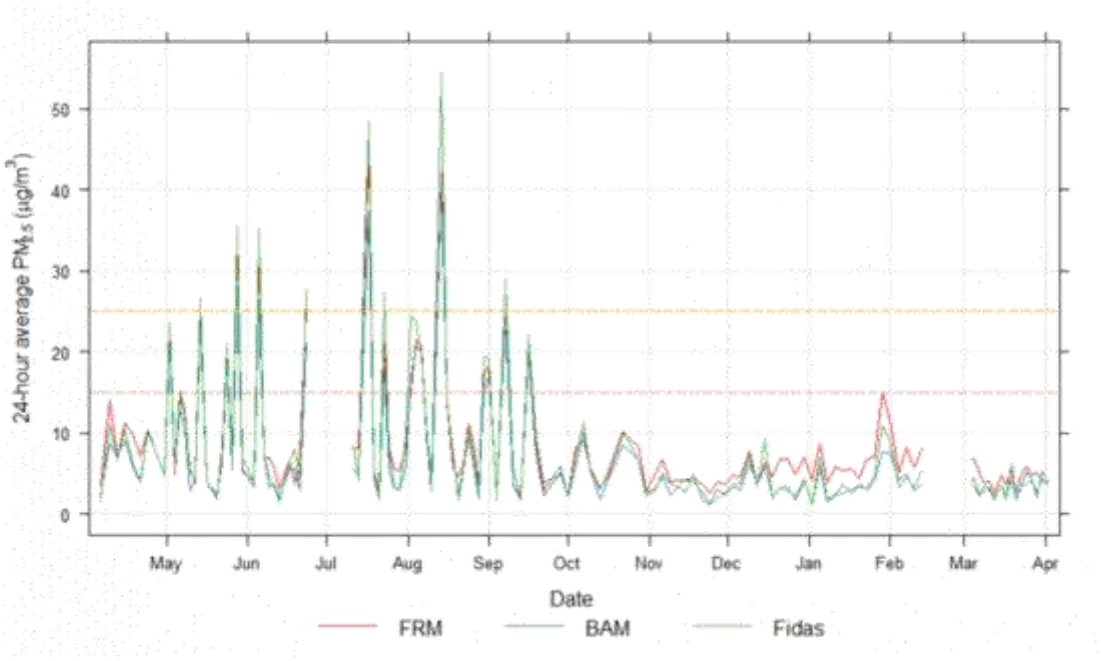

Figure 3-2: 24-hour average $PM_{2.5}$ values for all methods across the study period. The orange dashed line represents the WHO 2005 guideline of 25 µg/m³. The red dashed line represents the WHO 2021 guideline of 15 µg/m³.

3.2 Methods Comparison and Demonstrated Equivalence

Table 3-2 summarises the results of the demonstrated equivalence testing between the reference and candidate methods for all particle size fractions. The BAM $PM_{2.5}$ and Fidas PM_{10} pass the expanded relative uncertainty test when compared with the gravimetric reference method. However, none of the comparisons satisfied the requirements for passing the slope or intercept tests as set out in the AS/NZS standard for demonstrating equivalence. The BAM PM_{10} showed the greatest difference from the reference method, with a bias of -16.27 at the threshold of 50 µg/m³. When the Candidate Method data is adjusted using the slope and intercept of the regression, all the measurements meet the threshold for expanded relative uncertainty (Table 3-3).

Figure 3-3 presents the orthogonal regression plots for each of the measurement method comparisons. In plots **B** and **D** the regression lines are close to the line representing a 1:1 relationship, indicating that the Fidas and reference method have similar PM_{10} concentrations and the BAM and reference method have similar $PM_{2.5}$ readings. In plots **A**, **C**, **E**, and **F** there is a greater discrepancy between measurement methods.

Version

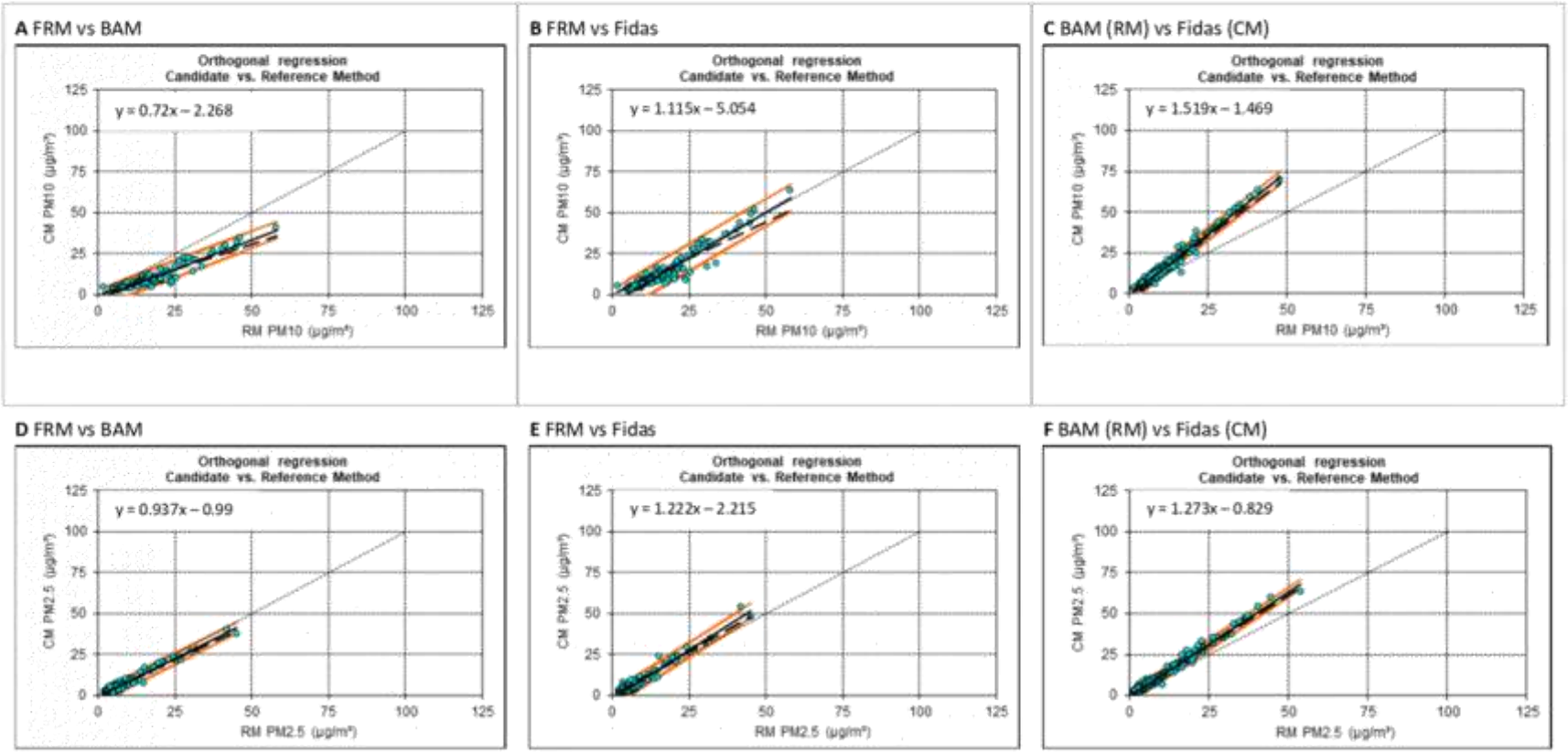

Figure 3-3: Plots comparing 24-hour average values for: A) Reference vs BAM PM_{10}, B) Reference vs Fidas PM_{10}, C) BAM vs Fidas PM_{10}, D) Reference vs BAM $PM_{2.5}$, E) Reference vs Fidas $PM_{2.5}$, and F) BAM vs Fidas $PM_{2.5}$. The orthogonal regression equation is in the top left corner of each plot and is represented by the solid black line on each graph (the dashed black line when forced through 0). The orange lines represent the 97.5% confidence interval.

Version

Table 3-2: Summary of the demonstrated equivalence analysis. The analysis is based on the results of an orthogonal regression between measurement methods (as used in Beijk (2018)). Threshold values for the bias are 50 µg/m³ for PM_{10} and 25 µg/m³ for $PM_{2.5}$. Cells highlighted green indicate an expanded relative uncertainty less than the threshold of 25% required to demonstrate equivalence as per the AS/NZS 3580.9.17:2018 Standard.

-

Measurement	Reference Method	Candidate Method	No. of samples	Slope (b)	Intercept (a)	R^2	Bias at threshold (µg/m³)	Expanded relative uncertainty (%)	Slope test	Intercept test
PM_{10}	FRM	BAM	123	0.72	-2.268	0.899	-16.27	65.7%	Fail	Fail
$PM_{2.5}$	FRM	BAM	132	0.937	-0.99	0.951	-2.56	23.4%	Fail	Fail
PM_{10}	FRM	Fidas	129	1.115	-5.054	0.889	0.7	15.0%	Fail	Fail
$PM_{2.5}$	FRM	Fidas	127	1.222	-2.215	0.953	3.32	30.7%	Fail	Fail
PM_{10}	BAM	Fidas	356	1.519	-1.469	0.975	24.49	98.2%	Fail	Fail
$PM_{2.5}$	BAM	Fidas	360	1.273	-0.829	0.982	6.01	48.9%	Fail	Fail

Table 3-3: Summary of the demonstrated equivalence analysis after data adjustment. The analysis is based on the results of an orthogonal regression between measurement methods (as used in Beijk (2018)). Threshold values for the bias are 50 µg/m³ for PM_{10} and 25 µg/m³ for $PM_{2.5}$. Cells highlighted green indicate an expanded relative uncertainty less than the threshold of 25% required to demonstrate equivalence as per the AS/NZS 3580.9.17:2018 Standard.

Measurement	Reference Method	Candidate Method	No. of samples	Slope (b)	Intercept (a)	R^2	Bias at threshold (µg/m³)	Expanded relative uncertainty (%)	Slope test	Intercept test
PM_{10}	FRM	BAM	123	1.017	-0.294	0.899	0.58	13.8%	Pass	Pass
$PM_{2.5}$	FRM	BAM	132	1.002	-0.014	0.951	0.03	12.9%	Pass	Pass
PM_{10}	FRM	Fidas	129	0.993	0.107	0.889	-0.22	14.9%	Pass	Pass
$PM_{2.5}$	FRM	Fidas	127	0.995	0.041	0.953	-0.08	13.3%	Pass	Pass
PM_{10}	BAM	Fidas	356	0.995	0.048	0.975	-0.21	4.4%	Pass	Pass
$PM_{2.5}$	BAM	Fidas	360	0.998	0.016	0.982	-0.04	6.8%	Pass	Pass

Version

3.3 Temporal Variation

Figure 3-4 shows how the monthly average PM_{10} concentrations vary throughout the year. Monthly means were higher for the FRM PM_{10} than the other methods during the summer, spring, and autumn months. However, this changes during the winter months when the average concentrations of the Fidas and FRM are very similar. The BAM PM_{10} is consistently lower than the other methods throughout the year. The relative difference between the seasonal mean concentrations also changes throughout the year (Figure 3-5). During summer months (D,J,F) the relative difference between the FRM and the two continuous methods is the greatest. The relative difference between the BAM and Fidas is greater during autumn (M,A,M) and winter (J,J,A).

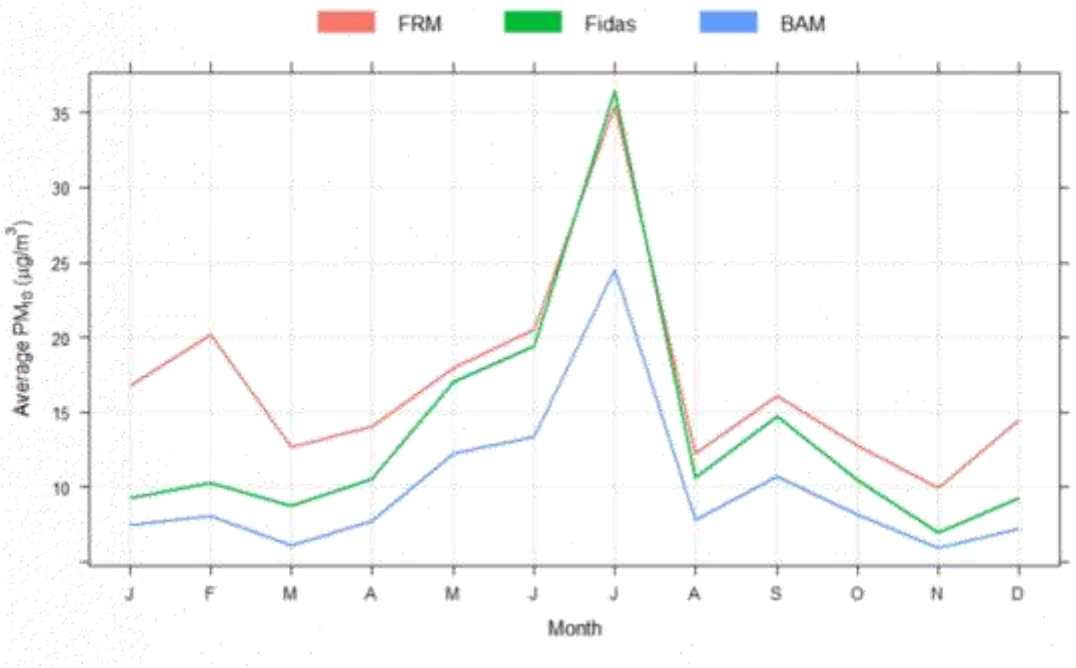

Figure 3-4: Monthly average PM_{10} across all three measurement methods for the study period.

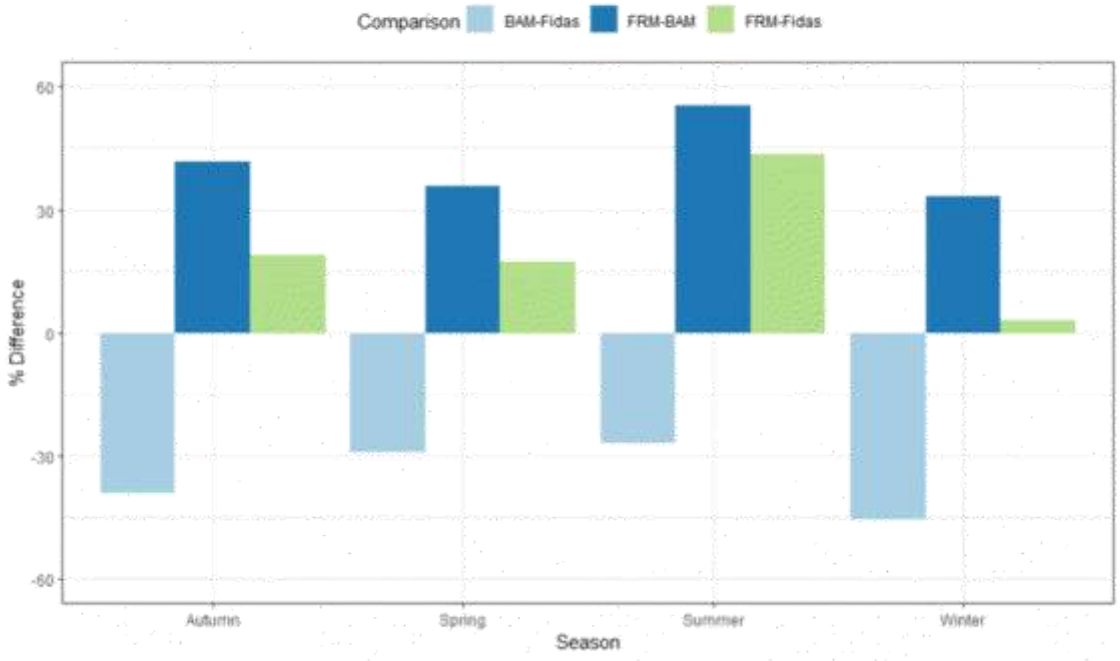

Figure 3-5: Percentage difference between the mean seasonal PM_{10} concentrations of the different measurement methods. The difference is expressed as a percentage of the reference method mean seasonal PM_{10} concentration. For the BAM-Fidas comparison the BAM is considered the reference method.

Figure 3-6 shows the variation in monthly average $PM_{2.5}$ concentrations. The averages for June and July may have been influenced by missing data during that period in the study. The FRM $PM_{2.5}$ and Fidas $PM_{2.5}$ exhibit a different relationship during the warmer months and colder months of the year. The FRM measures higher $PM_{2.5}$ concentrations during the summer while the Fidas measures the highest concentrations during the winter. The BAM again measures lower concentrations than the other methods, except in September when it is similar to the FRM monthly average. Overall, the relative differences between the $PM_{2.5}$ concentrations of all measurement methods are lower than for PM_{10} but the pattern remains the same. The relative difference between the FRM and the continuous methods is again the greatest during summer. The relative difference between the BAM and Fidas is the greatest during winter months (Figure 3-7).

Version

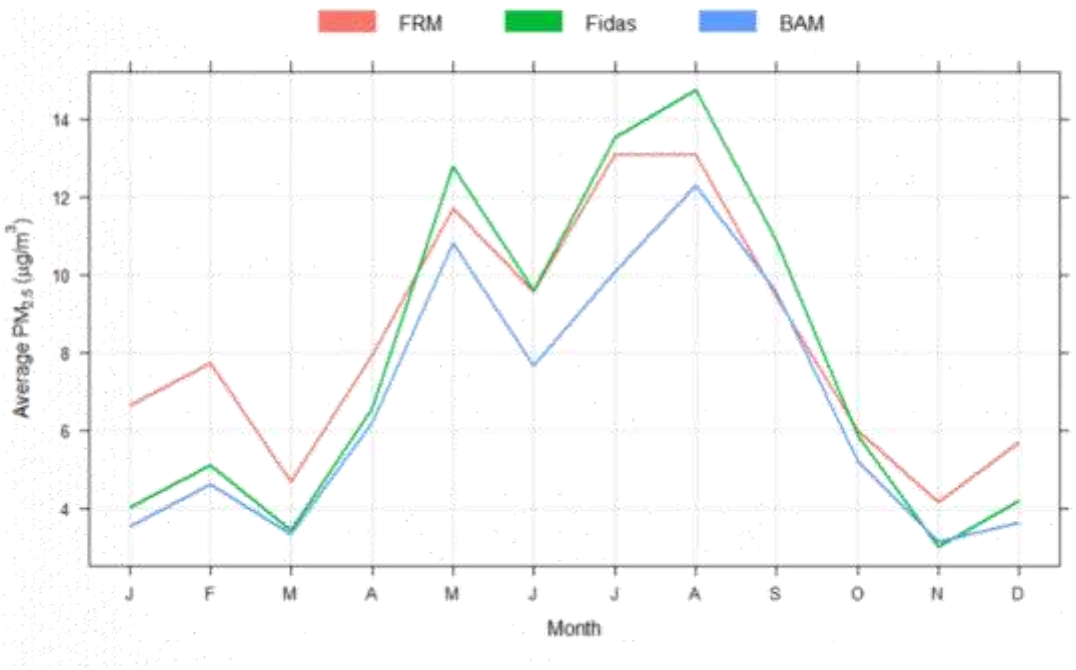

Figure 3-6: Monthly average $PM_{2.5}$ across all three measurement methods for the study period.

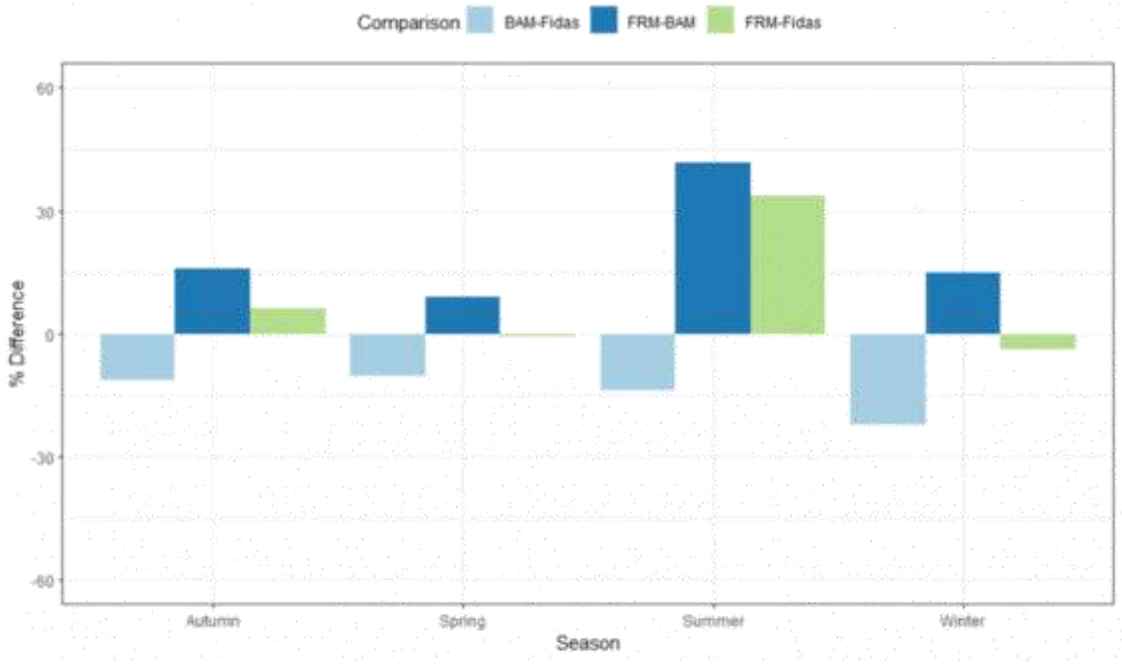

Figure 3-7: Percentage difference between the mean seasonal $PM_{2.5}$ concentrations of the different measurement methods. The difference is expressed as a percentage of the reference method mean seasonal $PM_{2.5}$ concentration. For the BAM-Fidas comparison the BAM is considered the reference method.

Further analysis of the BAM and Fidas data is possible due to the availability of a full year of data collected at a higher time resolution (Figure 3-8 and Figure 3-9). The diurnal patterns in PM_{10} concentrations for both the BAM and Fidas show a peak in concentrations during the evening. The Fidas is recording higher concentrations than the BAM in the evening peak and has a smaller peak in concentrations during the morning, around 8am, which is largely absent in BAM data. Both instruments have their highest average concentrations occurring on weekends, with a low point mid-week. The monthly average concentrations rise from low concentrations in the summer to a winter peak in July. The difference between Fidas and BAM readings is evident throughout the year (Figure 3-8).

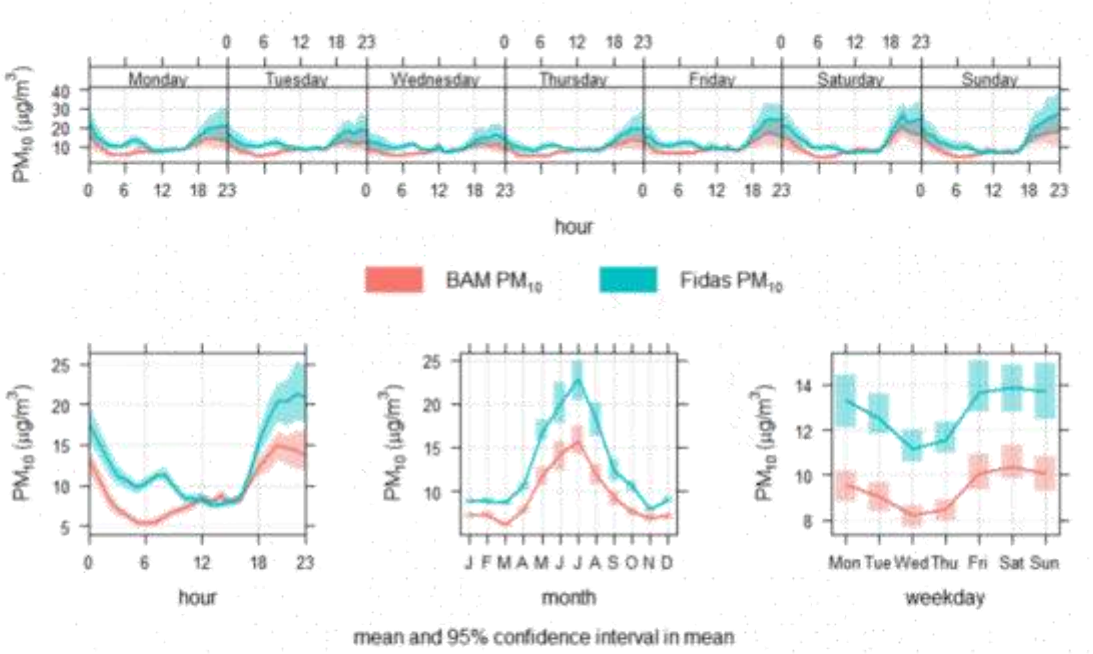

Figure 3-8: Time Variation plot of PM_{10} measurements from the BAM and Fidas for the study period.

Diurnal patterns in $PM_{2.5}$ concentrations follow a similar pattern to PM_{10}, with concentrations peaking in the evening for both measurement methods. Fidas concentrations are higher than the BAM in the evening and early morning while BAM concentrations are higher during the day. The BAM data exhibit a second, lower peak during the late morning which is absent from the Fidas data. The average concentrations for each day of the week peak during the weekend and are the lowest on Wednesdays and Thursdays. Monthly average concentrations exhibit a similar pattern to PM_{10} with a winter peak during July. Fidas and BAM concentrations are similar at the beginning and end of the year but spread apart during winter months (Figure 3.9).

Version

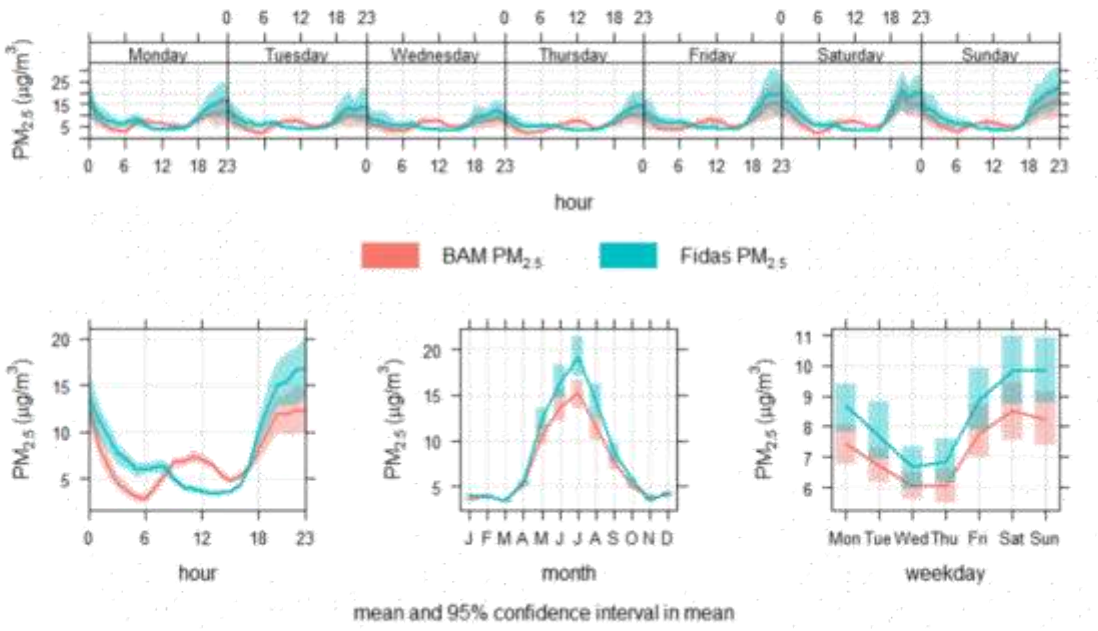

Figure 3-9: Time Variation plot of $PM_{2.5}$ measurements from the BAM and Fidas for the study period.

3.4 Meteorological Conditions

Climatic conditions in New Zealand during 2022 and early 2023 were influenced by the occurrence of La Niña bringing more sub-tropical, north-easterly winds than usual to the country (NIWA, 2023, 2024). For the Hawke's Bay region, La Niña conditions are typically associated with more northerly quarter winds (Fedaeff & Fauchereau, 2015). This pattern is evident in Figure 3-10, with more frequent northerly and north-easterly winds during the study period when compared to the long-term average. Winds with any westerly component were less frequent during the study period. Wind roses for each season of the study period reveal that the anomalous northerly winds mostly occurred during the summer and were mostly at wind speeds above 5km/h. A greater proportion of lower wind speeds from the south and southwest occurred during the autumn and winter (Figure 3-11). Average temperatures during the study period were similar to the long-term average during most months of the year, except for the winter months and November which were warmer than usual (Figure 3-12).

Version

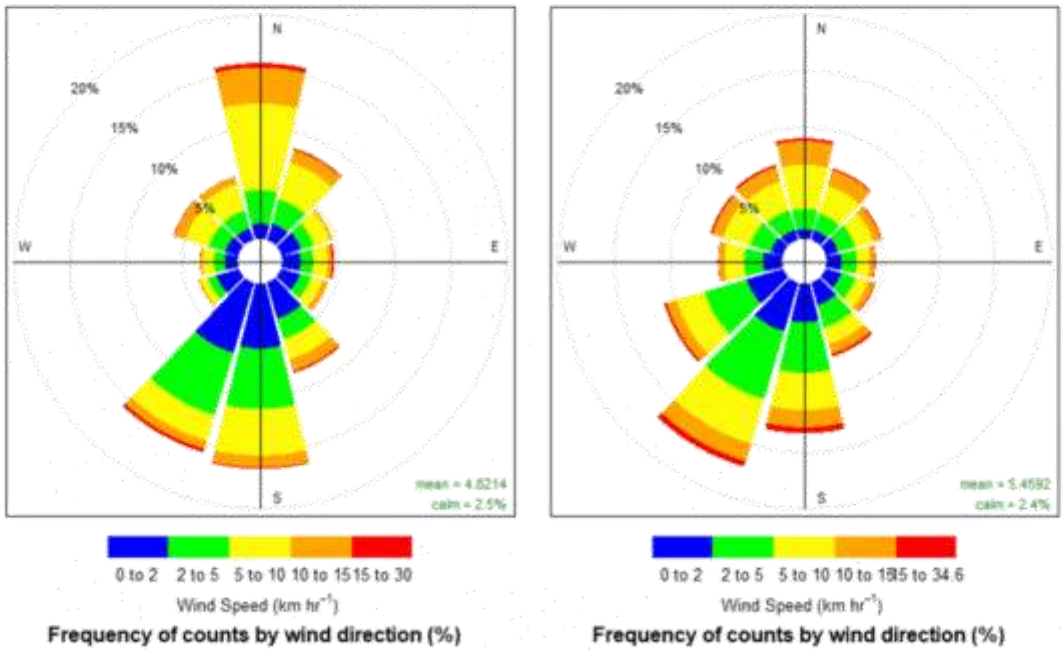

Figure 3-10: Frequency of wind direction and wind speed during the study period (left) and the entire data record (right) at the HBRC St John's Air Quality site.

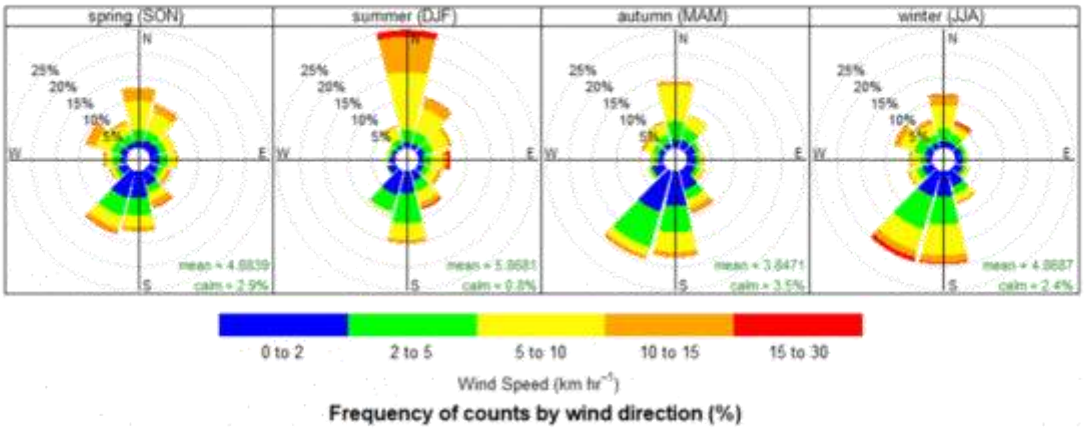

Figure 3-11: Frequency of wind direction and speed by season for the study period.

Version

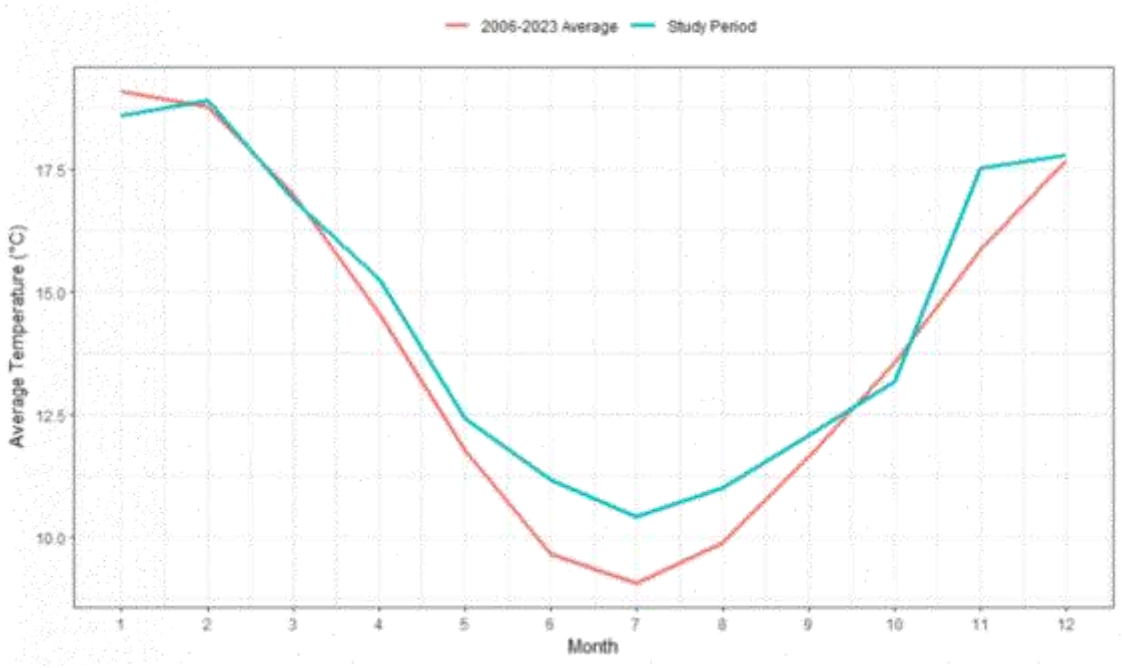

Figure 3-12: Monthly average temperatures for the study period and the entire data record at St John's Air Quality site.

4 Discussion

4.1 PM_{10}

The results of the equivalence testing reveal that the BAM measuring PM_{10} is under-reading 24-hour average concentrations by around 30% when compared to the reference method at the NESAQ standard of 50µg/m³. The Fidas provides a more accurate representation of PM_{10} concentrations than the BAM, with a bias of only 0.7µg/m³ when compared to the reference method. The results of the equivalence testing indicate that the Fidas is the most appropriate instrument to be using for NESAQ reporting, as the data does not need adjusting to meet the expanded relative uncertainty threshold. As the Fidas and BAM data did not demonstrate equivalence (bias of 24.49 at the 50µg/m³ threshold), an adjustment must be made to either of the data sets to maintain data continuity for robust trend analysis.

Analysis of the differences between measurement methods by season shows that the greatest discrepancy from the gravimetric measurements occurs in summer. This may reflect the ability of different measurement methods to detect particles from different sources. Source apportionment work using the gravimetric filters from this study revealed that the average contribution of marine aerosols to PM_{10} was greatest during the summer months of the study period (Davy & Trompetter, 2024). The summer wind rose in Figure 3-10 shows that winds from the north and northeast were particularly frequent during this season, which may have contributed greater amounts of marine aerosols in the air around Hastings.

The difference between Fidas and BAM PM_{10} concentrations is greatest during the autumn and winter months. This is when the contribution of biomass combustion to PM_{10} was the greatest (Davy & Trompetter, 2024), indicating that the Fidas may be more sensitive to detecting PM from this source.

4.2 $PM_{2.5}$

The $PM_{2.5}$ concentrations provided by all the monitoring methods showed better accuracy than the PM_{10} measurements. The results of the study suggest that the BAM can be considered equivalent to the reference method for $PM_{2.5}$ at this site while the Fidas cannot, although it is close (expanded relative uncertainty of 30.7%). The bias for the BAM and Fidas, -2.56 and 3.32 at 25µg/m^3 respectively, indicate these methods under/over-report $PM_{2.5}$ concentrations by about 10-15%. When compared with each other, the BAM and Fidas cannot be considered equivalent for $PM_{2.5}$ measurement which means that an adjustment/correction needs to be applied to some of the data to achieve stationarity of the $PM_{2.5}$ data record or for the purpose of trend analysis.

As with the PM_{10} data, the greatest difference between $PM_{2.5}$ readings of the continuous monitoring methods and the reference method occurs during the summer months. $PM_{2.5}$ from marine aerosol and secondary sulphate sources peak during the summer months (Davy & Trompetter, 2024), indicating that the continuous methods are less sensitive to $PM_{2.5}$ from these sources. Results for $PM_{2.5}$ from the Fidas were higher than the BAM and FRM during the winter, when the contribution to total $PM_{2.5}$ from biomass combustion was the greatest (Davy & Trompetter, 2024). This again points towards the Fidas having a higher sensitivity to PM from biomass combustion.

4.3 Implications of switching monitoring methods

Changing the method by which HBRC monitors PM_{10} and $PM_{2.5}$ at its air quality sites will have implications for the airsheds that are represented by this data. As shown by the results of this study, the proposed new method for monitoring (Fidas) returns higher PM_{10} and $PM_{2.5}$ concentrations than the existing method (BAM). Reporting on PM_{10} concentrations measured by the Fidas would result in 2 exceedances of the NESAQ during the study period, which is above the allowed number of exceedances in a 12-month period. NESAQ exceedances in the Hastings airshed have decreased over time to no more than 1 during 2020, 2021 and 2022 (Figure 2-2). This means the airshed is close to becoming classified as 'not polluted' (as defined in the RMA). Using the Fidas for NESAQ reporting would likely mean the airshed remains a 'polluted' airshed, warranting consideration of further management interventions by HBRC. Resource consent applicants are also affected with stricter controls on the discharge of PM_{10} or requirements to offset proposed discharges within the airshed.

The results of this study indicate that achieving the strategic goal of air quality meeting the WHO guidelines in Hawke's Bay by 2025 would be made more challenging by switching to monitoring PM_{10} and $PM_{2.5}$ with a Fidas. The Fidas recorded more exceedances of the daily limits in the WHO guidelines and higher annual averages, meaning more reductions in emissions would be required to meet these guidelines. However, with the Fidas showing greater sensitivity to PM from biomass burning and less sensitivity to PM from natural sources, management interventions aimed at reducing smoke from biomass burning may have a larger impact on PM_{10} and $PM_{2.5}$ concentrations measured using a Fidas.

Version

5 Acknowledgements

Thanks must be given to Environment Canterbury for the use of their reference monitors and in particular Nathan Cross for his help with the installation of these instruments and guidance on their operation.

6 Glossary of abbreviations and terms

BAM	Beta-attenuation monitor. Air quality monitoring equipment that uses the principle of beta-attenuation to measure the concentration of airborne particles.
FRM	Federal Reference Method - A sequential gravimetric reference method sampler. The instrument takes samples of PM10 and PM2.5 by drawing air through a sequence of filters.
Fidas	Fidas 200E aerosol spectrometer. An air quality monitoring instrument that uses an optical sensor to detect airborne particles.
HBRC	Hawke's Bay Regional Council
NESAQ	National Environmental Standards for Air Quality
PM10	Particulate matter with an aerodynamic diameter of less than 10 micrometers
PM2.5	Particulate matter with an aerodynamic diameter of less than 2.5 micrometers
RMA	Resource Management Act 1991
WHO	World Health Organisation

Version

7 References

Beijk, R. *Orthogonal regression and equivalence test utility, V2.9*. (2018). RIVM (Dutch Institute for Public Health and the Environment, dep. Centre for Environment Monitoring) https://joint-research-centre.ec.europa.eu/system/files/2016-10/aquila-rivm_pm_equivalence_v2.9.xls

Carslaw, D. C., & Ropkins, K. (2012). *openair—An R package for air quality data analysis. Environmental Modelling & Software, 27–28*, 52–61. https://doi.org/10.1016/j.envsoft.2011.09.008

Chappell, P. R. (2013). *The Climate and Weather of Hawke's Bay. 3rd Edition* (p. 44).

Davy, P. K., & Trompetter, W. J. (2024). *Air particulate matter composition and sources of air pollution in Hastings* (HBRC Report 5637). GNS Science. https://hbrc.sharepoint.com/sites/Publications/HBRC%20Publications/Forms/AllItems.aspx?id=%2Fsites%2FPublications%2FHBRC%20Publications%2FHastings%20Air%20Particulate%20Matter%20Composition%202023%5FFINAL%5FHBRC%2Epdf&parent=%2Fsites%2FPublications%2FHBRC%20Publications&p=true&ga=1

Fedaeff, N., & Fauchereau, N. (2015). *Relationship between Climate Modes and Hawkes Bay Seasonal Rainfall and Temperature* (HBRC Report 4835). NIWA. https://hbrc.sharepoint.com/sites/Publications/HBRC%20Publications/Forms/AllItems.aspx?id=%2Fsites%2FPublications%2FHBRC%20Publications%2F4835%5FRelationship%5FClimate%5FModes%5FRainfall%5FTemperature%5F010615%2Epdf&parent=%2Fsites%2FPublications%2FHBRC%20Publications&p=true&ga=1

NIWA. (2023). *2022 Annual Climate Summary*. NIWA. https://niwa.co.nz/sites/default/files/2022_Annual_Climate_Summary_FINAL_v3.pdf

NIWA. (2024). *2023 Annual Climate Summary*. NIWA. https://niwa.co.nz/sites/default/files/2024-01/2023_Annual_Climate_Summary_Final_1.pdf

WHO. (2006). *Air quality guidelines: Global update 2005 ; particulate matter, ozone, nitrogen dioxide and sulfur dioxide*. WHO Regional Office for Europe.

WHO. (2021). *WHO global air quality guidelines. Particulate matter (PM2.5 and PM10), ozone, nitrogen dioxide, sulfur dioxide and carbon monoxide.* World Health Organisation.